Cover Page

CO-PYROLYSIS OF E-WASTE AND BIOMASS FOR FUEL OIL PRODUCTION

A Thesis submitted to Gujarat Technological University

for the Award of

Doctor of Philosophy

in

Chemical Engineering

By

PRAJAPATI SONALBEN BACHUBHAI

189999911007

under supervision of

Dr. Shina Gautam

GUJARAT TECHNOLOGICAL UNIVERSITY

AHMEDABAD

April-2023

CO-PYROLYSIS OF E-WASTE AND BIOMASS FOR FUEL OIL PRODUCTION

A Thesis submitted to Gujarat Technological University

for the Award of

Doctor of Philosophy

in

Chemical Engineering

By

PRAJAPATI SONALBEN BACHUBHAI

189999911007

under supervision of

Dr. Shina Gautam

GUJARAT TECHNOLOGICAL UNIVERSITY

AHMEDABAD

April-2023

DECLARATION

I declare that the thesis entitled Studies on **"Co-pyrolysis of E-waste and Biomass for Fuel Oil Production"** submitted by me for the degree of **Doctor of Philosophy** is the record of research work carried out by me during the period from February 2019 to October 2022 under the supervision of **Dr. Shina Gautam** and this has not formed the basis for the award of any degree, diploma, associateship, fellowship, titles in this or any other Universityor other institution of higher learning.

I further declare that the material obtained from other sources has been duly acknowledged in the thesis. I shall be solely responsible for any plagiarism or other irregularities if noticed in the thesis.

Signature of the Research Scholar: ..... Date: 05/04/2023

Name of Research Scholar: **Sonalben B Prajapati**

Place: Ahmedabad

CERTIFICATE

I certify that the work incorporated in the thesis **"Co-pyrolysis of E-waste and Biomass for Fuel Oil Production"** submitted by **Sonalben B Prajapati** was carried outby the candidate under my supervision/guidance. To the best of my knowledge: (i) the candidate has not submitted the same research work to any other institution for any degree/diploma, Associateship, Fellowship, or other similar titles (ii) the thesis submitted isa record of original research work done by the Research Scholar during the period of study under my supervision, and (iii) the thesis represents independent research work on the part of the Research Scholar.

Signature of Supervisor: Date: 05/04/2023

Name of Supervisor: **Dr. Shina Ganutam**

Place: Ankleshwar

Course-work Completion Certificate

This is to certify that **Sonalben B Prajapati**, Enrolment no. **189999911007,** is a PhD scholar enrolled for PhD program in the branch chemical engineering of Gujarat Technological University, Ahmedabad.

(Please tick the relevant option(s))

1. He/She has been exempted from the course-work (successfully completed during M.Phil Course)
2. He/She has been exempted from Research Methodology Course only (successfully completed during M.Phil Course)
3. ✓ He/She has successfully completed the PhD coursework for the partial requirement for the award of PhD Degree. His/ Her performance in the course work is as follows-

Grade Obtained in Research Methodology	Grade Obtained in Self Study Course (Core Subject)
(PH001)	(PH002)
BB	AA

Supervisor's Sign (Dr. Shina Gautam)

Originality Report Certificate

It is certified that PhD Thesis titled **"Co-pyrolysis of E-waste and Biomass for Fuel Oil Production"** by **Sonalben B Prajapati** has been examined by us. We undertake the following:

a. Thesis has significant new work/knowledge as compared already published or is under consideration to be published elsewhere. No sentence, equation, diagram, table, paragraph or section has been copied verbatim from previous work unless it is placed under quotationmarks and duly referenced.
b. The work presented is original and own work of the author (i.e. there is no plagiarism). No ideas, processes, results or words of others have been presented as author own work.
c. There is no fabrication of data or results which have been compiled / analysed.
d. There is no falsification by manipulating research materials, equipment or processes, or changing or omitting data or results such that the research is not accurately represented in the research record.
e. The thesis has been checked using https://www.urkund.com (copy of originality report attached) and found within limits as per GTU Plagiarism Policy and instructions issued fromtime to time (i.e. permitted similarity index <=10%).

Signature of the Research Scholar: ..... Date: 05/04/2023

Name of Research Scholar: Sonalben B Prajapati

Signature of Supervisor: Date: 05/04/2023

Name of Supervisor: Dr. Shina Gautam

Place: Ahmedabad

Copy of Originality Report

Ouriginal by Turnitin

Document Information

Analyzed document	Thesis 29122022- latest.pdf (D154612554)
Submitted	12/29/2022 8:05:00 AM
Submitted by	sonal Prajapati
Submitter email	sonalchem20@gmail.com
Similarity	5%
Analysis address	sonalchem20.gtuni@analysis.urkund.com

Sources included in the report

SA	**JVB all chapters_VP.pdf** Document JVB all chapters_VP.pdf (D57411958)	11
SA	**SURESH KUMAR P THESIS.pdf** Document SURESH KUMAR P THESIS.pdf (D148914903)	4
SA	**BHAVNA FINAL pdf.docx** Document BHAVNA FINAL pdf.docx (D54110293)	5
SA	**Thesis complete.docx** Document Thesis complete.docx (D34594142)	1
SA	**RAHUL SINGH PROJECT REPORT-M.TECH(EE)-20210402019-new.docx** Document RAHUL SINGH PROJECT REPORT-M.TECH(EE)-20210402019-new.docx (D141854783)	1
SA	**literature review 17-10-17.docx** Document literature review 17-10-17.docx (D31425461)	1
W	URL: https://www.slac.stanford.edu/xorg/hfag/charm/FPCP07/figures/fig_plot_xy.eps Fetched: 10/14/2022 10:00:00 PM	3
SA	**Gajera Bhautik_REE_2017-04-04-64-02_M.Tech_May_2019.pdf**	7

PhD THESIS Non-Exclusive License to

GUJARAT TECHNOLOGICAL

UNIVERSITY

In consideration of being a Research Scholar at Gujarat Technological University, and in the interests of the facilitation of research at the University and elsewhere, I, **Sonalben B Prajapati** having Enrollment No. **189999911007** hereby grant a non- exclusive, royalty free and perpetual license to the University on the following terms:

a. The University is permitted to archive, reproduce and distribute my thesis, in whole or in part, and/or my abstract, in whole or in part (referred to collectively as the "Work") anywhere in the world, for non-commercial purposes, in all forms of media;

b. The University is permitted to authorize, sub-lease, sub-contract or procure any of the acts mentioned in paragraph (a);

c. The University is authorized to submit the Work at any National / International Library, under the authority of their "Thesis Non-Exclusive License";

d. The Universal Copyright Notice (©) shall appear on all copies made under the authority of this license;

e. I undertake to submit my thesis, through my University, to any Library and Archives. Any abstract submitted with the thesis will be considered to form part of the thesis.

f. I represent that my thesis is my original work, does not infringe any rights of others, including privacy rights, and that I have the right to make the grant conferred by this non-exclusive license.

g. If third party copyrighted material was included in my thesis for which, under the terms of the Copyright Act, written permission from the copyright owners is required, I have obtained such permission from the copyright owners to do the acts mentioned in paragraph (a) above for the full term of copyright protection.

h. I understand that the responsibility for the matter as mentioned in the paragraph (g) rests with the authors / me solely. In no case shall GTU have any liability for any acts/ omissions / errors / copyright infringement from the publication of the said thesis or otherwise.

i. I retain copyright ownership and moral rights in my thesis, and may deal with the copyright in my thesis, in any way consistent with rights granted by me to my University in this non-exclusive license.

j. GTU logo shall not be used /printed in the book (in any manner whatsoever) being published or any promotional or marketing materials or any such similar documents.

k. The following statement shall be included appropriately and displayed prominently in the book or any material being published anywhere: "The content of the published work is part of the thesis submitted in partial fulfilment for the award of the degree of Ph.D. in **Chemical Engineering** of the Gujarat Technological University".

l. I further promise to inform any person to whom I may hereafter assign or license my copyright in my thesis of the rights granted by me to my University in this nonexclusive license. I shall keep GTU indemnified from any and all claims from the Publisher(s) or any third parties at all times resulting or arising from the publishing or use or intended use of the book / such similar document or its contents.

m. I am aware of and agree to accept the conditions and regulations of Ph.D. including all policy matters related to authorship and plagiarism.

Date: 05/04/2023

Place: Ahmedabad

Signature of the Research Scholar

Recommendation of the Supervisor: Recommended.

Signature of Supervisor

Thesis Approval Form

The viva-voce of the PhD Thesis submitted by Sonalben B Prajapati, Enrolment No. **189999911007** entitled **"Co-pyrolysis of E-waste and Biomass for Fuel Oil Production"** was conducted on 5/4/23 at Gujarat Technological University.

(Please tick the relevant option(s))

☑ The performance of the candidate was satisfactory. We recommend that he/she be awarded the PhD degree.

☐ Any further modifications in research work recommended by the panel after 3 months from the date of first viva-voce upon request of the Supervisor or request of Independent Research Scholar after which viva-voce can be re-conducted by the same panel again.

☐ The performance of the candidate was unsatisfactory. We recommend that he/she should not be awarded the PhD degree.

Name and Signature of Supervisor with Seal

1) (External Examiner 1) Name and Signature

5/4/23 (Dr. Vimal Gandhi)

2) (External Examiner 2) Name and Signature

ABSTRACT

Printed Circuit Boards (PCB), one of the main fractions of E-waste, is now becoming a source of pollution due to the presence of brominated flame retardants, which unleash highly toxic materials when burnt in presence of oxygen. Co-pyrolysis, which employs two or more feedstock together to transform solid waste into valuable solid, gas, and liquid while minimizing toxins, is one of the greatest solutions for reducing this waste. In the present research, biomass as Cotton Stalk (CS) was used in different composition with PCB, and its effects on chemical and physical characteristics of pyrolysis oils and char were evaluated, as well as possible reaction pathway of brominated epoxy resin of PCB and reduced toxicity in co-pyrolyzed products were derived. The slow pyrolysis of PCB, CS and co-pyrolysis with different compositions have been carried out in a fixed bed reactor, for temperature up to 500 ℃, and heating rate 10 $℃/min$. The Produced oil had been analysed in GC-MS and fuel properties of the oil measured as per FAME and compared. The generated gas was also analysed in GC. Moreover, the raw sample and char degradation behaviour was evaluated using Thermo-Gravimetric Analysis and Derivative Thermogravimetric Analysis (TGA/DTG) and the influence of co-pyrolysis process on chemical composition and physical attributes of the produced char as well as the advantages and effects of different CS ratio on product yield was determined. The physicochemical properties and morphological aspects of char were determined using a variety of analytical techniques. As CS was raised, there was a noticeable rise in the quantity of oil produced as well as the presence of total phenol and phenolic compounds. The most essential aspect of char analysis was bromine content, which was found to be increased with co-pyrolysis, showing that the co-pyrolysis process assisted in reducing bromine content in oil and fixing it in char. Additionally, the CS:PCB 50:50 composition satisfies all requirements for an automotive fuel with the exception of the phosphorous content (10 mg/kg) and calorific value (28.41 MJ/Kg).

Keywords: Co-Pyrolysis, TGA, PCB, Biomass, GC/MS, Fuel Properties

ACKNOWLEDGEMENT

"In a family, every need is satisfied"

गुरुर्ब्रह्मा गुरुर्विष्णुः गुरुर्देवो महेश्वरः । गुरुः साक्षात् परब्रह्म तस्मै श्री गुरवे नमः ॥

"Dedicated to Dr. Shina Gautam (Guide)"

"Feeling Blessed…..Thank you Divinity"

The aforementioned sentences adequately convey my respect and acknowledgement to the one who truly involved in the accomplishment of this work.

I would like to express my deep and sincere appreciation to Dr. N. V. Bhate, an associate professor at MS University, Baroda, and Dr. Latesh Chaudhary, Principal of the R. N. G. Patel Institute of Technology, Bardoli, both of whom are members of the PhD progress committee. They provided essential advice and direction that made this research work possible. I owe a profound debt of gratitude to Dr. Alok Gautam, Dr. Paresh Rana, Dr. Imran Khan and Dr. Lakhan Chopda, who were always being supportive and encouraging.

I wish to express my sincere appreciation to Mr. Vaibhav Pandere for experimental setup related work and to Dr. Williams Koshy, Ms. Rekha Kanzariya and Ms. Dhrupa Patel, who was not only a close friend but also a steadfast supporter and a never-ending source of inspiration. The former principal of GEC, Bhuj, Dr. P.P. Rathod, deserves my heartfelt thanks. He permitted me to enrol in this PhD programme at Gujarat Technological University, Ahmedabad. I also want to respectfully thank everyone who has ever assisted, directly or indirectly.

S B Prajapati

Place: Ahmedabad

TABLE OF CONTENT

List of Abbreviations

Abbreviation	Meaning
ABS	Acrylonitrile-butadiene-styrene
ABS	Algal biomass
AAS	Atomic absorption spectroscopy
BJH	Barrett-Joyner-Halenda
BDE	Bond dissociation energy
BERs	Brominated epoxy resins
BET	Brunauer-Emmet- Teller
CCR	Conradson Carbon Residue
CFPP	Cold Filter Plugging Point
CNTs	Carbon Nano Tubes
CS	Cotton Stalks
CS30	CS:PCB mixture with 30 % CS
CS40	CS:PCB mixture with 40 % CS
CS50	CS:PCB mixture with 50 % CS
CS60	CS:PCB mixture with 60 % CS
CS70	CS:PCB mixture with 70 % CS
DTG	Differential Thermogravimetric Analysis
DS	Digested sludge
EEE	Electrical and Electronic Equipment
EI	Electron Ionization
eV	Electron volt
EFB	Empty fruit bunch
EG	Ethelene Glycol
EPDM	Ethylene-propylene-diene monomer
FAME	Fatty acid methyl esters
FE-SEM	Field Emission Scanning Electron Microscope
FCC	Fluid catalytic cracking
FWO	Flynn-Wall- Ozawa
FTIR	Fourier transform infrared spectroscopy
GC/MS	Gas chromatography–Mass spectrometry
GHS	Globally Harmonized System

HDPE	High density polyethylene
HDO	Hydrodeoxygenation
IUPAC	International Union of Pure and Applied Chemistry
JF	Joliflora
KAS	Kissinger-Akahira-Sunose
LOD	Loss on Drying
LDPE	Low density polyethylene
MF	Metallic fraction
NIST	National Institute of Standards and Technology
NCAA	Near-critical aqueous ammonia
NM-PCB	Non-metallic fraction of PCB
NBERs	Non-brominated epoxy resins
NMF	Non-metallic fraction
PPM	Parts per Million
PMC	Phosphoric moulding composites
PBB	Polybrominated biphenyls
PBDE	Polybrominated diphenyl ethers
PBDD/F	Poly-bromo dibenzodioxines/furans
PC	Polycarbonate
PCABS	Polycarbonate (PC) and acrylonitrile butadiene styrene
PCDD/F	Poly-chlorodibenzodioxines/furans
PHA	Polycyclic aromatic hydrocarbons
PE	Polyethelene
PET	Polyethylene-terephthalate
PHAH	Polyhalogenated aromatic hydrocarbons
PP	Polypropelene
PS	Polystyrene
PTFE	Polytetrafluoroethylene
PVC	Polyvinylchloride
PCB	Printed Circuit Boards
HZSM-5	Protonic type zeolite socony mobil-5
Py-GC/MS	Pyrolysis–gas chromatography–mass spectrometry
RH	Rice Husk
SAN	Styrene acrylonitrile
TCB	Tandem catalytic bed

TBBA	Tetra-bromo-bisphenol-A
TGA	Thermogravimetric Analysis
UPE	Unsaturated polyester
WEEE	Waste Electrical and Electronic Equipment
WPCB	Waste printed circuit boards
WT	Waste Tyre
XRD	X-ray diffraction
EDS	X-ray energy dispersive system spectroscopy
XRF	X-ray fluorescence spectroscopy
ZSM-5	Zeolite Socony Mobil-5
XRF	X-ray fluorescence spectroscopy

List of Symbols

Symbol	Meaning
E	Activation energy, (kJ/mol)
E_α	Apparent activation energy, (kJ/mol)
A_c	Area exposed by the pore where the physically adsorbed gas is desorbed
M_a	Average molecular weight of the pyrolysis gas
Q_v	Calorific value of mixed gas, $Kcal/m^3$
r_k	Capillary radius
a, b	Compensation Coefficients
α	Conversion degree
P/P_0	Equilibrium pressure over the saturated vapor pressure of the adsorbed gas
m_f	Final mass of the sample, (mg)
T_f	Final temperature of mass loss, (℃)
β	Heating rate, (℃/min)
HHV	Higher heating value, (MJ/kg)
m_0	Initial mass of the sample, (mg)
T_i	Initial temperature of mass loss, (℃)
g(α)	Integrated form of the reaction model
p(*x*)	Integrated form of the temperature
γ	Interfacial tension of the liquid nitrogen at its boiling point
m_t	Mass of the sample at a given time t, (mg)
T_m	Maximum temperature of mass loss, (℃)
$\tilde{v}$	Mole volume of the liquid nitrogen
M_i	Molecular weight of the i^{th} component gas
r_p	Pore radius
V_p	Pore volume
A	Pre-exponential factor of the Arrhenius equation, (min^{-1})
k(T)	Rate constant of the Arrhenius equation
f(α)	Reaction model
t	Statistical film thickness
T	Temperature, (℃)

Δt	Thickness of adsorbed layer of N_2
R	Universal gas constant, (kJ/mol K)
V_3	volume % of CH_4
V_4	volume % of C_nH_m
V_1	volume % of CO
V_2	volume % of H_2
V_i	Volume % of the i^{th} component gas

List of Figures

List of Tables

List of Appendices

CHAPTER 1

Introduction

1.1 Background:

The world is currently dealing with a number of environmental issues as a result of rapid growth in manufacturing activities, inappropriate management strategies, and existing waste management laws and regulations; more recently, e-waste has emerged as an emerging environmental issue as a result of short product life cycles and rapidly advancing technology in the province of EEE's (Electrical and Electronic Equipment), which has resulted in vast quantities of comparatively new electronics products being discarded, as a result, E-waste builds up three times quicker than other waste [1]. According to Z wang et al. [2], 20 to 50 million tonnes of e-waste are produced globally each year [3], with India ranking first among the top five e-waste producers with an estimated yearly production of 2 million tonnes [4]. As per A saha et al. [5] in his recent research, globally, 53.6 Mt of e-waste were created in 2019 and it is anticipated to hit 74.7 Mt by 2030. This is the most serious matter for developing countries, which serve as a collection point for dumped material from developed countries and escalate the problem due to a lack of recycling infrastructure. As a necessity, developing countries such as Asian and African, e.g., India, Pakistan, China, Nepal, Bangladesh, Bhutan, Ghana and Nigeria must find environmentally acceptable ways to dispose of or recycle E-waste.

Printed circuit boards (PCBs) which are a heterogeneous mixture of organic materials, glass fibres, and metals, make up around 3-6% of all electrical and electronic equipment, complicating the recycling process [6]. After mechanical separation of plastics and metals what remains behind is epoxy resin and this waste is just landfilled or incinerated causing release of toxic metals like Pb, Sn, Ca, Cu, Hg [7]. As per C Rosenberg et al. [8] PCBs are one of the major challenges in most electronic fractions, which are manufactured mainly

with epoxy or phenol resin containing a fire retardant, such as tetra-bromo-bisphenol-A (TBBA).

A Sepulveda et al. [9] described a number of PCBs treatment techniques and processes in China and India. Some of the processes employed include mechanical dismantling to separate plastics and metals, as well as thermal recycling, hydrometallurgical and pyrometallurgical facilities, leaching, and amalgamation to recover valuable metals [10]. However, there was no separation of plastics with brominated flame retardants and the leftover PCBs are just landfilled or incinerated. Landfilling of the brominated chemicals, like their chlorinated congeners, may seriously pollute the plant, soil, water and microbial species found in the nearby area; Whereas, incineration produces a high quantity of toxic polycyclic aromatic hydrocarbons (PAH), polyhalogenated aromatic hydrocarbons (PHAH) as well as PBDD/F (Poly-bromo dibenzodioxines/furans), PCDD/F (Poly-chlorodibenzodioxines/furans), and HBr with brominated phenols as by-products [11][12][13] which is catalytically amplified by the presence of heavy metals, especially copper and its oxides [14]; which pollutes air, ultimately contaminate our food chain and adversely affect to humans' skin, liver, and digestive tract. A number of studies have been carried out about the toxicity and the health risks concerning the human exposure in TBBA (tetrabromobisphenol-A) on recycling sites [9][5][15]. Therefore, environmentally acceptable disposal or recycling of waste PCB which can replace conventional traditional procedures with futuristic state of the art eco-friendly approaches is a big challenge [11][16][17]. By adopting more appropriate processing conditions during recycling, it is feasible to minimise the amount to which they are generated. Furthermore, it is need of the environment to find a simple, effective, and optional solution to increase the energy security of a nation, achieve effective waste management, and reduce dependency on fossil fuels [18].

1.2 Motivation and Definition of the Problem:

Pyrolysis of PCB has been demonstrated in several studies to be an effective waste valorisation approach to address the issues stated above [12][19]. It allows large polymer chains of PCBs to be broken up into lighter polymer compounds with smaller molecular weight. Slow pyrolysis (Temperature ~ 500 ℃ , hot vapor residence time ~ 2 sec, and very fast condensation to prevent the scope of secondary reactions) on the other hand, produces the maximum amount of oil while also producing solid char and gases [20][21]. The amount

of oil, solid char, and gas produced are mainly influenced by the temperature, raw material and hot vapour residence time with many other factors like additives, catalysts and technology [21][22].

The produced liquid oil can be hydro deoxygenated into fuels for automobile engines, fed into boilers alone or in combination with fossil fuels, or even employed as a more suitable resource of H_2 than biomass [14][23]. Conversely, this is only appropriate if the pyrolysis products have low halogen yields [24]. In fact, dehalogenation of oil products is one of the most important aspects of pyrolysis treatment. In this context, co-pyrolysis (a process which involves two or more different materials as feedstock) could be an alternative technology that improves these two criteria [25][26]. Co-pyrolysis of biomass has been shown in several studies to boost oil yield and quality while maintaining the overall process. Furthermore, biomass is renewable and underutilised in energy conversion technologies, and has been identified as a possible energy source owing to its low sulphur and nitrogen content [22]. A high amount of hydrogen present in biomass may lead to dehalogenation and prevention of PBDD/F which promotes HBr / HCl fixation in char [25][26]. Furthermore, the biomass has a higher H/C molar ratio than PCBs which can act as a hydrogen donor to PCBs during co-pyrolysis [26]. Water, one of the most abundant components in biomass, is expected to act as a reactive agent, promoting further cracking of the PCBs tar and the production of more volatile chemicals, hence improving pyrolysis oil yields; However, the product yields and characteristics are influenced by the temperature, residence time and blend ratio of the two feedstocks [27]. Moreover, because of the various reactivities of biomass and PCBs, this process is relatively complex.

In this work, Cotton Stalk (CS) as biomass was used because of its many benefits; Cotton is one of the most widely cultivated crops in Gujarat, India. Following cotton removal, the remaining cotton stalks are considered as waste and are simply burned to dispose of them, harming the environment. While characterization studies of cotton stalks suggest that it contains a high amount of volatile matter and a low O/C ratio [28][29] which can aid in improving the quality and quantity of bio-oil.

1.3 Scope of the research:

Based on the background information previously covered, the current study sheds light on the slow pyrolysis of PCB and CS and compares it with the co-pyrolysis of different CS and PCB compositions on a lab scale fixed bed equipment, and the synergistic effect is assessed. This research examines the impact of different CS compositions on co-pyrolysis products in order to obtain lower halogen yields and limiting toxic emissions while achieving increasing oil yield. Moreover, potential applications for pyrolysis oil, gas and char are explored. The present investigation also includes the comparison for morphological and physical attributes of co-pyrolyzed char with PCB, and CS char, including pore size distribution, surface area, porosity, structural properties, and elemental analysis. Most importantly, bromine content in char with respect to increased CS composition is evaluated.

As per the authors best knowledge, there was no single literature that focused on the thermal decomposition and co-pyrolysis of these residues. Its compositions might be the first expanding research effort to understand the synergistic behaviour of the mixture. Additionally, there are various studies available in literature on individual behaviour of PCB and Cotton Stalk pyrolysis, however, co-pyrolysis of the both and its product characterization has been evaluated first time from author best knowledge.

1.4 Objectives:

This research examines the impact of different CS:PCB compositions (like, CS30:PCB70, CS40:PCB60, CS50:PCB50, CS60:PCB40 and CS70:PCB30, named as CS30, CS40, CS50, CS60 and CS70, respectively) on the co-pyrolysis product in order to obtain lower halogen yields and reduced toxic emissions while achieving increasing oil yield. The principal objectives are listed below.

- To understand pyrolysis behaviour (such as initial degradation temperatures, thermal degradation rates, and residual weight) of PCB, CS and its mixture at different CS:PCB compositions by TGA/DTG analysis.
- To find pyrolysis kinetics of the main thermal decomposition processes and identify possible reaction mechanisms.
- To study oil characterization using GC/MS and find possible reaction pathways.
- To find the fuel characteristics of generated oil using FAME standards, and its potential applications. Moreover, application of generated gas is also explored.

- To compare the morphological and physical characteristics of the co-pyrolyzed CS:PCB char, as well as its potential applications.

1.5 Thesis structure:

The thesis structure contains seven chapters with appropriate sections, subsections, references, appendices, and the list of research publications.

1. **Introduction:** The chapter involves background for the research topic, problem statement and objectives with scope of the current research.

2. **Literature review:** This chapter explains the significance of PCB recycling, pyrolysis as a thermal degradation process, and the basic idea and mechanism of co-pyrolysis. More than 200 potential literature reviews are provided.

3. **Materials and methods:** This chapter includes detailed information on material preparation, lab scale experimental set-up and procedure, followed with detailed information on different equipment's and procedures used for oil, gas and char characterization including, TGA/DTG, GC/MS, FTIR, BET, FE-SEM, EDS, XRD, and XRF.

4. **Kinetic analysis:** This chapter covers a comparison of the thermal degradation behaviour of all above mentioned samples by TGA analysis at three distinct linear heating rates (5, 10, 15 ℃/min) in a nitrogen atmosphere. Three model-free non-isothermal methods such as Kissinger-Akahira-Sunose (KAS), Flynn-Wall-Ozawa (FWO), and Starink were used to calculate apparent activation energy (E_α) and pre-exponential factor (A). Furthermore, with calculated E_α values, the possible decomposition mechanism of all the samples was probed using the Criado differential-integral master plot.

5. **Oil and gas analysis:** The findings of the pyrolysis and co-pyrolysis processes on a lab-scale fixed bed pyrolizer are the basis for this chapter. Following oil characterization by GC/MS and possible reaction pathways identified for CS, PCB

and the mixtures, which gave an insight of the mechanism of different reactions taking place. Further, the fuel characteristics of the generated oil were also discovered using FAME standards, and its potential applications were discussed. The application of the generated gas, as well as the bromine content of the char, have both been assessed.

6. **Char Characterization:** The morphological and physical characteristics of co-pyrolyzed PCB and CS char, including their surface area, porosity, structural characteristics, and elemental analyses, are compared in this chapter.

7. **Conclusion:** The main conclusions from the current research are outlined in this chapter, followed by future scope.

CHAPTER 2

Literature Survey

2.1 What is PCB?

Printed circuit boards (PCBs) are common components in most electric and electronic equipment and can be considered the brain of the electronic equipment [30]. The manufacturing process and the raw materials used for PCB production depends on their applications. The mechanical support of a PCB is an insulating board, often made of epoxy resin and glass fiber (made from SiO_2, CaO, and Al_2O_3) [6]. PCBs can be single sided, double sided or multilayer types and can also be flexible, rigid or a combination of both. In order to produce all these different structures, it requires different layers of materials. The conductive pathways of circuits are made of copper, in order to connect, the electronic components soldered on the PCB [31].

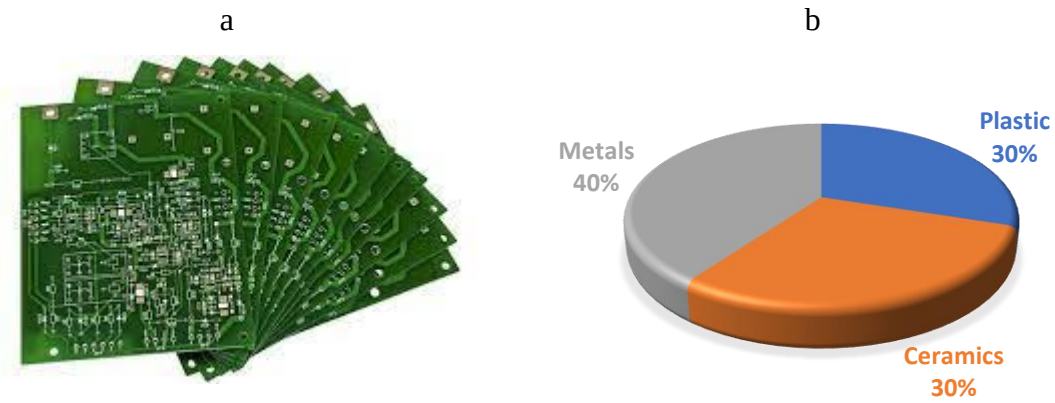

FIGURE 2.1: (a) Printed circuit Boards, (2) Composition of typical printed circuit boards.

Generally, the components of WPCB can be divided into metallic fraction (MF) and non-metallic fraction (NMF). Non-metallic fraction normally features 30 % plastics, which includes polyethylene, polypropylene, polyesters, PVC, epoxy resins, PTFE, acrylonitrile-

butadiene-styrene (ABS), styrene acrylonitrile (SAN) or ethylene-propylene-diene monomer (EPDM) and nylon. All of them also requires a hardener in order to form the cross linking of the resin which attach all their properties and creates a thermoset plastic. The most frequently used is the dicyanodiamide, sometimes diaminodiphenyl sulfone and diaminodiphenyl methane are also used [32]. Epoxy resins based on bisphenol A and its diglycidyl ether are high-quality materials that are effective insulators against harsh environments and contribute to the mechanical strength of the PCBs. The chemical structure of epoxy resin is shown in Fig. 2.2. The elemental analysis of a typical e waste is shown in Table 2.1.

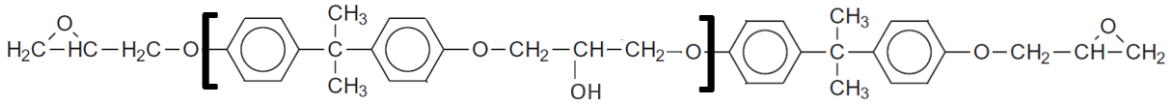

FIGURE 2.2: Chemical Structure of Epoxy Resin [11]

TABLE 2.1: Proximate, ultimate analysis of waste printed circuit boards.

Elemental Analysis					Proximate Analysis				HHV	Reference
C	**H**	**O**	**N**	**S**	**Moisture**	**Ash**	**Volatiles**	**Fixed Carbon**	**(MJ/kg)**	
28.2	2.40	7.36	0.83	0.04	0.69	43.2	51.8	4.35	-	[33]
16.04	1.46	3.15	0.20	0.14	0.48	73.73	20.69	5.58	11.26	[34]
24.51	2.55	6.84	0.39	0.55	0.75	64.91	23.26	11.08	10.59	[35]

The PCB contains 30% ceramic reinforced plastics [36], primarily silica or alumina with some amount of mica, alkaline earth oxides, and barium titanate [32]. Furthermore, it typically contains 40% metallic fraction, with copper (Cu) accounting for around 10% to 27% of the total weight of PCBs. Other precious metals found in it are platinum, palladium, silver and gold, makes it worth recycled. However, the amount present are in ppm level, see Table 2.2. Some, toxic and critical metals such as antimony, cadmium, lead, nickel, arsenic, mercury, and chromium, if not recycled carefully, can have major environmental consequences [36].

Moreover, the PCBs contain brominated and chlorinated organic compounds, which are flame retardants in order to prevent fire damage [32]. As per, Hall and Williams [37] the amount of halogens in plastic fractions only could reach up to 10.9 wt.% Br and 57.8 wt.% Cl [38]. Since the use of hazardous flame retardants, namely polybrominated biphenyls

(PBB) and polybrominated diphenyl ethers (PBDE), is limited in EU countries due to restriction by Directive 2011/65/EU in electrical and electronic equipment. As a result, the usage of the alternative materials, mainly phosphorous- or nitrogen-based has been increased [39]. However, halogenated flame-retardant use is steadily rising. Most are combined with inorganic compounds like aluminum or magnesium hydroxide ($Al(OH)_3$, $Mg(OH)_2$) and antimony trioxide (Sb_2O_3).

TABLE 2.2: Average composition of Plastics, ceramics and metals in waste PCBs.

Plastics (wt.%)		**Ceramics (wt.%)**		**Metals (wt.%)**	
PE	1.7	SiO_2	15-41.86	Cu	10-26.8
PP	0.9	Al_2O_3	6-6.97	Al	1.33-4.78
PS	3.6	CaO	6-9.95	Pb	0.99-4.19
PVC	1.1	Titanates, Mica	3	Zn	0.16-2.17
Epoxy resins	4.8			Ni	0.28-2.35
PTFE	2.4			Fe	1.22-8.0
ABS	8.9			Sn	1.0-5.28
SAN	0.6			Sb	0.06-0.4
EPDM	0.3			Au	80-1000 (ppm)
Nylon	0.9			Pt	4.6-30 (ppm)
PCABS	3.1			Ag	110-3301 (ppm)
Others	1.7			Pd	10-294 (ppm)

Reference from [24][32]

2.2 Recycling Methods and their Risks:

Before the recycling of the PCBs, a pretreatment stage is essential in order to remove the larger components for reuse, which covers manual dismantling, crushing and separation. Manual dismantling has always been the most popular technique throughout the previous few decades. After manual disassembly or by using high heat for de-solder using coal heated plate, capacitors, resistors, integrated circuit chips, thermistors and others are being removed and the leftover WPCBs are mainly composed of thermoset polymers and the attached solder, copper foil, and others, with high hardness and toughness. This process has drawbacks of low efficiency and environmental pollution. The emission of toxic gas during the de-soldering process, such as hexabromocyclododecane, polybrominated diphenyl ethers, polychlorinated biphenyls, and tetrabromobisphenol A, will be a threat to the worker's health [6]. In order to facilitate the subsequent recovery of both metal and energy after dismantling, crushing is used for the liberation of different fractions which determines the recovery rate and purity of materials.

After crushing, mechanical separation is the essential process of the mechanical−physical recycling process, technically, it could sort out the metallic materials from the non-metallic materials based on the difference of the physical properties of various particles (e.g., density, particle size, electrical conductivity, magnetic permeability), mainly involving density and magnetoelectric separation. Gravity separation (density separation) is according to the distinction in density and particle size among different materials. Miscellaneous particles are then layered by the fluid dynamics and mechanical forces. A metal and non-metallic mixture can be separated via magnetoelectric separation based on variations in electricity or magnetism. As the result of separation, copper is found be the most concentrated metal, and Ag, Au, and Cu occupy the highly valued metals [6]. However, the combination of manual dismantling, crushing, grinding and separation methods produce much dust and harmful particulate matters. Moreover, the precious metals may be lost during crushing and grinding as they usually adhere to the non-metallic powder. Also, this non-metallic powder can only be used as low-value products, viz. paint, paving material, plastic filling material etc. [17].

Other recycling methods include thermal and hydrometallurgy treatment. The thermal recycling includes the pulverizing of the PCB to fine particles' size and then the combustion of the polymeric components at high temperatures (1200 ℃). The polymeric compounds are evaporated and the residual is a black metal with high concentration of copper. The more precious metals are being separated by electro fining and they are being recovered afterwards by leaching, melting and precipitation routes from the anodic sludge [40]. In hydrometallurgy method, the metals are dissolved by concentrated nitric acid or hydrochloric acid or cyanide solution and the metal recovered from solution by electro-refining. The method is used mostly for gold recovery [41]. It is a low-cost treatment; however, it is time-consuming or is only moderately effective, also consumes large amounts of chemicals and generates a huge amount of wastewater [6][42]. Additionally, the procedure entails an exposure risk to acid vapours, acid in its liquid form, and of course, the exposure on cleaning solvents employed in the preparation of shreds [41].

Processes used in pyrometallurgy include combustion and melting in a molten bath. In this method, crushed scrap is charged into a molten bath to dissolve refractory oxides and polymers, forming a slag that contains valuable metals. However, only a limited recovery of metals could be achieved, and it produces dangerous byproduct gases. While, hydrometallurgical procedures are more precise, highly predictable, and controllable than

pyrometallurgy, many of the solvents employed, such as cyanides and chlorides, are extremely dangerous. The process also produces waste solutions and sludge that pollute the environment, involves multiple processes and has a high cost of recovery [17]. Other WPCB treatments include bioleaching and supercritical fluid, which offer large volume reduction and significant energy recovery but suffer from complicated methodologieswhich are less effective, demand a lot of energy, and are prone to secondary contamination [6].

The aforementioned PCB recycling techniques include recovering metallic fractions and come with significant risks and hazards. Furthermore, incorrectly discarding or disposing of non-metallic materials, which are composed of 60% inorganic and 40% organic elements, would result in a massive waste of resources and constitute a substantial risk to the environment. The dust of plastics, ceramics, metals, and silica produced by shredders and grinding during the size reduction process can be inhaled and applied topically by workers, posing a danger of contaminating the environment [42]. Excessive levels of cadmium and lead in the working environment in PCB recycling facilities can cause flu-like symptoms (chills, fever, and muscle discomfort), as well as harm to the brain and lungs. Disease of the kidneys, intestines, bones, and lungs can arise from chronic exposure. Lead exposure can have deleterious effects on the CNS, vitamin D, and blood pressure [43]. Other than those already mentioned, there are still some drawbacks associated with using physical recycling techniques for non-metallic fractions. These drawbacks include the challenges associated with separating efficiently metallic fractions from non-metallic fractions in PCB waste, determining how to improve the compatibility of non-metallic fractions with matrix materials, and deciding on a good way to stop hazardous substances from leaching out of the matrix materials.

Historically, landfills or incinerators were used to dispose of WPCBs. when burnt in presence of oxygen highly toxic polycyclic aromatic hydrocarbons (PAH), polyhalogenated aromatic hydrocarbons (PHAH) are produced. Importantly, PCB contains TBBA (Tetrabromobisphenol-A) as a fire retardant, which, produces PBDD/Fs (Polybromodibenzodioxins/furans) and PCDD/Fs, which is catalytically amplified by the heavy metals, especially copper and its oxides (Polychlorodibenzodioxins/furans), as well as high amounts of particulate matters, carbon oxides, and HBr are also produced, which can have negative impact on human health, while the landfill leads to the pollution of groundwater due to BFRs and heavy metals [14]. In order to lessen pollution, heavy metals

and BFRs must be removed or treated. While NMF-WPCBs with lesser economic efficiency must also be handled with care to protect the environment. In this regard, both non-metallic PP and PVC-based composite materials as well as phosphoric moulding composites (PMC), which are utilised in a range of fillers and binding agents, have been recovered from PCBs in a number of previous applications [44][45]. Non-metallic fraction of WPCBs were recycled by Hu et al. [46], as reinforcing filler in a kind of novel room temperature cured Unsaturated Polyester (UPE) composites. The results showed that UPE composites with WPCB nonmetals at the right content outperformed UPE matrix in terms of flexural strength, tensile strength and heat deflection temperature. Additionally, based on an investigation of the kinetics of thermal deterioration, Sohaili et al. [47] found that the addition of WPCB nonmetals increased the thermal stability of UPE matrix. In a study on the viability of employing nonmetals again as reinforcing fillers in polypropylene matrix, Zheng et al. [48] found that the mechanical and heat resistance of the nonmetals-filled PP were superior to those of the pure PP. In the following year of his research [49], he used a fluidized bed reactor and a low temperature combustion technique (400–600 ℃) to recover glass fibres from printed circuit boards with a 95 wt% recovery rate.

The glass fibres retaining their properties suitable for re-use. A wide range of glass fibre reinforced plastics have been investigated for their potential for the recovery of the glass fibre, including, polyester, epoxy, polypropylene, phenolic and polyethylene terephthalate resins [50][51].

In addition to the methods mentioned above, pyrolysis is another approach that may be employed for efficient processing because it can lessen the secondary environmental damage brought on by the combustion process [52]. It is one of the most reliable and promising developing technologies for the production of fuel from solid waste [53].

2.3 Pyrolysis:

Pyrolysis is the term for the thermal degradation of solid wastes without the presence of oxygen at a moderate to high temperature [29]. The word is a combination of two Greek words,: "lysis," which denotes breakdown into constituent elements, and "pyro," which means fire [54]. The three main products of pyrolysis are the char-like solid residue, condensable liquids including aromatics, water, products with low levels of polymerization,

tars, etc., and the non-condensable gases, primarily CO_2, CO, CH_4, H_2, and other light hydrocarbons [55]. In reality, phase transition events, heat and mass transport mechanisms, and chemical reaction kinetics all play significant roles in product distributions [56]. Pyrolysis technology was utilised for the manufacturing of charcoal and chemicals more than 5500 years ago in Southern Europe and the Middle East. As a result, the older literature typically compares pyrolysis to carbonization, in which a solid char is the main by-product [53]. Also, the oil obtained from the pyrolysis of different feedstock can exhibit the properties of fossil fuels such as higher heating value, low viscosity and volatility. The gas can be used as a source of energy [58]. Bio-char also has a wide range of intriguing prospective applications. For instance, because of its great capacity to be used as sorbent for the purification of compounds, water and nutrients [59], it can be employed as a soil conditioner to improve soil fertility, and activated carbon for the treatment of effluents [60]. As waste management and minimization are performed simultaneously with material and energy recovery, it is seen as a viable strategy for treating waste.

All the steps simply categorise as feed stock preparation, Feed stock drying, thermo-chemical conversion in the reactor, ash separation and liquid collection. Different reactor needs different sizes particle, that is why cutting and grinding is needed. Drying is essential to avoid adverse effects of water on stability, viscosity, corrosiveness and other liquid properties in the pyrolysis product. The sample is introduced into the reactor after being dried and ground, and the pyrolysis process occurs there at a certain heating rate and with a fixed flow rate of inert gas (N_2/Ar). Pyrolysis liquid is collected after quenching the volatile material by the vapours liquid condensers. This is the most important step of the whole process, without this only the char and gas would be generated. Therefore, rapid cooling of the pyrolysis vapours is required to produce a high liquid yield. Finally, solid residue and gas are collected separately.

2.3.1 Pyrolysis Classification

According to the operating conditions such as temperature, heating rates, solid residence time and raw material particle size, pyrolysis can be classified as conventional or slow (<400 ^{0}C), fast (400-600 ^{0}C) or high (flash), as shown in Table 2.3. There are specific applications and end products for each pyrolysis technique. As a result, it is feasible to create important

pyrolysis products (bio-oils, gas, or bio-char) in large quantities and of high quality by modifying the operational parameters.

TABLE 2.3: Classification of pyrolysis process based on operating parameters.

Pyrolysis Process	Temperature (℃)	Heating rate (℃/sec)	Particle size (mm)	Solid Residence Time (sec)	Product yield (%)		
					Oil	Gas	Char
Slow	300-500	0.1-1	5-50	300-550	30	35	35
Fast	600-1000	10-200	<1	0.5-10	50	20	30
Flash	800-1000	> 1000	<0.2	<0.5	75	12	13

Reference from [53][56].

2.3.1.1 Slow Pyrolysis

Since ancient times, slow pyrolysis has been employed to increase the production of char at lower temperatures and slow heating rates. It is a traditional pyrolysis process. The manufacturing of charcoal benefits from lower operational temperatures and higher vapour residence time, which causes the primary products to rupture. Additionally, the elements in the vapour phase keep reacting with one another, which increases the yield of solid char while negatively affecting the output of gaseous and liquid yield [61]. Additionally, extra energy input is required due to long residence times and poor heat transport [62][53].

2.3.1.2 Fast Pyrolysis

The fast pyrolysis process, employs high heat transfer by rapid heating, very short vapour residence time and a moderate temperature in the absence of oxygen, see Table 2.3. According to Ali et al. [29], depending on the feedstock utilised, fast pyrolysis typically yields 50%–75% of liquid oil, 15%–25% of solids, and 10%–20% of gaseous products. High heating rates, reaction temperatures nearby 500 ℃, and short vapour residence times (< 2 seconds) to reduce secondary reactions have all been demonstrated to produce the highest liquid yields [63]. Fast-pyrolysis technology is receiving incredible popularity in producing liquid fuels from different solid wastes. It also has potential to supply a number of valuable chemicals that offer the attraction of much higher added value than fuels. When compared to other processes, fast pyrolysis technology can have relatively low investment costs and great energy efficiency, especially on a small scale [53].

2.3.1.3 Flash Pyrolysis

Main parameter of flash pyrolysis includes reaction durations of a very few seconds and very high heating rates (>1000 ℃/min). It is a technology that shows promise for producing large amounts of liquid fuel (up to 75%) with a very little gaseous and solid yield. Under these operating conditions, molecular disruption is so severe and the particles are ejected so quickly that there is less time for the subsequent molecular corrections that result in the formation of charcoal. However, there are some technological limitations to this process, such as the produced oil contains solid particles, it is corrosive and has lower thermal stability, gradual increase in viscosity brought on by the catalytic action of the char, the dissolution of concentrated alkali in the char, and the creation of pyrolytic water [64].

The aforementioned classification is based on the conditions under which biomass is converted to bio-oil, char, and gas. Due to its great waste management potential, pyrolysis is currently receiving more attention for other solid wastes such as plastics, tyres, and discarded PCBs.

2.3.2 Important parameters

Numerous factors, such as the type of feedstock, temperature, heating rate, reaction time, and feed particle size, affect the pyrolysis process [26]. The impact of several variables on the optimum oil yield during the pyrolysis of biomass has been thoroughly discussed by Akhtar and Amin [65].

Research has shown that maximum liquid yields are obtained with high heating rates, at reaction temperatures around 500 ℃ and with short vapour residence times to minimise secondary reactions [61]. Since it will directly affect the rate of thermal breakdown, the stability of the input material, and the reaction products, temperature is possibly the most important parameter. It is evident that temperature favoured tar cracking, making it a factor that limits tar output [66]. However, the ideal temperature needed to yield the most oil depends on the properties of the feedstock. The majority of plastics begin to pyrolyze at 300 ℃; however, the presence of additives, flame retardants, stabilisers, etc. in the plastic has a significant impact on this beginning temperature [67]. To have a general idea of the material's thermal behaviour, characterization with relation to thermogravimetric analysis

should be done [68]. The pyrolysis of most polymers starts at approximately 300 ℃; however, this onset temperature is strongly affected by the presence of flame retardants, additives and stabilizers etc. in the plastic [67]. Temperatures above 400 ℃ and increased pressure result in more viscous liquid products, higher rates of pyrolysis, a higher coking tendency, increased amount of secondary products and more dehydrogenation [66][26]. In this regard, Hu et al., [52] pyrolyzed PCBs under argon atmosphere with the flow rate of 0.8 *l*/min and a heating rate of 30 ℃/min. The effect of heating temperature on the yield of solid residue was investigated in the range of 300 to 800 ℃ under the holding time of 60 min. The result showed that the yield of solid residue decreased dramatically from 97.23 to 94.26% when the temperature increased from 300 to 600 ℃. With the successive increase of the temperature to 800 ℃, the changes of the solid residue yields were not obvious, indicating that the organics were almost completely thermally decomposed at 600 ℃. De Marco et al. [69] pyrolyzed WEEE up to 500 ℃, indicating it is the optimum temperature for treating polymeric wastes by pyrolysis, since at lower temperatures complete decomposition of the organic matter is not achieved, and at higher temperatures there is not a significant variation of the amount and characteristics of pyrolysis products, only a slight increase in gas yield to the detriment of liquid yield. H. Chiang et al. [70], who aimed to figure out how particle size and process temperature affected the elemental compositions of PCBs and pyrolytic products also confirmed that temperature had a substantial impact on product yield, with 96 wt.% solid residues at 200 ℃ and 39 wt.% solid residues at 500 ℃.

Moreover, a direct correlation exists between residence time and the reaction temperature. To meet the demand for more thermodynamically stable products, the residence time should be extended [67]. Mankhand et al. [17] evaluated the rate of thermal degradation of PCB particles in the N_2 atmosphere by thermogravimetric examinations at various temperatures, including 300, 400, 500, and 600 ℃, with a constant heating rate of 40 ℃/min. It was shown that the total weight loss of PCB at 600 ℃ for 10, 30, and 50 minutes was substantially the same (25 wt%). However, the maximum weight loss, even after 50 minutes at 300 ℃, was only 16%. The experiment found that a temperature of 500 ℃ and a duration of 50 minutes are adequate for the effective removal of volatiles from PCB. While increase heating rate produce more liquid , Barontini and Cozzani [71] evidenced that in a pyrolytic condition for TBBA and electronic boards, higher heating rates resulted in a decrease of brominated

compounds named, 4-bromophenol, 2,4-dibromophenol and 2,4,6-tribromophenol in condensable, while a simultaneous increase of the HBr in gaseous products was observed.

Additionally, the flow rate of inert gas has a certain effect on the mass loss. To get a maximum oil yield, an optimum vapor residence time in the reactor is required. The other major reason is to minimize secondary reactions (i.e., repolymerization and thermal cracking). A very high vapour residence time at lower inert flow rate could result in high yields of solid char than oil. As well as a very short vapour residence time, higher N_2/Ar flow rate, contribute more yield of non-condensable gases and again decline oil yield. It is also important to maintain the flow rate of nitrogen that prevents the sample from escaping the reaction zone [72]. Generally, nitrogen (N_2) is an inert gas that is commonly used since it is found to be cheap compared to others. However, the use of inert gas is dependent on the type of reactor used. The fluid bed reactor, circulating fluid bed reactor, and entrained flow reactor are the types which need a high flow rate of inert gas [73]. For vacuum and ablative reactors, the use of inert gas is not compulsory [54]. For ablative reactors, according to Bridgwater and Peacocke, nitrogen purging and the use of any inert gases is not required, but is included in the laboratory tests for control purposes, to ensure safety in the feeder and residence time control in the reactor [74]. İilknur and Sevgi [72] has employed fixed bed pyrolysis experiments on a sample of hazelnut bagasse to determine the effects of heating rate, pyrolysis temperature, particle size and inert gas flow rate on the pyrolysis product yields. Under the various pyrolysis conditions viz., temperature range 350–550 ℃, 10 and 50 ℃/min heating rate, 0.224–1.800 mm particle size and 50–200 cm^3/min inert flow rate, the obtained char, liquid, and gas yield ranged between 26- 35, 23-34, and 25-32 in wt.%, respectively. The highest liquid yield of 34.40% was achieved at a final temperature of 500 ℃ with a heating rate of 10 ℃/min, 150 cm^3/min sweep gas flow rate, and a particle size of 0.425-0.600 mm.

Furthermore, the pyrolysis procedure and conditions are fully responsible for determining the type of pyrolysis reactor used in each pyrolysis operation. The rotatory kilns, drum, and screw/auger are among the reactors used most frequently for slow pyrolysis, while fluidized beds, fixed beds, augers, vacuums, entrained flows, rotating cones, ablative reactors, etc. can be used for fast pyrolysis [56][63]. However, due to its high biomass conversion efficiency for fast pyrolysis, fluidized bed is one of the most efficient reactors for producing liquid fuels

[29]. They feature faster devolatilization, ready scale-up, high heating rates, and ease of operation [56].

This thesis aims for the conversion of waste PCB in to valuable fuel oil, solid char and gaseous products. There are abundant literatures are available, which includes pyrolysis experiments of metal free waste PCBs with different operating conditions and with result of different oil, gas and char yield. Although the reaction process is influenced by chemical composition and residence time also, it is critical to develop methods and procedures for obtaining pyrolysis products with low halogen yields and reducing harmful emissions as much as possible. If the pyrolysis products have low yields of halogens, they can be utilized appropriately [36][67]. Furthermore, simplicity and effectiveness are especially important in developing a technique to produce the ideal synthetic liquid fuel. Moreover, PCB includes a relatively high content of ash, so its energy density (e.g., heating value) and thermolysis efficiency are low. It is possible to break down the organic component of WPCBs during pyrolysis in order to produce fuel or useful chemicals, but additional processing of the solid by-product can also make it possible to recover important metals rapidly and efficiently. The pyrolysis of discarded PCBs inhibits the formation of dioxins since it is performed in the absence of oxygen. Although there have been several studies on the pyrolysis of PCBs, the most of it has been done in nitrogen settings using analytical pyrolysis methods or laboratory size reactors with kinetics measurement and product characterization.

Some of the authors including, Hall and Williams [75], Chiang et al.[70] and Scharnhorst et al.[76], in their research were aimed to the process of separating the organic, metallic, and glass fibre fractions of PCBs much easier. When PCBs were heated to 800 ℃, in an inert environment, the organic resin decomposed to form volatile oils and gases leaving behind the metal and glass fibre fraction of the boards. The numerous fractions including metal parts, copper power boards and glass fibre were incredibly friable, making separation simple. With a focus on recovering and recycling rare and precious metals, the recovered metals could then be recycled using conventional methods. In a fixed bed reactor, Hall and Williams [75] pyrolyzed discarded printed circuit boards from computers, televisions, and mobile phones up to 800 ℃ at a heating rate of 10 ℃/min and maintained the temperature there for 135 min. They reported that copper was the largest concentration of metal in the residue after separation of the char, filler, and any reinforcement with concentrations of up to 33 wt% in the residue. In addition, high concentrations of calcium, iron, nickel, zinc, aluminium, lead,

and silver was also found with a small amount of gold from the PCB of waste computer and mobile phone ash. Some toxic metals like mercury and cadmium were very low in concentration. Most important metal he found was gallium arsenide, which is required in the semiconductor sector. Pyrolysis of waste PCB therefore a valuable resource for gallium, due to the difficulty of producing gallium arsenide and the fact that bauxite, the sole industrial supply of gallium, only contains 0.01% gallium. Chiang et al. [70] found that the smaller particle sizes of PCB feedstock resulted in higher copper concentrations. In the solid residue, there were substantial amounts of barium, manganese, antimony, nickel, lead and zinc. He also mentioned silicon, which comes from the reinforcing of glass fibre. Scharnhorst et al. [76] investigated the volatilisation of metals from printed circuit boards under oxidising and reducing conditions at 550 and at 880 ℃. They found that volatile metals, particularly antimony, arsenic and gallium, were volatilised during the thermal processing of the printed circuit boards and the atmosphere and temperature influenced the amount of volatilisation of the metals. The results imply that, if electronic scrap is thermally processed, attention has to be paid in particular to Sb (antimony), As (arsenic), and Ga (gallium). Due to the increasing use of these metals in third generation mobile phone networks and other modern electronic devices. According to Sun et al. [77], combining mechanical processing with microwave-induced pyrolysis is a reliable approach of recycling waste printed circuit boards (WPCBs). The final recycling rate and grade of metals in the separation step can amount to 95 wt.% and 96.5%, respectively. Huang et al. [78] pretreated PCB by conventional pyrolysis and microwave pyrolysis prior to acid leaching processes and the overall copper recovery rates found to be approximately 75 and 96%, respectively. Whereas, the gold recovery rate were approximately 69 and 80%, respectively. Given that the presence of base metals would lead to increased thiourea consumption and consequently low gold recovery, the higher gold recovery rate may be explained by the increased amount of copper that was leached out of the microwave-pyrolyzed PCBs.

Additionally, author Huang and Lo [34], contrasted traditional and microwave pyrolysis. For a 50-minute operation, the waste PCBs were heated using microwaves with powers ranging from 200 to 1000 W. While, with 1 *l/min* N_2 flow rate, waste PCBs were subjected to conventional pyrolysis in a muffle oven at temperatures of 300-800 ℃, at the interval of 100 ℃. As per his research compared to conventional pyrolysis, microwave pyrolysis can provide higher weight loss of waste PCBs by 3-5 wt.%. Because microwave heating involves energy conversion rather than heat transfer, it is quicker and more effective than traditional

heating. In general, long heating time, unfavourable heat distribution, and radiative energy loss caused by conventional heating can be prevented by using microwave heating. In comparison with conventional methods, the pyrolysis induced by microwave irradiation is capable of producing more gaseous and solid products but less liquid product [79].

Moreover, according to Abdou et al. [80] thermal decomposition of PCB starts at 250 ℃ and continues up to 900 ℃. The results showed that at 550 ℃ for 1 h, it was possible to obtain free carbon fibres from the polymeric matrix. SEM images showed that the morphology of fibres recovered was similar to virgin carbon fibres. Pyrolysis experiments above 550 ℃ degraded the material, and experiments below have not completely removed the polymeric matrix.

In addition to the recovery of valuable metals and carbon fibres as discussed above, pyrolysis of PCB is important to produce organic oils and gases that can be used as chemical feedstock to the petrochemical industry or as a fuel. To determine the viability of employing pyrolysis oil produced from scrap printed circuit boards as a precursor for advanced carbonaceous materials, Quan et al. (2010) [81] conducted pyrolysis experiments in a laboratory scale fixed bed reactor at 600 ℃ temperature for 30 minutes. However, the thermal degradation and composition of each pyrolysis product is depended on the kind of resin used to create the original printed circuit boards [82], as well as the degree of curing of the resin and the type of hardener used in resin preparation [32]. The presence of the metals of the printed circuit board can also influence the thermal degradation of the polymer and the products evolved via catalytic reactions. The sections that follow provide an overview of how essential pyrolysis variables such as temperature, residence time, heating rate, operation mode, and additives affect the quality and quantity of waste PCB pyrolysis products, see Table 2.4.

TABLE 2.4: Product yields reported by different researchers at different process conditions for PCBs.

Author	PCB From	Process Conditions						Product yield (%)			Ref
		Flow rate	Temperature, ℃	Heating rate	Time (min)	Particle Size	Reactor Type	oil	gas	char	
Hall & Williams (2007)	Computer Television Mobile Phone	N_2, -	800	10	135	1.5-2 cm^2	Fixed bed	22.7 28.5 15.2	4.7 6.5 2.3	68.9 60 82.2	[83]
De Macro et al. (2008)	Mixture	N_2, 1 dm^3/min	500	15	30	2 cm	Autoclave	16.2	7.3	76.5	[69]
Sun et al. (2011)	Mixture	N_2, 100 ml/min	800	-	30	2*2 cm	Microwave induced pyrolysis at 700 W power	15.7	5.7	78.6	[77]
Y. Zhou et al. (2010)	Type A (PCB made from cellulose paper reinforced phenolic resin)	Vacuum	600	40	30	10-15 cm^2	Lab scale vacuum reactor	27.73	4.3	67.97	[84]
	Type B (made from glass fiber reinforced epoxy resin)							21.45	6.35	72.2	
Jie et al. (2008)	Mixture	N_2, 200 ml/min	300 400 500 600 700	10	30	2*2 cm	Tubular Type oven	5.21 6.9 9.06 9.13 8.87	9.85 13.56 12.93 13.18 13.9	84.94 80.9 78 77.69 77.23	[85]

Chiang et al. (2010)	Mixture	N_2, 0.1 l/min	500	2 to 5	30	4-4.8 mm	electrical furnace quartz tube	39	37	24	[86]
Chien et al (2000)	Mixture	N_2, 100 ml/min	550	5	30		Fixed bed reactor	40.6	24.9	34.5	[87]
P. Evangelopoulos et al. (2017)	PCB main body PCB sockets	N_2, -	600	-	30	-	Batch reactor	20 42	2 5	78 53	[88]

2.4 Decomposition and Thermogravimetric Study:

Thermogravimetric analysis (TGA), a type of analytical technique, is widely used to precisely analyse composition, identify patterns of breakdown, and forecast product performance. It works by monitoring weight loss as temperature changes over time at a fixed heating rate. The apparent activation energy, which reflects the minimum energy required for the deterioration of the sample at each stage of analysis, can also be determined from the TGA curves. Various TGAs are available, including isothermal, Quasi- static and dynamic one. Whereas, a differential thermogravimetric (DTG) analysis, is a plot of the weight loss rate over time or temperature (the first derivative against time in %/min) [89][90]. The weak organic molecules are given some energy during pyrolysis in order to overcome the dissociation energy and breakdown their bonds. Following that, new, stronger bonds are made to produce new molecules like CO, CO_2, H_2, and so on. The energy released throughout the process is computed using the DTA curves since breaking down the molecules releases significantly less energy than creating new ones does.

Evangelopoulos et al. [14] aimed to investigate the pyrolytic behaviour of waste printed circuit boards (PCBs) by means of TGA at different heating rate from 5 to 40 K/min and analytical pyrolysis (Py–GC/MS). No mass change was observed from the beginning of the experiment until the temperature of 120 ℃ as a result of the minimal moisture content and the mass loss ends at a percentage of almost 70% of the initial mass which can be explained by the high ash content of the initial material. The higher mass loss rate occurs at temperature between 250 – 370 ℃. Grause et al. [91] examined the pyrolysis of TBBA-containing waste paper laminated PCB prepared from novolac in a temperature range of between 40 and 1000 ℃. The TGA was quenched for 80 min with a helium flow of 100 ml/min, 0.5 to 4 ℃/min heating rate. They discovered that PCB broke down in three stages, the first of which occurred below 270 ℃ and involved the evolution of H_2O and CO_2 from the paper laminate. In the second stage (270–370 ℃), the fire retardant degraded, yielding brominated aromatics plus HBr. In the third step, the phenol resin broke down and char developed at temperatures above 370 ℃. Barontini et al. [92] demonstrated that if a heating rate of 10 ℃/min is utilised, the thermal degradation of TBBA primarily occurs between 240 and 350 ℃ under a nitrogen environment. While Y. Kim et al. [93], who made TGA investigation of paper laminated phenolic-printed circuit boards at a heating rate 15 ℃/min with nitrogen flow rate of 120

ml/min. It was investigated that the degradation can be divided in four zones with temperature range 100 ~ 280 ℃ (the vaporization of phosphorous-based fire retardants), 280 ~ 370 ℃ (pyrolysis of the laminated paper), 370 ~ 500 ℃ (degradation of phenol resin), and 500 ~ 800 ℃ (char stabilization).

The slight variation in the above results was related to the varying concentrations of TBBA and phosphorous-based flame retardants in each PCB. According to the literature, the breakdown temperature range for phosphate-based and TBBA flame retardants was quite similar. While the decomposition of phenol resin occurred at a higher temperature than 370 ℃ and the DTG curve pattern was changed at approximately 500 ℃. The bromine content influences thermal degradation and the brominated epoxy resins (BERs) are thermally less stable than the non-brominated (NBERs) ones [94][70][95]. According to Kim et al. [12], the cleavage event of N-containing cross-linkage between BERs and NBERs to produce thermally stable intermediates was observed below 250 ℃ temperature. NBERs degraded slowly and at a broader temperature range between 250 to 500 ℃. BERs, however, degraded more quickly between 250 and 350 ℃. Also agreed by Luda et al. [96] who reported BERs decomposition at 295 ℃ and 336 ℃ for NBERs. According to the research by Kim et al. [12], using gas chromatography/mass spectrometry, brominated phenol and brominated bisphenol A, were primarily produced below 335 ℃, with a heating rate of 20 ℃/min, while non-brominated and branched phenols were produced at above 335 ℃. Finally, thermally stable intermediates slowly turned into char at temperatures between 500 and 600 ℃ as a result of HBr release from the resin intermediates. According to Grause et al. [91], just 2% of the bromine remained in the residue and 14% was fixed in brominated aromatics. Moreover, the thermogravimetric data for integrated printed circuit boards with 2 and 15 K/min heating rates showed a two-step thermal degradation. According to the theory, the first stage around 300 ℃ involved reactions between the amine and bromine groups, while the second stage 360-510 ℃ involved the devolatilization of the tar and aromatic amines that were produced during the first stage [70]. With the use of a thermogravimetric analyser, Barontini et al. [92] pyrolyzed the plastic component of printed circuit boards made of flame-retardant epoxy resin obtained from several manufacturers. They showed that almost negligible differences were present in the temperature range of the thermal degradation process, which takes place mainly between 280 and 350 ℃. The

breakdown then continued up to the final temperature of 800 ℃, leaving an approximately 65 wt% solid residues.

2.5 Reaction pathways:

N-containing cross-linking agent (i.e 4,4'-diaminodiphenyl methane, 4,4'-diaminodiphenyl sulphone, polyethylene polyamine and dicyandiamide) is used to blend the BERs diglycidyl ether of tetrabromobisphenol A DGETBBA and NBERs diglycidyl ether of bisphenol A DGEBA in different ratio during the PCB manufacturing process. The expected structure of prepared epoxy resin using 4,4'-diaminodiphenyl methane as curing agent is shown in Fig. 2.3.

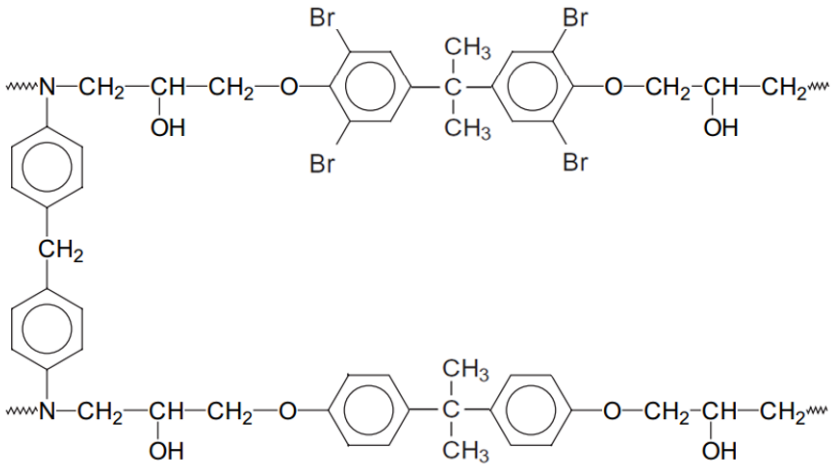

FIGURE 2.3: Possible structure of epoxy resin using 4,4' – diaminodiphenyl methane.

The possible pyrolysis reaction pathways of waste PCBs can be summarized as below [12]:

(1) Initial cleavage: The thermal decomposition of Waste PCBs is likely to be decomposed first by initial cleavage of N-containing cross-linkage which includes nucleophilic substitution through amines within the aromatic ring of BER to release HBr via the Hofmann–Matius reaction [97]. The HBr subsequently reacts with the amine curing agent to create dimethyl formamide, which destabilises the resins [12]. The separation of BERs and NBERs results in the generation of Bisphenol A and TBBA. Methylbromide, carbon dioxide, and acetone were also generated as a result of the initiation decomposition process [94].

(2) Independent decomposition of NBERs and BERs: Reaction pathway for NBERs via Bisphenol A was described by Quan et al. [11], see Fig. 2.4. Bisphenol A was formed due to the cleavage of O–CH_2 bond on both sides of the same monomeric structure. With Quan et al.[11], Y Kim et al. [12], also described possible reaction pathways by which bisphenol A, p-isopropenyl phenol, phenol and p-tert-butylphenol were produced. The breakdown of the bonds connecting the phenyl ring to an isopropylidene group would result in the formation of isopropenyl or isopropyl phenol and phenol, and phenol could also be produced by the decomposition of various intermediate products [98]. It was noticeable that the quantities of p-isopropenyl phenol was higher than that of p-tert-butylphenol in pyrolysis products, indicating the breakdown of the isopropyl–phenyl bond (Ar–$C(CH_3)_2$–) of the bisphenol A structure preferred to formation of isopropylidene double bonds [11]. The higher energy bond of C-O in phenolic compounds, brakes at higher temperatures and other aromatic substances such as styrene, methylstyrene, benzene, and toluene are being produced due to epoxy resin's decomposition [14]. Whereas, as per Marongiu et al. [99] the thermal degradation of Brominated epoxy resin, TBBA is a complex process takes place by bond cleavage between the aromatic rings and the methylene bridges. Debromination of the polymer fraction occurs mainly by the production of HBr [71]. However, some of the bromine remains bound to aromatic phenolic rings and produces bromophenols while the other part interacts with available methyl radicals to make bromomethane. i.e 2-bromophenol, 2,6-dibromophenol. With the help of hydrogen atoms, the generated radicals go through secondary reactions to generate phenol and methylphenols. [14].

(3) Char generation: Conversion of the intermediate (i.e. brominated and non-brominated phenoxy radical) and a substitutive addition reactions (i.e., polymerization) leading to a final residue named chars with relatively low oxygen, emission of hydrogen bromide and formation of dioxin [12][99].

The primary consequence of PCB pyrolysis is the creation of extremely hazardous compounds including benzofuran and dioxin precursors [96]. These products are mainly takes place by the cyclization of alkylphenols. However, low percentages of dioxins were identified at lower temperature, on high thermal processes with similar initial composition, produce high yields of dioxins due to catalytic effects and the high content of copper and nickel [96][14].

Higher temperature conditions favour the creation of aromatic hydrocarbons, while lower temperature conditions favour the formation of bisphenol A, brominated compounds, and phenol. Therefore, the chosen temperature conditions can help us to yield the desirable products according to their preference. However, benzofuranic structures are also formed at high temperatures, indicating that high temperature conditions should be avoided [14].

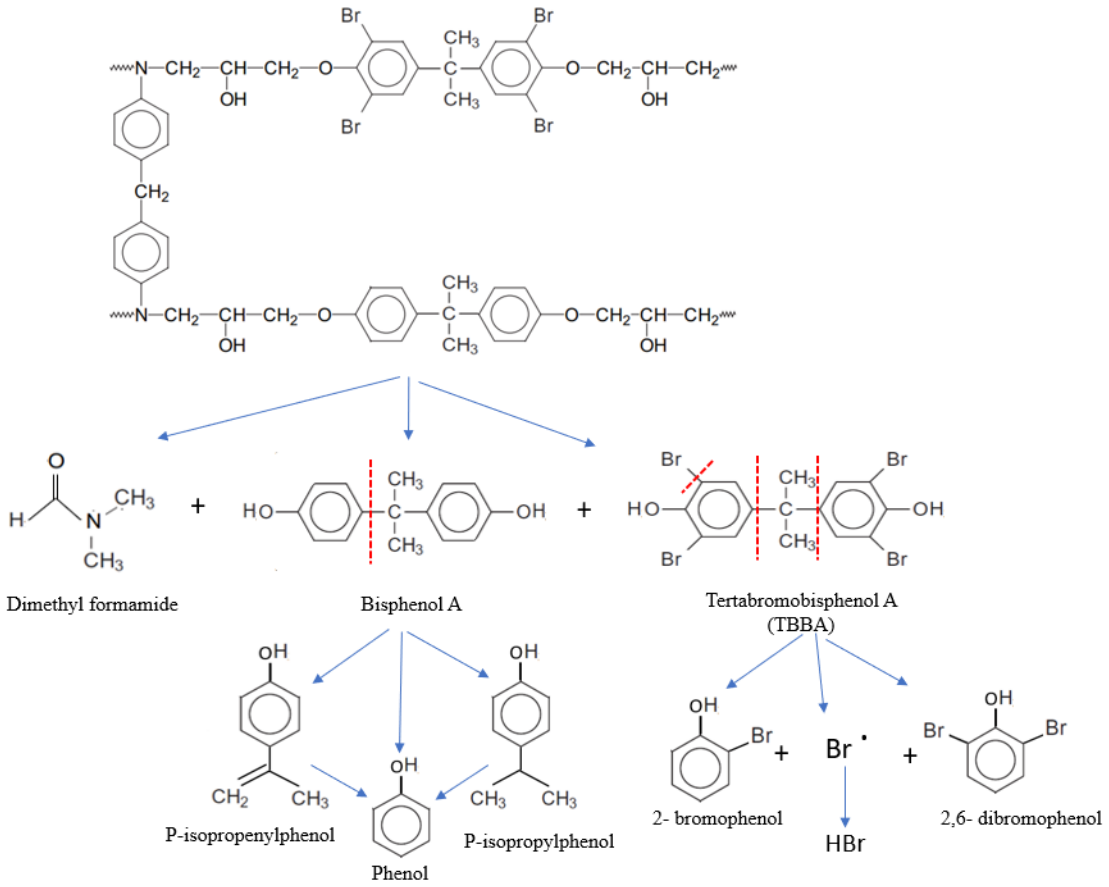

FIGURE 2.4: Reaction pathway for BFRs and NBFRs to produce phenol and brominated compounds.

2.6 Compounds identified by GC/MS in pyrolysis oil:

The liquid oil produced during the pyrolysis process is a complex mixture of condensable hydrocarbons, including oxygen containing 1–5 ring aromatic and complex polyaromatic hydrocarbons. It is thick, dark brown, and highly viscous liquid composition with some aqueous products. Depending on the raw material that was pyrolyzed, the oils' composition varies greatly. In reality, it has been observed that the degree of resin curing and the kind of hardener involved in resin preparation have an impact on the thermal decomposition of the PCB and the composition of the pyrolysis products [82][94][96][100].

De marco et al. [69] has shown the elemental composition of the pyrolysis oil produced from E-waste PCBs at 500 ℃, in an autoclave, where the H/C atomic ratio was near 1, which is indicative of a more aromatic/naphthenic nature. Since oxygenated polymers like polycarbonate (PC) and epoxy resins are parts of printed circuit boards, the liquids are almost entirely constituted of C and H with considerable amount of O. It also contains some amounts of nitrogen and other elements. The authors [69][70][85][77] have reported that this pyrolysis oil has a high calorific value and could be used as a fuel or a source of chemical materials. The calorific value of PCB oil was reported 26.5 MJ/kg by De Marco et al. [69]. Whereas, Chiang et al. [70] reported a calorific value of 31.4–37.7 MJ/kg for different particle size and temperature ranging from 5-40 mesh and 200-500 ℃, respectively. Jie et al. [85] observed that the pyrolysis oils created from computer printed circuit boards that were pyrolyzed at 500 ℃ had a gross calorific value of 30.5 MJ/kg. Nearby same result reported by Sun et al. [77] who used microwave induced pyrolysis and the calorific value of the oil was as high as 30 MJ/kg.

A preliminary characterization of PCB pyrolysis oil was carried out by many researchers [82][69][101][16][52][83][86][91][92][102]. While, researcher like M Siddiqui et al. [98] has focused on degradation of poly (bisphenol A- carbonate) based polymers by gas chromatography–mass spectroscopy (GC–MS), in order to get an idea of the nature and type of components present. Table 2.5 shows a summary of the main components, tentatively identified by GC–MS, reported by different researches.

The PCB sample's pyrolysis liquids are primarily made up of aromatic chemicals. They are rich in phenol and phenol derivatives, which very certainly originate from polycarbonate (PC) [67][69]. With substituted phenols, aromatic/aliphatic ethers are the predominant by-products of the heat decomposition of the non-brominated components of the epoxy resin, showing a preferred splitting of the O-CH_2, C(phenyl)-C, and C-N bonds [96]. Branda and Jima, [100] had also observed 2-methylphenol, 2,6-dimethylphenol, and 2-ethylphenol as the main pyrolysis products in liquid oil derived from epoxy resin.

Barontini et al. [92] used a laboratory size fixed bed tubular pyrolysis reactor at 800 ℃, with 10 ℃/min heating rate, and 80 ml/min N_2 flow rate to pyrolyze the plastic fraction of flame retarded epoxy resin based non-metallic printed circuit boards. He discovered several non-

volatile species as the most significant ones, including phenol (38%), 4-(1-methylethyl)phenol (11.7%), and bisphenol A (10.2%). These products originating from the thermal breakdown of the bisphenol A based epoxy resin. The PCBs from television, mobile phone and computers, were pyrolyzed by Hall and Williams [82], at 800 ℃ with a heating rate of 10 ℃/min in a fixed bed reactor. Reporting phenol and 4-(1-methylethyl) phenol as two of the primary components in the resulting pyrolysis oil, as well as 4-methylphenol and 4-ethylphenol were also present in the pyrolysis oils, generated from the subsequent breakdown of 4-(1-methylethyl) phenol [32].

In addition to methyl and ethylphenol, dimethylphenol and isopropyl phenyl revealed a high fraction at high temperature (i.e., >400 ℃) [86]. Moreover, 2-bromophenol, 4-bromophenol, 2,4- and 2,6-dibromophenols and 2,4,6- tribromophenol are major components of brominated compounds; they could be decomposed from the tetrabromobisphenol A and also associated with the sister product of 2,6-dibromo-4-(1,1-dimethyl ethyl)phenol [86][103]. G. Grause et al. [91] had pyrolysed TBBA containing paper laminated PCBs prepared from novolac by both TGA and in a quartz glass reactor between 40 and 1000 ℃. The GC–MS analysis of the liquid products indicated the presence of aromatic products only. With phenol, methylated phenols and methylated benzene, some brominated compounds were also detected named, 2-bromophenol, 2,4-dibromophenol, 2,6-dibromophenol and 2,4,6-tribromophenol. In addition to these compounds some poly aromatics such as methyl naphthalene and methyl anthracene, which are precursors for the formation of char were also detected.

De Marco et al. [69] reported 36.1% phenol and 26.9% phenol derivatives in pyrolysis oil, generated in autoclave at 500 ℃ for 30 min. In addition to this some toluene (1.6%), alkyl or alkenyl benzenes (5.1%), and N-containing aromatics (1.3%) were also found, with only 0.3% of non-aromatics. Agreed by F Diaz et al. [67], who conducted a comparative analysis on the degradation mechanism of PCBs in slow and fast pyrolysis. Except the compounds mentioned in Table 2.5, Evangelopoulos et al. [14] also found some lower molecular hydrocarbons like, butane, benzene, toluene and methylstyrene. Additionally, 1,3-Pentadiene as well as acetone were found. Meanwhile, 3-Ethylphenol, 2-Allylphenol, 1,3-Dimethylnaphthalene, 3,3', 4,4', and 2,2', 5,5' tetramethyl-1,1'-biphenyl were all reported by Quan et al. [81]. Toluene and benzene are broken down by (-OH) hydroxyl radicals, which

operate as a source of water by extracting hydrogen from any accessible methylene bond, making phenol formation more favourable at lower temperatures than 500 ℃. On the other hand, toluene can also be converted by partial oxidation reactions [104] to methylphenols like cresols, which cannot be fully oxidised because there is no free oxygen in the system and only a small concentration of other C-H oxidants. According to the findings, toluene should degrade at a temperature of 400 ℃.

As per literature, no higher polybrominated dibenzo dioxins/furans (PBDD/F) or polychlorinated dibenzo dioxins/furans (PCDD/F) were identified, in the product oil recovered from runs performed in inert atmosphere. However, Molto et al. (2008) [101], identified PCDDs, PCDFs and polychlorinated biphenyls in the off gases from pyrolysis of PCB derived from mobile phones at 500 ℃. According to the findings of earlier studies on the synthesis PBDD/F revealed that TBBA breakdown mostly produces mono- to tri-brominated PBDD and PBDF in the ppm range [105][106][71]. Whereas, brominated compounds mainly 2-bromophenol, 4-bromophenol, 2,4-dibromophenol, 2,6-dibromophenol, bisphenol A and dibromobisphenol A, tribromobisphenol A and Tetrabromobisphenol A were identified in pyrolysis oil by many researchers, see Table 2.5. Hall and Williams (2007) [82] had noted the presence of 2,6-dibromophenol (0.1%), 2,4-dibromophenol (0.01%) and a trace level of tetrabromobisphenol A. Moreover, none of the researchers, who worked on PCB pyrolysis found chlorinated compounds in the oil despite Hall and Williams (2006) [107] who identified hexadecyl chloroacetate and (4-chlorobutyl)benzene in mixed WEEE pyrolysis oil.

Additionally, phosphate-based compounds have been found in several liquid products, with triphenyl phosphate and isopropylphenyl diphenyl phosphate being the most prevalent ones [86][103][91]. While ortho and meta cresyl phosphate, a plasticizer and flame retardant used in PVC and polystyrene, was also reported by Hall and Williams [82] and Grause et al. [91], it was also discovered by Hall and Williams in a computer printed circuit boards pyrolysis oil, but at a very low concentration [82]. In addition, [83] had reported cresyl diphenylphosphate, which also has flame- retardant characteristics (Lee 1989- Dictionary of composite materials technology). Generally, triphenyl phosphate is a fire-retardant additive (Lassen and Lokke 1999) in PCB, but it is also the pyrolysis product of several other phosphated fire retardants, i.e., bisphenol A bis(diphenyl phosphate) [94], triphenyl (diphenoxyphosphinyl)phosphorimidate [29], and tetraphenyl imidodiphosphate [108]. It is

primarily utilised in thermoplastic polymers, such as poly(vinyl chloride), polystyrene, and others [86]. Therefore, the detection of phosphate flame retardants shows that, rather than the printed circuit boards themselves, the pyrolysis oil may have contained these compounds as a result of the pyrolysis of plastic-containing components that were attached to the boards [82].

TABLE 2.5: GC/MS identified compounds by different researchers.

	Reference								
	[92]	[82]	[83]	[101]	[86]	[109]	[103]	[14]	[98]
Compounds name									
Phenol	√	√	√	√	√	√	√	√	√
Styrene	√	n.d	n.d	√	n.d	√	n.d	√	n.d
2-Methyl phenol	√	√	√	√	√	√	√	√	n.d
4-Methyl phenol	√	√	√	√	n.d	√	n.d	√	√
2-Ethylphenol	√	√	√	n.d	√	√	n.d	n.d	n.d
4-Ethylphenol	√	√	√	√	√	n.d	√	n.d	√
2,6-Dimethylphenol	√	√	√	√	√	n.d	n.d	√	n.d
2,4-Dimethylphenol	√	n.d	n.d	n.d	√	√	√	n.d	n.d
2,4,6-trimethylphenol	n.d	n.d	n.d	n.d	√	n.d	n.d	n.d	n.d
1-Ethenyl-4-ethylbenzene	n.d	n.d	n.d	√	n.d	n.d	n.d	n.d	√
2-Propylphenol	√	n.d	n.d	√	n.d	n.d	n.d	n.d	√
4-isopropenylphenol	n.d	n.d	n.d	√	n.d	n.d	n.d	n.d	√
4-isopropylphenol	√	√	√	n.d	√	√	√	n.d	√
p-hydroxydiphenyl	n.d	√	√	√	n.d	n.d	n.d	n.d	n.d
Methyl-4(1-methylethyl)phenol	√	√	n.d	√	n.d	n.d	n.d	n.d	n.d
(1-methylpropyl)phenol	√	n.d	n.d	n.d	n.d	n.d	n.d	n.d	n.d
bis(1-methylethyl)phenol	√	n.d	n.d	n.d	n.d	n.d	n.d	n.d	n.d

Naphthalene	n.d	n.d	n.d	√	n.d	n.d	n.d	n.d	n.d
Methylnaphthalene	n.d	n.d	n.d	√	n.d	n.d	n.d	n.d	n.d
Biphenyl	n.d	n.d	n.d	√	n.d	n.d	n.d	n.d	n.d
Anthracene/Phenanthrene	n.d	n.d	n.d	√	n.d	n.d	n.d	n.d	n.d
1,3-Diphenylpropane	n.d	n.d	n.d	√	n.d	n.d	n.d	n.d	n.d
Benzofuran	n.d	√	n.d	√	n.d	n.d	n.d	√	n.d
2-furanmethanol	n.d	n.d	n.d	n.d	√	n.d	√	n.d	n.d
2-Methylbezofuran	√	√	n.d	√	n.d	√	n.d	√	n.d
2-methyl-2,3-dihydrobenzofuran	√	n.d	n.d	n.d	n.d	√	n.d	n.d	n.d
3,4-Dihydro-2H-1-benzopyran	√	n.d	n.d	√	n.d	n.d	n.d	n.d	n.d
3,4-dihydro-2H-1-benzopyran-3-ol	√	n.d	n.d	n.d	n.d	n.d	n.d	n.d	n.d
1-phenoxy-2-propanone	√	n.d	n.d	n.d	n.d	n.d	n.d	n.d	n.d
Dibenzofuran	√	n.d	n.d	√	n.d	n.d	n.d	n.d	n.d
methylenbis(phenol)	√	n.d	n.d	n.d	n.d	n.d	n.d	n.d	n.d
Benzene-1-ethenyl-4-ethyl	n.d	n.d	n.d	√	n.d	n.d	n.d	n.d	n.d
oleic acid	n.d	n.d	n.d	n.d	√	n.d	n.d	n.d	n.d
Ethylstyrene	n.d	n.d	n.d	√	n.d	n.d	n.d	n.d	n.d
Dimethylpyrazine	√	n.d	n.d	n.d	n.d	n.d	n.d	n.d	n.d
Methylbenzofuran	n.d	n.d	n.d	√	n.d	n.d	n.d	n.d	n.d
Hydroxybiphenyl	√	n.d	n.d	√	n.d	n.d	n.d	n.d	n.d
Bisphenol A	√	√	√	√	n.d	n.d	n.d	√	√

Hexadecanoic acid	n.d	n.d	n.d	n.d	n.d	n.d	√	n.d	n.d
Heptadecanenitrile	n.d	n.d	n.d	n.d	n.d	n.d	√	n.d	n.d
Brominated Compounds									
Bromomethane	n.d	n.d	n.d	n.d	n.d	n.d	n.d	√	n.d
2-Bromophenol	√	n.d	n.d	√	√	√	n.d	√	n.d
3-Bromophenol	n.d	n.d	n.d	n.d	n.d	n.d	√	n.d	n.d
4-Bromophenol	√	n.d	n.d	√	√	n.d	n.d	n.d	n.d
2,4-Dibromophenol	√	√	√	√	n.d	n.d	√	√	n.d
2,6-Dibromophenol	√	√	n.d	n.d	√	n.d	√	n.d	n.d
Bromobenzene	n.d	n.d	n.d	√	n.d	√	n.d	n.d	n.d
Phenol, 2-bromo-4-methyl-	n.d	n.d	n.d	√	n.d	n.d	n.d	n.d	n.d
Benzamine, 4-bromo, 2-6-dimethyl	n.d	n.d	n.d	√	n.d	n.d	n.d	n.d	n.d
2-bromo, 14 -dioxine	n.d	n.d	n.d	√	n.d	n.d	n.d	n.d	n.d
3,6-dibromo-2,5-xylidine	n.d	n.d	n.d	√	n.d	n.d	n.d	n.d	n.d
phenol,2,6-dibromo	n.d	n.d	n.d	√	n.d	n.d	n.d	n.d	n.d
2,6-Dibromo-4-(1-methylethyl)phenol	√	n.d	n.d	n.d	n.d	n.d	n.d	n.d	n.d
2,6-Dibromo-4-(1-methylethenyl)phenol	n.d	n.d	n.d	n.d	n.d	n.d	n.d	n.d	n.d
2-bromo-4-(1-methylethenyl)phenol	n.d	n.d	n.d	n.d	n.d	n.d	n.d	n.d	n.d
2-bromo-4-(1-methylethyl)phenol	√	n.d	n.d	n.d	n.d	√	n.d	n.d	n.d
2,6-dibromo-4-(1,1-dimethyl ethyl)phenol	n.d	n.d	n.d	n.d	√	n.d	n.d	n.d	n.d

2,4,6-Tribromophenol	n.d	n.d	n.d	n.d	√	n.d	√	n.d	n.d
1-Bromo-3-phenoxy-2-propanol	√	n.d	n.d	n.d	n.d	n.d	n.d	n.d	n.d
1,3-Dibromo-2-propanol	n.d	n.d	n.d	n.d	n.d	n.d	n.d	n.d	n.d
Bromobisphenol A	√	n.d.	n.d	√	√	n.d	n.d	n.d	n.d
2-Bromo-3-methoxyacetophenone	n.d	n.d.	n.d	√	n.d	n.d	n.d	n.d	n.d
Dibromobisphenol A	√	n.d.	n.d	√	n.d	n.d	n.d	n.d	n.d
Tribromobisphenol A	√	n.d.	√	√	n.d	n.d	n.d	n.d	n.d
Tetrabromobisphenol A	√	√	n.d	n.d.	n.d	n.d	n.d	n.d	n.d
2-Bromo-p-cymene	n.d	n.d	n.d	n.d	n.d	√	n.d	n.d	n.d
Phosphate based									
Triphenyl phosphate	n.d	√	√	n.d.	√	n.d	√	n.d	n.d
o-Cresyl phosphate	n.d	√	n.d	n.d.	n.d	n.d	n.d	n.d	n.d
m-Cresyl phosphate	n.d	√	n.d	n.d.	n.d	n.d	n.d	n.d	n.d
cresyl diphenylphosphate	n.d	n.d.	√	n.d.	n.d	n.d	n.d	n.d	n.d
Isopropylphenyl diphenyl phosphate	n.d	n.d	n.d	n.d	√	n.d	√	n.d	n.d

The pyrolysis by-products include pyrolysis gases, which are mostly made up of H_2, CO, CO_2, CH_4, and light hydrocarbons linked as C_mH_n mainly composed of C1-C4 [85], as well as inorganic halogens, depending on the type of raw material pyrolyzed and the experimental conditions. Chiang et al. [86] has also identified NO_x, but the quantity was very less (72-265 ppm). As per [69] the gross calorific value of the printed circuit boards gases generated at 500 ℃ was 30 MJ/m^3, which was as high as 70 MJ/m^3 for the gases produced from computer-based PCBs at 300 to 700 ℃ temperature range [85]. Gases with such high calorific values are adequate to meet the process plant's energy needs. On the other hand, if CO_2 is present, the gases created during pyrolysis can have a decreased calorific value. However, systems now exist for removing CO_2 from gas streams (International Energy Agency, 2004) [82]. Sun et al. (2011) [77] used below formula to calculate calorific value of pyrolysis gas,

$$Q_v = 30.5V_1 + 25.7V_2 + 84.7V_3 + 170V_4 \quad (2.1)$$

Where, Q_v is the calorific value of mixed gas, Kcal/m^3: V_1, V_2, V_3 and V_4 are the volume % of CO, H_2, CH_4 and C_nH_m in the total pyrolysis gas. The yield of the pyrolysis gas was obtained in terms of mass by difference. To obtain gas volume, the average molecular weight of the pyrolysis gas is required, which can be calculated as follows,

$$M_a = \frac{\sum MiVi}{\sum Vi} \quad (2.2)$$

Where, M_a is the average molecular weight of the pyrolysis gas, M_i and V_i are the molecular weight and the volume % of the i^{th} component gas, respectively.

As the temperature rises, there will be a reduction in the amount of C_2-C_4 hydrocarbons, but a significant increase in the production of CH_4 and H_2 was observed [66]. The release of CO was primarily concentrated at 500 ℃ or higher, according to Xiong et al. [16], who employed TGA-FT-IR and GC/MS to determine the release of NM-PCB compounds at different temperatures. As the temperature rose, the amount of CH_4 and H_2O releases increased, reaching their maximum levels at 600 ℃ - 800 ℃ and 400 ℃ - 600 ℃, respectively. The presence of CO and CO_2 in pyrolysis gases is attributed to the oxygenated structures in the polymeric components of the polycarbonates and epoxy resins, released nearby 360-400 ℃.

It could also have been formed by the decomposition of calcium carbonate fillers in the polymer. Hall and Williams (2007) [82] observed some amount of ethene, propene, butane and butene/butadiene at different temperature ranging from temperature 400 – 550 ℃ for PCBs from computer, television and mobile phones. Propene release during the pyrolysis of the computer circuit boards occurred very rapidly for a short time peaking at 400 ℃, the same temperature that CO_2 and CO release peaked at. The fact that propene, CO_2, and CO were all released at the same time suggests that the decomposition of the epoxy group either leads to the release of CO that is later oxidised to CO_2 or the release of a hydroxyl group leaving an allyl radical which reacts with a hydrogen radical to form propene. As the temperature increased above 600 ℃, the release of CO_2 and CO increased, presumably due to further decomposition of the char.

The generation of off-gases during the pyrolytic breakdown of PCBs has already been covered in a number of studies [67][52][107]. It was determined that beyond 500 ℃, where the pyrolysis gas is rich in H_2 and CH_4 [85], there is no additional temperature influence on gaseous products. However, there were trace amounts of bromine in every printed circuit board pyrolysis gas. Barontini et al. [92] and Cozzani [71], in addition to Chien et al. [87] and Xiong et al. [16], performed in-depth research on HBr and the generation of brominated chemicals during pyrolysis. They all came to the same conclusion that bromoethane (C_2H_5Br) and methyl bromide (CH_3Br) were evaluated together with the synthesis of HBr at high temperatures and rapid heating. Using a TG-FTIR-GC/MS coupled system, Xiong et al. [16] explored the fate of bromine and thermal degradation pathway for non-metallic PCBs. They discovered that HBr, CH_3Br, and C_2H_5Br released at their highest rates at 545 ℃, 597 ℃, and 673 ℃, respectively. The reaction pathways demonstrated tetrabromobisphenol-A (TBBA) decomposition into C_6H_5BrO and HBr, which further reacted with small molecules forming brominated derivatives. Due to the fact that hydrogen halides are highly corrosive to boiler tubes, the low concentration of halogens in the pyrolysis gases is advantageous if the gases are to be utilized as fuel. However, already in use technology, including wet or dry cleaning systems, are able to address the problems brought on by the modest levels of brominated substances [82][77].

Coke [67] is a solid char residue from pyrolysis that is predominantly composed of glass fibres, metals (in the form of metal balls and copper foil), and carbon [77]. According to Diaz et al. [67], only a limited amount of carbon is created during the secondary tar-cracking

events that include the polymerization of unsaturated products like dienes and olefins or coke precursors, such as aromatics.

2.7 Dehalogenation of Pyrolysis Oils:

The utilisation of the pyrolysis oils as potential fuels or refinery feedstocks becomes limited if they contain significantly high concentrations of bromine or chlorine. As was already mentioned, the presence of TBBA in PCBs enables char formation and is to blame for the brominated chemicals release during combustion. The main product of the degradation of TBBA is HBr, with brominated phenols formed as by products [110]. In fact, one of the most crucial components of pyrolysis treatment is dehalogenation of oil products, and increasing oil production is another difficult task to do. In order to solve this problem, Barontini et al. [92] suggested a fundamental process for the formation of dibenzodioxin structures that promotes debromination by fixing this matrix in char. When compared to chlorinated dibenzodioxins, the brominated dibenzodioxins remain predominantly encased in the char matrix because of the higher molecular weight of the bromine atom than the chlorine atom and the lower binding energy of the carbon-bromine bond compared to the carbon-chlorine link [111]. Different PBDD/F sources and manufacturing methods were carefully analysed by Yang et al. [112] in order to comprehend PBDD/F environmental contamination and human exposure levels. However, investigations also indicate the release of PBDD and PBDF during the degradation process were at ppb and ppm levels as discussed above.

2.7.1 Catalytic debromination

By selecting better pyrolysis processing conditions, it is feasible to lessen the degree to which they are generated. While several writers have utilised debromination using various catalysts, Bockhorn et al. in 1999 [113] recommend adding calcium carbonate to the electronic waste before pyrolysis to capture generated bromine in char. The amount of bromine in the residue was increased by a factor of two for an addition of 20 % calcium carbonate at a pyrolysis temperature of 400 ℃. Additionally, it has been demonstrated that calcium-based additives are readily available, inexpensive, and very effective at removing halogens from pyrolysis oils and gases. In a fluidized bed pyrolysis reactor with a temperature range of 430-510 ℃, Jung et al. [114] successfully completed the thermal degradation of acrylonitrile-butadiene-styrene containing brominated flame retardants

utilising Ca-based additives (calcium oxide, calcium hydroxide, and oyster shells). When $Ca(OH)_2$ was used, the oil's total bromine and chlorine concentrations fell to 0.05 and 0.04 wt.%, respectively. Vasile et al. [115] used a coupled thermal, catalytic ($CaCO_3$/cracking), and dehalogenation (absorption) approach to produce pyrolysis oils from waste computer printed circuit boards with low levels of heteroatoms (Br, Cl, N, and O). They stated that the halogen content of the oils produced by pyrolysis had significantly decreased.

Blazso and Czegeny [116] used a number of catalysts, including ALM-MCM-41 and Na Y-zeolite for the debromination of epoxy resin containing TBBA and discovered that the bromobisphenols and bromophenols could be removed by Na Y-Zeolite catalyst. While, Li et al. [33] used tri-iron tetroxide sorbent (Fe-O) to degrade brominated epoxy resin from WPCBs. As per his investigation adding 1:1 ratio, bromine concentration of pyrolysis oil decreased up to 98.2%. Meanwhile, Ng et al. [117] concentrated on increasing oil yield and employed catalytic pyrolysis of PCBs over different catalysts such as FCC (fluid catalytic cracking), zeolite socony mobil-5 (ZSM-5), H-Y-type zeolite and dolomite. They discovered that the maximum yield of liquid products with a significant amount of phenol was produced by the FCC catalyst at 275 ℃ with an FCC:PCB ratio of 10:90. Whereas, Hall and Williams [37] who pyrolyzed acrylonitrile–butadiene–styrene, flame retarded with tetrabromobisphenol A and high impact polystyrene (HIPS), which was flame retarded with decabromodiphenyl ether in a fixed bed reactor at 440 ℃ temperature, found that Y- Zeolite were more effective to remove organobromine compounds from the volatile pyrolysis products. The removal of antimony bromide, however, was less successful. Wang et al. [118] used activated Al_2O_3 with a catalyst feed ratio of 1.0:1.5 and a pyrolysis temperature of 600 ℃ for reduced bromine in oil. While, Natural clays like, bentonite, dolomite, and olivine were used as in-situ catalyst as well as ex-situ HY(30, SiO_2/Al_2O_3) were used by Park et al. [119]. Additionally, pyrolysis and catalytic reforming at 500 ℃, utilising iron oxide as a catalyst along with biochar and electronic waste char were carried out by C. Areeprasert and Khaobang [114].

On the other hand, some authors had suggested modification in pyrolysis process for debromination instead of using catalyst. Luda et al. [120] looked into the effect of alkali pretreatment in the form of NaOH or $Na_2CO_3/Ca(OH)_2$ to de-brominate flame retarded brominated high impact polystyrene and epoxy resin during pyrolysis and discovered that the procedure resulted in the recovery of bromine from the residue by washing. Grause et al.

[91] focused on analysing how brominated compounds degraded during the pyrolysis of paper laminated PCBs that included tetrabromobisphenol-A. Experiments were conducted in an electric heated quartz tube with a nitrogen at a flow rate of 100 ml/min, heated from 50 to 800 ℃, with a heating rate of 10 K/min. The findings demonstrate that brominated compounds are only generated between 270 and 400 ℃ , and that the bromine is only released at higher temperatures (>450 ℃) in the form of HBr. They recommended to avoid 270- 400 ℃ temperature range during pyrolysis to get less brominated phenolic compounds and accelerating fixation of it by the formation of char. Later on, Y. Shen in 2018 [121] proved that the formed HBr can react with NaOH to generate NaBr at high temperature by sodium hydroxide (NaOH) pretreatment and the Br fixation efficiency of char can reach up to 53.6%. Terakado et al. in their research on thermal degradation of tetrabromobisphenol A [122] and printed circuit board containing brominated flame retardant (2013) [123] reported that adding metal oxides can fix bromine and prevent the creation of HBr and organobromine compounds. Whereas Xiu et al. [124] in their research created an innovative method for debromination of waste PCBs as well as for the recovery of copper and nitrogen-containing fine chemicals from waste PCBs, using low temperature, near-critical aqueous ammonia (NCAA). In a batch reactor, the experiment was conducted with reaction periods of 30 to 90 minutes and temperatures of 200 to 350 ℃. The outcome had demonstrated that the NCAA could remove and trap 99.9% of the Br in waste PCBs by heating them to 300 ℃. After NCAA treatment, no brominated organic chemicals were found in the oil products, not even at low temperature of 200 ℃. Additionally, by using this process, two novel, highly valuable chemicals (pyrazine and pyridine compounds) were produced. Huang et al. [34] used microwave pyrolysis heated under 300 W irradiation, the oil and gas produced was composed of less brominated compounds, as the process resulted in approximately 92% of bromine converted into HBr, much higher than that produced by conventional pyrolysis (approximately 75%).

According to the abovementioned research, catalysts are useful for both improving pyrolysis products and eliminating bromine. However, the use of expensive catalysts, such as HY and HZSM-5 zeolites, limits their applications because the activities of these catalysts are markedly reduced by coke formation during the pyrolysis process [125][126], as well as S Jung et al. [114] found reduction in oil yield in the thermal degradation of BFRs with Ca-based additives. On the other hand, the activity and selectivity in the catalytic cracking depend largely on the chosen catalyst, and factors such as pore size or acidity wield a

decisive influence upon its performance. Additionally, Hydrodeoxygenation (HDO) is an upgrading technique that works well for producing hydrocarbons from low-grade pyrolysis oil. However, the expensive equipment, the demand for catalyst additions, and the high-pressure requirements for the reaction make the procedure complicated and expensive [26]. Therefore, improved PCB pyrolysis processes or low-cost catalysts are required, in addition to BFR debromination [127]. Furthermore, simplicity and efficiency must be given great consideration while developing a process to produce the best synthetic liquid fuel. In this context, the concept of co-pyrolysis can be a flexible technique that has potential by satisfying the aforementioned requirements.

2.8 Co-pyrolysis:

Co-pyrolysis is a procedure in which the feedstock consists of two or more distinct components. Numerous research have demonstrated that the oil amount and quality were successfully increased by co-pyrolyzing biomass with various polymeric wastes without any changes to the system process [128][129][130][131]. The key advantage of employing the co-pyrolysis approach is the ability to drastically reduce waste volume as more trash is used as feedstock. Additionally, it reduces the need for a landfill, lowers waste treatment expenses, and resolves a number of environmental issues.

2.8.1 Mechanism of Co-Pyrolysis Process

The mechanisms of co-pyrolysis and normal pyrolysis are almost the same. The most important thing is the particles size which should be less than 2-3 mm to achieve homogeneous mixture of totally different material, which can also help to achieve high heating rate. In contrast to normal pyrolysis, co-pyrolysis has a special parameter which is called the ratio of feedstocks. This parameter is very important since it has a significant effect, leading to the production of extra oil. According to researchers [133][134][135], reaction parameters such as feedstock types, blending ratios, heating rates, temperatures, and reactor types have an impact on the distribution and properties of co-pyrolytic products.

The co-pyrolysis process is significantly influenced by the type of reactor employed. Each reactor has known operational and scalability benefits and downsides. The fluidized bed reactor is suggested for fast pyrolysis due to its relatively simple operation and easy

scalability in comparison to other reactor types. However, the majority of co-pyrolysis experiments [136][137][138][128][25] used a fixed-bed reactor, in order to accomplish synergistic effect by providing close contact between the fuel particles and their produced volatiles [26]. The auger reactor is, however, more efficient for co-pyrolysis, according to Martinez et al. [139]. Using two separate reactors, the fixed-bed reactor and the auger reactor, waste tyres (WT) and biomass were co-pyrolyzed. According to the findings of their comparative investigation, the auger reactor yields more liquid for the 90/10 biomass/waste tyre blend than the fixed-bed reactor. The experimental findings from the auger reactor also revealed a significant improvement for various liquid parameters, including a decrease in the total acid number, a decrease in density, an increase in pH, a rise in calorific value, and a decrease in oxygen content.

Co-pyrolysis has been used by many authors for PCB with various materials with major goals being debromination and better oil quality. In this context, C. Ma et al. [140] has investigated synergistic effects on the product features and heteroatom migration by co-pyrolyzing the NMF-PCBs and waste tyres combined in various ratios. The use of WT as an H-donor source greatly enhanced the synthesis of phenol (40–51%) and p-isopropylphenol (24–92%), by improving decomposition of Bisphenol A in PCB. However, there was a considerable decrease in the generation of key chemicals from WT pyrolysis, such as isoprene and D-limonene. Additionally, the co-pyrolysis caused effective elimination of hazardous substances, i.e. 26-47% decrease in tetrabromobisphenol A, and a 50-59% decrease in the generation of benzothiazole.

Moreover, according to analysis of the pyrolytic char, the process was useful for converting sulphur compounds into sulphates and the addition of 75% waste tyre was able to capture 12 times as much amount of bromine. Same author in their recent research [141], has reported effect of fast co-pyrolysis of PCB and waste tyre (WT) for value added recovery and heteroatom transformation. Using various fitting models, the yields of key products were reliably predicted and the outcomes were helpful for adjusting the experimental conditions to maximise the production of desired products. Blazso et al. [102] demonstrated change in yield and composition of brominated species, generated during co-pyrolysis of the circuit board with various basic additions, such as NaOH, Na_2CO_3, and CaO. In particular, an increased bromomethane evolution and a decreased brominated phenol production were seen during co-pyrolysis with NaOH. Whereas, Chen et al. [142] has co-pyrolyzed PCB with

oxides and salts of iron. As per research, $FeCl_2$, $FeCl_3$, or $FeSO_4$ were effective to improve the yield of a liquid product that was high in phenol and its homologues by co-pyrolyzing it with PCB. The release of brominated organics to liquid was also decreased due to fixation of Br as $FeBr_3$ in solids or release as HBr. In comparison to other $FeCl_2$ shown the highest ability to decrease the transfer of organics containing Br to liquid. A Hornung et al. [143] has employed polypropylene as a reductive medium for debromination, between temperature range of 300-400 ℃ and residence time 10-30 min in an inert atmosphere. Additionally, Y M Kim et al. [144] has used catalytic co-pyrolysis of PCB with PP and HDPE over HZSM-5 and HY by Pyro-GC/MS at 600 ℃ temperature, approved debromination and generation of value-added compounds. Some authors like J Guan et al. used calcium based compounds [145] and reported debromination by adsorption of HBr due to calcium compounds, but at the cost of reduced liquid yield, whilst Z Ye et al. [146] used Fe_3O_4+4A additives as second feedstock in PCB co-pyrolysis, reported increase in oil yield from 16.43% to 18.25% for the increased 4A amount for the ratio WPCBs:Fe_3O_4:4A, 1:1:0.5 to 1:1:1 and reduction in bromine content was observed 10.45 mg/g.

2.8.2 Importance of Biomass

The development and utilization of biomass energy has attracted more and more recognitions and concerns [147]. Furthermore, biomass is renewable and underutilised in energy conversion technologies, and has been identified as a possible energy source owing to its low sulphur and nitrogen content [22]. Pyrolysis of biomass to obtain bio-oil is an important way to develop and utilize biomass energy. Through pyrolysis, the organic components of biomass can be transformed into high value-added liquid products [148]. However, there are still bottlenecks existing in the follow-up utilization of these liquid products. First of all, it is well known that bio-oils have a series of disadvantages, like high oxygen, low calorific value, strong corrosion, ignition delay and storage instability, and so on, which greatly limits the utilization of bio-oils as power fuels [149][150]. The high oxygen concentration of the pyrolysis oil has reportedly been reduced using a variety of oil upgrading techniques, including catalytic pyrolysis, hydrogenation, steam reforming, molecular distillation, supercritical fluids, hydrodeoxygenation (HDO), esterification, and emulsification. Catalytic cracking and high-pressure hydrogenation processing are now the two major approaches for upgrading the bio-oil [151][152][153]. To cope up with this issue, in recent years, co-pyrolysis of biomass with different feed stocks have been increasingly concerned by

researchers, since it has ability to the reduction of pollutants emission as well as the synergetic effects might occur, which can result in a reduced activation energy and the improvement of products yield and quality.

Basically, the main components of biomass, most especially, the lignocellulosic biomass are cellulose (30–60%), hemicellulose (polysaccharides) (20–35%), and lignin (15–30%), together with some resins and minerals [154][155][18], while other forms of biomass such as the algae is generally categorized based on the two main groups of algae, namely; the macroalgae (i.e., the seaweeds), which contain mainly fatty compounds, soluble polysaccharides and proteins [156], and the microalgae which also consists of three main biochemical compositions, namely; lipids, carbohydrates and proteins, and the nature of the compositions of the algae is the major factor for the viability of its utilization in a variety of high-value products, mainly pigments (chlorophylls and carotenoids), PBPs (Penicillin-binding proteins), fatty acids, carbohydrates, vitamins, nutraceuticals and fuel production [157].

C Quan and Gao [158] investigated the properties of the char created by the rubber/sawdust, two-step co-pyrolysis, named "pyrolysis and activation process," that transforms rubber/sawdust with low value-added into activated carbon with high value-added. According to the findings, upgraded carbon exhibited a BET surface area between 600 and 900 m^2/g, which is more than activated carbon. Additionally, Hopa et al. [159] suggested a few potential synergistic mechanisms that could occur during the co-pyrolysis of coal/biomass mixtures. The study findings suggested possibility for the production of liquid fuels with better properties by using different biomass sources that exhibited interaction. In a fixed bed reactor operating at 550 ℃ in a nitrogen environment, equal amounts of binary and ternary blends were used to co-pyrolyze sugarcane bagasse, poppy capsule pulp, and rice husk. While, the rice husk and sugarcane bagasse produced the highest bio-oil yield (28.4%). The highest calorific value, on the other hand, was obtained through the pyrolysis of a mixture of sugarcane bagasse and poppy capsules, and it was 29.68 MJ/kg. Sourabh Chakraborthy [160] employed mixtures of digested sludge (DS), algal biomass (AB), and cedar wood (CW) in his investigation, both with and without the catalyst ZSM-5. The bio-oil contained primarily naphthalene, anthracene, and its methyl derivatives as aromatic hydrocarbons. It was proven that adding catalyst to blends decreased the energy needed for pyrolysis. The bio-oil with the highest aromatic hydrocarbon production, 89.38

wt.%, was produced by the 2:1 wt/wt ZSM-5: biomass mix, which was used in equal weight fractions of the three biomasses.

The use of discarded tyres as a fuel source through the co-pyrolysis process is gaining more and more attention from researchers. According to Sunarno et al. [161], the enhanced hydrogen index that is possible with polymers is one of the most crucial characteristics for co-pyrolysis with biomass. The effect of mass ratio of palm empty fruit bunch (EFB) to waste tyre was evaluated with the temperature of co-pyrolysis and yield and composition of the product were monitored. The experiment was made on different EFB: Waste tyre (100:0; 75:25; 50:50; 25:75 and 0:100) in a tube type reactor, heated at 400 – 600 ℃, with N_2 as a carrier gas at a flow rate of 400 m*l*/min for 45 minutes. Where addition of 75% tire waste in the co-pyrolysis and at a temperature of 500 ℃, resulted bio-oil yield was 44.3%, and the composition of hydrocarbons in bio-oil was 59.55% with a bio-oil heating value of 33.1 MJ/kg.

M Hossain et al. [163], in their study co-pyrolyzed rice husk and tire waste by varied percentage of blends at 450 ℃ in a fixed bed reactor to investigate their suitability as feedstock for the conversion into biofuels and chemicals. The highest liquid output was 52 wt% for a 50:50 composition, running for 60 minutes with no N_2 gas flow. Liquid products obtained at these conditions were characterized by physical properties, chemical analysis and fractional distillation. The findings demonstrated that if the pyrolysis conditions were selected appropriately, it was possible to produce liquid products from the specified wastes that were comparable to petroleum fuels and valuable chemical feedstock. Other researchers had also worked on co-pyrolysis of waste tyre with different biomass. Q Cao et al. [136] used Co-pyrolysis of sawdust and waste tyre with catalysts such as SBA-15, MCM-41 and HZSM-5 in a fixed-bed reactor at 500 ℃ for a period of 1 h. The outcome demonstrates that co-pyrolysis is helpful in preventing polycyclic aromatic hydrocarbons (PAHs) from being formed from tyres. SBA-15 as a catalyst is more significant than MCM-41 or HZSM-5 for reducing the density and viscosity of the oil and it can effectively decompose some large molecular compounds into small ones and thereby improving the quality of the oil. The liquid yield reached 45.0 wt.%, 46.2 wt.% and 47.0 wt.% when tires mass occupied 25%, 50%, and 75% in the mixture, respectively. The liquid derived from pyrolysis of sawdust alone had a HHV of 28.51 MJ/kg, while the value was increased to 42.44 MJ/kg when tire mass accounted for 50% of the mixture. Experiments in a fixed bed reactor at 500 ℃ was

done by, M Siva[164] in order to determine how oily wastes from ships (bilge water oil and oily sludge) affect the pyrolysis of waste tyres. The catalysts used in the pyrolysis were a commercial refinery catalyst and an industrial by-product containing iron. The co-pyrolysis oils (except flash point and sulfur content) had similar fuel characteristic with the commercial diesel. It was also found that the amounts of metal impurities in all pyrolytic oils were smaller than 0.3 ppm. The pyrolysis gases were found to have gross calorific values between 20.4 and 26.4 MJ/Nm^3. It had been demonstrated that the oils produced by co-pyrolysis include aromatic and olefinic compounds than oils produced only from scrap tyres. S. A. Babajo et al. [132] has made review of co-pyrolysis of waste tyre with different biomass and reported that co-pyrolysis technique can improve the characteristics of pyrolysis oil, e.g., increase the oil yield, reduce the oxygen content, reduce the water content, and increase the calorific value of the oil.

TABLE 2.6: Proximate analysis of some plastics and tires in wt.%.

Feedstock	Moisture	Volatile Content	Fixed carbon	Ash
PE	0.3	99.5	0.2	0
PS	0.25	99.63	0.12	0
PVC	0	94.8	4.8	0.4
PP	0.18	97.85	0.16	2
LDPE	0	100	0	0
HDPE	0	98.57	0.03	1.4
Tyre	1.22	62.36	29.45	6.97

Reference from [165].

Different plastics, in addition to recycled tyres, are also utilised in the co-pyrolysis process, and there is a plethora of research on this. It is worth noting that in analyzing the interactions between biomass and plastic during the co-pyrolysis process, the types of plastics commonly used include, among others, the polyethylene (PE), polypropylene (PP), polystyrene (PS) and polyethylene-terephthalate (PET). Moreover, the proximate analysis results of different plastic types disclosed that plastic consists mainly of volatile matters, for example, PP (95.08–100.00%), PS (97.85–99.80%), PE (98.87–99.80%), PVC (92.14–98.57%) and PET (88.61–91.75%), followed by fixed carbon contents but with low ash contents and very little or no moisture, see Table 2.6. This property of plastic make it a desirable co-feeding medium for improving the quality of biomass fuels during co-pyrolysis. Also, presence of alkali and alkaline-earth metals, as well as silica, can play important roles in the thermochemical

process [27]. Plastics are a good source of liquid hydrocarbons due to their high carbon and hydrogen contents. Therefore, when pyrolyzing plastics alongside biomass, this method can increase not only the quantity but also the quality of the bio-oil generated [18]. A recent study by Z. Wang et al. [166] on the co-pyrolysis of three different biomass materials (Rice Husk, Sugar Bagasse, and Poplar Wood) and PP, however, revealed a negative synergistic effect at low temperatures. This may be because the PP melts at low temperatures (< 400 ℃), preventing the volatilization of the biomass materials. While at higher temperatures, a favourable synergistic effect was observed. Many of the review papers are published, which covered research papers from 2001 to 2018 including, [167][153][165][168]. Some of the most recent research from 2018 to 2021 are presented in Table 2.7.

Sharypov et al. [169] conducted a study on the co-pyrolysis of wood biomass and a synthetic polymer. According to their research, the feed ratio, as opposed to temperature and reaction time, had the greatest impact on the production of liquid yield. Abnisa et al. [130], who looked into the co-pyrolysis of waste mixtures made of polystyrene and palm shells for the generation of liquid fuel, observed the same result.

TABLE 2.7: Most recent research on co-pyrolysis between different biomass and plastics.

Biomass	Plastic	Reactor and Operating Conditions	Catalyst	Results	References
Bamboo	PP	Microwave assisted co-pyrolysois, 550 ℃ temperature	HZSM-5	The highest bio-oil yield was achieved at a temperature of 250 ℃ with a feedstock/catalyst ratio of 1:2 and a bamboo/PP ratio of 2:1. Evidently, the ratios of aromatic and naphthenic hydrocarbons in bio-oil have also improved.	[170]
Corn stover	LDPE	Analytical pyrolyzer at 600 ℃ for 30 s with heating rate of 10 ℃/s	Tandem catalytic bed (TCB) of CeO_2 and HZSM-5	Results indicated that CeO_2 could remove oxygen from acids, aldehydes and methoxy phenols, producing a maximum yield of hydrocarbons of 85% and highest selectivity of monocyclic aromatics of 73%.	[171]
Lignocellulose	PP	Semi-batch reactor, at 510 ℃, Lignocellulosic Biomass to plastic (1:2, 1:1, and 2:1), at a heating rate of 10 ℃/min and a holding time of 1 h.	Spent FCC	At an LB to PP ratio of 0.5, the liquid yield and aromatic yields were at its highest 43 wt.% and 49% C, respectively.	[172]
Juliflora	PE	Indigenous reactor, At 450, 500, 550, 600, 650, and 700 ℃ temperature, heating rate 10 ℃ /min, different JF:LDPE ratio 1:0, 1:1, 1:2, 2:1, and 0:1.	-	With a blend ratio of 1:2 (JF and LDPE), the oil obtained was 32%, with 27.14 MJ/kg calorific value.	[109]

Bamboo sawdust	LLDPE	Analytical Pyrolyzer, at 600 ℃, heating rate 2000 ℃/s and the retention time 30 s. helium (99.999%) as inert gas	CeO_2/γ-Al_2O_3 and HZSM-5	By employing synthetic dual catalyst, CeO_2/-Al_2O_3 to HZSM-5 with a mass ratio of 1:3 in co-pyrolysis, the concentration of aromatic hydrocarbons was maximized. It was discovered that a 75% LLDPE percentage was more favourable for the production of monocyclic aromatic hydrocarbons.	[173]
Rice straw	Polythene	Cylindrical fixed bed reactor, at 450-500 ℃ temperature and 60 min holding time	-	For 50 wt.% polythene and 50 wt.% rice straw, the maximum liquid yields were 60.7 wt.% at reactor temperature 450 ℃ with a heating value 38.13 MJ/kg.	[174]
Mahua Seeds	PS + Waste Nitrile Gloves	Semi-batch reactor, 550 ℃ temperature, 80 ℃/min heating rate, and 100 mL/min N_2 flow rate	-	80:20 WNG:Biomass produced 44.18 wt.%, while 80:20 PS:Biomass produced 45.89 wt.% of liquid yield. Additionally, a significant decrease in viscosity, oxygen content, and moisture as well as a rise in the gross heating value, carbon content, and acidity were attained.	[175]
Sugarcane bagasse	HDPE	Fixed-bed reactor, 400–700 ℃, 45 min, heating rate of 10 ℃/min.	-	A maximum variation in oil output of 6.02 wt.% was observed at 600 ℃ and a composition of 60:40 HDPE:biomass. However, with a 40:60 HDPE:biomass ratio, the suppression of oxygenated compounds was most pronounced at the same temperature.	[176]

Considering above, adding biomass to the pyrolysis of Printed circuit boards is worth a try. Since a high hydrogen concentration would normally result in the creation of HBr/HCl and its fixing in the char [25][26], benefits include preventing the development of PBDD/F. Furthermore, because the biomass has a higher H/C molar ratio than PCBs, it can serve as a hydrogen donor during co-pyrolysis [26]. One of the most common components in biomass is water which is expected to act as a reactive agent, promoting further degradation of the PCBs polymer matrix and the production of more volatile substances, hence increasing pyrolysis oil yields. As per Y Shen et al. [27] cellulose in biomass could improve the thermolysis efficiency of NMF of PCB, whilst lignin can adjust the activation energy and thus, the co-pyrolysis with biomass can improve the fuel property.

Very little work had been done till now in this direction. One of them is W. J. Liu et al. [25], who conducted experiments on the co-pyrolysis of WEEE and waste biomass (sawdust) and found that the oil yield was 62.3%, which was significantly higher than the individual pyrolysis of WEEE (53.1%) and biomass (46.3%), where 90% of bromides were enriched in the pyrolysis oil and char. Wu and Qiu in their research [150] and [177] investigated the influence of mass ratio of reactants and heating conditions on co-pyrolysis of Chinese Fir Sawdust and Waste Printed Circuit Boards. Comparing with individual feedstock pyrolysis oils, the co-pyrolysis oils have advantages of more active phenolic compounds (phenol, 4-isopropylphenol, bisphenol A, etc.) from the WPCBs part and more soft phenolic compounds (guaiacol, 4-methylguaiacol, etc.) from the CFS part for polymerization, which guaranteed the high performance (especially the mechanical properties) of the synthesized phenolic resin. According to the data of liquid yields and total phenol contents of the pyrolysis oils, relatively low temperature and short holding time is beneficial to the formation of relatively long molecular chain compounds, while high temperature (500 ℃) and long holding time (30 min) is good for the formation of relatively shorter molecular chain compounds.

2.8.3 Cotton Stalk as Biomass

In this work biomass was used because of its many benefits namely [178]:

- It is renewable and has been identified as a possible energy source owing to its low sulphur and nitrogen content.

- Biomass is also abundantly available and underutilised in energy conversion technologies.
- Cotton is one of the most widely cultivated crops in Gujarat, India. While characterization studies of cotton stalks suggest that it includes a high amount of volatile matter and a low O/C ratio [12][28][29], which can aid in improving the quality and quantity of bio-oil [25][28].

Additionally, employing cotton stalk offers other advantages that researchers have addressed are shown below.

G Mailto et al. [179] examined the kinetic properties of the Cotton stalk and Rice Husk samples under conditions of pure nitrogen 99.9% and pure oxygen 99.9%. The temperature was increased from the ambient level to 900 ℃ while maintaining a 10 ℃/min heating rate. The kinetic characteristics such as (pre-exponential factor, the order of reaction and activation energy) were calculated for both selected materials. The activation energies calculated under nitrogen environment for CS (68.77 kJ/mole) was lower than RH (72.31 kJ/mole). While D Chen et al. [180] examined the pyrolysis kinetics of cotton stalk and sweet sorghum bagasse at five heating rates (15, 25, 35, 45, and 55 ℃/min). It was discovered that the average activation energy required for SSB and CS were 154.61 and 142.93 kJ/mol by the KAS methods and 155.61 and 145.39 kJ/mol by the FWO method, respectively. This indicates that CS requires less energy than SSB.

A Saad et al. [22] examined the burnout temperatures for sugarcane bagasse and cotton stock (defined as the temperature at which the rate of weight loss constantly drops to less than 1%/min). The burnout temperature for cotton stalks was the lowest (500 ℃), while that for sugarcane bagasse was significantly higher (520 ℃), proving that cotton stalks burn somewhat more easily. Furthermore, fast pyrolysis of cotton stalk was conducted by N Ali et al. [29] in the bubbling fluidized bed reactor at temperatures of 360–540 ℃ , and influence of pyrolysis temperature and feed size on the yield of bio-oil and coproducts was investigated. The yield of bio-oil and gas was increased with the increase in temperature, whereas yield of charcoal was decreased. The maximum bio-oil yield obtained was 36 wt.% at temperature of 490 ℃ at feed size of 1.0 mm. whereas, 51 wt.% bio-oil was obtained by P Madhu [28] with same particle size. The author used fluidised bed reactor, under the

operating parameters of 450 ℃ at sweep gas flow rate of 1.75 m^3/h. Additionally, S.A.Y. Shah et al. [181] examined the effect of waste tyre (WT) and cotton stalk (CS) co-pyrolysis with an emphasis on the quantity and quality of the liquid co-pyrolysis yield. In a fixed bed reactor, experiments were conducted with different mix ratios of the two feedstocks (e.g., CS/WT 1:0, 4:1, 3:2, 2:3, 0:1) at 20 ℃/min heating rate up to 550 ℃ with 50ml/min flowrate of N_2 gas. Maximum oil yield (48 wt.%) was shown by the blend ratio of CS/WT (2:3) with considerable rise in carbon content and a drop in oxygen content, resulted in a higher calorific value (41MJ/kg). Additionally, X Yuan et al. [129] looked into how co-pyrolysis affected the properties of solid char, such as yield, pH, elemental analysis, specific surface area, etc., as well as their ability to remove Pb(II). The bio-chars were made by co-pyrolyzing cotton stalks and low-density polyethylene (LDPE) in the following ratios: 1:0, 3:1, 2:1, and 1:1 (w/w) at 400, 450, and 500 ℃, respectively, and then maintaining the temperature for one hour. As a consequence, removing Pb(II) from blended bio-char at 500 ℃ temperature was more successful than removing Pb(II) from biochar made from cotton stalks alone, which was dominated by monolayer adsorption with a maximum capacity of about 200 mg/g. Additionally, W Zhipu et al. [182] looked at the effects of adding CS during co-pyrolysis with sewage sludge in a 1:1 weight-to-weight ratio on the physicochemical, surface characteristics, and ecological dangers of bio-chars for the pyrolysis temperatures ranged from 350 – 750 ℃. The increased temperatures encouraged the conversion of heavy metals from mobile to stable components, which significantly reduced the ecological concerns and made all biochar mesoporous.

Conclusion

Based on the preceding literature, it would be worthwhile to try pyrolyzing printed circuit boards with cotton stalk added as biomass. Which can aid in increased oil quality and quantity, while reducing brominated compounds. Up until recently, no effort has been done in this approach. So, the aim of this thesis is to work on co-pyrolysis of waste printed circuit boards and cotton stalks to find the best compositions, i.e., CS:PCB (30:70, 40:60, 50:50, 60:40, and 70:30) which can contribute to increased oil yield as well as improved fuel properties and value-added chemicals. In addition to this, debromination of the PCB pyrolysis oil is main concern of co-pyrolysis with cotton stalk. Furthermore, properties of gas and solid char generated through the co-pyrolysis process were also investigated in the foregoing chapters.

CHAPTER 3

Materials and Methods

3.1 Sample Preparation:

The cotton stalk waste samples used in this work were collected from the local farm (Gandhinagar, Gujarat), located in India. The samples were crushed and air-dried. On the other hand, the PCB waste samples were collected from Shivalik solid waste management, Punjab, India which was already pre-treated to remove metals. The samples were grounded and sieve analysis had been done for both samples individually. The particle retained on 100 µm screen and passed from 210 µm screen were taken for the experiments for CS and PCB. During mixing of PCB and CS samples partitioning method had been used to obtain a near homogeneous representative sample, see Fig. 3.1. The particle size is a crucial factor to take into account; as particle size increases, a temperature gradient is produced within the particle, leading to an incomplete pyrolysis process that, in turn, reduces pyrolysis volatiles and lowers the output of pyrolysis oil.

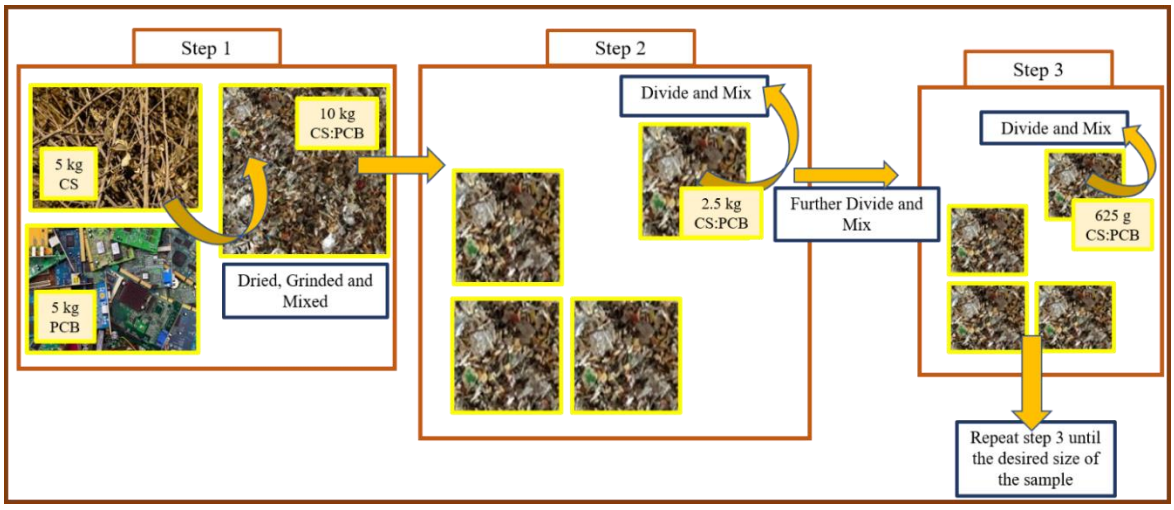

FIGURE 3.1: Sample preparation steps for pyrolysis experiment.

In order to investigate the chemical properties of the feedstock, ultimate and proximate investigation were carried out on dry wt. % basis. The higher heating value (Gross calorific value) in Table 3.2 was calculated using Dulong's formula [184] as below:

$$\text{HHV (MJ/kg)} = \left[338.2 * \text{C}\,\% + 1442.8 * \left(\text{H}\,\% - \frac{\text{O}\,\%}{8}\right)\right] * 0.001 \quad (3.1)$$

In order to analyse metals, 10 g of PCB sample was dissolved in 100 ml of aqua-regia (1:3 - HNO_3: HCl) at room temperature. The solution was then filtered and sent to BEIL-Ankleshwar for AAS analysis, Table 3.1. Copper is the most abundant metal in the printed circuit board, as expected from the literature [185][186]. Iron is the second most common component of PCB.

TABLE 3.1: Heavy metals contents (ml/l) obtained by AAS analysis.

Sample	Copper	Zinc	Nickel	Chromium	Manganese	Lead	Iron
PCB	3937	25	22	4	44	18	1304

3.2 TGA Analysis of raw sample:

Thermogravimetric analysis (TG-DTG), was performed using Mettler Toledo analyser. The system was purged with 50 ml/min flow rate of N_2 gas to avoid combustion. The drying step of TGA had heating rate of 10 ℃/min for all three samples, whereas the pyrolysis stages used three distinct heating rates: 5, 10, and 15 ℃/min with approximately 10 mg of each sample. The sample was placed in a ceramic crucible within the furnace and heated to 700 ℃, after which the TG and DTG curves were calculated using an analytical computer system. The conventional furnace has a temperature precision of ± 2 ℃. The mass change of the sample with temperature during the course of the heating process is recorded and the findings are utilised to compute the degradation kinetics. It must be noted that experiments were performed for same samples for four times to see repeatability of the results.

3.3 Pyrolysis experiments:

A SS 316 fixed bed cylindrical reactor, see Fig. 3.2, was used to carry out pyrolysis experiments with a 100 mm ID (inner diameter), height of 320 mm and 7 mm thickness, surrounded by three parallel electrical heaters each of 2 kW and appropriately insulated with

glass wool. The top of the reactor was open from where 200 g of sample was fed for each experiment and sealed by bolts. Nitrogen was purged at 50 ml/min flow rate through silica frit from the reactor bottom. According to TGA/DTG analysis, the majority of the mass loss occurred up to 500 ℃ temperature only, exceeding this temperature did not result any gas or oil generation. Moreover, the % residue with 10 ℃/min heating rate was lower. The reactor temperature was therefore raised from ambient to 500 ℃ at 10 ℃/min heating rate. As the temperature increased, the feed vapours evolved and passed through glass condenser connected to a chiller which is maintained at 2 ± 0.1 ℃ temperature and generated liquid and non-condensable gases were collected. After the experiment was done, the top of the reactor was opened to remove the char, and the yields of the generated solid and liquid were weighed and their corresponding percentages were calculated.

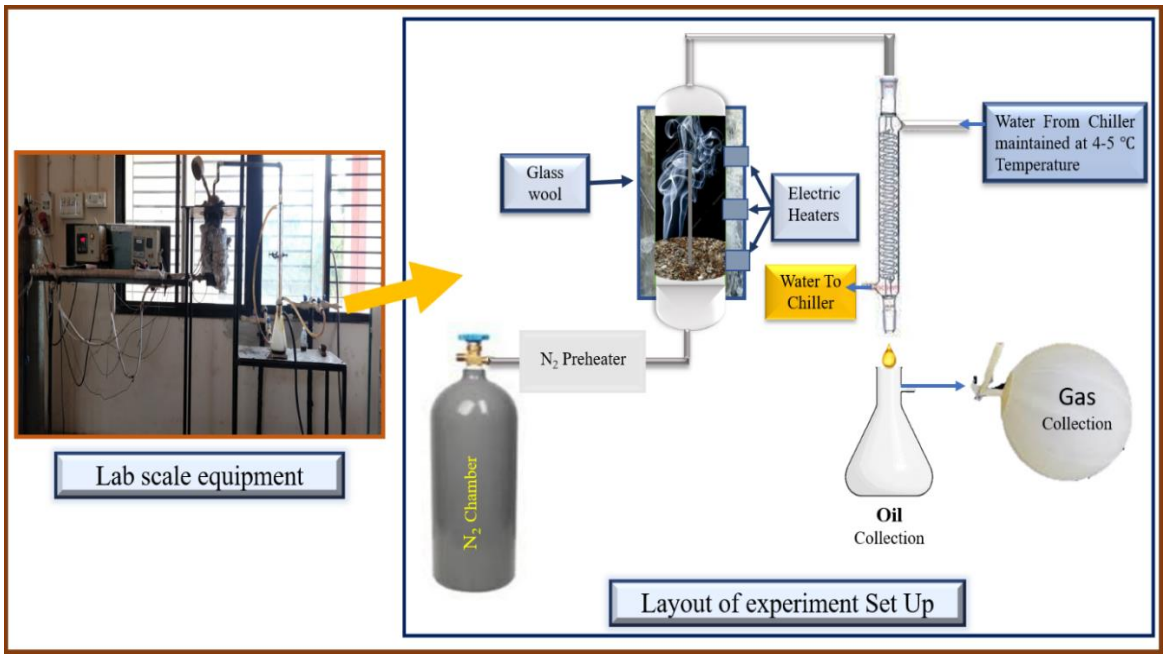

FIGURE 3.2: Lab scale equipment with layout of experimental setup.

3.4 Oil and gas analysis:

Chemical composition of the pyrolysis oil was determined using GC-MS (Gas chromatography–mass spectrometry) analyser by Thermo Scientific TSQ 8000 equipment. The MS element of the system consists of a Triple Quadrupole paired with a TRACE 1300 GC and an auto-sampler for automated sample processing. Helium was used as the carrier gas flowing at 1.2 ml/min through a 15-meter-long, 0.25-mm- ID and 0.25-mm-thick film (SQC). The oil samples were prepared as 10% solution in acetone and peaks were scanned

in the *m*/*z* range from 40 to 650 with an ionizing voltage of 70 eV (electron volt) and an emission current of 350 A of electron ionization (EI) and the results are displayed in **section 5**. Collected gas samples were analysed by gas chromatography with model Shimadzu GC-2014, results are shown in **section 5.8**. Additionally, oil samples were analysed according to FAME standards to determine its fuel characteristics.

3.5 Char Analysis:

Several characterization techniques were utilized to examine and determine the char attributes, such as TGA/DTG was performed using N_2 as inert gas on Mettler Toledo with 10 ℃/*min* heating rate. The sample was kept in a ceramic crucible inside the furnace and heated from ambient temperature to 1000 ℃. The Brunauer-Emmet- Teller (BET) Quanta Chrome Nova 2200e with nitrogen gas physisorption method was used to determine pore volume and surface area. The Barrett-Joyner-Halenda (BJH) approach was used to calculate the amount of nitrogen absorbed and the cumulative volumes of pores from the desorption isotherms. The morphology and surface of char were typically observed using the Field Emission Scanning Electron Microscope (FE-SEM) and X-ray energy dispersive system spectroscopy (EDS). In this investigation, powder was dispersed on carbon tape and analysed using a cold field FESEM Hitachi SU8010 electron microscope with a 5KV acceleration and a theoretical resolution of 1*nm*.

Additionally, the analysis of elements was carried out by X-ray energy dispersive system spectroscopy (EDS) using Brukers EDS XFlash 6130. Fourier Transform-Infrared (FTIR) spectra was used to determine the functional groups which were measured in the range of 250-4000 cm^{-1} present in char samples using a Perkin Elmer spectrum RX-IFTIR spectrometer. The spectral data was collected at a resolution of 1 cm^{-1} and 120 scans. Furthermore, powder XRD (X-ray diffraction) was used to analyse phase and crystalline variant of char samples and data were collected using a PANalytical X'Pert PRO MPD X-ray diffractometer with graphite monochromatized Cu K_α radiation ($\lambda = 0.15406$ nm) and step scanning at $2\theta = 0.020^\circ$ per second from 5˚ to 80˚

CHAPTER 4

Non-isothermal Kinetic Analysis

4.1. Introduction:

The knowledge of the pyrolysis kinetics of the main thermal decomposition process is very important for predicting the pyrolysis behaviour of a material and helps to design a suitable reactor, as well as mathematical modelling of the reactor for process optimization. Process parameters, heat and mass transport limits, physical and chemical properties of the sample, and systematic errors are all factors that might affect the kinetic parameters.

The main purpose of this study is to understand pyrolysis behaviour (such as initial degradation temperatures, thermal degradation rates, and residual weight) of PCB (printed circuit boards with non-metallic fraction) and CS. The present study provides a comparison of the thermal degradation behaviour of the two totally different samples. TGA was used to carry out the pyrolysis process in a nitrogen atmosphere, and thermal analysis curves were generated at three distinct linear heating rates (5, 10, 15 ℃ /min). Three model-free non-isothermal methods such as Kissinger-Akahira-Sunose (KAS), Flynn-Wall- Ozawa (FWO), and Starink were used to calculate apparent activation energy (E_α) and pre-exponential factor (A). Furthermore, with calculated E_α values, the possible decomposition mechanism of all the samples were probed using the Criado differential-integral master plot.

4.2. Kinetic modelling:

The concept of the single-step, solid-state reactions can be represented by Arrhenius equation. It means that the reactant molecules are in an endothermic equilibrium with the active molecules that are involved in the reaction.

$$K(T) = Ae^{\left(-\frac{E}{RT}\right)} \tag{4.1}$$

In Equation (4.1), *E* is the activation energy (the heat of activation) in kJ/mol, *A* is the pre-exponential factor, 1/min, *R* is the gas constant in kJ/mol K, *T* is the temperature in K and *K(T)* is a rate constant. The value of E was supposed to be a constant for single step reactions and it is the energy needed to turn inactive molecules into active molecules. To describe the status of a reacting solid for a single phase reaction, Lewis [187] used the degree of conversion, α. So, the thermogravimetric results can be expressed as,

$$\frac{d\alpha}{dt} = K(1-\alpha)^{n} \tag{4.2}$$

Where n is reaction order. A general kinetic Equation (4.2) is based on an assumption that the rate of process dα/dt is a function of two variables only: degree of conversion (α) and temperature (T). Assuming that the function of two variables can be substituted by a product of two functions variables, *K(T)* and f(α). So, the rate of heterogeneous solid reactions can be described as, [188].

$$\frac{d\alpha}{dt} = K(T)f(\alpha) \tag{4.3}$$

where, *K(T)* is a rate constant, *t* is time and α is the conversion of the raw materials, ranging from 0 to 1, and f(α) is the reaction model that represents a certain solid-state mechanism [189]. Where, the conversion can be defined as:

$$\alpha = \frac{m_0 - m_t}{m_0 - m_f} \tag{4.4}$$

where m_0 is the initial mass of the sample, m_t is the mass of the sample at time *t*, and m_f is the final mass of the sample. Putting values of Equation (4.1) into Equation (4.3), rate of a solid-state reaction will be as,

$$\frac{d\alpha}{dt} = Ae^{-E/RT} f(\alpha) \tag{4.5}$$

Parameters *E*, *A* and reaction model *f(α)* in Equation (4.5) is called kinetic triplets [188]. If the reaction is studied under non-isothermal conditions at a linear heating rate, *β=dT/dt*. In which Equation (4.5) becomes:

$$\frac{d\alpha}{dT} = \frac{A}{\beta} e^{-E/RT} f(\alpha) \tag{4.6}$$

In actual solid state, reaction is complex, which includes multiple solid-gaseous reactions with different rates, like adsorption, desorption, sublimation of gaseous products or reactants on the surface of a reacting solid and diffusion of gaseous products or reactants through a solid [190][187].

Therefore, the effective activation energy derived from the overall kinetic data is a composite number determined by the activation energies of the individual stages and their relative contributions to the overall reaction rate. As a result, the effective activation energy is usually a function of either temperature and conversion, or merely temperature. That's why the concept of variable activation energy E_α is more suitable to the non-elementary nature of heterogeneous solid-state reactions. It should be used to explain how overall reaction rates are affected by temperature [190]. As per previous study, this obtained activation energy is the apparent one and does not have any mechanistic significance [191].

4.2.1 Model Free Methods

There are two basic methods to find the kinetics triplets of complex solid-state reactions, one is model-fitting, and the second is a model-free method, also called iso-conversion method. The model-fitting approaches use a single, unpredictable heating rate [191][192], whereas the model-free method use several heating rates, which eliminates mass transfer constraints. As per Z Yao et al. [193][194], model free techniques have two key benefits: they allow for an evaluation of the variable activation energy, E_α without assuming any particular reaction model and can avoid errors associated with the choice of kinetic model. A Dhaundiyal et al. [195] and H Mahmood et al. [196] employed a model fitting approach (Coats Redfern method [197] based on the Arrhenius equation to test the validity of the model-free method and produce the best appropriate reaction model for the decomposition of weed and lignocellulosic materials, respectively. They observed that kinetic parameters derived at various heating rates for models, as shown in Table 4.1, differed significantly from those

computed using the model-free method. The force-fitting of non-isothermal data to a hypothetical reaction model is the initial cause of disagreement between model-free and model-based runs. Arrhenius parameters are calculated in the form of $g(\alpha)$ in the model fitting of Coats Redfern method, which is previously assumed and not able to discriminate separately temperature dependence of rate constant and conversion, resulting in erroneous estimates of Arrhenius parameters. The possibility of multi-reaction pathways is another key cause of disagreement, as the activation energy determined using the model-based method is a function of T and α. However, the calculated value of activation energy represents the average value for the overall process, which is derived in such a way that it is invariant to the reaction mechanism and kinetics with change in temperature and degree of conversion. With model free methods, there's an opportunity for estimating the relative reactivity of solids by comparing the respective estimated times to accomplish the same extent of conversion at the same temperature. Therefore, these are called the iso-conversion method, and the parameters are calculated as a function of conversion rate [190][191]. In other words, these methods used the rate data associated with a constant conversion to eliminate the reaction rate dependency on the conversion [192][198]. Therefore, Model free iso-conversional approaches, as recommended by [8][9][32], are more realistic and exact when modelling non-isothermal pyrolytic kinetics.

Furthermore, iso-conversional methods can be classified as Iso-thermal and Non-Isothermal methods. The non-isothermal methods are the most commonly used for performing the kinetic analysis of solid-state reactions and were originally developed by assuming a 'n-order' kinetic model. A number of papers on this topic have been already published [188][199][200][201][202][203].

Moreover, we may also categorise Isoconversional methods as differential and integral non-isothermal methods. Differential methods such as Friedman [191][204][205], evaluate the reaction rate at an equivalent stage of the reaction for different heating rates. It uses plotting $d\alpha/dt$ versus $1/T$. It tends to be numerically unstable and extremely subtle to experimental noise. Whereas, Integral methods involve the plotting of logarithmic function versus $1/T$, which depends on the heating rate and often the temperature. This logarithmic function depends on the mathematical approximation for the temperature integral used [206], which is different for the different methods. This approximation causes inaccuracies which depend on the type of approximation chosen. M J Starink in 2003 [204] explained this approximation

of the temperature integral to understand different methods. Differential method would be more accurate if transformation rate can be measured with a precision. In certain cases, however, it would be difficult to guarantee that the rate of transformation will be calculated to the precision, and in these cases, Integral methods for activation energy analysis are suggested [191][204]. This is the reason we have chosen Integral methods to find kinetics and, as different methods use different mathematical approximation, it is necessary to evaluate kinetics with different methods and conclude which one is more suitable for particular solid decomposition.

Integrating Eq. (4.6), and replacing *E/RT* by *x* and after rearranging it leads to,

$$g(\alpha) = \frac{A}{\beta}\int_{To}^{Tmax} e^{\left(-\frac{E}{RT}\right)}\, dT = \int_0^{\alpha} \frac{d\alpha}{f(\alpha)} = \frac{AE}{\beta R} p(x) \tag{4.7}$$

Where, *p(x)* is a function known as the Arrhenius integral, which can be calculated numerically or by using various approximations. When we utilise Doyle's estimate [207][204] for *p(x)* we get the popular equation proposed by Ozawa [208] for determining the activation energy by iso-conversion methods from Equation (4.3). Doyle has found that for *20< E/RT <60, log p(E/RT)* may be closely approximated by Equation below, [207][208]

$$Log\ p\left(\frac{E}{RT}\right) \cong -2.315 - 0.457\ \frac{E}{RT} \tag{4.8}$$

That reduces to Flynn wall Ozawa equation [195][208];

$$ln\ \beta = ln\ \frac{AE_\alpha}{g(\alpha)R} - 5.330 - 1.052\ \frac{E_\alpha}{RT} \tag{4.9}$$

where, E_α is the apparent activation energy or can also be called as variable activation energy. The plot of *ln β* against *1/T* at different heating rate gives straight line with slope $-1.052E_\alpha/R$. Finding the slope for different (α) reveals the dependency of E_α on α [198][206].

Murray and White [204][209] provide a more precise estimate for *20< E/RT <50* in the form of Kissinger, sometimes known as the Kissinger–Akahira–Sunose (KAS) Equation [200][210];

$$ln\left(\frac{\beta}{T^2}\right) = ln\left(\frac{AE_\alpha}{Rg(\alpha)}\right) - \frac{E_\alpha}{RT} \quad (4.10)$$

For a constant value of α, plotting $ln(\beta/T^2)$ vs. $1/T$ will give a straight line with a slope of E_α/R. The profile of apparent activation energy can be generated for the different conversion [211]. Starink approximated expression of FWO and KAS method, which can be transformed into the same general formula as [212]:

$$ln\left(\frac{\beta}{T^S}\right) = C - \left(B\frac{E_\alpha}{RT}\right) \quad (4.11)$$

where, parameters $s=0$, $B=0.4567$ and $s=2$, $B=1$ for FWO and KAS method, respectively. As per Starink both the parameters can be adjusted to $s=1.8$, $B=1.0033$, respectively. As a result, the Starink Equation can be rewritten as [200][204][205];

$$ln\left(\frac{\beta}{T^{1.8}}\right) = C - 1.0037\left(\frac{E_\alpha}{RT}\right) \quad (4.12)$$

where, $C = ln\left(\frac{AE_\alpha}{Rg(\alpha)}\right)$, for a given conversion fraction α, the points of $ln(\beta/T^{1.8})$ versus $1/T$ at different heating rates can be fitted to a straight line and the slope of the line corresponds to $-1.0037\left(\frac{E_\alpha}{RT}\right)$. As a result, the slope of the straight line can be used to estimate the apparent activation energy E_α [191][205].

4.2.2 Criado method

Many studies that have examined experimental data for the solid-state mechanism have used reference theoretical curves, referred to as "master plots" in their analyses [213][214][215]. It uses the concept of reduced time plots, introduced by Ozawa [191][208] for α against t/t_α, where t_α is the time to reach a certain value of α (usually 0.5 to 0.9). In this sense, the master plot is a characteristic curve independent of the measurement condition, which is readily obtained from experimental results [213][216].

To use this method for determination of reaction mechanism, known value of apparent activation energy is required. For that, experimental data can be compared against a collection of theoretical model plots and the model that exactly match the data can be chosen. This makes it possible to view the data in terms of the mechanism described by the chosen

reaction model. The master theoretical curves can be generated through the *Z(α)* function [13], where,

$$Z(\alpha) = f(\alpha)\, g(\alpha) \tag{4.13}$$

Thus, *Z(α)* versus *α* for different reaction mechanisms can be plotted as presented in Table 4.1 [197][199][214]. The equation is given by,

Theoretical curve $$\frac{Z(\alpha)}{Z(0.5)} = \frac{f(\alpha)g(\alpha)}{f(0.5)g(0.5)} \tag{4.14}$$

Experimental curve (Master curve) $$\frac{Z(\alpha)}{Z(0.5)} = \left(\frac{T_\alpha}{T_{0.5}}\right)^2 \frac{(d\alpha|dt)_\alpha}{(d\alpha|dt)_{0.5}} \tag{4.15}$$

TABLE 4.1: Different degradation mechanisms with f(α) and g(α).

No.	Function name	Mechanisms	f(α)	g(α)
m1	Jander equation	Diffusion, 3D (spherical symmetry)	$3/2(1 - \alpha)^{2/3}[1 - (1 - \alpha)^{1/3}]^{-1}$	$[1 - (1 - \alpha)^{1/3}]^{1/2}$
m2	G–B equation	Diffusion,3D (column symmetry)	$3/2[(1 - \alpha)^{-1/3} - 1]^{-1}$	$1 - 2\alpha/3 - (1 - \alpha)^{2/3}$
m3	Anti–Jander equation	Diffusion, 3D	$3/2(1 + \alpha)^{2/3}[(1 + \alpha)^{1/3} -1]^{-1}$	$[(1 + \alpha)^{1/3} - 1]^2$
m4	Z–L–T equation	Diffusion, 3D	$3/2(1 - \alpha)^{4/3}[(1 - \alpha)^{-1/3} - 1]^{-1}$	$[(1 - \alpha)^{-1/3} - 1]^2$
m5	Avrami–Erofeev Equation	Random nucleation and nuclei growth, n=3	$3(1 - \alpha)\,[-\ln(1 - \alpha)]^{2/3}$	$[-\ln(1 - \alpha)]^{1/3}$
m6	Avrami–Erofeev Equation	Random nucleation and nuclei growth, n=2	$2(1 - \alpha)\,[-\ln(1 - \alpha)]^{1/2}$	$[-\ln(1 - \alpha)]^{1/2}$
m7	Avrami–Erofeev Equation	Random nucleation and nuclei growth, n=3/2	$3/2(1 - \alpha)\,[-\ln(1 - \alpha)]^{1/3}$	$[-\ln(1 - \alpha)]^{2/3}$
m8	Avrami–Erofeev Equation	Random nucleation and nuclei growth, n=4/3	$4/3(1 - \alpha)\,[-\ln(1 - \alpha)]^{1/4}$	$[-\ln(1 - \alpha)]^{3/4}$
m9	Geometrical contraction	Shrinkage geometric shape ((column symmetry)	$3(1 - \alpha)^{2/3}$	$1 - (1 - \alpha)^{1/3}$
m10	Geometrical contraction	Shrinkage geometric shape, (spherical symmetry)	$2(1 - \alpha)^{1/2}$	$1 - (1 - \alpha)^{1/2}$
m11	Reaction order n=2	Chemical reaction	$(1 - \alpha)^2$	$(1 - \alpha)^{-1} -1$
m12	Reaction order n=1	Chemical reaction	$(1 - \alpha)$	$-\mathrm{Ln}(1-\alpha)$
m13	Reaction order n=3	Chemical reaction	$(1 - \alpha)^3$	$((1 - \alpha)^{-2} -1)/2$

Plotting the graph of $\frac{Z(\alpha)}{Z(0.5)}$ vs α for different mechanisms, a theoretical curve will be obtained. By the derived apparent activation energy plot, experimental curve (master curve) can be made. By comparing these two curves, the best match of the reaction mechanism can be found.

4.3 Result and Discussion:

4.3.1 Characterization of Raw Material

An ultimate and proximate analysis of the PCB, CS and different CS:PCB compositions with different ratios are shown in Table 4.2**,** on dry wt.% basis. High volatile matter of CS indicates the high reactivity compared to PCB. The PCB sample had a smaller loss on drying (LOD) (14.05 %) than the CS sample (23.93 %), which can be related to dehydration response of water content as well as release of more volatile components such as CO_2, CO, and CH_4. Therefore, with increasing CS ratio, amount of LOD in each CS:PCB composition increasing and it is highest for CS70 (21.28 %). The presence of high amount of incombustible inorganic material in PCB results in increased amount of ash in the CS:PCB composition.

TABLE 4.2: Proximate and Ultimate analysis of the PCB, CS and Compositions.

Sample	HHV MJ/kg	LOD (%)	Proximate Analysis (Dry wt. % basis)			Ultimate Analysis (Dry ash wt. % basis)					
			Ash (%)	Volatile Material (%)	Fixed C (%)	C (%)	H (%)	N (%)	S (%)	O (%)	Others * (%)
PCB	6	14.05	43.95	41.87	0.13	23.27	2.51	1.87	0.22	28.18	43.95
CS	10	23.93	5.49	70.51	0.07	36.54	4.54	2.45	0.16	50.82	5.49
CS30	10	7.12	35.31	57.45	0.12	30.66	3.32	2.14	0.05	28.52	35.31
CS40	9	8.12	23.48	68.32	0.08	29.97	4.01	1.7	0.10	40.74	23.48
CS50	11	12	23.73	64.2	0.07	29.76	5.45	2.86	0.15	38.05	23.73
CS60	7	10.16	19.88	69.87	0.09	26.69	4.15	2.35	0.22	46.84	19.75
CS70	6	21.28	16.03	62.58	0.11	26.17	4.21	2.08	0.14	51.37	16.03

* Calculated from difference of C, H, N, S and O.

The higher heating value (Gross calorific value) of all the samples was calculated using Dulong's formula [217] as per Equation (3.1).

The solid char residues for the co-pyrolysis, however, ought to exhibit a similar pattern to that of the ash content. Since this feedstock have low N and S contents, there will be fewer harmful gas emissions when they are thermally degraded. However, it is most important to understand that, the results produced here are based on a composition that is a heterogeneous blend of CS and PCB, which is most crucial to comprehend. This PCB is a complex mixture of epoxy resin and some residual metals and polymers from the separation process. So, the results of proximate and ultimate analysis based on very small amount may slightly vary with the bulk quantity of the sample pyrolyzed, ultimately affects the thermal degradation behaviour.

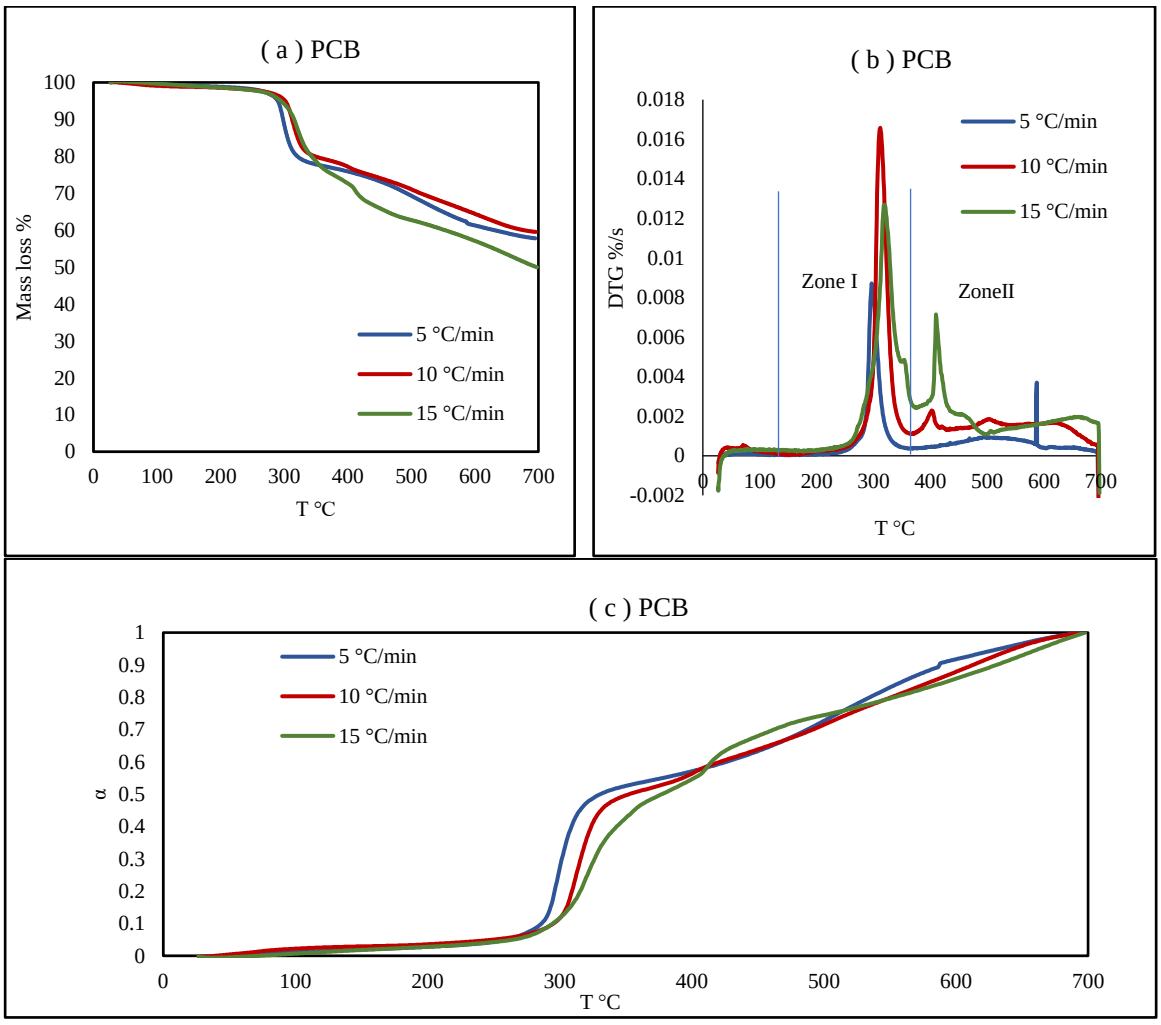

FIGURE 4.1: Thermogravimetric, DTG and variation of conversion as a function of temperature for the pyrolysis of PCB (a, b, c) at heating rates of 5, 10 and 15 ℃/min.

4.3.2 Thermogravimetric Analysis

The mass loss in %, DTG and conversion curves from TGA data for PCB, under inert atmosphere from ambient to 700 ℃ temperature, are shown in Fig. 4.1. Whereas, Fig. 4.2, 4.3 and 4.4 shows mass loss in %, DTG and conversion data curve for CS and its different composition with PCB, respectively. As shown in Fig. 4.1 (b) and 4.3**,** DTG curves, the three steps that make up the entire thermal process are the small loss zone (referred to as Demosturization zone), the first zone (active pyrolysis), and second zone (passive pyrolysis). Notably, the conversion displayed a predictable pattern for a sample heated at three different heating rates 5, 10 and 15 $℃/min$, See Fig. 4.1 (c) and 4.4.

TABLE 4.3: Mass loss in % for First and second zone of all samples.

Sample	Heating Rate ℃/min	First Zone ℃				Second Zone ℃			
		T_i	T_{max}	T_f	Mass loss %	T_i	T_{max}	T_f	Mass loss %
PCB	5	180.99	297.13	359.59	22	360.34	494.47	577.15	14
	10	207.69	312.03	369.60	19	370.43	402.22	577.12	13
	15	207.46	319.39	377.30	24	378.05	410.31	577.19	16
CS	5	147.94	279.26	350.78	48	351.45	434.09	571.67	34
	10	172.08	292.39	374.51	50	375.35	436.04	577.11	27
	15	173.50	300.23	376.56	50	377.31	433.13	577.79	30
CS30	5	122.09	298.13	342.12	36	342.87	388.70	577.41	33
	10	188.11	288.01	376.38	44	376.38	423.65	577.14	28
	15	181.87	303.25	371.78	32	372.53	477.50	577.01	22
CS40	5	161.50	300.85	334.51	19	335.26	401.01	577.21	55
	10	168.25	313.32	363.47	37	364.29	491.53	576.89	32
	15	180.87	302.25	370.78	32	371.53	399.08	577.01	22
CS50	5	121.34	297.37	341.37	36	342.12	387.93	577.41	33
	10	152.22	289.72	371.71	42	372.54	430.32	576.88	28
	15	152.25	317.36	366.15	36	366.88	489.98	577.74	27
CS60	5	172.31	279.11	340.68	36	341.42	358.00	562.27	32
	10	187.26	288.00	375.54	44	376.38	423.65	577.14	28
	15	176.93	298.29	377.45	45	378.19	461.01	577.39	31
CS70	5	175.75	280.41	352.43	44	353.10	444.04	577.30	37
	10	179.69	292.15	368.74	44.5	369.58	443.70	576.89	27.5
	15	187.15	293.52	352.65	23	353.37	388.56	577.09	45

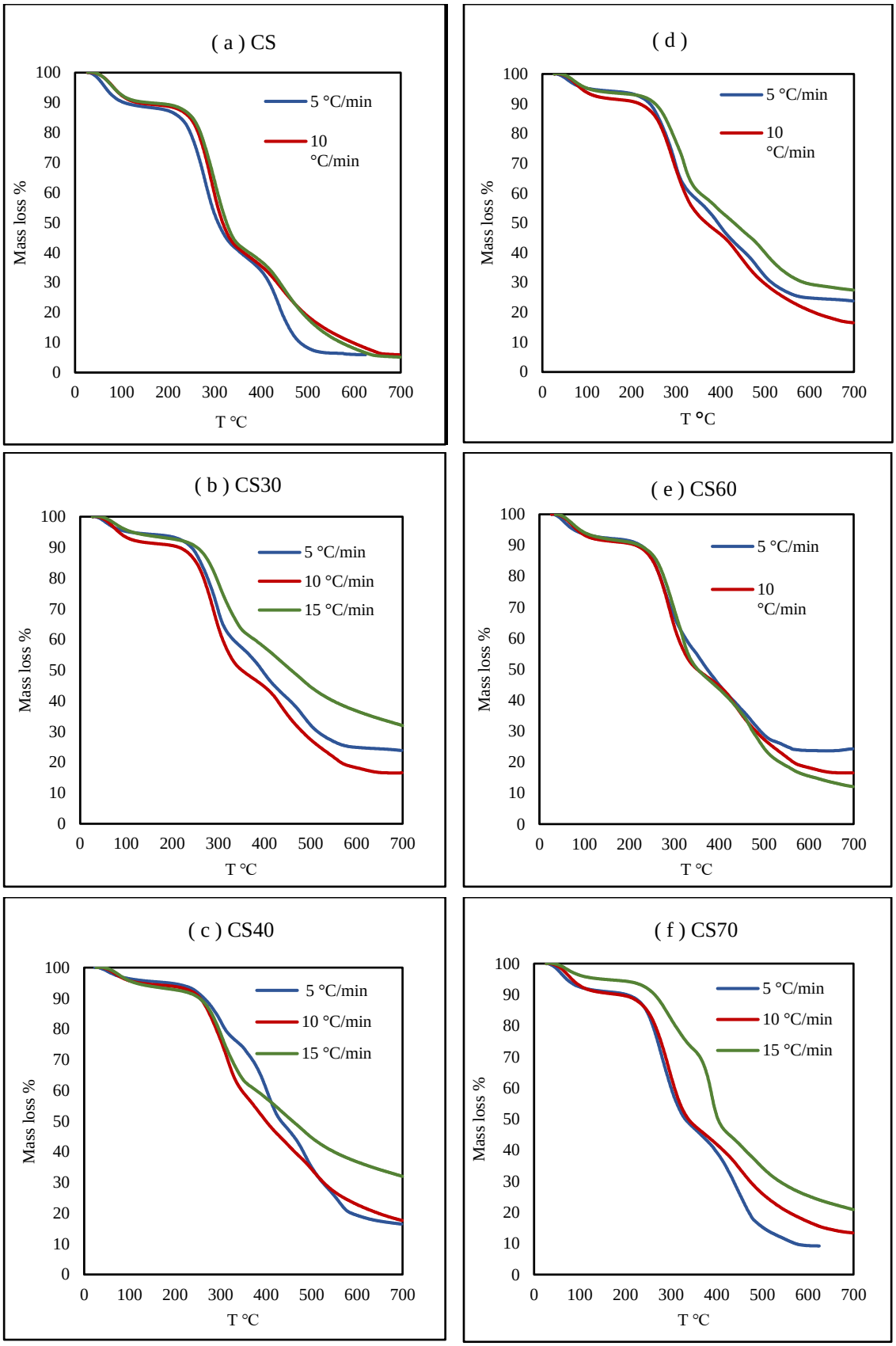

FIGURE 4.2: Mass loss % plots at heating rates of 5, 10 and 15 ℃/min for CS, CS30, CS40, CS50, CS60 and CS70.

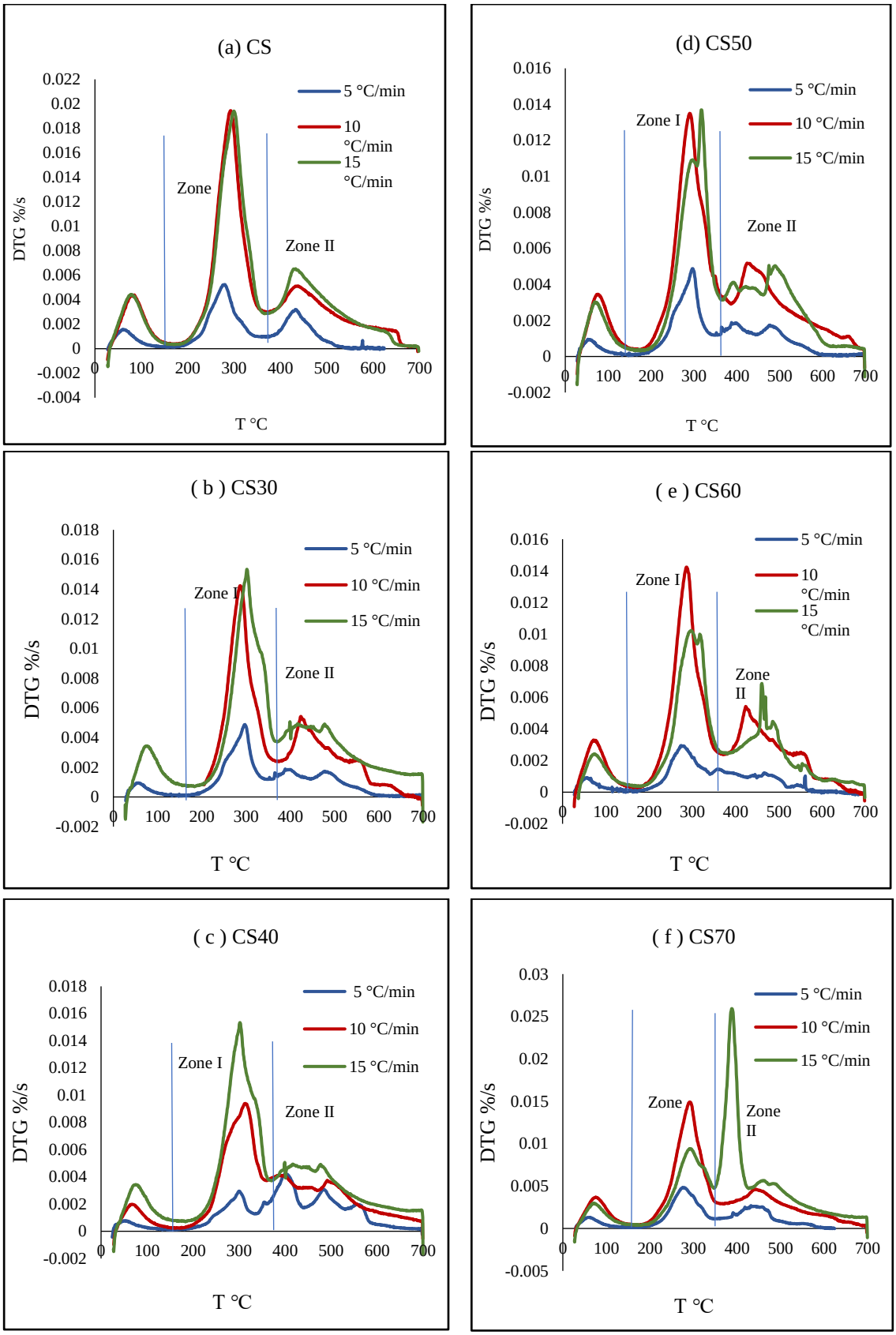

FIGURE 4.3: DTG plots at heating rates of 5, 10 and 15 ℃/*min* for CS, CS30, CS40, CS50, CS60 and CS70.

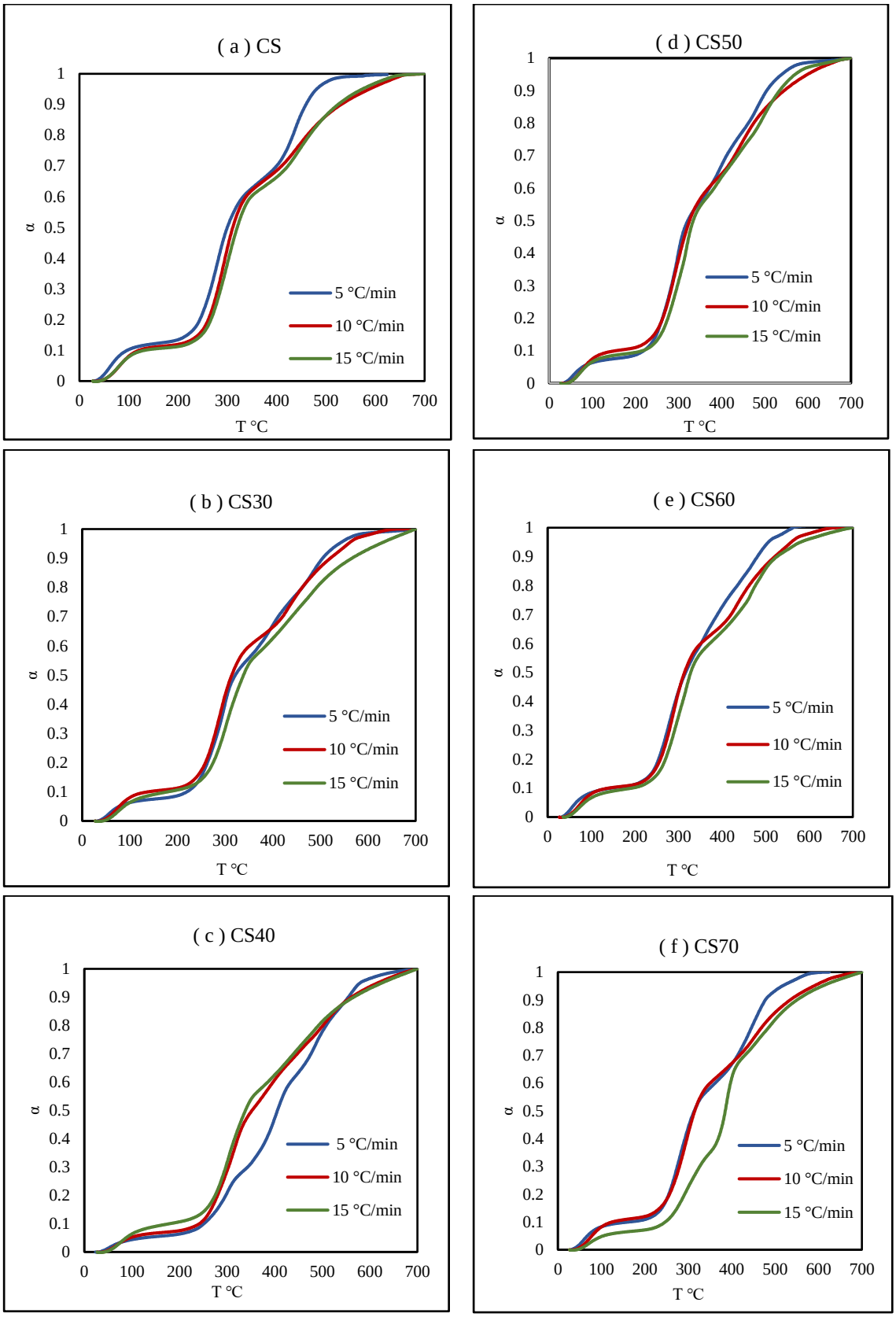

FIGURE 4.4: Conversion vs Temperature plots at heating rates of 5, 10 and 15 $℃/min$ for CS, CS30, CS40, CS50, CS60 and CS70.

Table 4.3 displays the mass loss in Zones I and II together with T_{in}, T_f, and T_{max} (initial, final and maximum temperature of mass loss, respectively) at the DTG peak. Aboulkas and Harfi

[210] claim that the emission of water as well as low-molecular-weight gases caused the sample to soften and undergo molecular rearrangement prior to breakage at Demosturization stage. According to Quan et al. [218], the mass loss (nearby 1%) at demoisturization zone in PCB indicates the elimination of water, HBr, CO_2, CH_4, and CH_3COCH_3. While the depolymerization and vitrification transition in CS cause moisture loss that results in a 10–11% mass loss [22][180], and in CS:PCB composition this mass loss varied from 6–10% when heated at different rates, see Table 4.4. The position of the TG curve, the rate of degradation, and the location of the maximum temperature (T_m), in DTG peaks are all influenced by the heating rate. Although the reaction time is reduced with a higher heating rate, a higher temperature is also needed for the sample to breakdown [195].

TABLE 4.4: Mass loss in % for Demoisturisation and Char generation.

Sample	**Heating Rate** ℃/min	**Demosturization**	**Char Generation**	**Overall Mass loss %**	**Residue %**
		Mass loss %	Mass loss %		
PCB	5	1	5	42	58
	10	1.5	6.5	40	60
	15	1.5	8.5	50	50
CS	5	11	1	94	6
	10	11	6	94	6
	15	10	5	95	5
CS30	5	5	2	76	24
	10	9	3	84	16
	15	7	7	68	32
CS40	5	5	5	84	16
	10	6	7	82	18
	15	7	7	68	32
CS50	5	5	2	76	24
	10	8	6	84	16
	15	6	4	73	27
CS60	5	8	0	76	27
	10	9	3	84	16
	15	9	3	88	12
CS70	5	10	0	91	9
	10	10	5	87	13
	15	5	6	79	21

Moreover, the rate of mass loss is temperature dependent: the higher the temperature, the larger the mass loss because pyrolysis process proceeds fast at higher temperatures [219][220]. According to Manon et al. [221], the breakdown of cellulose and hemicellulose is responsible for the production of a sharp DTG peak in CS, also approved by S. Munir et al. [222]. For PCB sample, this is due to the rupture of ether bonds in brominated resin into bisphenol A, propyl alcohol, and tetra-bromo-bisphenol-A, also the epoxy group may rupture, resulting in the release of small molecules [13]. However, the degradation of hemicellulose and lignin for CS and tetra-bromo-bisphenol-A for PCB can be seen as less pronounced shoulders in the second zone.

For different heating rates ranging from 5 to 15 ℃/min, main pyrolysis process starts at approximately 180-207 ℃, 147-173 ℃, 123-182℃, 162-181℃, 121 – 152 ℃, 172-176℃, and 175-187℃, for the Zone I and quickly moves to the Zone II with increasing temperature until about 359-377 ℃, 350-376 ℃, 342-371℃, 334-370℃, 342-367 ℃, 340-377℃, and 352-368℃ for PCB, CS, CS30, CS40, CS50, CS60, and CS70, respectively. Here, only the first and second zones of pyrolysis, which correspond to the actual stages of pyrolysis, were used for the kinetic analysis and mechanism prediction. After then, weight loss gradually reduces with varying heating rates, reaching 577 ℃, at which point devolatilization stops, indicating the stage of char production and carbonization. The mixture of carbon and ash generated throughout the entire degradation along with some unreacted material is referred to as a % residue, see Table 4.4. In samples with low volatile components and high ash, this residue value was higher. The amount of PCB residue left over is relatively very high (50-60 wt.%) and the results are consistent with earlier investigations [223][218]. However, only 5–6% of solid residue was found in the case of CS, whereas for CS:PCB composition, minimum solid residues about 9 % for CS70 at 5 ℃/min heating rate and maximum 32 % of solid residue for CS30 and CS40 at 15 ℃/min is found. This demonstrates the combined effects of the presence of more inorganic compounds and a shortened reaction time due to a faster heating rate, as was previously discussed. It should be noted that with a heating rate of 10 ℃/min for all compositions, the value of % residue is at a minimum and consistent with 13–18%. It indicated that the co-pyrolysis of PCB with CS increased the thermolysis efficiency at this heating rate, especially with CS70 composition (with % residue 13).

4.3.3 Kinetic analysis

The results of thermogravimetric analysis were intended to measure the kinetic parameters using model-free methods. Using KAS, FWO, and Starink methods the activation energy (E_α) and pre-exponential factor (A) were obtained.

To determine the kinetic parameters, the value of α ranging from 0.1 to 0.9 during the major thermal decomposition process were chosen, at different heating rate. Further, the results before 0.2 conversion and after 0.9 conversion are having very low value of correlation coefficient and were not reliable, so average value was chosen from 0.2 to 0.9 conversion. The FWO, KAS, and Starink plots for different values of conversion of zone I and II were calculated with Equation (4.9), (4.10) and (4.12) for PCB and CS samples as shown in Fig. 4.5, Fig. 4.6, respectively. Whereas, the comparison of plots for the same methods with different composition are shown in Fig. 4.7, 4.8 and 4.9, respectively. The apparent activation energies were obtained from the slopes and compiled in Table 4.5 to Table 4.11 for PCB, CS and CS:PCB compositions, respectively. The calculated correlation coefficients, R^2, correspond to linear fittings and were higher for all cases except PCB second zone. This could be the result of a complex reaction mechanism, implying that the activation energy values are reliable. The reactivity and sensitivity of a reaction rate are also determined by activation energy. A higher value of activation energy indicates the presence of a complex reaction. From results, it can be observed that apparent activation energy for FWO, KAS, and Starink methods are varying significantly for all conversions which shows the presence of a multi-step complicated process in the solid-state matrix. It can be seen from Fig. 4.5 to 4.9, that all the data points are fitting in straight lines at different conversion degrees and are nearly parallel through the iso-conversion methods, which represent the unchanged reaction mechanisms of a single zone of the pyrolysis process in all the samples. The slower the reaction rate, the bigger the space between two consecutive fitting lines. As a result, the scenario suggests that the reaction rate changes as the conversion degree increases. Furthermore, in TG curves, a smaller distance equates to a steeper slope, but in DTG curves, a smaller distance corresponds to a higher reaction rate [180].

The kinetic parameters computed using the Starink approach followed the same pattern as those calculated using the KAS method, as shown in Tables 4.5 – 4.11. The FWO approach yields somewhat higher energy values than KAS and Starink, as evidenced by literature.

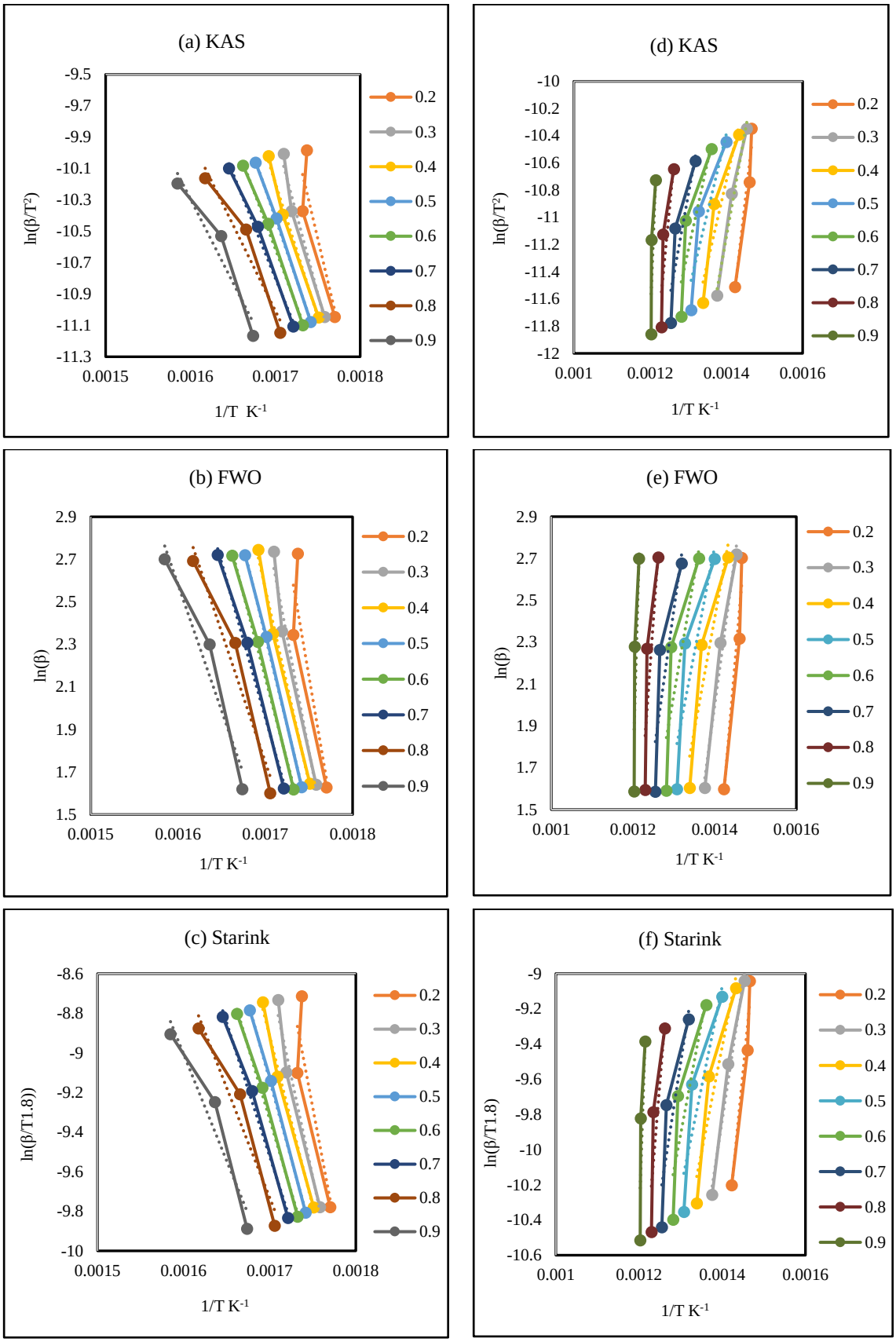

FIGURE 4.5: Curve fittings to kinetic model proposed by KAS, FWO and Starink for PCB 1st (a,b,c) and 2nd (d,e,f) Zone.

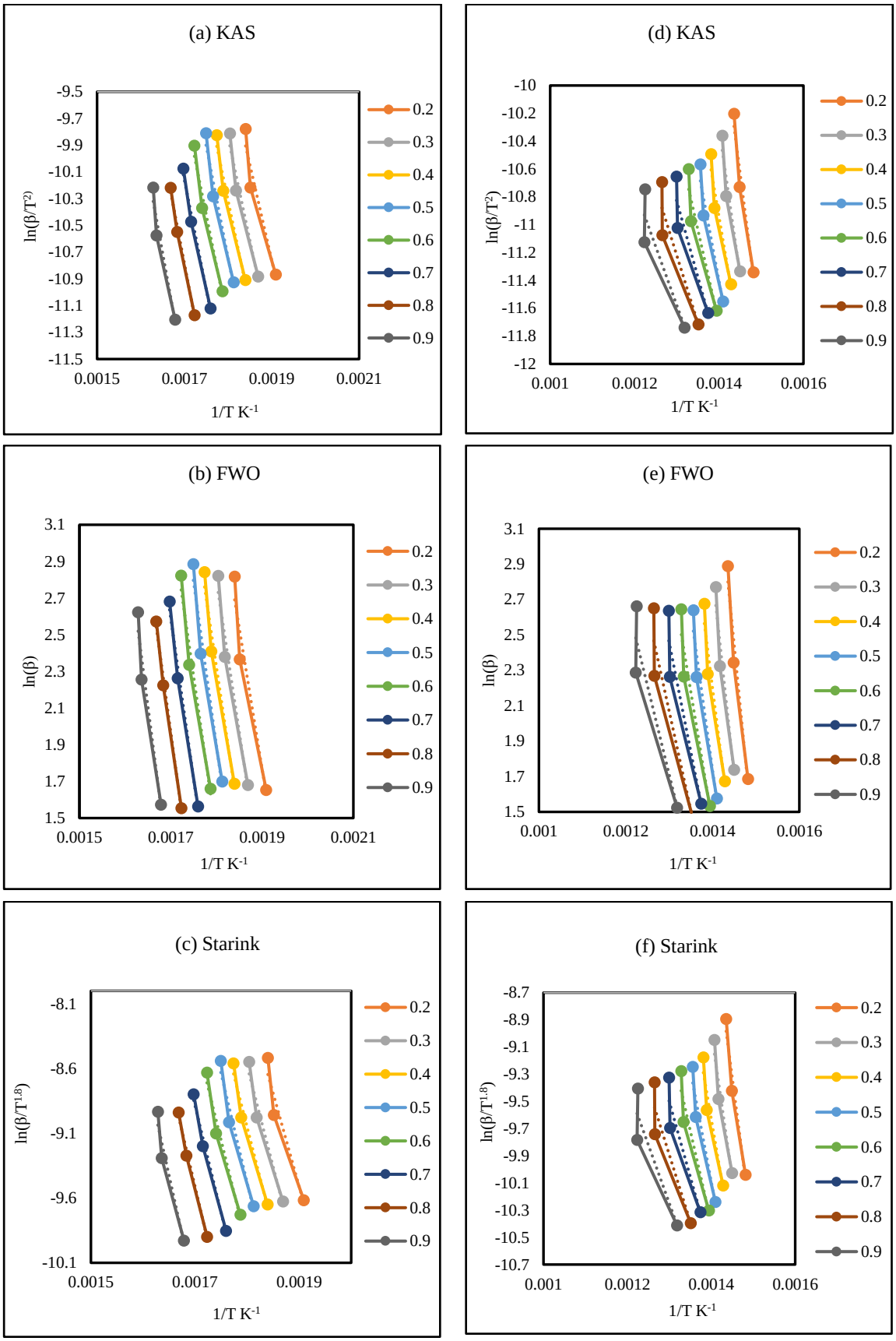

FIGURE 4.6: Curve fittings to kinetic model proposed by KAS, FWO and Starink for CS 1st (a,b,c) and 2nd (d,e,f) Zone.

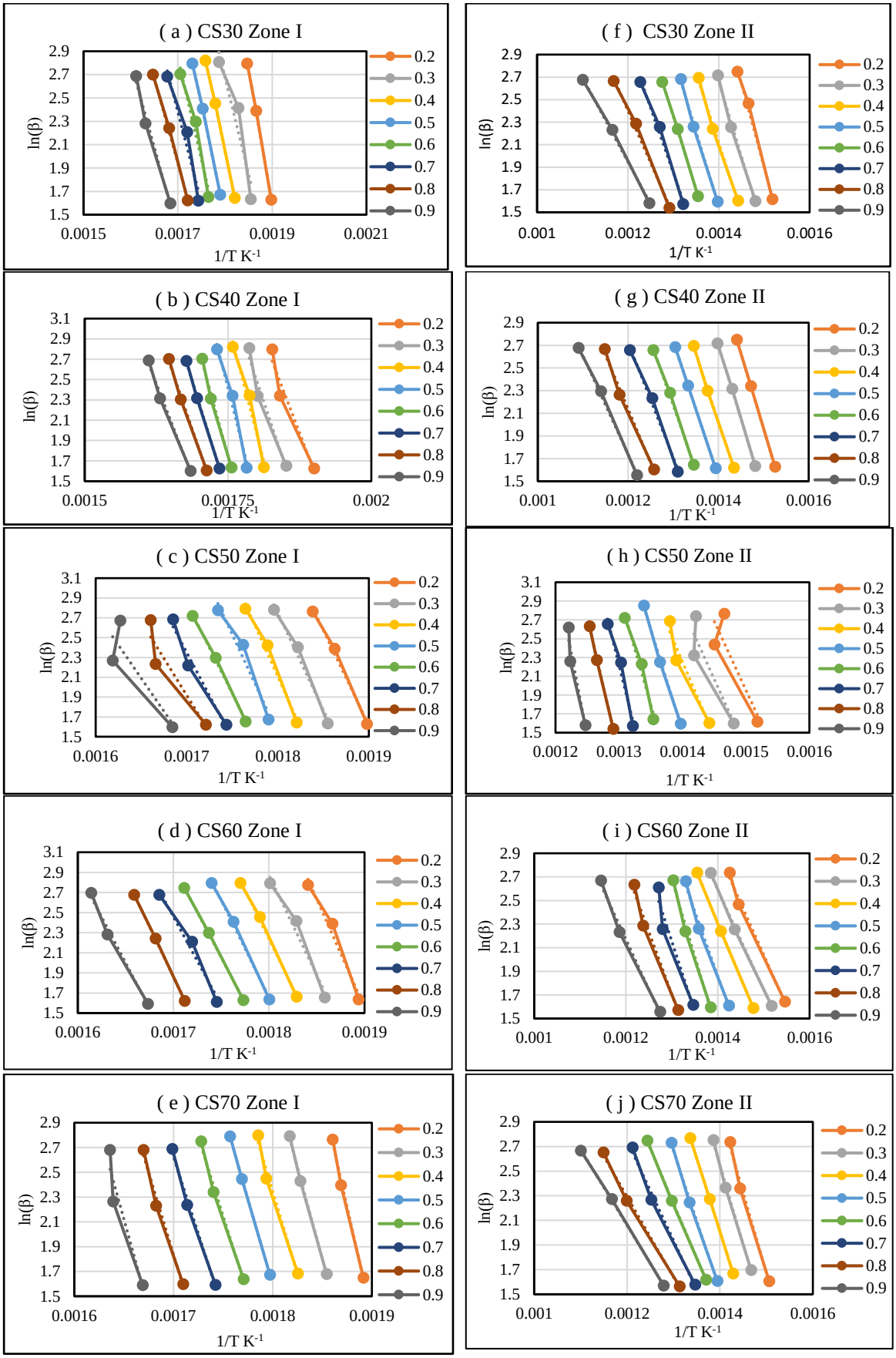

FIGURE 4.7: FWO plots of co-pyrolyzed samples for the First (a,b,c,d,e) and second zone (f,g,h,i,j).

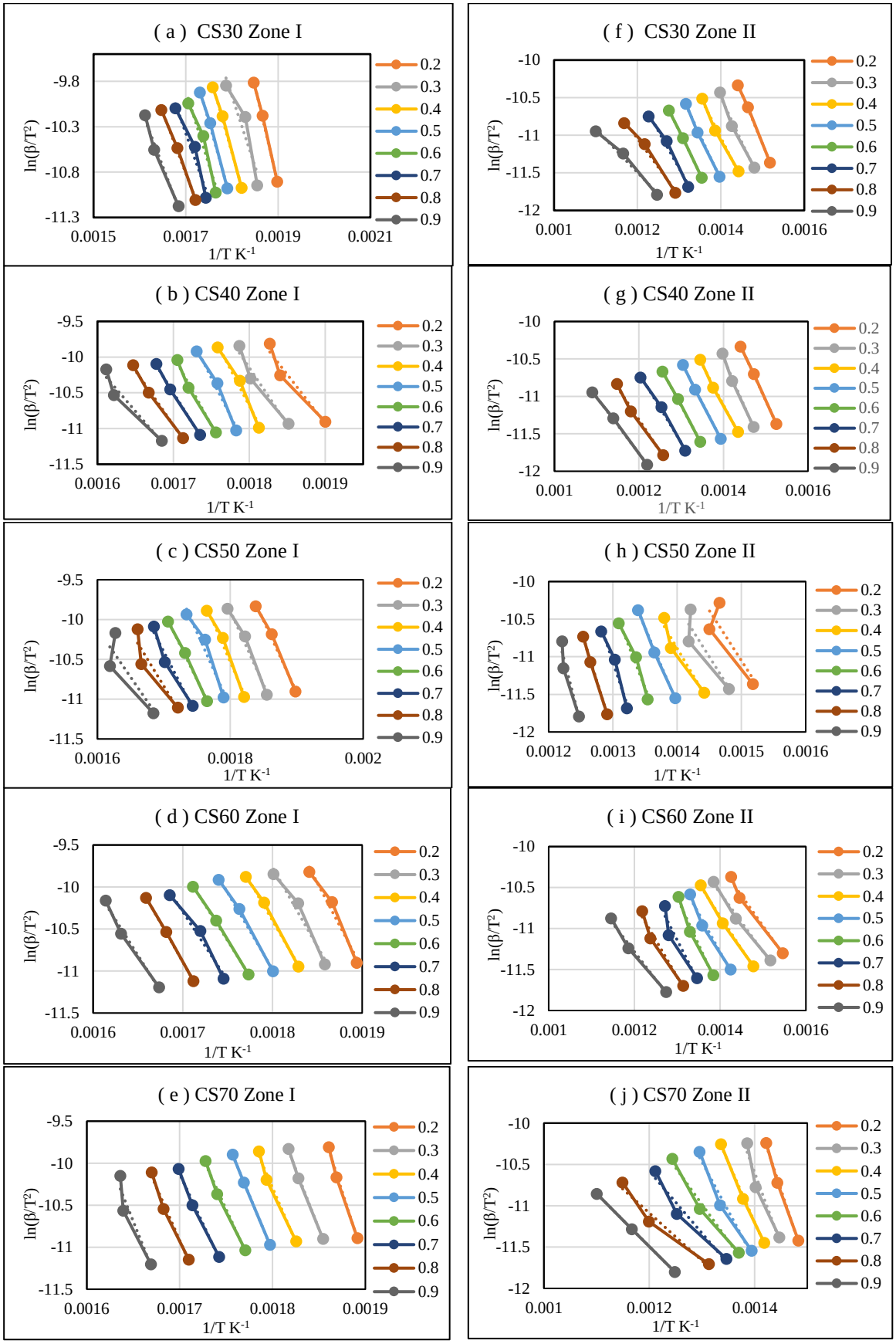

FIGURE 4.8: KAS plots of co-pyrolyzed samples for the First (a,b,c,d,e) and second zone (f,g,h,i,j).

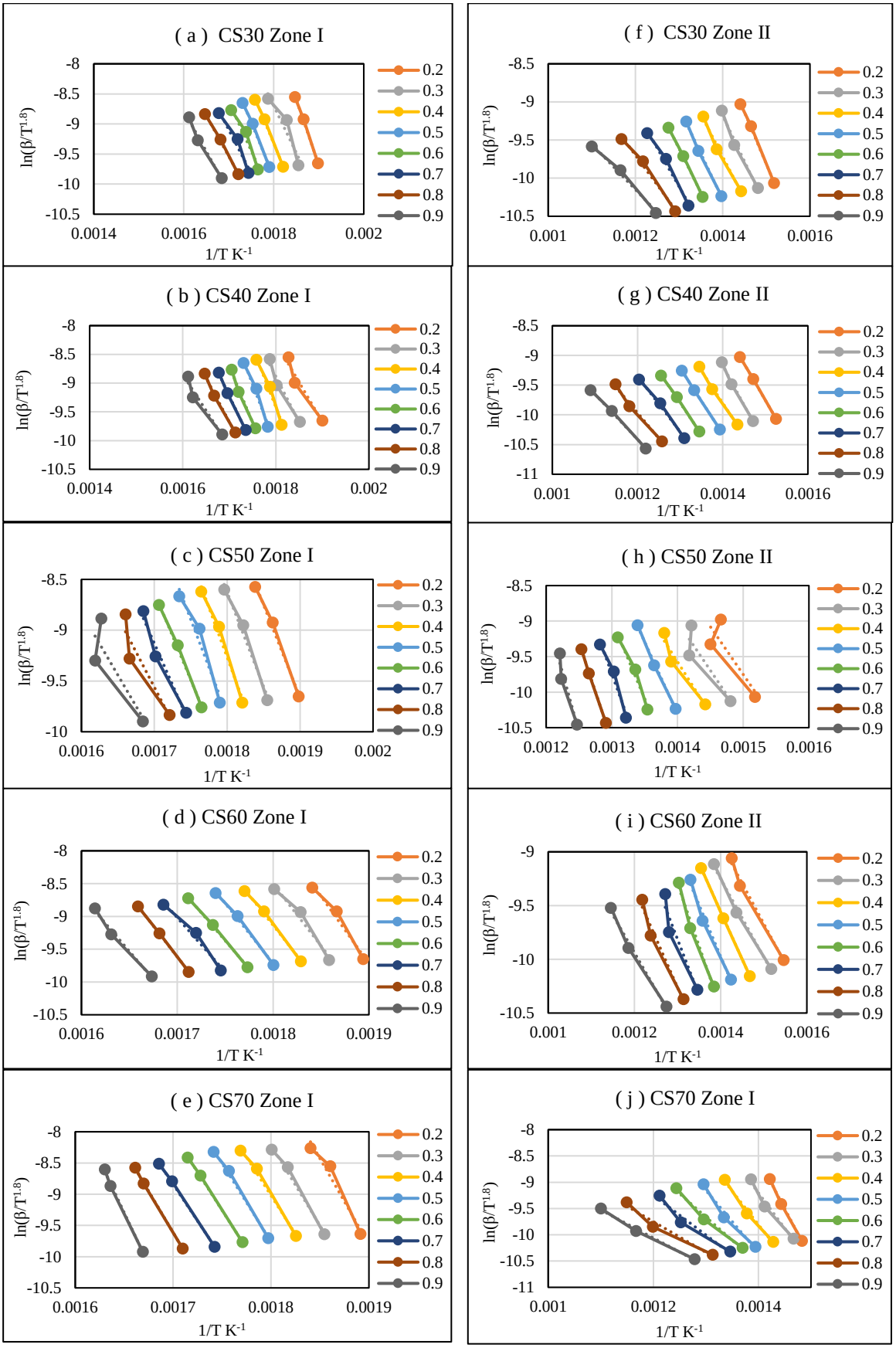

FIGURE 4.9: Starink plots of co-pyrolyzed samples for the First (a,b,c,d,e) and second zone (f,g,h,i,j).

TABLE 4.5: Activation energy obtained by model-free methods for PCB.

PCB (α)	First Zone						Second Zone					
	KAS		FWO		Starink		KAS		FWO		Starink	
	E (KJ/mol)	R^2	E (KJ/mol)	R^2	E (KJ/mol)	R^2	E (KJ/mol)	R^2	E (KJ/mol)	R^2	E (KJ/mol)	R^2
0.1	165.98	0.57	166.57	0.59	166.29	0.57	-724.18	0.88	-677.79	0.88	-720.40	0.88
0.2	190.61	0.77	190.21	0.79	190.85	0.77	-202.37	0.95	-181.41	0.94	-200.47	0.95
0.3	168.27	0.97	169.06	0.97	168.60	0.97	-131.06	0.98	-113.41	0.97	-129.41	0.98
0.4	141.89	0.99	144.05	0.99	142.33	0.99	-101.62	0.90	-85.21	0.87	-100.05	0.89
0.5	130.58	0.99	133.37	0.99	131.07	0.99	-97.11	0.83	-80.65	0.79	-95.53	0.83
0.6	120.59	0.99	123.94	0.99	121.12	0.99	-106.57	0.79	-89.36	0.75	-104.93	0.79
0.7	111.12	0.99	115.02	0.99	111.70	0.99	-128.65	0.80	-110.03	0.76	-126.90	0.79
0.8	91.42	0.94	96.42	0.95	92.08	0.94	-242.42	0.76	-217.76	0.74	-240.20	0.76
0.9	88.55	0.92	93.88	0.94	89.24	0.93	-596.35	0.70	-553.80	0.69	-592.79	0.70
Avg. (0.2-0.9)	130.38		133.24		130.87		-200.77		-179.95		-198.78	

TABLE 4.6: Activation energy obtained by model-free methods for cotton stalk.

CS (α)	First Zone						Second Zone					
	KAS		FWO		Starink		KAS		FWO		Starink	
	E (KJ/mol)	R^2	E (KJ/mol)	R^2	E (KJ/mol)	R^2	E (KJ/mol)	R^2	E (KJ/mol)	R^2	E (KJ/mol)	R^2
0.1	102.82	0.89	105.90	0.91	103.30	0.9	149.96	0.95	153.04	0.96	150.50	0.96
0.2	118.88	0.93	121.43	0.94	119.33	0.93	195.91	0.96	197.06	0.96	196.33	0.96
0.3	128.57	0.96	130.81	0.96	129.00	0.96	177.49	0.93	179.77	0.94	178.00	0.93
0.4	130.40	0.96	132.7	0.97	130.84	0.96	149.04	0.92	152.92	0.93	149.68	0.93
0.5	139.12	0.96	141.11	0.96	139.54	0.96	135.95	0.93	140.65	0.94	136.64	0.93
0.6	134.81	0.96	137.15	0.97	135.26	0.96	111.55	0.91	117.64	0.92	112.36	0.91
0.7	136.10	0.98	138.50	0.98	136.55	0.98	90.66	0.87	98.00	0.90	91.56	0.88
0.8	141.63	0.99	143.94	0.99	142.09	0.99	80.86	0.87	88.95	0.90	81.83	0.87
0.9	149.72	0.94	151.88	0.95	150.17	0.94	70.26	0.84	79.22	0.88	71.30	0.84
Avg. (0.2-0.9)	134.90		137.19		135.35		126.47		131.78		127.21	

TABLE 4.7: Activation energy obtained by model-free methods for CS30.

CS30 (α)	First Zone						Second Zone					
	KAS		FWO		Starink		KAS		FWO		Starink	
	E (KJ/mol)	R^2	E (KJ/mol)	R^2	E (KJ/mol)	R^2	E (KJ/mol)	R^2	E (KJ/mol)	R^2	E (KJ/mol)	R^2
0.1	117.73	0.9955	120.08	0.9961	118.15	0.9956	101.63	0.917	108.37	0.9461	102.49	0.9205
0.2	179.14	0.9973	181.77	0.9987	179.68	0.9975	111.51	0.9986	117.66	0.9948	112.31	0.9983
0.3	128.78	0.8877	131.10	0.9008	129.21	0.8891	98.65	0.9868	105.29	0.9946	99.49	0.9879
0.4	148.90	0.9965	149.75	0.9989	149.21	0.9968	91.11	0.9913	98.14	0.9953	91.98	0.9918
0.5	149.40	0.9959	150.51	0.9986	149.74	0.9963	98.65	0.9973	105.42	0.9978	99.51	0.9974
0.6	135.15	0.9538	137.69	0.9644	135.62	0.955	94.80	0.9993	102.13	0.9995	95.71	0.9993
0.7	119.67	0.9454	123.00	0.9531	120.20	0.9462	82.68	0.9865	91.00	0.9902	83.68	0.9869
0.8	111.69	0.9975	115.56	0.9979	112.26	0.9976	63.62	0.9882	73.18	0.9949	64.72	0.9891
0.9	111.34	0.9843	115.42	0.9867	111.93	0.9846	48.20	0.9875	59.16	0.9978	49.42	0.9893
Avg. (0.2-0.9)	135.51		138.10		135.98		86.15		94.00		87.10	

TABLE 4.8: Activation energy obtained by model-free methods for CS40.

CS30 (α)	First Zone						Second Zone					
	KAS		FWO		Starink		KAS		FWO		Starink	
	E (KJ/mol)	R^2	E (KJ/mol)	R^2	E (KJ/mol)	R^2	E (KJ/mol)	R^2	E (KJ/mol)	R^2	E (KJ/mol)	R^2
0.1	94.22	0.8776	97.74	0.8951	94.74	0.8795	140.66	0.9996	144.08	0.9997	141.23	0.9996
0.2	114.03	0.9441	116.87	0.9514	114.51	0.9449	133.22	0.9787	104.72	0.9964	133.85	0.979
0.3	131.10	0.9554	133.35	0.9612	131.53	0.9561	108.86	0.9941	102.67	0.9951	109.61	0.9942
0.4	170.94	0.9801	171.17	0.9759	171.22	0.9797	94.70	0.961	94.86	0.9989	95.53	0.9619
0.5	176.12	0.9798	176.28	0.9754	176.39	0.9793	129.23	0.9478	94.69	0.997	129.99	0.9487
0.6	161.29	0.9898	162.92	0.993	161.70	0.9901	141.75	0.9327	89.89	0.9975	142.51	0.9338
0.7	141.46	0.9975	144.10	0.9988	141.94	0.9977	127.24	0.9772	80.41	0.9998	128.09	0.9776
0.8	126.54	0.9945	130.04	0.9968	127.10	0.9948	112.30	0.9957	75.30	0.9967	113.26	0.9958
0.9	102.88	0.9428	115.12	0.9936	103.50	0.9438	85.72	0.9762	68.97	0.9994	86.85	0.9769
Avg. (0.2-0.9)	140.55		143.73		140.99		116.63		88.94		117.46	

TABLE 4.9: Activation energy obtained by model-free methods for CS50.

CS50 (α)	First Zone						Second Zone					
	KAS		FWO		Starink		KAS		FWO		Starink	
	E (KJ/mol)	R^2	E (KJ/mol)	R^2	E (KJ/mol)	R^2	E (KJ/mol)	R^2	E (KJ/mol)	R^2	E (KJ/mol)	R^2
0.1	131.23	0.9912	132.90	0.9923	131.61	0.9913	90.21	0.6451	96.07	0.6956	90.95	0.6506
0.2	150.59	0.9923	151.60	0.9932	150.92	0.9924	110.74	0.7304	113.07	0.9493	111.44	0.7344
0.3	153.61	0.9803	154.67	0.9825	153.95	0.9805	112.85	0.8085	114.38	0.9227	113.57	0.8116
0.4	161.97	0.9832	162.78	0.985	162.30	0.9834	120.41	0.935	125.65	0.9453	121.14	0.9361
0.5	155.81	0.9531	157.08	0.9582	156.18	0.9537	167.41	0.9971	170.68	0.9975	168.00	0.9972
0.6	142.63	0.9975	144.69	0.9978	143.06	0.9975	182.74	0.9706	185.59	0.9743	183.31	0.971
0.7	135.02	0.9657	137.56	0.97	135.49	0.9662	212.90	0.9653	214.51	0.9691	213.38	0.9657
0.8	113.93	0.8647	117.64	0.8829	114.48	0.8667	229.07	0.9992	230.15	0.9993	229.52	0.9993
0.9	101.11	0.7331	105.67	0.7687	101.74	0.737	275.90	0.917	275.07	0.924	276.22	0.9177
Avg. (0.2-0.9)	139.33		141.46		139.76		176.50		178.64		177.08	

TABLE 4.10: Activation energy obtained by model-free methods for CS60.

CS60 (α)	First Zone						Second Zone					
	KAS		FWO		Starink		KAS		FWO		Starink	
	E (KJ/mol)	R^2	E (KJ/mol)	R^2	E (KJ/mol)	R^2	E (KJ/mol)	R^2	E (KJ/mol)	R^2	E (KJ/mol)	R^2
0.1	180.51	0.982	179.77	0.9837	180.69	0.9822	66.48	0.9759	74.20	0.9885	67.39	0.9776
0.2	170.35	0.9708	170.39	0.9736	170.60	0.9711	61.27	0.9858	69.22	0.9922	62.19	0.9866
0.3	156.44	0.9675	157.35	0.9709	156.77	0.9678	57.52	0.8968	66.88	0.9986	58.46	0.9003
0.4	150.03	0.933	153.56	0.9972	150.39	0.9338	68.98	0.9545	73.78	0.9998	69.93	0.9566
0.5	147.78	0.9343	152.50	0.9971	148.17	0.935	78.47	0.9835	86.49	0.9918	79.43	0.9846
0.6	136.82	0.9447	142.78	0.9997	137.26	0.9454	95.07	0.9827	102.78	0.9927	96.02	0.984
0.7	136.36	0.9736	138.84	0.977	136.82	0.974	85.67	0.9086	94.21	0.9866	86.69	0.9122
0.8	155.82	0.9997	157.49	0.9998	156.23	0.9997	74.63	0.9698	83.88	0.9824	75.71	0.9714
0.9	140.79	0.9892	143.44	0.9905	141.28	0.9893	56.75	0.9883	66.99	0.992	57.91	0.9888
Avg. (0.2-0.9)	149.30		152.04		149.69		72.30		80.53		73.29	

TABLE 4.11: Activation energy obtained by model-free methods for CS70.

CS70 (α)	First Zone						Second Zone					
	KAS		FWO		Starink		KAS		FWO		Starink	
	E (KJ/mol)	R^2	E (KJ/mol)	R^2	E (KJ/mol)	R^2	E (KJ/mol)	R^2	E (KJ/mol)	R^2	E (KJ/mol)	R^2
0.1	451.58	0.9921	437.41	0.9924	450.77	0.9921	119.01	0.9872	111.18	0.9687	118.37	0.9857
0.2	286.59	0.9958	280.85	0.996	286.42	0.9958	159.12	0.9954	103.70	0.9986	158.06	0.9965
0.3	237.02	0.9981	233.91	0.9983	237.04	0.9981	144.80	0.9473	101.68	1	143.67	0.952
0.4	213.95	0.9854	212.13	0.9865	214.08	0.9855	136.03	0.9832	94.20	0.9999	134.56	0.9859
0.5	221.17	0.9998	219.13	0.9998	221.28	0.9998	135.02	0.9052	89.40	0.9945	134.12	0.912
0.6	201.84	0.9925	200.90	0.9931	202.05	0.9926	83.66	0.9337	70.49	0.9792	83.53	0.9393
0.7	196.73	0.9931	196.19	0.9937	196.96	0.9932	62.34	0.9558	63.93	0.992	62.60	0.9609
0.8	210.47	0.9869	209.41	0.988	210.68	0.987	47.95	0.9609	51.73	0.9961	48.42	0.9665
0.9	230.34	0.9043	228.52	0.9114	230.49	0.905	56.76	0.9766	48.73	0.9921	57.60	0.9802
Avg. (0.2-0.9)	224.76		222.63		224.88		103.21		77.98		102.82	

Different approximations in equations could be a reason for the discrepancy. Although the precision of the two iso-conversion procedures differs, the variation tendency of activation energy is the same [13]. The R^2 values derived from the FWO method were higher, therefore, this method was selected for the decomposition mechanism study in the following section.

The ability to recognise multi-step processes and forecast the response "kinetic scheme" over a large temperature range is enabled by understanding E_α vs α. A change in the slope of E_α dependence is usually linked to a change in the overall reaction mechanism's rate limiting step. The similar kinetic model was presented to simulate intricate polymerization, and the evaluation of the E_α dependency and its modifications revealed vital information about the change in the rate limiting steps which concluded that the assumption of a single-step equation's validity constrained to a fixed value of α, holds true for complex processes.

Typically, a change in the rate-limiting step of the overall reaction mechanism corresponds to a change in the slope of the E_α dependency [224]. The upward trend of E_α for progressive degree of conversion α values may be attributed to the exothermic nature of the decomposition reaction, while the downward trend is associated to an endothermic reaction. As per research, [69] the higher E_α values have been assigned to the solid carbonaceous char, which protects the larger molecules from further breakdown and leaving behind a significant amount of solid residue.

For PCB, with FWO method, the calculated E_α for conversion from 0.2 -0.9 values decreased from 190.21 to 93.88 kJ/mol in the first zone where average E was 133.25 kJ/mol. In the second zone it was found fluctuating, average E was 178.95 kJ/mol, with a positive slope (negative activation energy) that indicates the rate of reaction decreases with increasing temperature. It can be seen from Table 4.3 that there is a significant weight loss in this zone so the degradation in this temperature range can’t be neglected. Moreover, in Table 4.5, the negative activation energy was observed which may take place due to the presence of multi-steps in the process of pyrolysis where the activation energy of one of the steps becomes negative, while the activation energy of the other step remains low, thus making the total sum negative, there may be regimes of spontaneous reactions occurring during pyrolysis

[225]. According to the researcher Siddiqui et al. [98] who worked on poly (bisphenol A carbonate)-based polymers originating in waste electric and electronic equipment, the process of heat deterioration is easy to initiate because of the weak link points in the polymer chain. Random scission becomes the limiting phase of degradation when these weak linkages are depleted, and the activation energy rises to the steady-state value, which is generally between 210 and 260 kJ/mol. Higher E_α values have also been assigned to the solid carbonaceous char, which protects the polymer from further breakdown and results in a significant amount of solid residue (more than 20%), as agreed by literature [57][69].

For CS with FWO method, apparent activation energy is increased from 121.43 to 151.88 kJ /mol (average E, 137.19 kJ/mol) with α ranging from 0.2 to 0.9, it is increased in second zone up to 0.2 conversion then decreased at the end of the conversion (α = 0.9) to 79.22 kJ/mol (average E, 131.78 kJ/mol), it may be due to the formation of porous chars, which enhanced the diffusion of volatiles, as discussed by Z Yao et al. [13]. For a similar kind of biomass, researchers have found activation energy for the cellulose and hemicelluloses as 152.0527 kJ/mol and 133.549 kJ/mol, respectively which is consistent with present results of model-free methods [27][195].

The prominent effect of PCB can be seen on degradation mechanism of the co-pyrolyzed samples. The majority of E_α variations happen in the Zone I, and it was ranged from 90 to 200 KJ/mol. While for the Zone II, it is between 70 and 150 KJ/mol. With CS30 the average activation energy is 138.10 KJ/mol, rising to 222.63 KJ/mol for the first zone of CS70 with a higher CS ratio. Which can be associated with the presence of several reactions that occur in parallel together with the high thermal stability of C–C bonds, thus needing more energy to break the chemical bonds [226]. The higher E_α also indicates slower reaction and better thermal stability of generated char [227]. While in the second zone of CS70, a faster reaction is evidenced by a reduction in apparent activation energy with increased conversion (0.6-0.9). It may be attributed to the addition of CS, which aided in the production of porous chars and enhanced the diffusion of volatiles, as discussed in literature [16][228]. Additionally, alkalis metals including K, Na, Mg, and Ca from reinforcing materials in NMF of PCB operate as catalysts [229], resulting in a decrease in apparent activation energy for the second zone under high conversion conditions (above 0.6) with the exception of CS50.

4.3.4 Determination of the most probable reaction model

Plotting the graph of $\frac{Z(\alpha)}{Z(0.5)}$ vs α for different mechanisms (using Equation 4.14), theoretical curves were obtained. By using known value of activation energies, the experimental $\frac{Z(\alpha)}{Z(0.5)}$ value was derived (See, Equation 4.15) and overlapped to check best match of the reaction mechanism. Here, 10 ℃/min heating rate was randomly selected. In Fig. 4.10**,** CS70 sample is shown for reference, while the Criado plots for other samples are shown in Appendix A.

The acquired experimental curve, for the second zone of all five compositions, is highly equivalent to the m13 mechanism of Table 4.1. While, for the first zone, CS60 demonstrates the m13 mechanism, CS30 exhibits the m12, and CS40 exhibits the m11 reaction mechanism.

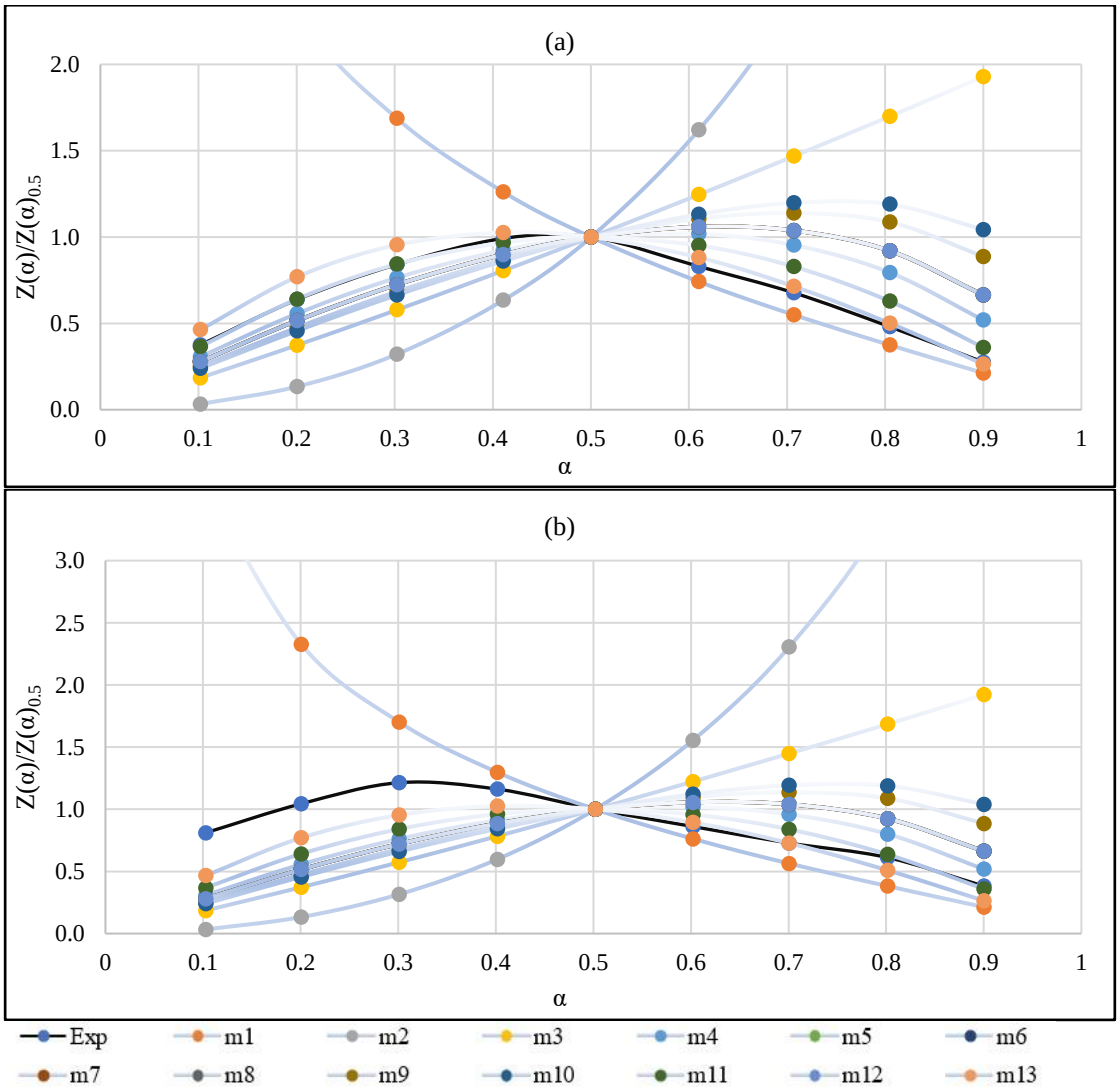

FIGURE 4.10: Criado plots of CS70 for first zone (a) and second zone (b).

Importantly, the CS70 for the first zone demonstrates two distinct reaction mechanisms, m11 for α = 0.2–0.5 and m13 for α = 0.2–0.5. The variation in reaction mechanisms could be the reason for treatment of the TGA data which may have an impact on the recognized E_α values; Other potential contributing factors include the size distribution of the sample particles and the chemical composition, which varies for different PCB parts.

4.3.5 kinetic compensation effects

Increasing activation energy increases the overall rate of reaction, whereas activation energy must be decreased to accomplish higher conversion rate. This fact implies that the experimental values of *A* and *E* could be correlated. We can fit the experimental data to a rate equation by adjusting the values of *A* and *E* in such a compensating manner that their simultaneous change does not affect the overall rate [192]. This correlation is known as a compensation effect and is typically found in the following form [193][200],

$$ln\, A = aE + b \tag{4.19}$$

where, a and b are constants and refer to the compensation coefficients.

Above equation represents linear relation between *In A* and *E* for a series of related reactions or for the same reaction carried out in a series of different conditions, known as a compensation effect [230].

TABLE 4.12: Pre-exponential factor derived using FWO method.

Conversion	**First Zone (lnA)**					**Second Zone (lnA)**				
(α)	**CS30**	**CS40**	**CS50**	**CS60**	**CS70**	**CS30**	**CS40**	**CS50**	**CS60**	**CS70**
0.1	19.79	14.51	23.00	34.01	96.38	11.48	18.09	9.28	5.28	11.61
0.2	33.81	18.80	27.00	31.35	57.04	13.42	16.87	13.14	4.90	18.11
0.3	21.84	22.36	27.50	28.24	45.47	11.24	12.77	13.56	5.11	15.54
0.4	25.70	30.63	29.21	26.87	40.15	10.03	10.47	14.80	6.64	13.54
0.5	25.60	31.49	27.88	26.41	41.32	11.20	15.71	22.24	8.36	14.36
0.6	22.67	28.36	25.20	24.20	37.57	10.72	17.45	24.47	11.14	7.47
0.7	19.43	24.36	23.87	24.23	36.43	9.16	15.27	28.99	9.96	5.13
0.8	17.75	21.54	20.20	28.42	39.28	6.93	13.29	31.42	8.78	3.91
0.9	17.48	18.79	18.67	26.15	43.52	5.99	10.45	38.52	7.27	6.62
Avg (0.2-0.9)	22.68	24.54	24.94	26.98	42.60	9.84	14.03	23.39	7.77	10.58

It means that the reduction in rate expected to result from an increase in activation energy does not occur for the set of reactions obeying Equation (4.19), due to a compensatory increase of *A*. In fact, the compensating effect offers a potential way to anticipate how experimental conditions would affect kinetic parameters. In other words, for any change in the experimental activation energy resulting from the modification of experimental conditions, a corresponding change in *A* also occurs, thus we could correlate various parameters under various experimental conditions.

(a)

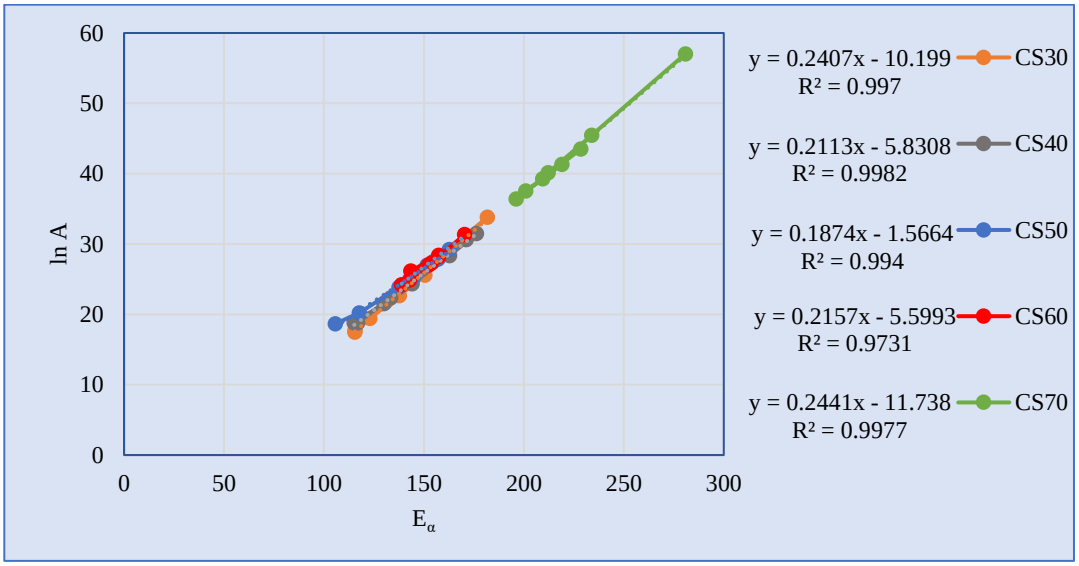

(b)

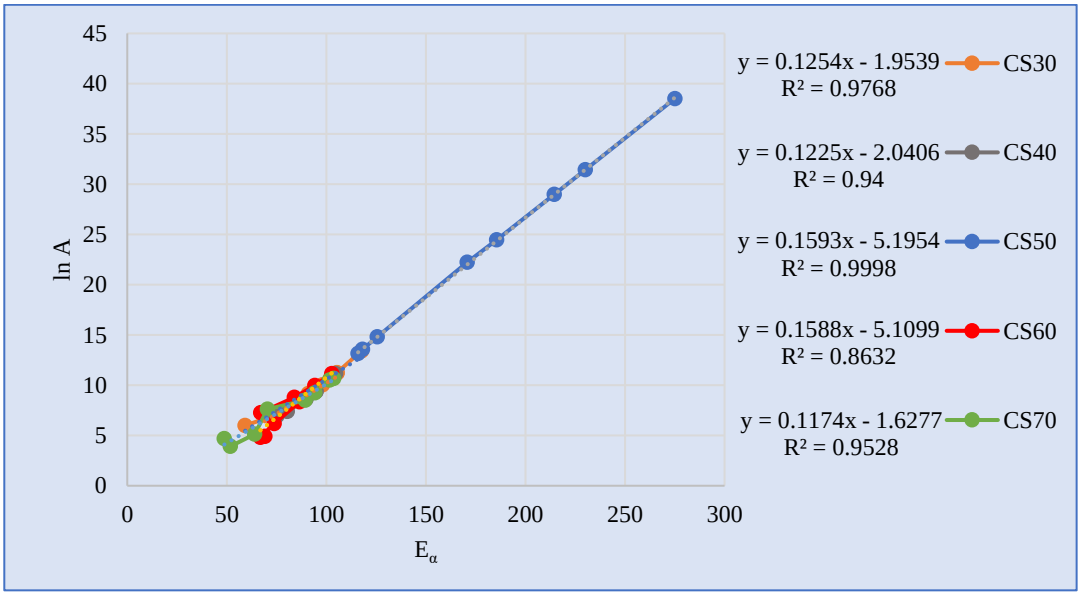

FIGURE 4.11: Compensation effect between lnA and E_α using Eq. (4.19) with first zone (a) and second zone (b).

Table 4.12 displays the value of the pre-exponential factor in the form of *ln A*, obtained by substituting E_α and $g(\alpha)$ values in Equation (4.9). The $g(\alpha)$ values were determined based

on approximated reaction mechanism by Criado master plots. As illustrated in Fig. 4.11, plotting *lnA* vs E_α results in an excellent linear relationship with greater R^2 values for all five samples. Demonstrating that there was a compensating impact between the apparent E_α and *lnA* during the pyrolysis.

4.4 Conclusion:

The pyrolysis kinetics of PCB and CS were investigated in this study using a number of TG tests, and comparisons were made with various CS:PCB compositions with CS ratios of 30, 40, 50, 60, and 70.

The TG analysis revealed that the decomposition process can be divided into three stages, named Demosturization zone and two main pyrolysis zones, Zone I and Zone II. The % residue of the co-pyrolyzed samples has decreased significantly compared to PCB (lowest with CS70), indicating comparatively increased reactivity.

For main pyrolysis process zones, the apparent activation energies were calculated using FWO method, which did not show large variations with progressing value of α, for PCB, CS and different CS:PCB compositions (varies between 90 – 150 KJ/mol), except PCB, which exhibited negative activation energy in second zone indicating complex reaction mechanism. Moreover, comparatively higher E_α values of CS70 (~ 200 KJ/mol) indicates slower reaction and better thermal stability of generated char.

The reaction mechanism of co-pyrolyzed material for second zone followed the m13 model (rection order n=3). While for the first zone, CS30 and CS40 displayed m12(n=1) and m11(n=2), respectively, while CS50 and CS60, displayed m13 (n=3) reaction mechanisms. Most importantly, the CS70 has demonstrated two distinct reaction mechanisms at first zone, m11 for α = 0.2–0.5 and m13 for α = 0.2–0.5. This variance in mechanism may be caused by TGA processing, differing chemical compositions, and the size distribution of various PCB components. Finally, the value of *lnA* were calculated based on associated reaction mechanism and were overall higher for CS70, falling between 36 and 57 for the first zone and between 3 to 18 for the second zone, with α rising from 0.2 to 0.9. Moreover, the pre-exponential factor and the apparent activation energy were found to have a kinetic compensation effect.

CHAPTER 5

Oil and Gas Analysis

5.1 Introduction:

This Chapter demonstrates the slow pyrolysis of PCB, CS and compares results with co-pyrolysis of various compositions of CS with PCB (CS:PCB) on a lab scale fixed bed equipment, designed and fabricated at the Shroff SR Rotary Institute of Chemical Technology-Ankleshwar, Gujarat (India). The research examines the impact of different CS compositions on co-pyrolysis products in order to obtain lower halogen yields and limit toxic emissions as much as feasible while also increasing liquid yield. Produced gas is also identified and the quantity is compared. Moreover, potential applications for pyrolysis oil and gas are explored.

5.2 Pyrolysis Experiments:

Pyrolysis experiment of all seven samples were performed on the lab scale instrument set up as discussed in chapter 3. Each sample ran 3 times to confirm product yields, as the repeatability of the experiments is necessary when the heterogeneous nature of the samples was taken into consideration. As per TGA analysis discussed above the optimum temperature for producing maximum oil is in the range of 200 - 500 ℃. Above 500 ℃, very slow degradation takes place which reduces liquid and char production and provides increased amount of gas, this reduction at higher temperature could be the reason of secondary reaction of the liquid fraction of the volatiles and the further decomposition of the char particles. Several studies [17][231][232] have looked into the same effects. Whereas, too lower a temperature can cause incomplete decomposition of the biomass [11][178]. The pyrolysis technique, as discussed in chapter 3, produced varying fractions of oil, char, and

gas for different samples, and the yield of this components with reference to % fraction is provided in Fig. 5.1 (a) and (b).

5.3 Results and discussion:

5.3.1 Effect of different composition on product yield

Fig. 5.1 (a) shows that for PCB, the amount of oil is lowest (19.6%) and the amount of char is largest (59.6%); however, for CS, the contrary is evident, with the highest oil (36%) and lowest char (28%). Furthermore, because CS contains more volatile components and moisture, the amount of oil generated by co-pyrolysis rose significantly as CS was increased, peaking at CS70 (31.5 %). This synergistic effect can also be explained by the fact that CS has a higher H/C ratio than PCB and provide a source of hydrogen during co-pyrolysis, while the water present in it can function as a reactive compound causing PCB tar to break even more and help to produce more oil, as shown above in an elemental analysis [12].

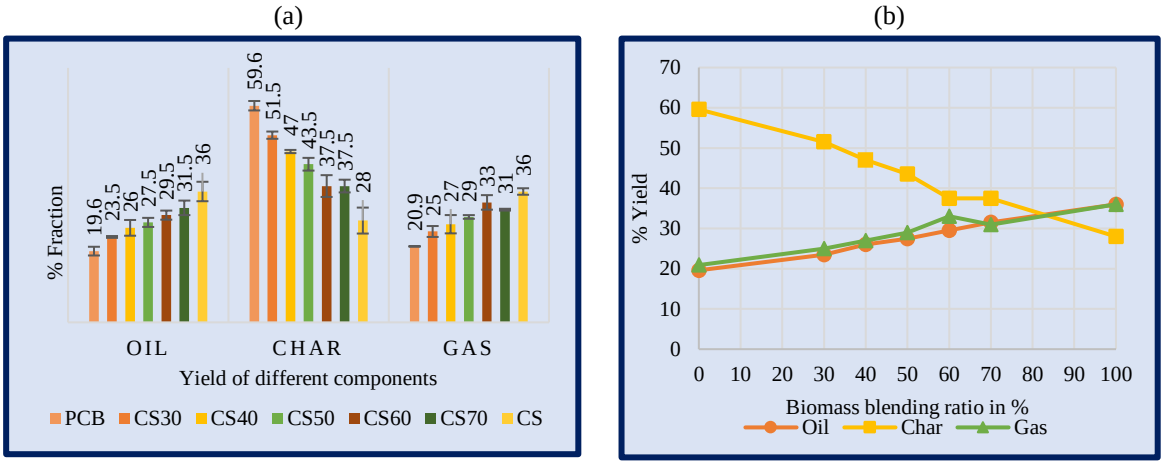

FIGURE 5.1: (a) Comparison of % fraction generated in each sample, (b) Yield of the different sample with different biomass blending ratio.

Similarly, the amount of gas produced by co-pyrolysis grows dramatically with increasing CS up to 60 %, then somewhat drops with 70 % CS, owing to the fact that numerous big hydrocarbon molecules have been broken into smaller molecules [233]. Furthermore, as the amount of CS increases, the amount of char created falls dramatically until it reaches a plateau at 70 % CS composition.

The higher water content of CS, as shown in Fig. 5.2, results in a comparatively clear texture, lower energy density, and may be a cause of corrosivity and chemical instability [234][235]. Additionally, due to the presence of lignin, solid particles are adsorbed with it, causing gummy tars and making phase separation difficult [26][236]. Sensoz and Angin [237] concluded that a lower lignin percentage in the feedstock is preferable in order to minimise larger molecular weight components and generate a more homogeneous liquid.

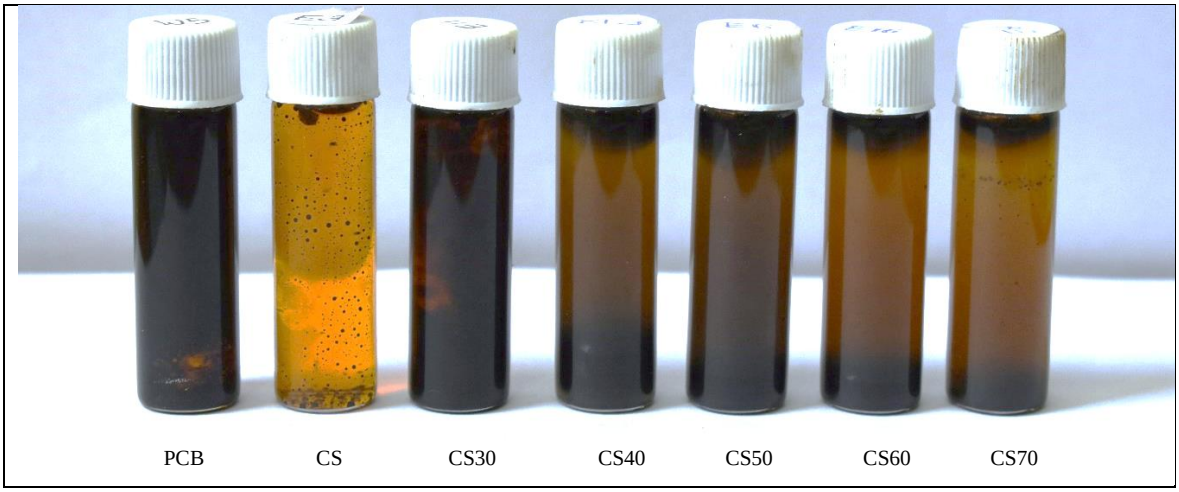

FIGURE 5.2: Pyrolysis oil of PCB, CS and its different composition.

However, PCB oil has a lower water content, which can lead to high viscosity, whereas a co-pyrolysis oil product, as suggested by [238][234], can impart the required amount of water, which can add positive effects to using it as a fuel, with supplementary benefits such as reduced pollutant emissions, reduced viscosity, enhanced oxidation, and contributes to micro explosion of droplets in combustion. In fact, radical interaction can aid the creation of a stable pyrolysis oil that prevents phase separation during the co-pyrolysis reaction [236].

5.3.2 Liquid oil characterisation

The GC-MS analysis of the collected oil is used to determine the nature and type of components present without breaking them down [29]. The chromatograms are shown in Fig. 5.3, and the compounds discovered after performing a library search on mass spectrometry and matching mass spectra data with the NIST library are specified in Table 5.1, 5.2 and 5.3. More than 25 unique aromatic and aliphatic compounds were found in each sample during the 40 minutes of GC-MS spectra acquisition, and we will only discuss the

compounds with an area percent of more than 0.1. The % of a compound in the oil was equivalent to the area percent of the peak for that component.

a

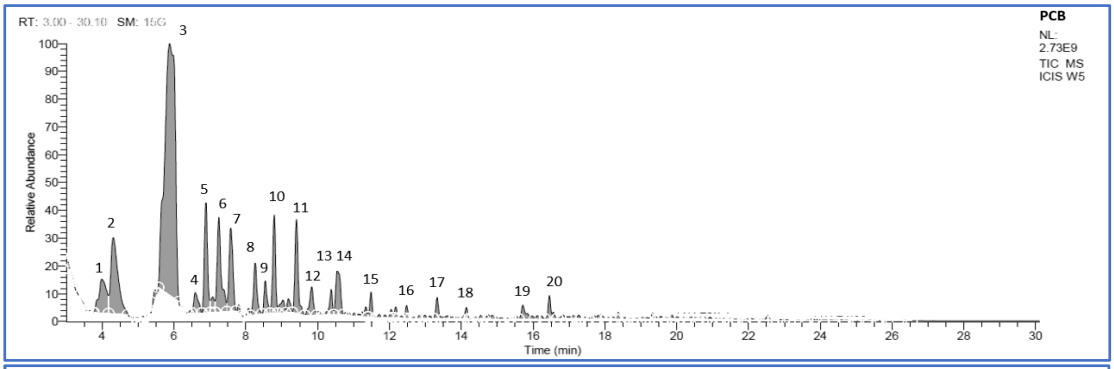

b

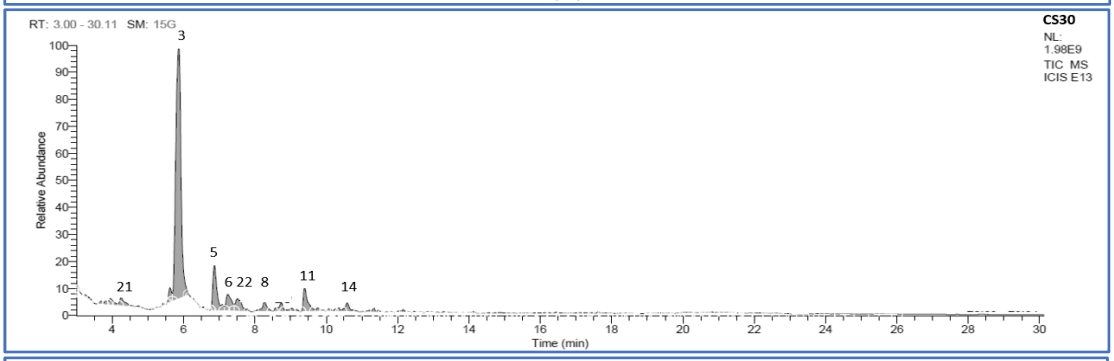

c

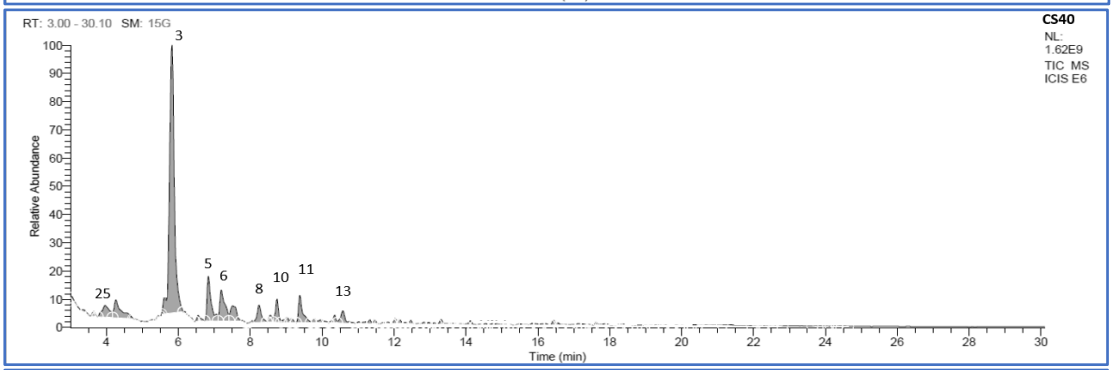

d

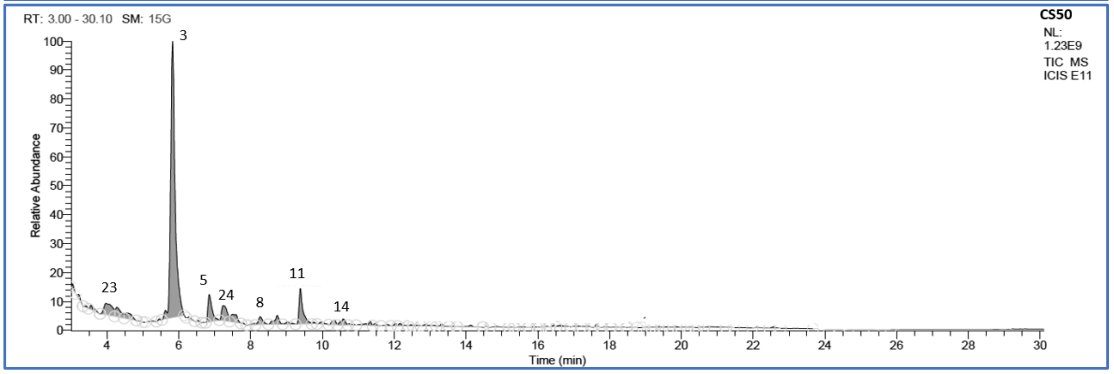

e

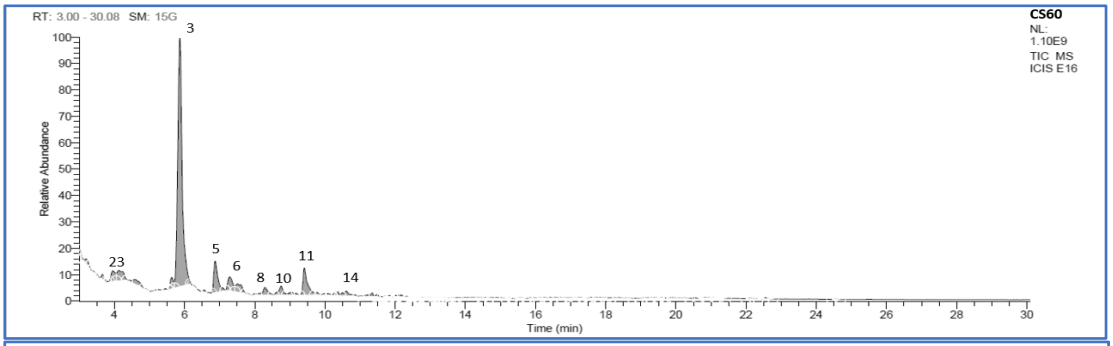

f

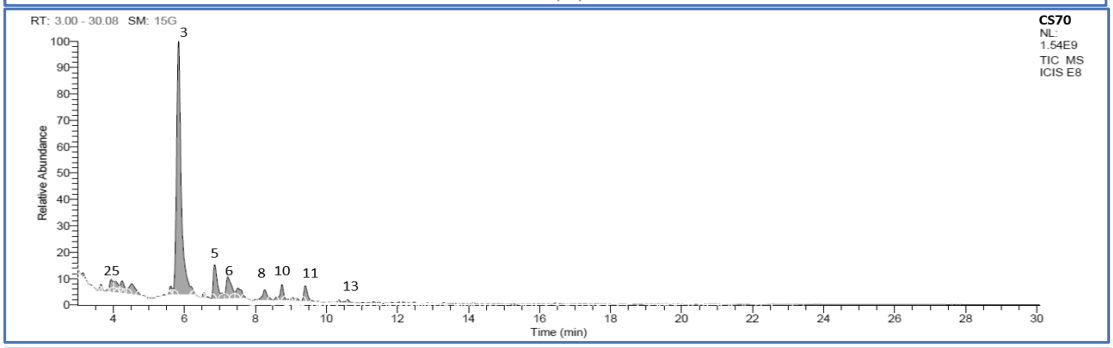

g

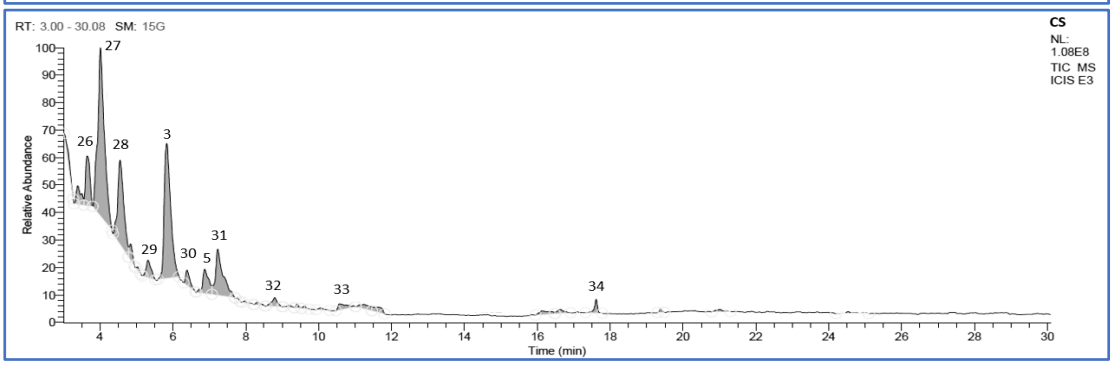

1. Xylene
2. Styrene
3. Phenol
4. Benzene,1-ethynyl-4-methyl
5. 2-methyl, phenol
6. 4-methyl, Phenol
7. 1h-pyrrolo[2,3-b]pyridine,1-methyl-
8. phenol, 3,4-dimethyl-
9. phenol, 3-ethyl
10. Naphthalene
11. phenol, 3-(1-methylethyl)
12. 1,2-Benzenedicarbonitrile
13. Naphthalene, 2-methyl-
14. P-isopropenylphenol
15. naphthalene, 2-ethenyl
16. Acenaphthylene
17. Dibenzofuran
18. Fluorene
19. 3-Hydroxybiphenyl
20. Anthracene
21. 3H-2-Benzopyran-3-one, 1,4-dihydro
22. 2H-1-Benzopyran-3-ol, 3,4-dihydro-,acetate
23. 1,6:2,3-Dianhydro-4-O-acetyl-beta-d-gulopyranose
24. phenol, 2,3-dimethyl
25. 4,6-octadiyn-3-one, 2-methyl
26. 2-pentanone, 4-hydroxy-4-methyl
27. Guanidine, N,N-dimethyl
28. Pyridine, 2,3-dimethyl-
29. 2-cyclopenten-1-one, 3-methyl
30. 1-Methoxy-1,3-cyclohexadiene
31. 2-cyclopenten-1-one, 3,5,5-trimethyl
32. 3,4-Dihydro-1-methylpyrrolo[1,2-a]pyrazine
33. 9-Undecenal, 2,10-dimethyl-
34. Pentadecanoic acid, 14-methyl-, methyl ester

FIGURE 5.3: GC/MS analysis result with detected compounds for (a) PCB, (b) CS30, (c) CS40, (d) CS50, (e) CS60, (f) CS70 and (g) CS.

The GC-MS analysis revealed that the major products of PCB and its compositional pyrolysis oil are fragments of the polycarbonate epoxy resin, with phenol being the most abundant component. According to literature [14][21], they are formed between 450 - 500 ℃, however their quantity decreases as the temperature rises above 500 ℃, due to secondary reactions that may further decompose it in smaller molecules. The quick degradation of polymeric macromolecules also produces some phenolic compounds, such as 2-methyl-

phenols, 4-methyl-phenol, phenol,3,4-dimethyl-, phenol,3,4,5-trimethyl-, phenol,3-(1-methylethyl) and p-isopropenylphenol, in minor amounts, which escape the reaction system without further decomposition to phenol [14]. Table 5.1 describes the value of phenol and phenolic compounds identified in PCB, CS, and different CS:PCB combinations. PCB had total of 60.67% phenol and phenolic compounds, while CS had just 25.94%. However, when co-pyrolysis was used, the amount increased, which can be attributed to the combined effect of bisphenol A decomposition in epoxy resin of PCB and lignin decomposition of CS. It's worth noting that in the presence of biomass, pyrolysis of polycarbonate (Bisphenol A) can lead to an increase in phenol chemicals in the oil [239]. Total phenol and phenolic compounds generated in the co-pyrolyzed oil products vary from 78.63, 69.77, 76.82, 75.29, and 74.3 % area for CS compositions 30, 40, 50, 60, and 70%, respectively. It can be concluded that CS30 has highest amount of phenol and phenolic compounds, whereas CS50 has a greater number of phenolic derivatives. If we compare total of phenol and phenolic compounds in each composition then we can write: CS30>CS50>CS60>CS70>CS40.

TABLE 5.1: The amount of phenol and phenolic compounds identified in each sample, expressed as % area.

Compound name	% Area						
	PCB	CS	CS30	CS40	CS50	CS60	CS70
phenol	38.47	21.85	56.74	48.28	54.83	55.21	55.78
2-methyl, phenol	5.07	-	8.42	6.76	5.04	6.4	6.92
4-methyl, Phenol	5.66	3.73	3.9	5.94	3.77	3.35	5.5
phenol, 2,3-dimethyl	-	-	-	-	2.36	-	-
Phenol, 2-ethyl	0.28	-	-	-	0.3	-	-
phenol, 3,4-dimethyl-	2.54	0.36	2.14	2.92	1.62	2.01	2.6
Phenol, 3,4,5-trimethyl-	-	-	1.01	0.85	0.54	0.93	0.7
phenol, 3-(1-methylethyl)	4.31	-	4.58	4.12	6.17	5.97	2.8
Phenol, m-tert-butyl-	-	-	-	-	0.88	-	-
P-isopropenylphenol	2.94	-	1.84	-	1.31	1.42	-
phenol, 4-ethyl	1.4	-	-	0.9	-	-	-
Total	60.67	25.94	78.63	69.77	76.82	75.29	74.3

Table 5.2 indicates the list of compounds found in the different CS:PCB compositions, excluding phenol and phenolics, and the concentration is compared with 100% PCB and CS samples. Those compounds are classified based on some of the functional groups which involves alkyne, ketone, ester, siloxane, nitrile, furan, pyridyl, PAHs and phosphate ester. Table 5.3 highlights chemicals discovered in PCB and CS pyrolyzed oil only; they are

completely missing in co-pyrolyzed oil due to the differing reaction mechanism and feedstock.

Furthermore, Fig. 5.4 represents polycyclic aromatic hydrocarbons (PAHs) present in PCB and co-pyrolyzed oil products. Whereas CS oil contains most of aliphatic hydrocarbons, ranging from C3-C34.

TABLE 5.2: Compound found other than phenol and phenolics and categorised based on functional groups.

Functional Group	Compound Name	% Area						
		PCB	CS30	CS40	CS50	CS60	CS70	CS
Alkyne	Benzene,1-ethynyl-4-methyl	1.3	0.15	0.77	-	0.25	0.81	-
	4,6-octadiyn-3-one, 2-methyl	-	1.4	3.27	-	-	2.17	-
ketone	2-pentanone, 4-hydroxy-4-methyl	-	0.4	0.5	-	0.73	0.79	5.44
	Ethanone, 1-(2,3-dihydro-1H-inden-5-yl)-	-	0.57	0.5	0.22	0.32	0.09	-
	5',6',7',8'-Tetrahydro-2'-acetonaphthone	0.6	0.75	0.6	0.98	0.79	0.26	-
	Methanone, (2-methylphenyl)phenyl-	0.3	0.18	0.27	0.16	0.14	0.08	-
Ester	Pentadecanoic acid, 14-methyl-, methyl ester	-	0.2	0.3	0.28	0.37	0.14	1.07
Siloxane	Cyclotetrasiloxane, octamethyl-	0.5	0.24	0.14	0.18	0.18	0.13	-
Nitrile	Benzonitrile	-	1.73	-	-	1.71	1.14	-
	Pentadecanenitrile	0.1	0.09	0.08	0.23	0.15	0.03	-
Furan	Benzofuran, 2-isopropenyl-3-methyl-	0.4	0.41	0.43	0.42	0.35	0.16	-
	Dibenzofuran	0.8	0.29	0.55	0.36	0.26	0.18	-
Pyridyl	1h-pyrrolo[2,3-b]pyridine,1-methyl-	4.6	3.62	3.38	-	2.54	3.03	-
PAHs	Acenaphthylene	0.4	0.11	0.31	0.12	0.1	0.13	-
	Fluorene	0.4	0.28	0.45	0.4	0.44	0.19	-
	Anthracene	1	0.23	0.64	0.23	0.16	0.21	-
	Fluoranthene	0.2	0.13	0.21	0.13	0.15	0.09	-
	Naphthalene	4	1.8	2.58	1.89	1.96	2.91	-
	Naphthalene, 2-methyl-	1.1	0.67	0.87	-	-	0.4	-
	Naphthalene, 2-ethenyl	0.9	0.26	0.37	0.31	0.23	0.15	-
Phosphate ester	Triphenyl phosphate	0.2	0.29	0.36	0.2	0.21	0.14	-

*4,6-octadiyn-3-one, 2-methyl is fall under alkyne and ketone functional groups. *2-pentanone, 4-hydroxy-4-methyl falls under ketone and alcohol group.

It has been found that PCB generated oil, as well as oil samples with different CS compositions to it, has remarkable amount of PAHs, in the form of acenaphthylene, anthracene, naphthalene, naphthalene,2-methyl, naphthalene,2-ethenyl, fluoranthene, and fluorene. Meanwhile, more PAHs like Pyrene, naphthalene,1,7-dimethyl, naphthalene,2,3-dimethyl and 4H-Cyclopenta[def]phenanthrene and many others listed in Table 5.3, are also present in PCB oil, which covers 13.92% area covered, and are totally eliminated from all co-pyrolyzed oil.

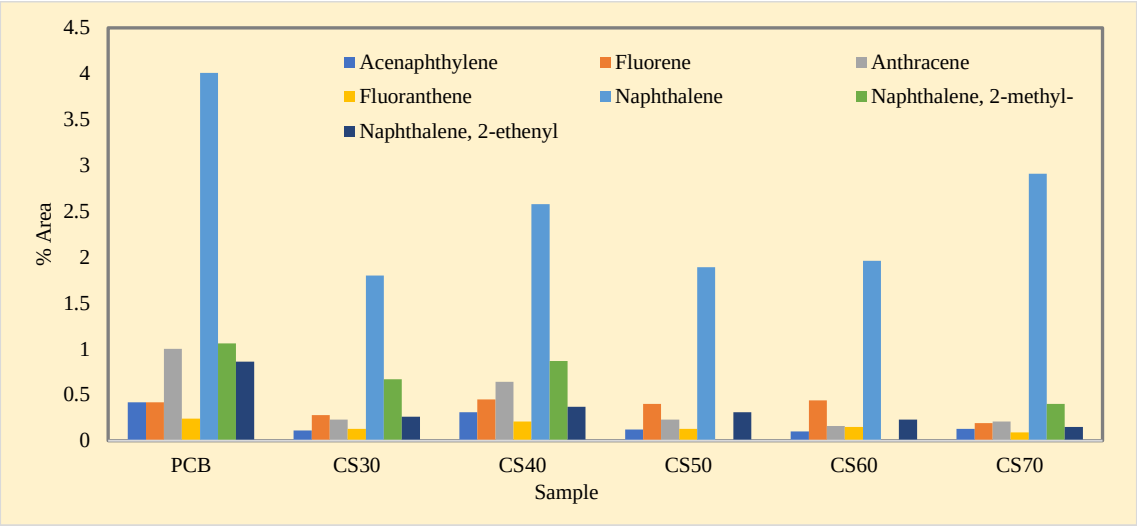

FIGURE 5.4: Comparison of different PAHs found in GC/MS analysis of Pyrolysis oil.

Overall, PCB contains aromatic hydrocarbons ranging from C6 to C18, Whereas CS composition to it has incorporated some aliphatic components like pentadecanenitrile (C15) and pentadecanoic acid,14-methyl-, methyl ester (C17) with less than 0.5 area %.

5.3.3 Reaction Pathways

5.3.3.1 Reaction Pathways of PCB

The basic reaction mechanism of the PCB breakdown pathway is depicted in Fig. 5.5. Brominated epoxy resin start decomposing with an increase of process temperature up to 335 ℃ and let the debromination start with release of HBr and bisphenol A formed with cleavage of O–C bond on both sides of the same monomeric structure [16][24][240]. Bisphenol A breakdown happens between phenyl ring and an isopropylidene group and will release phenol, and p-isopropylphenol, which is further led to the presence of 4-methylphenol, 4-ethylphenol and p-isopropenylphenol [11]. 2-methylphenol and 2-ethylphenol were also found in the pyrolysis oil, which are characteristic of the compounds generated when epoxy novolac is pyrolyzed [83]. Also, the breakdown of numerous other precursor intermediates would yield phenol [13]. By a further increase of temperature, larger organic compounds and later char are produced, while CH_4 and CO are emitted [24].

It’s also important to remember that slow pyrolysis totally destroys the bisphenol A structure, as none of the pyrolysis oils contained bisphenol A. [16][83] has described the

debromination process for brominated flame retardants to tetrabromobisphenol A, which was then converted to C_6H_5BrO, CH_3Br, C_2H_5Br, C_3H_5Br, C_3H_7Br, and HBr. While no evidence of such compounds were discovered in any of the oil and gas samples in our study, this could be attributed to the GC/MS detection limit or further degradation to Br.Furthermore, Y Shen et al. [241] has worked on the pyrolysis process for waste electronics with NaOH pretreatment and proved that it can help to fix produced HBr in the char by inhibiting Br release into the oil and gas. As shown in Fig. 5.6, our char XRF analysis confirmed the literature [11][241] and revealed a considerable amount of Br content in pyrolyzed char. Additionally, the bromine concentration in char is increasing with increased amount of biomass and is highest with CS60 and then decreased with CS70.

TABLE 5.3: List of compounds found only in the pyrolysis oil of PCB and CS feedstock, and completely absent from the co-pyrolysis oil product.

PCB				CS			
Area %	**Compound Name**	**Molecular Structure**	**Molecular Weight**	**Area %**	**Compound Name**	**Molecular Structure**	**Molecular Weight**
7.95	Styrene	C_8H_8	104.15	27.72	1,3-dioxolane,2,2-dimethyl	$C_5H_{10}O_2$	102.3
3.83	P-xylene	C_8H_{10}	106.16	12.82	N-cyano-2-methylpyrrolidine	$C_6H_{10}N_2$	110.16
1.59	1,2-benzenedicarbonitrile	$C_8H_4N_2$	128.13	8.71	2-cyclopenten-1-one, 3,5,5-trimethyl	$C_8H_{12}O$	124.18
1.4	Phenol, 3-ethyl	$C_8H_{10}O$	122.16	2.25	2-acetyl-2-methyl-succinonitrile	$C_7H_8N_2O$	136.15
0.99	3-hydroxybiphenyl	$C_{12}H_{10}O$	170.2	2.19	2-cyclopenten-1-one, 3-methyl	C_6H_8O	96.13
0.86	1-Naphthalenol, 5,8-dihydro-	$C_{10}H_{10}O$	146.2	1.62	1-Methoxy-1,3-cyclohexadiene	$C_7H_{10}O$	110.15
0.8	N-(1-Cyanovinyl)benzamide	$C_{10}H_8N_2O$	172.18	1.54	Acetic formic anhydride	$C_3H_4O_3$	88.06
0.63	2-Propenal, 2-methyl-3-phenyl-	$C_{10}H_{10}O$	146.2	1.32	Pyridine, 2,3-dimethyl-	C_7H_9N	107.15
0.29	Naphthalene, 2,3-dimethyl-	$C_{12}H_{12}$	156.2	1.32	9-Undecenal, 2,10-dimethyl-	$C_{13}H_{24}O$	196.33
0.29	4H-Cyclopenta[def]phenanthrene	$C_{15}H_{10}$	190.24	1.27	3,4-Dihydro-1-methylpyrrolo[1,2-a]pyrazine	$C_8H_{10}N_2$	134.18
0.28	9h-xanthene	$C_{13}H_{10}O$	182.2	1.16	7-Hydroxy-6-methyloct-3-enoic acid	$C_9H_{16}O_3$	172.22
0.27	4-Cyclohepta-2,4,6-trienyl-phenol	$C_{13}H_{12}O$	184.2	1.14	Cyclohexanol,3-(acetyloxymethyl)-2,2,4-trimethyl-	$C_{12}H_{22}O_3$	214.3
0.25	Cyclopentasiloxane, decamethyl	$C_{10}H_{30}O_5Si_5$	370.77	1.02	2-Octanol, 2-methyl-6-methylene-	$C_{10}H_{20}O$	156.26
0.23	Benzoic acid, 2(cyanomethyl), methyl ester	$C_{10}H_9NO_2$	175.18	0.71	8-Methyl-6-nonenamide	$C_{10}H_{19}NO$	169.26
0.23	Naphthalene, 2-phenyl-	$C_{16}H_{12}$	204.3	0.43	Bis(tridecyl) phthalate	$C_{34}H_{58}O_4$	530.8
0.22	2(5H)-furanone, 3-hydroxy-4,5-dimethyl-	$C_6H_8O_3$	128.1	0.41	Eicosane, 9-cyclohexyl-	$C_{26}H_{52}$	364.69
0.21	9H-Fluoren-9-ol	$C_{13}H_{10}O$	182.2	0.32	2-Azidomethyl-1,3,3-trimethyl-cyclohexene	$C_{10}H_{17}N_3$	179.26
0.19	1,1'-Biphenyl, 4-methyl-	$C_{13}H_{12}$	168.2	0.3	5,8-Decadien-2-one, 5,9-dimethyl-, (E)-	$C_{12}H_{20}O$	180.29
0.19	1H-Indene, 1-(phenylmethylene)-	$C_{16}H_{12}$	204.3	0.28	Pyrazine, 2,5-dimethyl-3-(1-propenyl)-, (E)-	$C_9H_{12}N_2$	148.2
0.18	Phenanthrene, 4-methyl-	$C_{15}H_{12}$	192.3	0.27	Z-8-methyl-9-tetradecenoic acid	$C_{15}H_{28}O_2$	240.38
0.17	Pyrene	$C_{16}H_{10}$	202.3	0.22	1,4-Dioxanyl hydroperoxide	$C_4H_8O_4$	120.1
0.16	Ethanone, 1(3-bromo-4-hydroxyphenyl)	$C_8H_7BrO_2$	215.04				
0.16	9H-Fluorene, 4-methyl-	$C_{14}H_{12}$	180.24				
0.15	2,4,4-Trimethyl-3,4-dihydroquinoline	$C_{12}H_{15}N$	173.25				
0.14	1,1'-Biphenyl, 2-methyl-	$C_{13}H_{12}$	168.2				
0.14	2-hydroxyfluorene	$C_{13}H_{10}O$	182.2				
0.13	7H-Benzo[c]fluorene	$C_{17}H_{12}$	216.28				
0.12	Anthracene, 9-ethyl-9,10-dihydro-9,10-dimethyl-	$C_{18}H_{20}$	236.4				
0.11	Silane, trimethyl-2-thienyl-	$C_7H_{12}SSi$	156.3				
0.1	Naphthalene, 1,7-dimethyl	$C_{12}H_{12}$	156.2				

This could be the combined effect of metals present in PCB and CS samples as well as the higher H content provided by CS biomass.

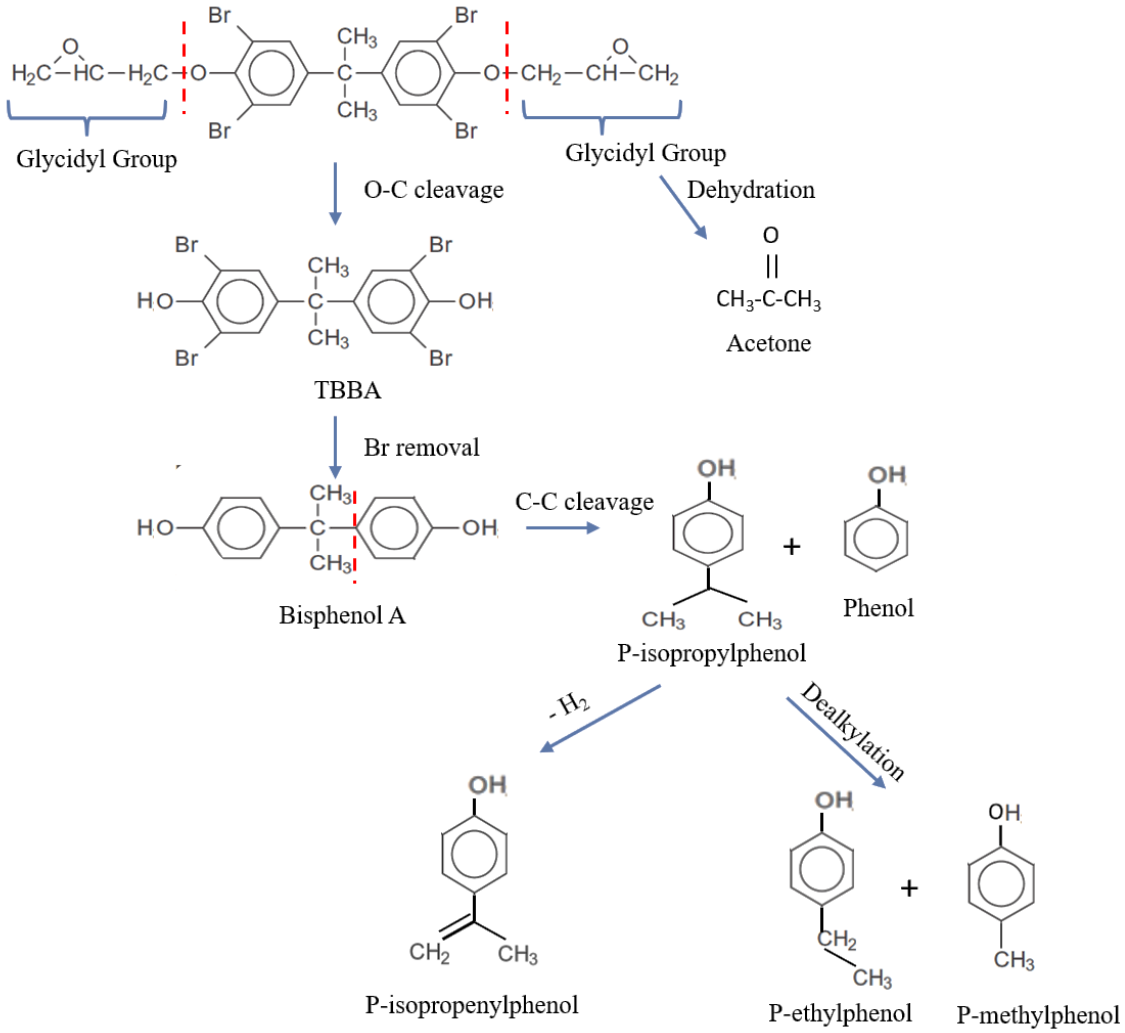

FIGURE 5.5: Possible reaction pathway of PCB for the production of phenol and phenolic compounds.

After the harvest of seed cotton, the cotton stalk is available as lignocellulosic biomass, which is high in cellulose, hemicellulose, and lignin.

Cellulose is a linear polysaccharide made up of 4000–8000 glucose units joined by β-1,4 glycosidic linkages. The most prevalent component detected in CS according to our GC/MS analysis is 1,3-dioxolane,2,2-dimethyl (27.72 area%). Which is derived solely from the breakdown of cellulose. Fig. 5.7 depicts the probable reaction pathway for producing 1,3-dioxolane,2,2-dimethyl from cellulose. Hydrolysis (cellulose to glucose), retro-aldol reaction (glucose to glycolaldehyde), and hydrogenation (glycolaldehyde to ethane-1,2-diol)

are all steps in the process of converting cellulose to ethane-1,2-diol [242]. Finally, 1,3-dioxolane,2,2-dimethyl is formed from ethane-1,2-diol in the presence of acetone.

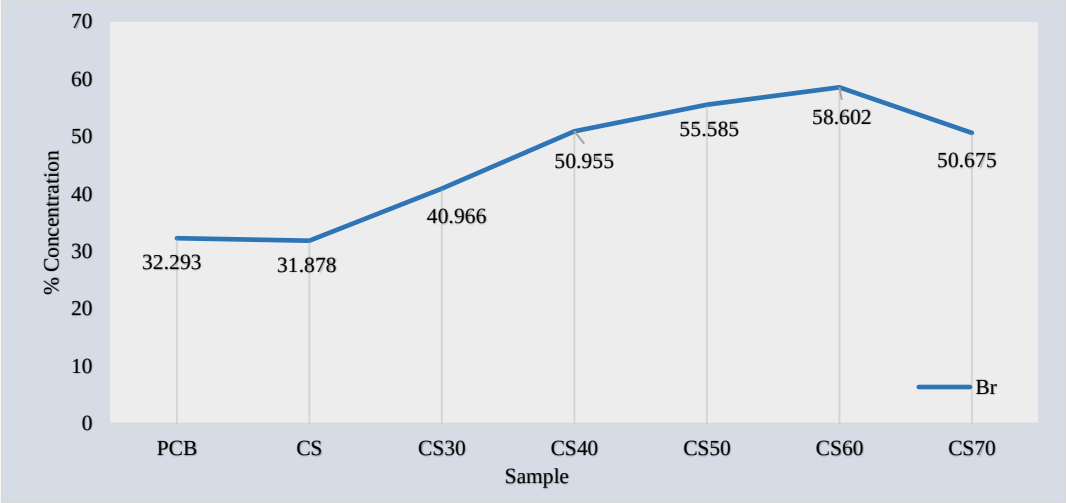

FIGURE 5.6: The amount of total Br found in each sample's char product by XRF analysis.

5.3.3.2 Reaction Pathways of CS

Hemicelluloses are non-cellulosic carbohydrates, and the pyrolysis chemistry of hemicelluloses is frequently studied using xylan. The pyrolysis occurs primarily by a free radical process with some furans, hydro-sugars and small molecule compounds [243]. Because of its lower degree of polymerization, xylan decomposes at a lower temperature than cellulose and lignin (220-315 ℃ [244]).

Lignin is a complex three-dimensional highly branched phenolic heteropolymer connected by C-O (β-O-4, α-O-4, 4-O-5 linkage) and C-C (β-5, 5-5, β-1, β–β linkage) bonds [243][245] Cotton stalk has more lignin (30 wt%) than other biomass. The relative amount of the monolignols (p-coumaryl alcohol/H, coniferyl alcohol/G and sinapyl alcohol/ S) differs significantly between the three biomass types (Hardwood, softwood and herbaceous crops). Cotton stalks have lignin that is made up of G-type units (coniferyl alcohol) and S-type units (sinapyl alcohol), similar to most hardwoods.

The presence of the most abundant β-O-4 ether linkages in hardwood lignin is due to the larger percentage of S-type unit in hardwood lignin compared to softwood lignin. This β-O-4 ether bonds has comparatively lower bond dissociation energy (BDE) than other ether bonds (5- 5, β-β, β-5, β-1) [246], which influences the synthesis of phenol and phenolic

monomers. A hypothesised chemical reaction route for the formation of phenol from G-type and S-type lignin in CS is shown in Fig. 5.8.

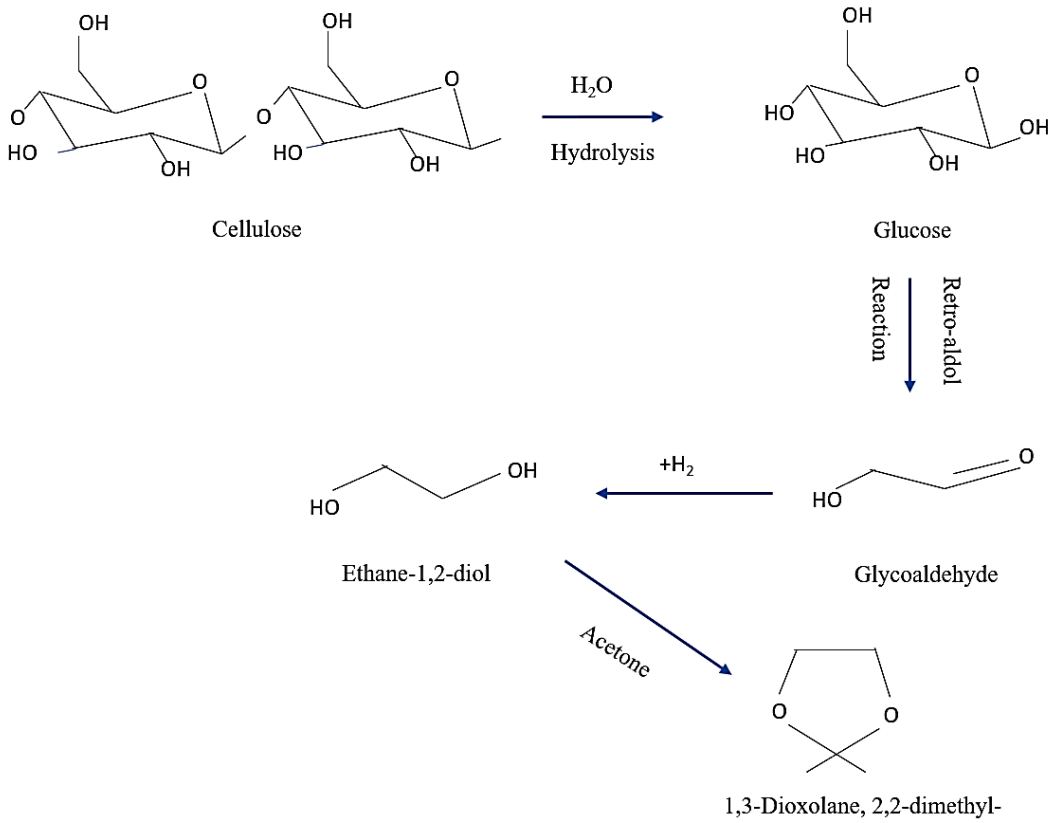

FIGURE 5.7: CS possible reaction pathway for the production of 1,3-dioxolane,2,2-dimethyl.

G-type lignin and S-type lignin are reductively fractionated to provide p-propylguaiacol and p-propylsyringol, respectively. Furthermore, because the bond energy of Ar- OCH_3 (356 kJ/mol) is lower than that of Ar-OH (414 kJ/mol), the methoxy group can be removed before the alkyl group without losing aromaticity or the phenolic hydroxyl moiety, which is a necessary step in the production of phenol. Demethoxylation of p-propylguaiacol and p-propylsyringol compounds yields p-propylphenol, which is subsequently trans-alkylated to create p-methylphenol and 3,4-dimethylphenol, which is then dealkylated to yield phenol. Huang et al. [247] looked into combining demethoxylation and dealkylation for lignin-derived monomers.

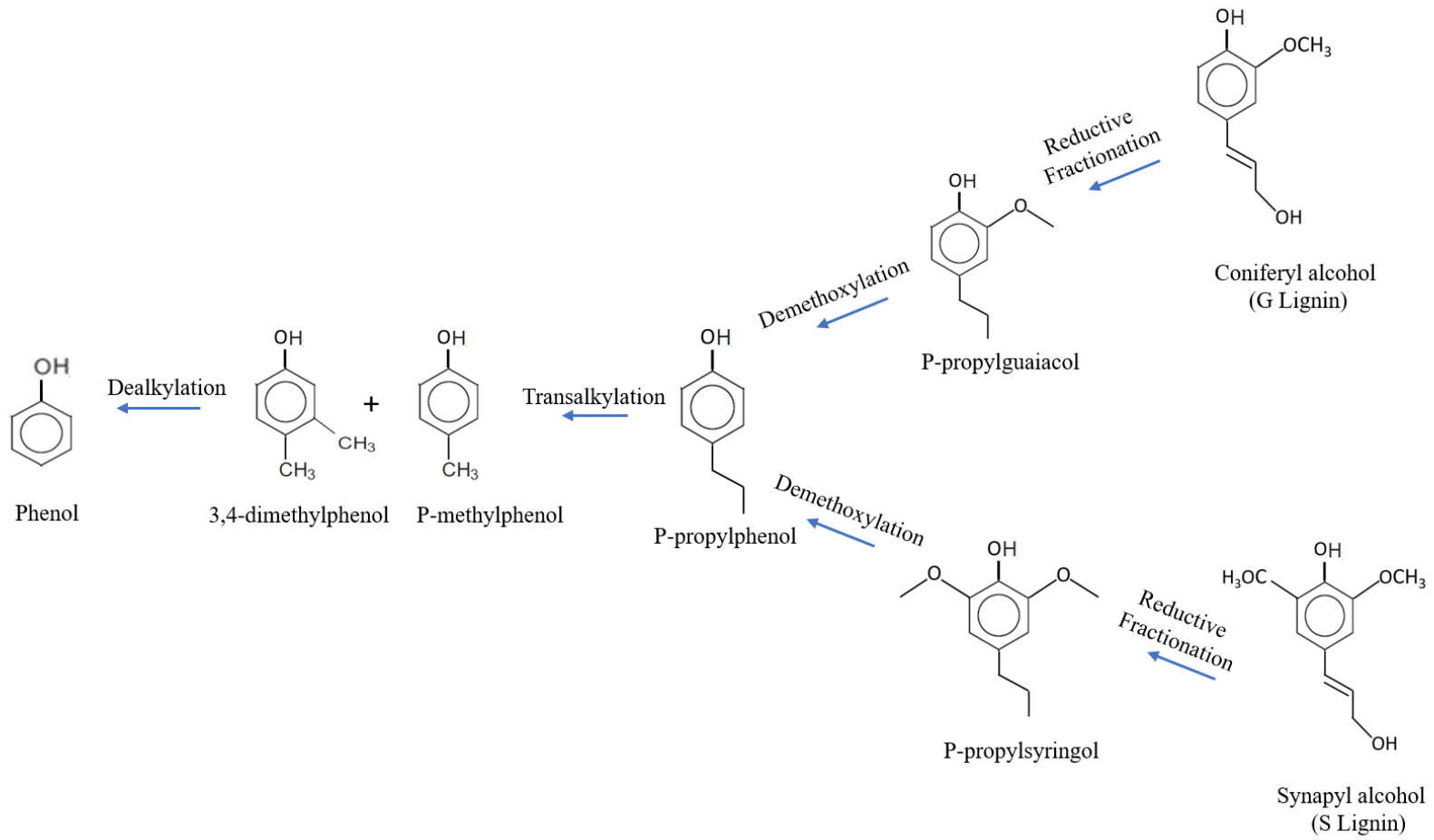

FIGURE 5.8: CS possible reaction pathway for the production of phenol.

5.3.3.3 Reaction Pathways of CS:PCB

In our studies, co-pyrolysis of CS:PCB resulted in higher amount of phenol and phenol derivatives, with a maximum for CS30. This could be due to the numerous metals found in PCB (e.g. Ni, Mo, Fe, Si, Ti) [248], which can aid in sufficient demethoxylation and transalkylation activity, followed by p-propylphenol or direct conversion from guaiacol/ syringol into phenol (See Fig. 5.8), coproducing small amount of cresol and other phenol derivatives mentioned in Table 5.1. In addition, the presence of 1,3-dioxolane,2,2-dimethyl in CS oil has completely vanished. As illustrated in Fig. 5.9, the interaction of Ethane-1,2-diol (Ethylene glycol (EG)) from CS with PC from PCB is the second possibility. PC and EG will be transformed to Bisphenol A, Ethylene carbonate, CO_2, and phenol,m-tert butyl by random scission. Finally, The C-C cleavage of bisphenol A and the dealkylation of phenol,m-tert butyl will produce phenol and phenolic compounds.

As per J. G. Kim [249], direct hydrolysis of polycarbonate in the presence of H_2O in CS can also aid to conversion in Bisphenol A and CO_2. The influence of reaction temperature on the rate of depolymerization of PC with EG was examined by Kim et al. [250]. According to him, high temperatures (>220 ℃) accelerate depolymerization and reduce induction time.

It should be mentioned that the focus of this study is on the elevated levels of phenol and phenolic compounds in co-pyrolyzed oil. As a result, the probable reaction routes detailed here are only for the formation of phenol and phenolic compounds.

5.3.4 Reduced toxicity

As per C. Ma and T. Kamo [251] in their research, HBr, bromophenol, dibromophenol and other derivatives were found in liquid products, due to debromination of BFRs in PCB, but here in our GC/MS result, only ethanone,1(3-bromo-4-hydroxyphenyl) was found in PCB oil with a very small amount (0.16 % area) and totally removed or below detection limit by co-pyrolysis products. This can be explained because the bromophenol is aromatic compound and the higher temperature can provide enough energy to partially break chemical bond and decompose it to compounds with lower molecular weight [21][252][253].

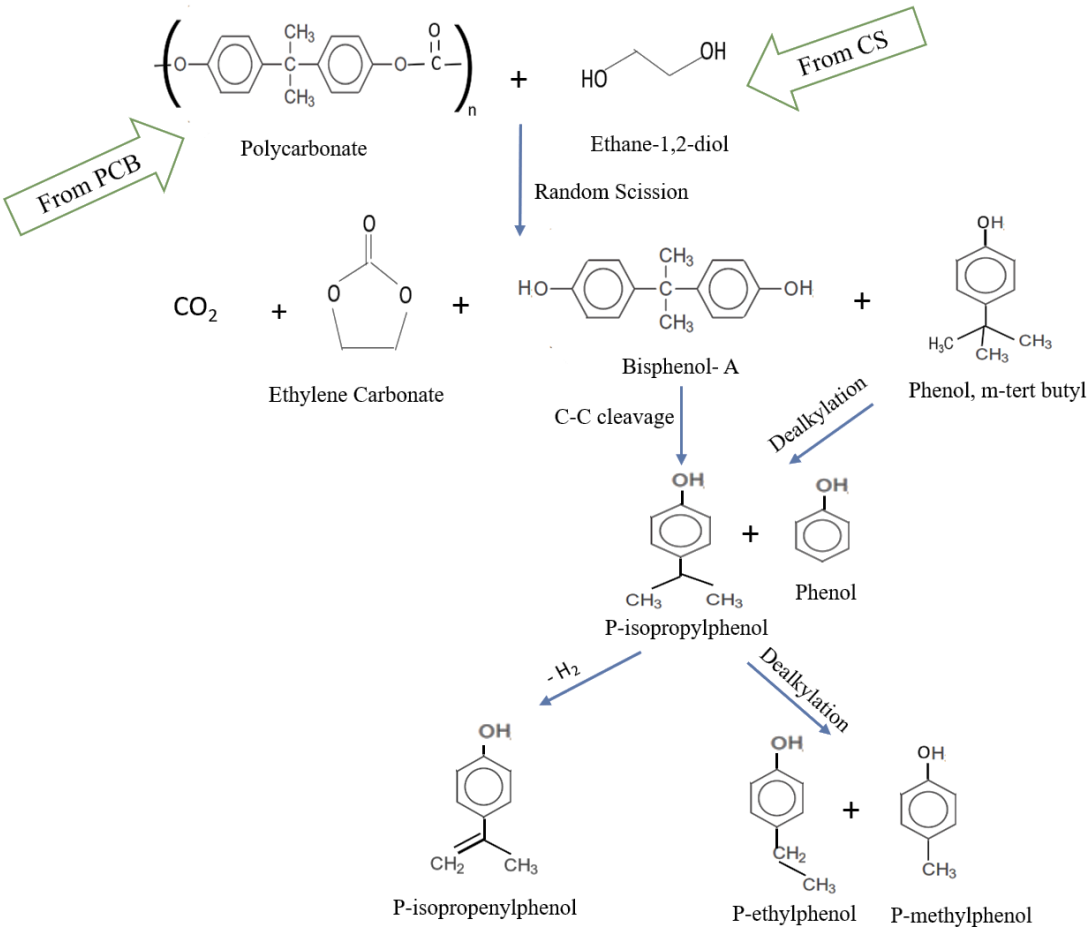

FIGURE 5.9: CS:PCB possible reaction pathway for the enhancement of phenol and phenolic compounds.

A Balabanovich et al. [95] supports this occurrence, as a significant number of Br radicals are formed at an early stage due to the poor C-Br bond strength, forming HBr by H-abstraction from the polymer chain and other brominated products via debromination reaction. Meanwhile, biomass acts as a hydrogen donor in the debromination reaction, and the increased supply of hydrogen in the phenol resin aids in the conversion of most organic bromine to inorganic HBr and its fixation in char [91][251]. Whereas, Mohammad et al. [21] has discovered evidence of HBr in the PCB pyrolysis oil, but GC/MS was unable to detect it in our case, possibly because to the lower molecular weight. Moreover, many authors have found that the amount of bromophenols generated during the pyrolysis process is affected by the presence of metals [83].

Furthermore, as shown with the GC/MS data in Table 5.1-5.3, none of the oil samples contain PBDD/Fs (product of TBBA fire retardant in presence of oxygen), attributable to the reductive environment of the pyrolysis process, which makes the formation of de-hydrogen

or de-hydroxyl radicals impossible [24]. This could also be reason of higher temperatures, which makes brominated materials undergo debromination and additional deterioration, inhibiting production of PBDD/Fs [92]. In addition, a very little amount of triphenyl phosphate, a phosphorus-based fire retardant, was discovered. Phosphate-based fire retardants are primarily utilised in thermoplastics [83], therefore their presence in PCB oil could be due to plastic attachments left with PCB, and co-pyrolysis had no discernible effect on any of the compositions.

The highly toxic furans produced in the form of Benzofuran, 2-isopropenyl-3-methyl and dibenzofuran are the most detrimental aspect of the PCB pyrolysis process feasibility. Table 5.2 concluded that with co-pyrolysis (CS60 and CS70 only), Benzofuran, 2-isopropenyl-3-methyl amount decreased, while for dibenzofuran co-pyrolysis with CS for all the composition helps to decrease the amount but cannot diminish it totally. The concentration of furans in pyrolysis oil rises with increasing temperature, although the quantity can be reduced at lower temperatures, as shown by [14][254]. Moreover, Benzoic acid, 2(cyanomethyl), methyl ester was also found in PCB oil and totally removed in co-pyrolysis products. As per GHS (Globally Harmonized System) of classification and labelling of chemicals this chemical is toxic if inhaled and the exposure to it can cause serious oral, dermal and ocular irritation.

5.3.5 Gas Analysis

Gas Chromatogram indicated H_2 and CH_4 as the most abundant pyrolysis gas in all the samples. Whereas, very small amount of other hydrocarbons like C_2H_6 and C_2H_4 was also there. From Fig. 5.10, It is seen that H_2 concentration in PCB is 46.38 % area, which decreases with increasing CS concentration from 30% to 40% and if we examine different CS composition then it is maximum with CS50 (44.49 % area). Methane, on the other hand, is found 41.26 area % in PCB gas and the values start increasing up to CS 40% composition and then it is lowest at CS50 (51.84 % area) and maximum at CS70 (66.13 % area).

Total of Hydrogen and Methane found in the sample ranges from 87.64, 98.58, 94.15,96.1, 95.77, 98.14 and 97.75 for PCB, CS30, CS40, CS50, CS60, CS70 and CS respectively. We can deduce from the results that using a 70 % CS in PCB composition can assist increase the

quantity of methane, which is one of the key fuels in industries, but using a 50:50 CS:PCB composition can maximise the amount of Hydrogen in gas. There are no indications of halogen gases, which is a plus because hydrogen halides are extremely corrosive and can cause the development of dioxins and furans when used as fuel.

(a) (b)

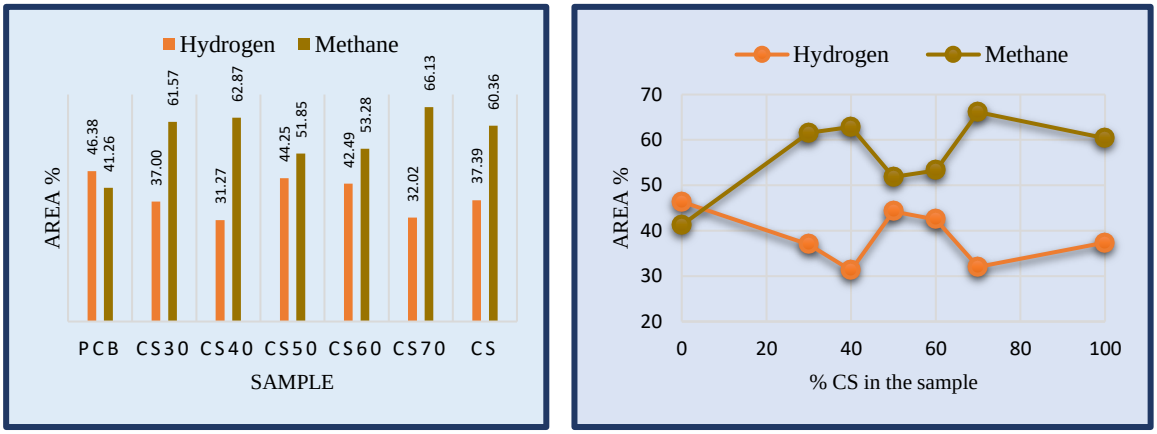

FIGURE 5.10: (a) amount of gas produced in % area, (b) Comparison chart of effect of CS composition on gas yield.

5.3.6 Physical Properties of generated oil

It is required to examine the chemical composition as well as the physical properties of the generated oil in order to determine its feasibility for application. The type of feedstock used and the procedures used to produce it have a great impact on the quality of the oil [231][255]. Compared to biodiesels, pyrolysis bio-oils and PCB oils are unsuitable for fuel atomization, due to their high viscosity and high-water content, resulting in lower calorific value and flame instabilities. Also, lower calorific value, causes slow vaporization, which leads to delayed ignition and decreased burning rate. Furthermore, since pyrolysis oils are extremely oxygenated, they are immiscible with fossil fuels [256]. As shown in Fig. 5.2, PCB pyrolysis oil is dark brown in colour, whilst CS generated oil is clearer and light orange. This appearance is significantly influenced by the existence of micro carbons, the amount of water in the oil, and the chemical composition of the oil [12][53]. Also, the samples have an acrid smoky smell, due to presence of lower molecular weight acids and aldehydes [53]. In this study, pyrolysis oil of PCB, CS, and various CS:PCB compositions were tested using FAME (Fatty acid methyl esters) test methods, which are known to define the product to be used as automotive diesel fuel and required criteria are compared to automotive diesel fuel Bharat

Stage VI (IS 1460-2017) and FAME requirements, as shown in Table 5.4. The results show that all of the pyrolysis oils' qualities fail to meet the IS automotive diesel fuel and FAME criteria, with the exception of CS50, which meets all of the requirements except for phosphorous content and calorific value. This implies that changing the CS:PCB ratio to 50:50, can enhance pyrolysis fuel qualities to some extent. Very importantly, the amount of water in the fuel oil is reduced below the limit by CS50. In contrast, the higher fuel water content in other samples indicates delayed ignition, poor fuel atomization, instability of combustion, and decreased combustion rates, all of which result in increased emissions [256]. The high flash point of CS50 indicates a higher level of safety during storage, usage, and transportation [28][237], as well as flammability difficulties. Furthermore, it is very important to reduce bromine content in generated oil, as bromine is corrosive to human tissue in a liquid state and its vapours irritate eyes and throat. Also, bromine vapours are very poisonous when inhaled [253]. So, Br_2 concentration in oil is also analysed to ensure that the amount of Br_2 in the co-pyrolysis oil product is minimised. H William [257] investigated the pyrolysis of brominated high impact polystyrene and acrylonitrile-butadiene-styrene in the presence of a waste fluidized catalytic cracker (FCC) catalyst in a fixed bed reactor, and discovered that the FCC catalyst was effective at reducing the bromine content of the pyrolysis oils. On the other hand, extra hydrogen from biomass aids in the reduction of bromine in oil and its fixation in char [26]. Here, in our investigation, bromine content in PCB oil was found to be 77.53 mg/100g of sample, whereas, it was found 48.41 mg/100g in CS and addition of CS resulted in a reduced Br_2 in different CS:PCB pyrolysis oils. Importantly, in CS40 oil it was found to be lowest (29.88 mg/100 gm).

The acid value is related to organic acids, most likely acetic and formic acids, and is above 0.2 mg KOH/gm (Max. limit of Automotive diesel fuel) for all pyrolysis oils, but below 0.5 mg KOH/g, satisfying the requirements of FAME limits. The higher acid value can result in corrosion of typical construction materials such as carbon steel and aluminium [236]. Importantly, the calorific value (the amount of energy released by full combustion of a fuel) of all the samples was determined using an oxygen-bomb colorimeter, and the results ranged from 22 to 26 MJ/Kg, with CS50 resulting in a little increase (28.41 MJ/Kg). Indeed, it is still very lower than automobile diesel requirements (43-46 MJ/Kg) due to the possible detrimental impact of high-water content and high oxygen content [255].

5.3.7 Possible applications of the oil

Many studies [233][258] discovered bio-oil to be a high-quality fuel oil that may be used to generate heat, power, and chemicals in replacement of fossil fuels. It can be used in boilers, furnaces, turbines, and traditional diesel engines that run at medium and slow speeds [53].

While a number of publications [53][238] revealed that these pyrolysis oils cannot be used directly as transportation fuels, so some possible solutions and upgrading treatments were suggested. For example, A. Oasmaa and S. Czernik [236] discussed bio-oils fuel quality aspects, which can cause major problems for combustion applications, and revealed that the high ash content and high viscosity crude bio-oils could only be used as a substitute for No. 6 fuel oil. However, adopting relatively simple processes like solvent addition to lower viscosity and boost chemical stability, filtration to remove char and alkali, bio-oil can be upgraded to meet the same quality standards as No. 2 fuel oil. S Zhang et al. [259] has pyrolyzed sawdust in a fluidized bed at a temperature of 470 ℃ and short residence time of up to 2 seconds. The generated oil phase was upgraded into liquid fuel by hydrotreatment using sulfidic Co–Mo–P in an autoclave with tetralin as solvent, which result in a significant decrease in oxygen content and increased heating value from 21.3 MJ/kg to 41.4 MJ/kg.

Y. Xu [260] recommends adding certain solvents to limit polymerization via esterification and emulsifiers to avoid phase separation difficulties, as well as increasing calorific value, lowering pH, and lowering viscosity. According to Y. Y. Chong et al. [261], one of the direct applications for bio-oil is emulsification with diesel. By varying the bio-oil, diesel, and surfactant ratios, the researcher explored the impact of emulsification parameters on the combustion qualities of a bio-oil (produced from Palm Kernel Shell biomass at 500 ℃ temperature) diesel emulsified combination. For maximum heating value (42.19 MJ/kg), pH (3.29), and lowest density (0.86 g/cm^3), the best ratio was determined to be 90% diesel and 10% bio-oil with 10% surfactant. M Bardalai and D Mahanta [255] compared the properties of the pyrolysis oil and the thermally treated pyrolysis oil of different biomass like, mesquite saw dust, pine saw dust and wheat shell. He noticed that, in the treated oil, the Conradson Carbon Residue (CCR) was relatively very low. There are numerous possibilities for research in to the optimization of various parameters and operating conditions, as well as the application of different processes, in order to obtain a suitable oil product.

According to our findings, pyrolysis oil produced from CS50 meets most of the criteria for usage as an automobile fuel, with the exception of a few constraints such as a lower calorific value and a higher phosphorous content. The lower the calorific value, the less heat is produced with complete combustion, whereas the greater the phosphorous concentration, the more damage is done to emission control systems [262]. As a result, considerably more work is needed on oil stabilisation and upgrading, as well as hydrodeoxygenation, catalytic cracking, and steam reforming of bio-oils, which are all extremely complicated procedures

TABLE 5.4: Fuel properties of the pyrolyzed oil samples, compared with automotive diesel fuel and FAME standards.

Test Parameters	Unit	PCB	CS	CS30	CS40	CS50	Cs60	CS70	Bharat stage VI (IS 1460-2017)	FAME Limits	Test Methods (FAME)
Density 15°C	g/cm³	0.912	0.923	0.915	0.908	0.88	0.911	0.903	0.815-0.845	0.86-0.9	EN 14214:2003
Kinematic Viscosity @ 40 °C	mm²/s	4.4	4.46	5.12	4.95	4.11	5.25	4.26	2.0-4.5	3.5-5	EN 14214:2004
Distillation	%@ °C	90%	93%	94%	85%	95%	92%	79%	-	-	EN 14214:2005
Flashpoint	°C	120	123	122	119	126	114	114	66 @ 40°C	Min. 101	EN 14214:2006
CFPP	°C	45	43	48	45	45	51	40	6 °C winter, 18 °C summer	-	EN 14214:2007
Cloud point	°C	-31	-29	-32	-29	-32	-30	-27	-	-	EN 14214:2008
Sulphur	mg/kg	18	15	19	28	8	30	23	Max10	Max. 10	EN 14214:2009
CCR 100%	%mass	19	16	22	18	18	26	15	-	-	EN 14214:2010
Carbon residue (10 % dist.residue)	%mass	0.56	0.4	0.55	0.52	0.22	0.49	0.47	0.3	Max.0.30	EN 14214:2011
Sulphated ash	%mass	0.067	0.056	0.045	0.056	0.012	0.032	0.04	-	Max. 0.02	EN 14214:2012
Oxid ash	%mass	0.33	0.25	0.61	0.34	0.14	0.54	0.26	-	-	EN 14214:2013
Water	mg/kg	840	852	829	831	413	824	827	Max. 200	Max 500	EN 14214:2014
Total contamination	mg/kg	32	29	28	31	24	25	28	max. 24	24	EN 14214:2015
Cu corrosion	3h/50°C	1	1	1	1	1	1	1	Not worse than No.1	class 1	EN 14214:2016
Oxidation stability	hrs;110°C	6 hours	6 hours	6 hours	6 hours	6 hours	6 hours	6 hours	-	Min. 6 hours	EN 14214:2017
Cetane number		47	49	53	48	51	56	44	Min. 51	Min. 51	EN 14214:2018
Acid value	mgKOH	0.45	0.38	0.52	0.4	0.43	0.43	0.36	0.2	0.5	EN 14214:2019
C(x:4) & greater unsaturated esters	%mass	1	1	1	1	1	1	1	-	Max. 1	EN 14214:2029
Phosphorus	mg/kg	18	15	31	28	10	28	31	-	4	EN 14214:2030
PAHs	%mass	0.25	0.32	0.35	0.52	0.42	0.18	0.2	Max. 8	-	EN 14214:2034
Lubricity/ wear	µm at 60 °C	15	8	12	16	10	9	13	Max. 460	-	EN 14214:2035
Bromine Content	mg of Br_2 per 100 gm of sample	77.53	48.41	82.47	29.88	43.1	32.45	56.18	-	-	ASTM D1159-07(2017)
Calorific value	Mj/kg	23.16	24.19	25.16	22.45	28.41	26.52	20.95	43-46 [28][231][232]	-	By Bomb Calorimeter

that require reliable and fully developed reactors [238]. In contrast, pyrolysis oil contributes to a production of high value chemical compounds that are more valuable than fuel oil. It is a large resource of phenol and phenolic compounds, which have recently drawn interest because of its potential applications as fuel additives and chemical precursors. After separation, some phenols and phenol derivatives can be employed as food antioxidants, transportation fuel additives, chemical product precursors (pesticides, dyes, pharmaceutical products), and resin industry products [263]. Moreover, T Rieger et al. [258] demonstrated that achieving a high yield of phenol requires close contact between the Au/TiO_2 de-methoxylation catalyst and the HZSM-5 trans-alkylation catalyst. Furthermore, C Quan et al. [81] suggests that the more feasible application for PCB generated oil is to use it as a carbon source. The researcher explained synthesis method of the CNTs (Carbon Nano Tubes) and porous carbons from PCB waste pyrolysis oil with formation mechanism. In our research, GC-MS result revealed that the major concentration of PCB, CS composition are phenol and phenolic compounds, and the concentration increases with co-pyrolysis. Indeed, CS60 can be a major source of phenol, without using any catalyst or process modification.

5.4 Conclusion:

Pyrolysis of non-metallic PCB waste produces valuable liquid, gas, and char, aids in reducing waste and energy generation. Most importantly, nowadays more research being conducted on the production of pyrolysis oils that can be used as automotive fuels. This is only conceivable if the oil product is halogen free and meets the required fuel specifications.

In this regard, to improve oil quality and quantity while lowering brominated compounds, co-pyrolysis with various CS compositions (CS30, CS40, CS50, CS60 and CS70) was performed and physical and chemical characterization of the generated oil is made. Also, possible reaction pathways, upgradation techniques and applications are discussed in detail and the benefits of the different composition of co-pyrolysis results are discussed below.

PCB has a lower volatile content (41.87 wt%) than CS (70.51 wt%) because it contains more inorganic elements and ash. As a response, as the value of biomass increases, the residual percent decreases, allowing the volatile quantity to rise and therefore improving the oil yield. Pyrolysis of PCB had generated lowest amount of oil (19.6%), Whereas, the amount of oil

generated by co-pyrolysis rose significantly as CS was increased, peaking at CS70 (31.5 %), also radical interaction of PCB and CS prevents phase separation during the co-pyrolysis reaction.

PCB had total of 60.67 % phenol and phenolic compounds, while CS had just 25.94 %. However, when co-pyrolysis was used, the amount increased, which can be attributed to the combined effect of bisphenol A decomposition in epoxy resin of PCB and lignin decomposition of CS. Total phenol and phenolic compounds generated in the co-pyrolyzed oil products vary from 78.63, 69.77, 76.82, 75.29, and 74.3 % area for CS compositions 30, 40, 50, 60, and 70 %, respectively.

Biomass acts as a hydrogen donor in the debromination reaction, and the enhanced quantity of hydrogen in the phenol resin aids in the conversion of most organic bromine to inorganic HBr and its fixation in char. XRF analysis of char revealed that the bromine concentration in PCB char is lowest (32.29 %), increases with increased amount of biomass, and is maximal with CS60 (58.60 %). Whereas, bromine content in PCB oil was found to be 77 mg/100g of sample, and decreased significantly in co-pyrolysis oil products. Importantly, in CS60 oil it was discovered to be 30.45 mg/100g, whereas, in CS40 oil it was found to be lowest (29.88 mg/100 gm). Perfect reaction mechanisms, on the other hand, are still need to be invented.

Hazardous compounds such as benzoic acid,2(cyanomethyl),methyl ester, and ethanone,1(3-bromo-4-hydroxyphenyl) were discovered in minor amounts in PCB oil and were completely eliminated in co-pyrolysis oil products. In addition, the amount of benzofuran, 2-isopropenyl-3-methyl, and dibenzofurans in all co-pyrolysis oil products is reduced.

A CS70 composition can assist increase the quantity of methane in generated gas, which is one of the most essential fuels in industry, whereas a CS50 composition can help increase the amount of oxygen in gas. Furthermore, when all of the pyrolyzed oil samples fail to meet the automotive fuel criteria, CS50 meets all of them except for phosphorous concentration (10 mg/kg) and calorific value (28.41 MJ/Kg). So, with CS50 even if it has some benefit like increased amount of oxygen in gas and meeting most of fuel criteria, still more work is

needed on upgrading, which may include hydrodeoxygenation, catalytic cracking, and steam reforming, which are all extremely complicated procedures that require reliable and fully developed reactors. On the other hand, CS60 can contribute to a production of high value phenol and phenolic compounds, that are more valuable than fuel oil.

CHAPTER 6

Char Analysis

6.1 Introduction:

Solid chars are acquiring popularity these days due to a variety of applications based on their quality, including adsorbents, carbon fuel cells, supercapacitors, soil amendment, gasification and co-combustion [264][265], formation of activated carbons, and graphene production [266]. Valorisation of biomass-generated char has become more of a research focus. According to [265][267], biomass pyrolysis char can be utilised as a heat source for the pyrolysis process and as a biofuel feedstock for domestic use, as well as in existing coal power plants. Additionally, compared to commercial activated carbon products, Deng et al., [268] claimed that biochar with good magnetic properties is easily separated from liquid and is better suited for livestock wastewater treatment. In recent years, biochar has become a popular topic of study in the realm of wastewater treatment [269][270]. Biochar can also be utilised as a slow-release fertiliser and has agricultural environment-friendly qualities [271] due to its high nitrogen and phosphorus adsorption ability. However, its specific applications are dependent on its physicochemical characteristics, which might vary depending on the feed stalk and processing method used to obtain it; consequently, it is critical to understand its chemical and physical properties in order to find an appropriate application [272].

Till date researchers had characterized pyrolyzed char generated from different biomass or PCB individually and found potential applications of it [273][274][276]. However, not a single literature is available for the characterization and potential applications of the char produced from the co-pyrolysis of PCB with cotton stalk. The result of this investigation showed that the co-pyrolysis of PCB and CS is more favourable than pyrolysis of CS or PCB separately. It had proven to be an economical and alternative waste management approach,

as well as a way to contribute to energy security by lowering dependency on fossil fuels. In this regard, present study examines the morphological and physical characteristics of co-pyrolyzed PCB and CS char, including the distribution of pore sizes, surface area, porosity, structural characteristics, and chemical analyses.

6.2 Result and Discussion:

6.2.1 Characterization of CS:PCB char

An ultimate and proximate analysis of CS, PCB and different mixtures are shown in Table 6.1. It can be seen that hydrogen concentration for various compositions of CS:PCB char samples decreased with increasing biomass concentration in comparison to PCB, while the carbon content was increased except for CS60. Moreover, oxygen content of CS50 and CS70 is much lesser. This suggests that hydrogen and oxygen are lost at a faster rate than carbon in these co-pyrolyzed char. The PCB sample had a larger loss on drying (LOD) than the CS sample, which can be related to dehydration response of water content as well as release of more volatile components such as CO_2, CO, and CH_4.

TABLE 6.1: Proximate and ultimate analysis of the char sample.

Properties	PCB	CS	CS30	CS40	CS50	CS60	CS70
Proximate analysis (wt. %)							
LOD	4.41	0.92	1.12	2.03	1.26	1.14	1.19
Ash	68.59	8.96	75.15	79.13	78.71	64.92	78.76
VM	16.51	56.69	21.25	17.99	18.9	22.29	19.04
Fixed Carbon (%)	10.49	33.43	2.48	0.85	1.13	11.65	1.1
Ultimate Analysis (wt %)							
Hydrogen	1.89	2.51	0.96	0.85	0.71	1.98	0.47
Carbon	23.87	23.1	32.71	55.91	82.5	32.12	88.17
Nitrogen	1.32	4.52	1.58	1.85	1.12	2.44	1.18
Sulphur	0.074	0.605	0.174	0.17	0.287	0.277	0.304
Oxygen	31.44	16.19	47.06	22.51	10.09	46.24	7.62
Others*	41.406	53.075	17.516	18.71	5.293	16.943	2.256
HHV(MJ/Kg)	5.13	8.51	3.96	16.08	27.11	5.38	29.12
H/C	0.08	0.11	0.03	0.02	0.01	0.06	0.01
O/C	1.32	0.70	1.44	0.40	0.12	1.44	0.09

*Others calculated from difference of ultimate analysis (C, H, N, S, O).

An amount of LOD in each CS:PCB composition was nearly same, with exception of CS40, which was slightly more (2.03 wt.%). The ash content of PCB char was 68.59% consisted incombustible inorganic material, was increased with co-pyrolysis and highest value was

achieved for CS40 (79.13%). This higher ash content of co-pyrolysis char may be the reason of thermal breakdown of organic molecules, resulting in CO_2 emission and formation and condensation of mineral elements [273].

The higher heating value (Gross calorific value) of all the char samples was calculated using Dulong's formula [273] as per Equation (3.1). The sample CS70 has a high quantity of total carbon, lower H/C and O/C ratio as well as higher HHV (29.45 MJ/Kg), indicates that removing ash from CS70 char could lead to its use as a solid fuel. Furthermore, fuels with lower H/C and O/C ratio as CS70, is highly favourable due to lower smoke generation, water vapor production and loss of energy during combustion. According to Shaaban et al. [274], low oxygen content increases the char's surface hydrophobicity. In this regards CS70 has highest amount of C (88.17 %) and lowest amount of O (7.62 %), which could make it useful for operations such as removing contaminants from aqueous matrices.

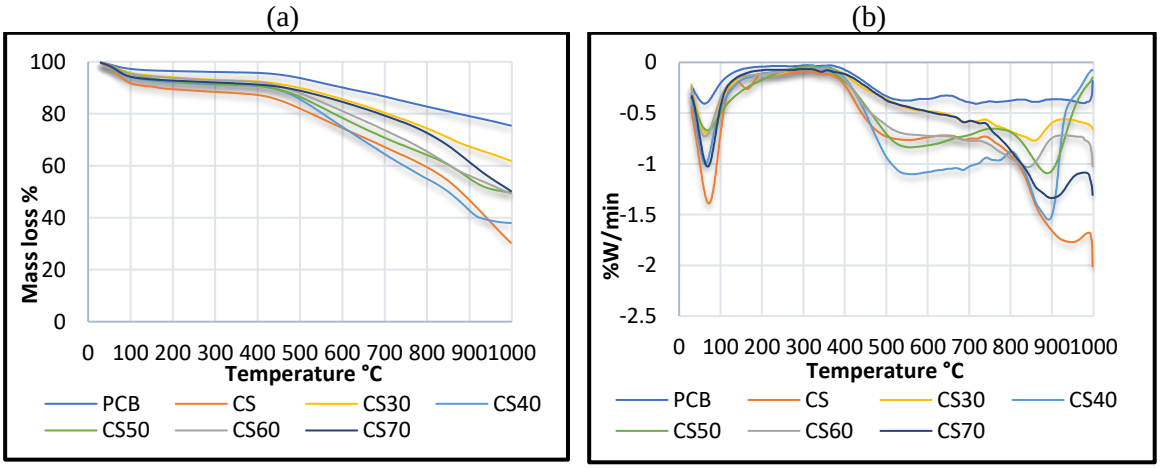

FIGURE 6.1: (a) TGA curves and (b) DTG curves obtained in an inert atmosphere at 10 ℃/min heating rate for char samples of PCB, CS and CS:PCB mixture.

TGA Fig. 6.1(a) and DTG Fig. 6.2(b) curves show endothermic heat effects for different char samples. The samples were heated from ambient to 1000 ℃ in an inert atmosphere with 10 ℃/min. A very slow and initial weight loss was visible up to 150 ℃ for PCB and co-pyrolyzed samples, the reason may be release of moisture and smaller molecules. The same behaviour was attributed to CS sample before 120 ℃, after that no apparent change in the sample weight was observed up to 400 ℃. The high rate of decomposition for PCB, CS and the mixture char began about 370 ℃, whereas for the mixture CS50 it started around 320 ℃.

The maximum rate of breakdown for PCB char was occurred close to 540 ℃, followed by very gradual and continuous mass loss, whereas the highest rate of decomposition for the CS and mixtures occurred above 500 ℃, associated with degradation of cellulose followed by hemicellulose degradation and above 800 - 900 ℃ the minor decomposition was associated with lignin decomposition. The co-pyrolysis most likely resulted in a stable carbon form that can endure higher temperatures, hence improved thermal stability.

Moreover, Fig. 6.1(a) shows that the overall mass loss for PCB was 25% explaining high ash content. For CS it was found 70%. However, the overall mass loss for co-pyrolyzed char sample for CS30 was 38%, whereas it was around 50% for CS50, CS60, and CS70 and was highest at CS40 (62%). This observation indicated that CS30 char took longer to decompose and more thermally stable structure than other compositions at the same operating temperature and heating rate.

6.2.2 Surface area and porosity

The surface area of char has a significant impact on its reactivity and combustion behaviour [275], and porosity and pore-size distribution are the most critical variables that determine the bulk of its mechanical and chemical properties, including flow and fluid behaviour [276]. N_2 adsorption isotherms disclose details on size distributions in the micro, meso, and macro porosity ranges (approx. 0.5–200 nm) when performed over a broad array of relative pressures (P/P_0) [277]. where P and P_0 are the absolute equilibrium pressure and the condensation pressure of nitrogen, respectively.

TABLE 6.2: BET surface area and porosity of the samples.

Sample	Average pore diameter (nm)	BET Surface area (m^2/g)	Total pore volume (cm^3/g)
PCB	3.458	2.575	0.005
CS	25.604	4.535	0.024
CS30	3.475	16.791	0.027
CS40	3.484	3.187	0.006
CS50	3.507	0.736	0.002
CS60	3.484	2.913	0.006
CS70	3.485	6.226	0.011

The International Union of Pure and Applied Chemistry categorize pores depending on the size (IUPAC). Micropores are those with a diameter of less than 2 nm, mesopores are those with a diameter of 2–50 nm, and macropores are those with a diameter higher than 50 nm.

Micropore filling (which aim on filling pore space instead of surface coverage), capillary condensation and multilayer adsorption filling mechanism prevail in micropores, mesopores and macropores, respectively. The primary surface properties of all char samples were determined using BET analysis (Table 6.2). The samples exhibited an average pore diameter of 2 to 50 nm, indicating that they were mesoporous materials filled by capillary condensation. It's worth noting that capillary condensation implies, filling of residual pore space left after multilayer adsorption with the condensate which is separated from the gas phase by menisci [272].

PCB and CS has a BET surface area 2.575 m^2/g and 4.535 m^2/g, respectively, CS30, on the other hand, has a comparatively higher surface area of 16.791 m^2/g, and the total volumes/g of the samples is also higher than other samples, indicating a significantly higher adsorption capacity than PCB, CS and other co-pyrolyzed char samples. The lowest surface area and total pore volume of CS50, may be due to persistent volatile materials, which causing the co-pyrolyzed char porosity to be blocked, indicating a very low reactivity [277].

6.2.3 Textural properties

The relationship between the amount of gas adsorbed and the gas's equilibrium pressure at constant temperature is known as the adsorption isotherm. The IUPAC classifies the adsorption isotherms into six types: Type I to Type VI. A detailed description of the isotherm classification is presented in [277].

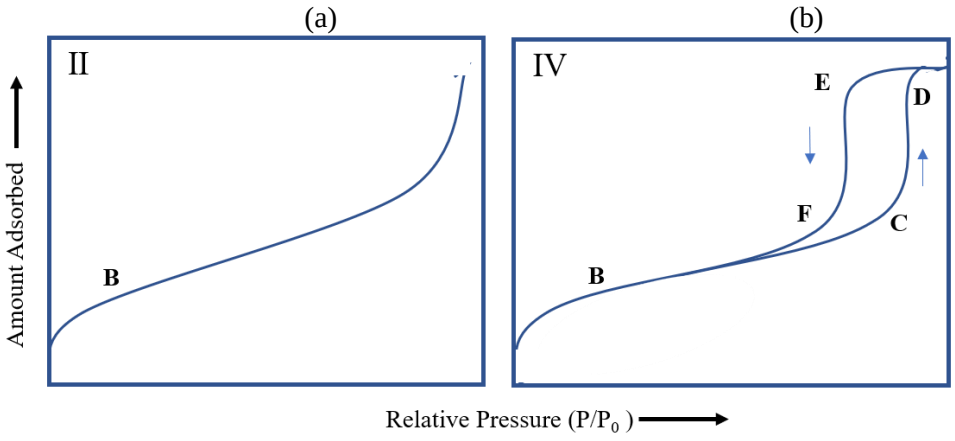

FIGURE 6.2: Type II and IV N_2 adsorption desorption isotherm pattern.

In our investigation, all of the char samples involve a combination of types II and IV adsorption-desorption isotherms. So, for a better understanding, Type II and Type IV isotherms are explained in detail (see, Fig. 6.2 (a) and (b)).

A non-porous or macro-porous material will have a completely reversible Type II isotherm, implying the substance is nonporous or only has pores with diameters greater than micropore dimensions. The completion of monolayer coverage and the start of multilayer sorption are shown by the inflection point B. There will be no hysteresis because adsorption and desorption will take the same path (See Fig. 6.2 (a)).

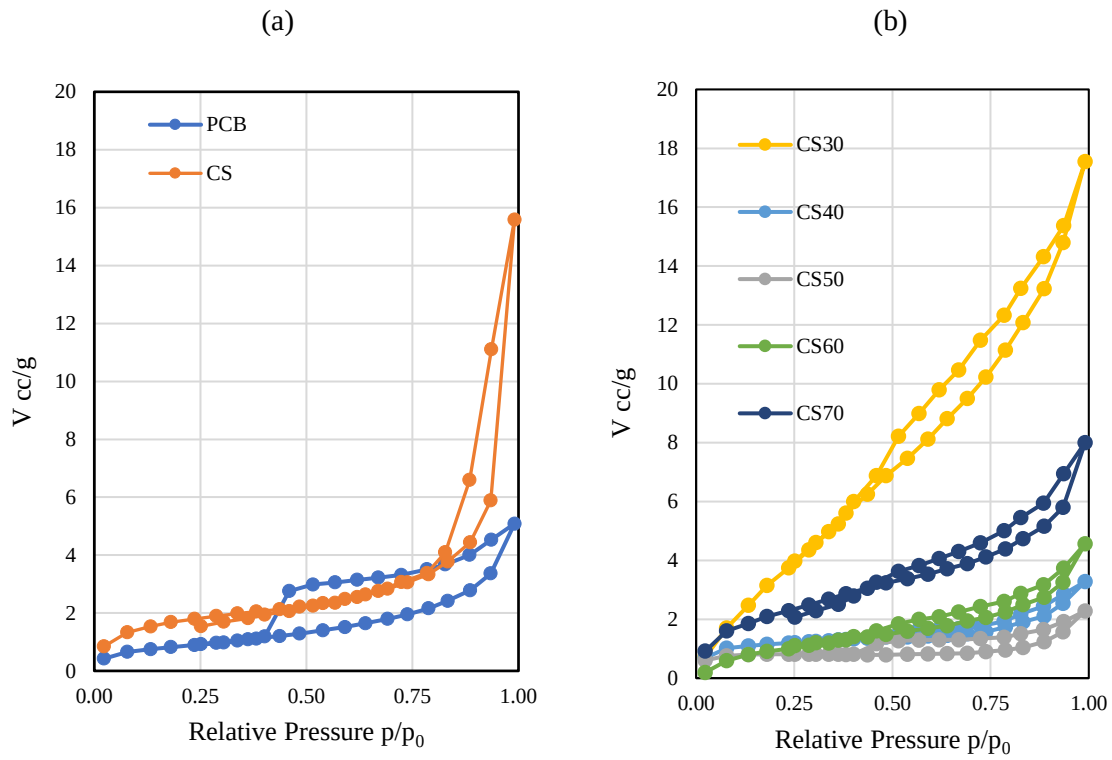

FIGURE 6.3: Type II and IV N_2 adsorption desorption isotherm pattern for PCB and CS (a), N_2 adsorption-desorption isotherms for co-pyrolyzed char samples (b).

Whereas, a type IV isotherm with hysteresis loop will exist in a purely mesoporous material, which is connected with capillary condensation and evaporation in mesopores (See Fig. 6.2 (b)). At lower relative pressures, the isotherm exhibits a concave form, indicating completion of micropore filling and single layer adsorption ($P/P_0 \approx 0.01$) and commencement of multi-layer adsorption ($P/P_0 < 0.2$) (at point B). Finally, at higher relative pressures ($P/P_0 > 0.4$), the adsorption quantity grows quickly, with a convex shape to the P/P_0 axis. The hysteresis

loop here is the indication of presence of mesopores and occurrence of capillary condensation phenomenon. Point C indicates initiation of capillary condensation and point D is the indication of completion of pore filling by capillary condensation. Finally, curve E → F shows desorption phenomena. Fig. 6.3 (a) and (b) represents the N_2 adsorption-desorption isotherms of the chars exposed to N_2 gas at constant cryogenic liquid nitrogen temperature 77 K and the volume of adsorbed gas on the solid surface is determined at distinct pressures over the relative equilibrium adsorption pressure (P/P_0) range of 0.075 – 1.0. The hysteresis pattern and isotherm shape provide important information about the physical adsorption mechanism and may thus be used to identify different types of pores in the adsorbent.

The hysteresis loop's shape and size can also be used to interpret relevant information about the kind of pores contacted by N_2 during sorption. A thin distribution of cylindrical pores is indicated by a wider plateau region of the loop at increasing P/P_0, as seen in Fig. 6.2 (b). An extremely tapered hysteresis loop that stretches beyond much of the plateau region of the adsorption curve to a somewhat lower P/P_0 implies thin slit shaped pores. The IUPAC divides hysteresis patterns into four categories: Type H1, Type H2, Type H3, and Type H4 [275].

It can be seen from Fig. 6.3 (a), that the PCB char exhibits type IV isotherm with hysteresis pattern H4 associated with narrow slit-like pores. CS sample shows type IV isotherm with H3 hysteresis loop, is observed with aggregates of plate-like particles which result in slit-shaped pores. CS40, CS50, CS60 and CS70 shows an almost reversible Type II nitrogen isotherm. On the contrary, the hysteresis loop H4 in these isotherms, is commonly related to capillary condensation in mesopore structures. The lack of steep slopes in the relative pressure range (0.98-1.0) and the amount adsorbed at very low-relative pressure ($P/P_0 <$ 0.01) indicate that CS40, CS50, and CS60 have insignificant or non-existent micropores and macropores compared to CS70. Whereas, CS30 char displays maximal adsorption and a substantial hysteresis pattern, but unlike the Type IV isotherm, it does not show a plateau at high P/P_0. For this, J Groen et al. [277] suggested to use designation Type IIB isotherm for this type of pattern, which implies that the material contains higher mesopores, which are responsible for hysteresis, as well as macropores, which results in the absence of the plateau

seen during mesoporous Type IV isotherms and steep slopes (as in the H3 hysteresis pattern with slit-like pores) in the P/P_0 range of 0.98–1.00. The isotherms also indicate a 'forced closure' of the desorption branch around $0.4 < P/P_0 < 0.5$ due to a sharp decline in the volume adsorbed, a phenomenon known as the 'tensile strength effect' [278]. This indicates that CS30 has a significantly larger amount of small mesopores with diameter < 4 nm [277]. Also, the volume uptake at P/P_0 near 1.0 indicates the total porosity of materials up to the ~200 nm pore-size range. So, CS30 has larger pore volumes near 200 nm size range compared to the other co-pyrolyzed char samples. Furthermore, there is no micropores in any of the samples, as indicated by a no adsorbed volume at very low relative pressure ($P/P_0 < 0.01$) [275].

6.2.4 Pore size distribution

For various chars, the BJH method was used to determine pore size distributions (the distribution of pore volume vs pore size) and pore areas. Using the kelvin model of pore filling, this method derives pore size distribution using experimental isotherms. It only applies to mesopores and small macropores, and it assumes there are no micropores. The most significant assumptions are that (1) the pore channel is stiff and (2) all of the pores to be identified have been filled at the largest relative pressure (P/P_0). Real core samples, on the other hand, have micropores with a complicated pore structure that are not simple cylindrical pores. As a result, the BJH method's restriction and pore size distribution errors are rather substantial.

The capillary radius (r_k) could be calculated when capillary condensation occurs by kelvin Equation (6.1). The cumulative pore volume distribution curve can then be shown as a correlation with capillary radius (r_k) also called as kelvin radius and liquid N_2 molar volume ($\tilde{v}$).

$$\ln\frac{p}{p_0} = -\frac{2\gamma\,\tilde{v}cos\theta}{r_k\,RT} \tag{6.1}$$

and,

$$r_p = r_k + t \tag{6.2}$$

Where, P/P_0 is the equilibrium pressure over the saturated vapor pressure of the adsorbed gas; $\tilde{v}$ is the mole volume of the liquid nitrogen; γ is the interfacial tension of the liquid nitrogen at its boiling point, r_p is the pore radius and t is the statistical film thickness of the adsorbed multilayer, which can be derived from standard isotherms [279].

a

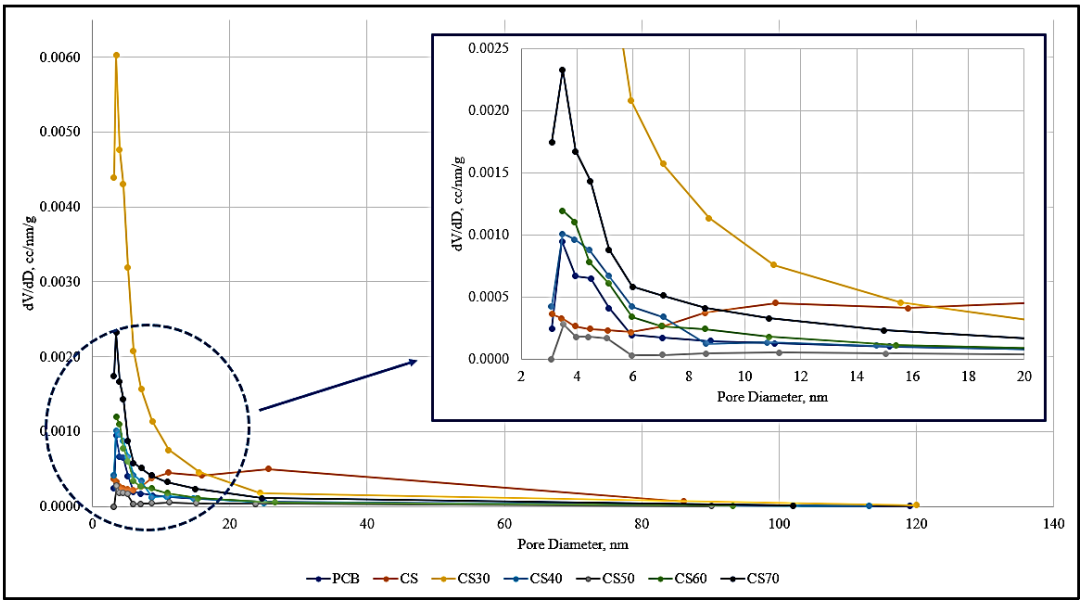

b

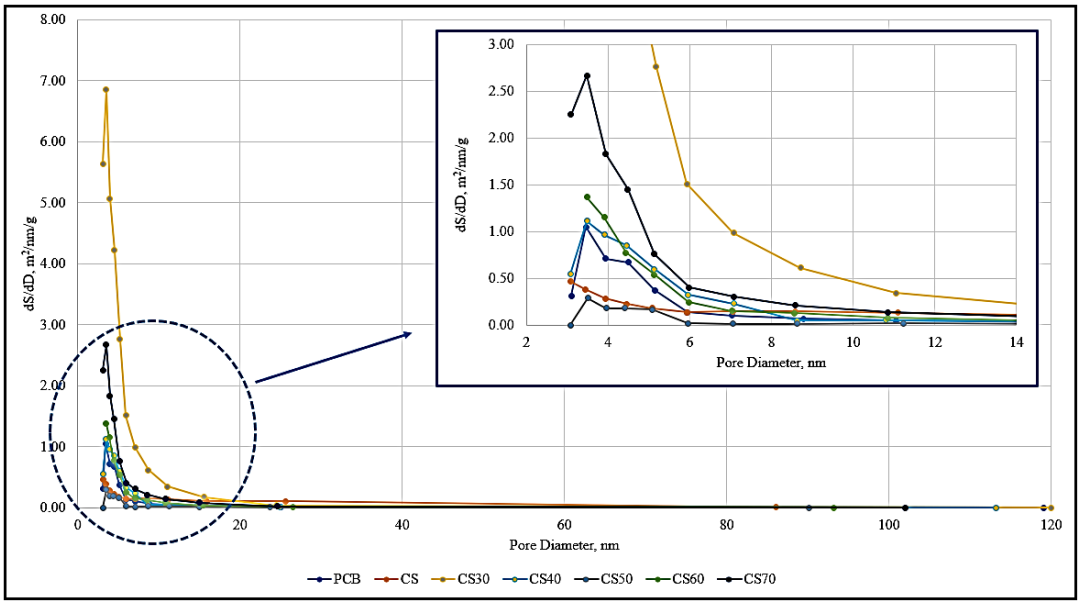

FIGURE 6.4: Pore size distributions comparison of PCB char with different composition char.

BJH proposed below equation to find pore volume,

$$V_{pn} = \left(\frac{r_{pn}}{r_{kn}+\Delta t_n/2}\right)^2 \left(\Delta V_n - \Delta t_n \sum_{j=1}^{n-1} Ac_j\right) \quad (6.3)$$

Where, r_p is the pore radius, V_p is the pore volume, Δt is the thickness of adsorbed layer of N_2 and A_c is the area exposed by the pore where the physically adsorbed gas is desorbed. The change in pore volume (dV) with respect to pore diameter (dD) is represented by the vertical coordinate dV/(dD) in Fig. 6.4 (a). The holes that create PCB and CS:PCB char were mostly concentrated in the 3 - 16 nm pore size range. Furthermore, Fig. 6.4 (b) represents change in surface area per unit pore diameter. when the pore size was reduced, the char's specific pore surface area increased, demonstrating that the small-diameter pore's specific surface area played a significant role in the overall specific surface area of the char. With pore diameters smaller than 6 nm, the pore area of PCB, CS40, and CS60 char increased substantially from 3.0 - 3.48 m^2/nm/g. Whereas CS and CS50 have much lower pore area with pore diameters less than 6 nm, whilst CS30 has a much larger pore area ranging from 1.5 - 6.8 m^2/nm/g, indicating that with CS50 co-pyrolysis, there are fewer small pore structures and the average pore size is smaller, and their distribution is more uniform. It's worth noting that, although having equal average pore diameters, the pore areas of CS50 char were smaller than those of PCB.

6.2.5 FE-SEM and EDS analysis

FESEM pictures of chars generated in a fixed bed reactor are shown in Fig. 6.5 (a-h). All chars revealed the existence of tiny particles and pores, with a rough texture, a heterogeneous surface, and a diversity of randomly distributed pore sizes. The FESEM image of PCB char Fig. 6.5 (a) shows the presence of a number of metals (Cu, Sn, Zn etc.) as bright spots and carbon as dark regions. CS shown in Fig. 6.5 (c) consisted of large particles with a smooth surface, whereas, small globular vesicle formation has been seen in CS30 char during char formation Fig. 6.5 (d).

Lignin particles melted and released volatile materials, leading in the production of open pores on the particle with rough surface and irregular outlet, resulting in a significantly increased surface area (16.791 m^2/g), see Table 6.3. However, if volatiles are not completely diffused out, larger vesicles are generated and stick to the surface, which can lead to pore blockage. Water permeation into the pores is another cause of pore blockage which diminishes surface area and could be the case for the reduced BET surface area for other CS:PCB compositions.

According to Sharma et al. [280], alkali metal K enrichment of cotton stalk char can cause agglomeration and even severe devolatilization, and plastic transformation may occur due

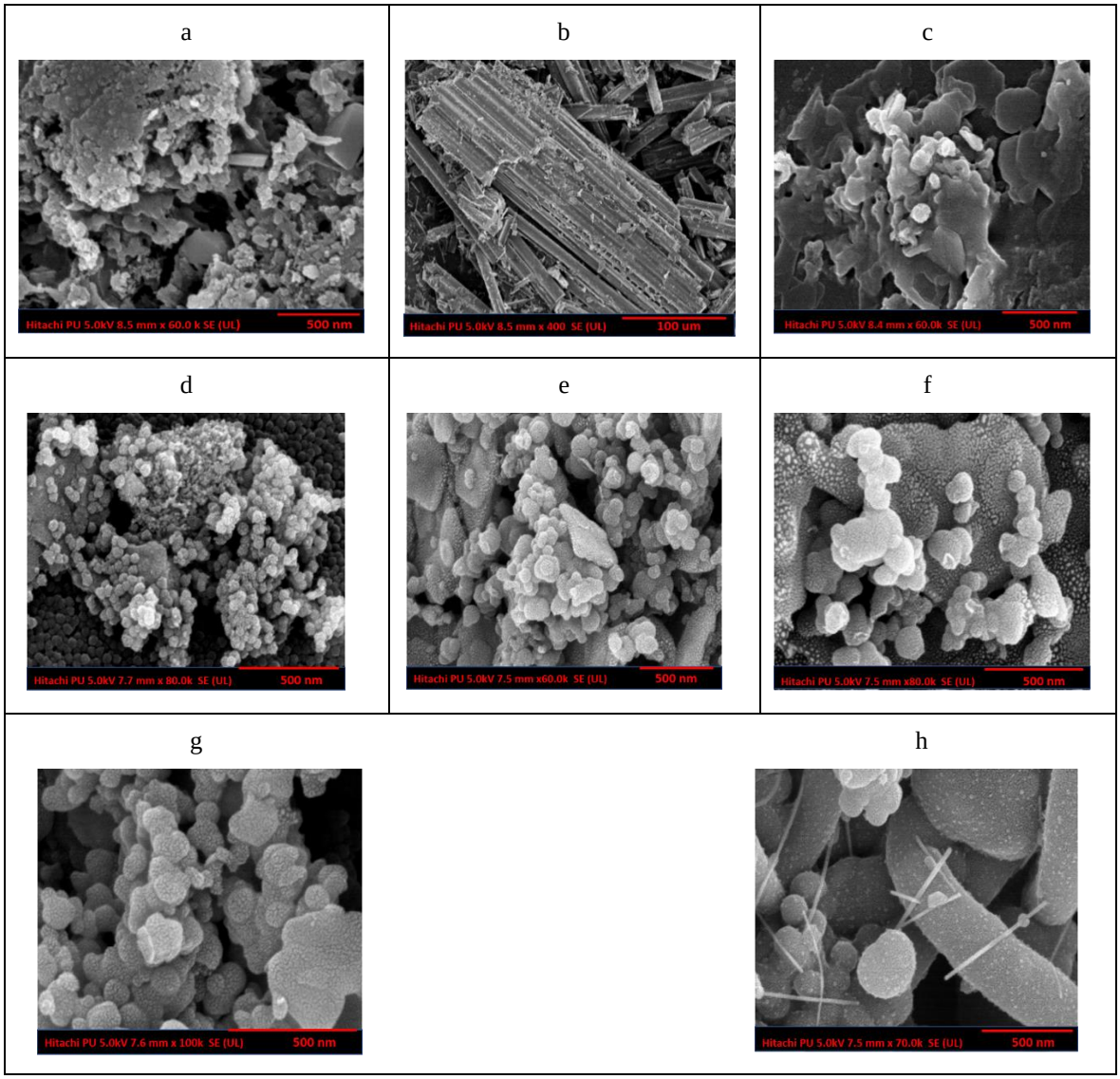

FIGURE 6.5: FESEM micrographs of (a) 500 nm resolution PCB char (b) 100 nm resolution PCB char, (c) CS, (d) CS30, (e) CS40, (f) CS50, (g) CS60 and (h) CS70 at 500 nm resolution.

to solid matrix softening and cell structure melting, resulting in pore closure. However, increased CS ratios, such as CS40 and above, Fig. 6.5 (e-h), could result in the strengthening of the degradation reaction and forceful release of gaseous substances that did not entirely diffuse out and then condensed during the cooling process, resulting in the generation of more twisted agglomerated and rough vesicles. EDS examination verified the existence of nonmetal-inorganic elements like Si and Ca from ceramic and glass fibre, as well as metals like Al, Fe. Oxygen was also present which can contribute to develop slag oxides (Al_2O_3, Fe_2O_3, SiO_2, etc.) and can be seen as light grey patches. Additionally, the presence of N, C,

Mg, K, Ca, Fe, S, and P are nutrient components for plant growth [281], and the increased C elements (See Table 6.1) are an indicator of condensed aromatic rings, which are likely to stick with soils.

TABLE 6.3: % of mineral content present in each sample by FESEM-EDS.

	K	S	Al	Si	Ca	Fe	N	P	Mg	Cl
PCB	-	-	4.88	14.13	10.71	1.77	2.24	0.69	0.27	-
CS	19.33	4.53	-	-	-	-	1.68	1.35	0.05	0.76
CS30	0.2	0.18	5.01	13.8	4.9	0.06	2.83	0.17	0.55	0.08
CS40	1.08	0.14	10.36	5.51	2	0.19	-	-	0.09	1.35
CS50	0.9	-	-	-	-	-	3.2	1.85	0.35	-
CS60	0.44	0.09	2.89	7.01	5.53	0.93	3.86	0.13	0.15	0.26
CS70	0.74	0.24	0.18	1.09	0.06	0.52	-	0.37	0.03	0.02

Furthermore, PCB char was largely made up of large fibrous textures, primarily glass fibre, organic elements such as epoxy resin components with irregular forms deposited on the surface and certain voids, as illustrated in Fig. 6.5 (b). Elements and trace metals present on the char surface of different CS, PCB and CS:PCB are shown in Table 6.3.

6.2.6 FTIR analysis of produced Char

The FTIR spectrum of the pyrolysis chars are shown in Fig. 6.6. The peak at 3423 cm^{-1} corresponds to the free O-H stretching in PCB, whereas in CS and the mixture it is attributed to decomposition of hemicellulose and cellulose. The peak at 3248 cm^{-1} reveals H bonded N-H. Peaks near to 1383 - 1394 cm^{-1} for CS and CS:PCB mixtures are attributed to lignin, mainly due to rings of type C=C. No aliphatic functional groups (C-H bonds) were found in any samples, may be at higher temperature compounds were converted to aromatics which was attributed to peaks at 2036- 2045 cm^{-1}; which denote framework vibration of benzene functional group caused by the stretching of carbon–carbon bonds of benzene rings [272]. The peaks observed around 1628 cm^{-1} may attributed to C=C and C=O, primarily aldehydes and ketones formed by dissociation of cellulose and hemicellulose of CS and epoxy resin of PCB. The absorption peaks near 600-950 cm^{-1} indicate mono and polycyclic aromatic groups [239] Whereas, the peak at 1110 cm^{-1} for CS and 1112 cm^{-1} for the mixture is associated with C-O-C bond stretching arising from hemicellulose groups like quinine and lactone. In the FTIR analysis, the chars produced by CS30 showed considerably higher carbonyl (1624-1633 cm^{-1}), and OH (3450-3460 cm^{-1}) groups.

Mainly because of the hydrolysis reactions and possible free radical reactions; phenolic compounds can be produced.

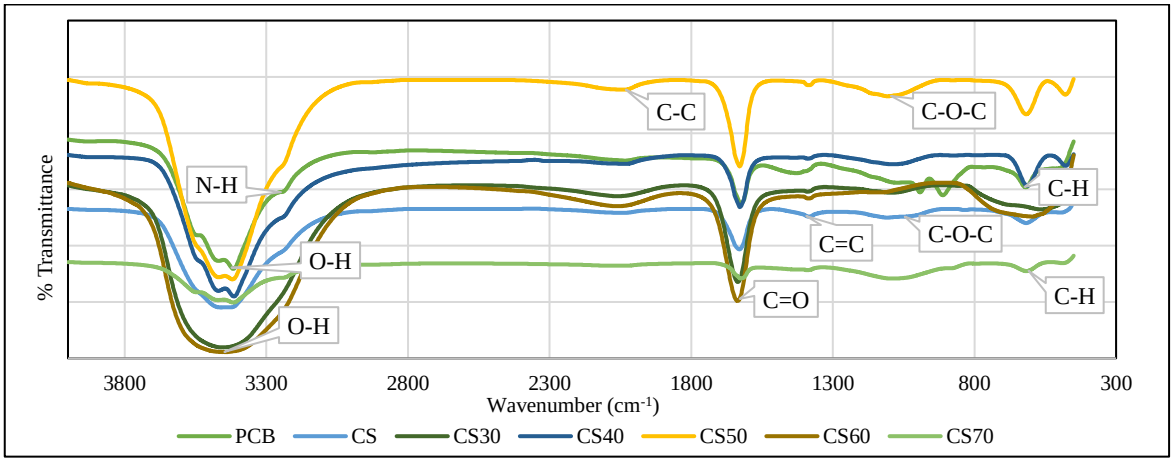

FIGURE 6.6: FTIR spectra of all the char samples.

These phenolics can further depolymerize and contribute to more char with aromatic properties. This could be a possible reason for higher char generation of CS30 (51.5 wt. %), See Fig. 5.1. Even CS60 with highest carbonyl and OH group shows lower pore volume due to condensation of gaseous substance as discussed in section 6.2.5. This result is supported by the above-mentioned observations on N_2 adsorption-desorption and BET surface area.

6.2.7 XRD (X-ray diffraction) Analyses

In general, diffuse and broad bands in XRD patterns characterize the existence of short-range order in the carbon structure, while the sharp and narrow peaks confirm to highly crystalline phases with high degree of long-range order over the examined 2θ range (5 - 80°). In PCB XRD pattern (see Fig. 6.7), sharp diffraction peak nearby 10 ° (2θ) and at 25~30° (2θ) indicates presence of apophyllite and crystal carbon structure (graphite), respectively. The presence of hematite can be seen in PCB as a peak about 43° (2θ) and 62° (2θ) and a peak nearby 40°, 44° and 50° (2θ) indicated the presence of magnetite. Whereas, several small sharp peaks belongs to various oxides such as silica, alumina, etc. and residual metals like Na, Fe, Ca, K and Mg, also observed by V Sahajwalla et al. [254]. In co-pyrolysis, the number of peaks and their intensities were found to be reduced, indicating mineral

disintegration. As well as the peak become wider and the arrangement of carbon crystal lattice are comparatively less arranged.

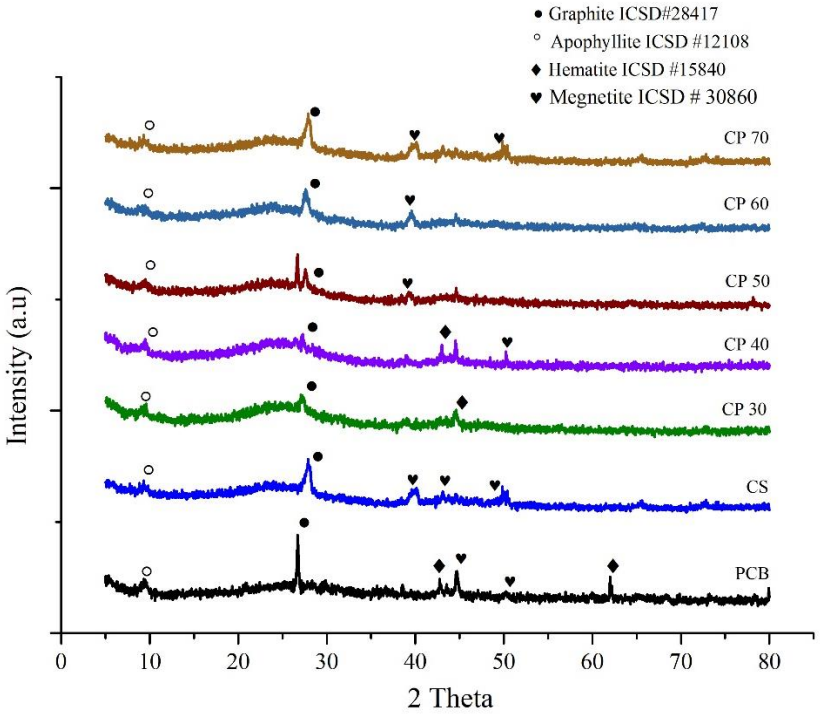

FIGURE 6.7: XRD results of all char samples.

6.2.8. X-ray Fluorescence Analyses

XRF (X-ray Fluorescence) analysis was done to determine the principal metals and other elements quantity. The bromine content in PCB char is the source of brominated fire retardants in epoxy resins, which is due to CS as the hydrogen donor assisted in the release of brominated compound in the form of HBr and its fixation in char. As shown in Fig. 6.8, Br content was 32% in PCB char and 31.8% in CS char, which increased in co-pyrolyzed chars with elevated CS concentration from 30 to 60%. For CS30, CS40, CS50, and CS60 bromine concentrations were 40.97, 50.95, 55.58, and 58.60%, respectively (Also discussed in chapter 5, section 5.4.1). Other major compound in PCB like SiO_2 (13.12%), Fe_2O_3 (7.9%), CuO (12.86%) was decreased in co-pyrolyzed char and minimum in CS50 to 4.8%, 2.49%, and 8.4% respectively. The chlorine content in PCB was very less 0.5% which was increased to maximum 2.41% with CS70. Also, Pb concentration was increased from 0.7% in PCB to 1.93% in co-pyrolyzed CS30 char. Phosphate was also present in PCB char (0.41%) due to phosphate-based fire retardants and concentration in char had slightly increased with co-pyrolysis to maximum 1.3% for CS70.

Many other metals like, barium, sulphur, aluminium and manganese were also present as shown in Fig. 6.8.

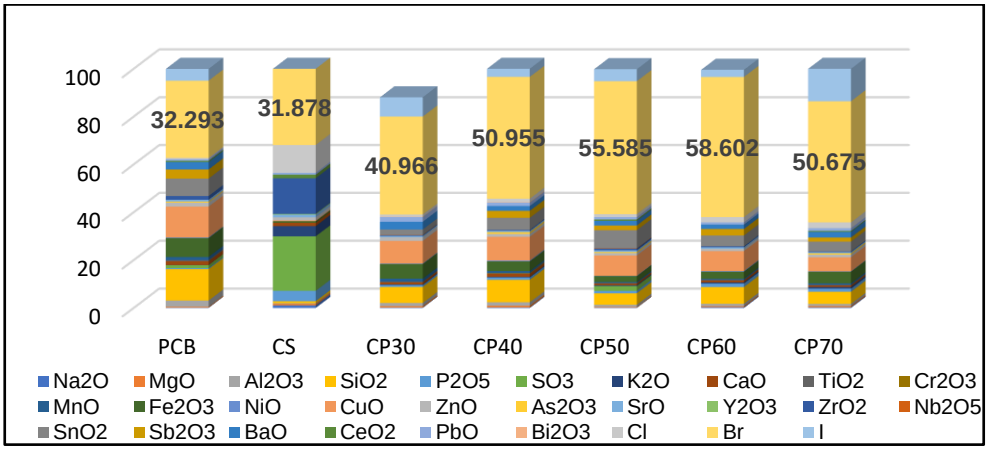

FIGURE 6.8: XRF analysis data comparison of metals oxides and other elements like bromine present in all char samples.

6.2.9 Indecisive applications of CS:PCB Char

It is feasible to investigate potential uses for CS:PCB co-pyrolysis char using the physicochemical characteristics stated above. For instance, due to mesoporous structure (pore diameters less than 3 nm) and enhanced surface areas of CS70 (6.226 m^2/g) and CS30 (16.79 m^2/g) it can be used to improve the catalytic activity for esterification and transesterification process [282][283]. The inclusion of nitrogenous functional groups in CS50, CS60, and CS70 (see Fig. 6.6) may aid physical CO_2 adsorption on CS:PCB char surfaces [284] which can then be converted in to the fuel. CS70 sample's HHV is 29.12 MJ/kg, which is within the range of industrial coals used for power generation (16–32 MJ/kg). This HHV values can further be increased by removing ash. Furthermore, because CS70 has an excellent thermal stability at higher temperatures (> 800 ℃), gasification would be slower. However, the inclusion of metals such as Al, Cu, and Ni, which acts as a catalyst, increasing the number of active sites on the char surface through the adsorption of gasifying entities, strengthening the chars' capacity to replace coal in power plants [284]. The presence of N, C, Mg, K, Ca, Fe, S, and P in the CS:PCB biochar could confirm the addition of these nutrients into a very poor soil, improving its fertility significantly [285][286].

In addition to the aforementioned applications, the carbon-rich char produced by CS:PCB co-pyrolysis can be employed in gas purification, vehicle colouring, water treatment, and as

a filler for composites [284]. However, before taking into consideration any of the aforementioned uses, it is necessary to take into account the existence of metal concentrations because different applications call for different levels of elimination. Also, bromine removal techniques must be developed, which must be focused on upcoming study.

6.3 Conclusion:

In the current study co-pyrolysis of PCBs with CS was examined and the influence of increasing amount of CS with PCB was found to be very effective in changing the morphology and texture of the char produced. In case of PCB pyrolysis, char yield was 60%, however, with co-pyrolysis amount was reduced due to CS early deterioration and char secondary decomposition at higher temperatures. CS30 showed a maximum yield (52 wt.%) because of the presence of more carbonyl and OH groups as per FTIR analysis.

TGA observation indicated that CS30 char took longer to decompose and more thermally stable structure than other compositions at the same operating temperature and heating rate. It also had more micro pores as well as larger pore volumes near 200 nm size range and has a surface area of 16.791 m^2/g, indicating a significantly higher adsorption capacity than other co-pyrolyzed char samples. However, it still needs to be activated before it can be used for sorption. In same sample compositions small globular vesicle formation were observed during char formation, resulting in a significantly increased surface area.

The bromine content in PCB char is the source of brominated fire retardants in epoxy resins, which was due to CS as the hydrogen donor assisted in the release of brominated compound in the form of HBr and its fixation in the char was increased with increasing amount of CS in co-pyrolysis. As per EDS analysis, CS70 has highest amount of C (88.17 %) and lowest amount of O (7.62 %) higher heating value (29.12 MJ/kg), as well as a reduced level of ash content which could make it useful for operations such as removing contaminants from aqueous matrices. However, the given applications can only be taken into consideration if the bromine content has been removed

CHAPTER 7

Conclusions and Scope of Future Work

7.1 Conclusions:

Waste electrical and electronic equipment (WEEE) consisting Printed circuit boards (PCBs) are the most hazardous material with a complex chemical composition, making it difficult to reuse and recycle. Pyrolysis has thus far been demonstrated to be a viable alternative for energy and material recovery in the form of gas, solid char, and especially liquid oil.

In the study, the pyrolysis of PCB, CS (Cotton Stalk) its different compositions are examined by thermogravimetric analysis (TGA) using a non-isothermal technique. The thermal degradation was carried out for the temperature range 25 to 700 $^{\circ}$C, in the presence of N_2 atmosphere, with 50 *ml/min* flow rate using three different heating rates 5, 10 and 15 $^{\circ}$C/min. The thermal decomposition at non-isothermal conditions for WPCBs, CS, and their mixture were investigated. The degradation profiles of different CS:PCB compositions were initiated at a lower temperature compared to PCBs and CS alone. The E_α from three model-free methods namely, KAS, FWO and Starink were found varying significantly. This exhibits the existence of a complex multi-reaction mechanism within the solid matrix which shows that the activation energy is dependent on conversion mechanism. The kinetic parameters calculated using the FWO method was considered the most reliable method for the reaction mechanism. For the first zone, with increased CS ratio the average *E* values for the different CS:PCB compositions were increased from 138.10 KJ/mol for CS30 to 222.63 KJ/mol for CS70. Whereas, with the second zone, a faster reaction is evidenced by a reduction in apparent activation energy with increased conversion (0.6-0.9) and the average *E* values also decreases with the increased CS ratio and ranged between 94 KJ/mol for CS30 and 77.98 KJ/mol for CS70. The reaction mechanism of co-pyrolyzed material for second zone

followed the *m13* model (rection order *n*=3). While for the first zone, CS30 displayed *m12* (*n*=1), CS40 displayed *m11* (*n*=2) and CS50, CS60, displayed *m13* (*n*=3) reaction mechanism. Most importantly, the CS70 demonstrated two distinct reaction mechanisms at first zone, *m11* for α = 0.2–0.5 and *m13* for α = 0.2–0.5. Moreover, the study of the kinetic compensation effect was used to characterize the dependence of *E* and *lnA* indicated that a compensation effect existed between the apparent activation energy and the pre-exponential factor during the pyrolysis process.

TABLE 7.1: Important results of the co-pyrolyzed sample products.

Sample	**Liquid Property**				**Gas Property**			**Char Property**	
	Quantity of oil (%)	**Phenol and Phenolic Compounds** % Area	**Br_2 mg/100gm**	**Liquid HHV MJ/kg**	**H_2 (%)**	**CH_4 (%)**	**Br Fixation in char (%)**	**Other Important property**	**Solid HHV MJ/kg**
CS30	25.3	78.63	82.87	25.16	30.7	61.57	40.96	Increased BET surface area (16.17 m^2/gm)	3.96
CS40	26	69.77	29.88	22.45	31.27	62.87	50.95	-	22.51
CS50	27.5	76.82	43.10	28.4	44.22	51.85	55.58	Fulfils all oil fuel FAME/ Bharat VI criteria except calorific value	27.11
CS60	29.5	75.29	32.45	26.52	42.49	53.28	58.60	-	5.38
CS70	31.5	74.3	56.18	20.95	32.02	66.13	50.67	High fixed and Total C, Reduced level of ash content.	29.12

Based on data from TGA analysis a lab-scale co-pyrolysis experiments were employed, in order to increase oil quality and quantity while reducing brominated compounds, using a variety of CS:PCB compositions (CS30, CS40, CS50, CS60, and CS70) and comparison was done by their physical and chemical characterisation. PCB had total of 60.67% phenol and

phenolic compounds, while CS had just 25.94%. However, as CS composition was increased during co-pyrolysis, the amount of phenol and phenolic compounds were increased and with CS50 the highest amount (78.63%) of phenol and phenolic compounds were observed.

The advantage of using cotton stock with PCB was, it acted as a hydrogen donor in the debromination reaction and aided in conversion of most organic bromine to inorganic HBr and its fixation in char. A CS70 composition showed an increase in methane in generated gas which is one of the most essential fuels in industry, whereas a CS50 composition showed an increase in the amount of hydrogen. Oil from CS50 composition met all FAME parameters except for phosphorous concentration (10 mg/kg) and calorific value (28.41 MJ/kg) to be used as a fuel. Further investigations are required into upgrading fuel oil, which may entail hydrodeoxygenation, catalytic cracking, and steam reforming.

Moreover, the influence of increasing amount of CS with PCB was found to be very effective in changing the morphology and texture of the char produced. In case of PCB pyrolysis, char yield was 60%, however, with co-pyrolysis amount was reduced due to CS early deterioration and char secondary decomposition at higher temperatures. TGA observation indicated that CS30 char took longer to decompose and more thermally stable structure than other compositions at the same operating temperature and heating rate. It also had more micro pores as well as larger pore volumes near 200 nm size range and has a surface area of 16.791 m^2/g, indicating a significantly higher adsorption capacity than other co-pyrolyzed char samples. However, it still needs to be activated before it can be used for sorption. In same sample compositions small globular vesicle formation were observed during char formation, resulting in a significantly increased surface area.

As per proximate, ultimate analysis, CS70 has highest amount of C (88.17 %) and lowest amount of O (7.62 %) higher heating value (29.12 MJ/kg), as well as a reduced level of ash content which could make it useful for operations such as removing contaminants from aqueous matrices. Additionally, other indecisive applications of the created chars were also reliant on the existence of nutritional components and their physicochemical properties, which could only be taken into account once the bromine content was removed, which might be the future focus of the new research. Most importantly, looking in to the results of Table

7.1, one has to choose the appropriate composition based on requirements. According to the authors' knowledge, CS50 can be used as a fuel and a value-added component in the synthesis of phenol and phenolic compounds. Additionally, an increased H_2 content in the gas has favourable economic effects.

7.2 Scope of Future work:

CS50 fulfils all fuel oil FAME/ Bharat VI criteria except calorific value, however, adopting relatively simple processes like solvent addition to lower viscosity and chemical stability, filtration to remove char and alkali, bio-oil can be upgraded to meet the same quality standards. One of the direct applications for bio-oil is emulsification with diesel. Other upgrading technologies could also be applied, like Hydrodeoxygenation, catalytic cracking, and steam reforming of bio-oils, which are all extremely complicated procedures that require reliable and fully developed reactors.

CS30 char having higher BET surface area, which can further be improved by adopting reliable process to be used as adsorber in different applications.

CS70 has good calorific value and acceptable solid fuel properties, but it needs to be bromine free before using it as a solid fuel. So, the most important future scope is to find the economical, acceptable bromine removal techniques for solid char.

List of References

[1] F. Cucchiella, I. D'Adamo, S.C. Lenny Koh, P. Rosa, Recycling of WEEEs: An economic assessment of present and future e-waste streams, Renew. Sustain. Energy Rev. 51 (2015) 263–272. https://doi.org/10.1016/j.rser.2015.06.010.

[2] Z. Wang, B. Zhang, D. Guan, Take responsibility for electronic-waste disposal, Nature. 536 (2016) 23–25. https://doi.org/10.1038/536023a.

[3] A. Kumar, M. Holuszko, D.C.R. Espinosa, E-waste: An overview on generation, collection, legislation and recycling practices, Resour. Conserv. Recycl. 122 (2017) 32–42. https://doi.org/10.1016/j.resconrec.2017.01.018.

[4] R.M.R. Turaga, K. Bhaskar, S. Sinha, D. Hinchliffe, M. Hemkhaus, R. Arora, S. Chatterjee, D.S. Khetriwal, V. Radulovic, P. Singhal, H. Sharma, E-Waste Management in India: Issues and Strategies, Vikalpa. 44 (2019) 127–162. https://doi.org/10.1177/0256090919880655.

[5] Ankit, L. Saha, V. Kumar, J. Tiwari, Sweta, S. Rawat, J. Singh, K. Bauddh, Electronic waste and their leachates impact on human health and environment: Global ecological threat and management, Environ. Technol. Innov. 24 (2021) 102049. https://doi.org/10.1016/j.eti.2021.102049.

[6] Q. Wang, B. Zhang, S. Yu, J. Xiong, Z. Yao, B. Hu, J. Yan, Waste-Printed Circuit Board Recycling: Focusing on Preparing Polymer Composites and Geopolymers, ACS Omega. 5 (2020) 17850–17856. https://doi.org/10.1021/acsomega.0c01884.

[7] N. Raje, E -Waste: Characterization and Disposal through Solid State Route, Int. J. Environ. Sci. Nat. Resour. 23 (2020) 33–43. https://doi.org/10.19080/ijesnr.2020.23.556106.

[8] C. Rosenberg, M. Hämeilä, J. Tornaeus, K. Säkkinen, K. Puttonen, A. Korpi, M. Kiilunen, M. Linnainmaa, A. Hesso, Exposure to flame retardants in electronics recycling sites, Ann. Occup. Hyg. 55 (2011) 658–665. https://doi.org/10.1093/annhyg/mer033.

[9] A. Sepúlveda, M. Schluep, F.G. Renaud, M. Streicher, R. Kuehr, C. Hagelüken, A.C. Gerecke, A review of the environmental fate and effects of hazardous substances released from electrical and electronic equipments during recycling: Examples from China and India, Environ. Impact Assess. Rev. 30 (2010) 28–41. https://doi.org/10.1016/j.eiar.2009.04.001.

[10] S. Salhofer, E-waste collection and treatment options: A comparison of approaches in Europe, China and Vietnam, Handb. Environ. Chem. 63 (2018) 227. https://doi.org/10.1007/698_2017_36.

[11] C. Quan, A. Li, N. Gao, Research on pyrolysis of PCB waste with TG-FTIR and Py-GC/MS, J. Therm. Anal. Calorim. 110 (2012) 1463–1470. https://doi.org/10.1007/s10973-011-2048-x.

[12] Y. Kim, S. Kim, J. Lee, Y. Park, Pyrolysis Reaction Pathways of Waste Epoxy-Printed Circuit Board 1,2, 30 (2013) 706–712. https://doi.org/10.1089/ees.2013.0166.

[13] Z. Yao, J. Xiong, S. Yu, W. Su, W. Wu, J. Tang, D. Wu, Kinetic study on the slow pyrolysis of nonmetal fraction of waste printed circuit boards (NMF-WPCBs), Waste Manag. Res. (2020). https://doi.org/10.1177/0734242X19896630.

[14] P. Evangelopoulos, E. Kantarelis, W. Yang, Investigation of the thermal decomposition of printed circuit boards (PCBs) via thermogravimetric analysis (TGA) and analytical pyrolysis (Py-GC/MS), J. Anal. Appl. Pyrolysis. 115 (2015) 337–343. https://doi.org/10.1016/j.jaap.2015.08.012.

[15] N. Singh, H. Duan, O.A. Ogunseitan, J. Li, Y. Tang, Toxicity trends in E-Waste: A comparative analysis of metals in discarded mobile phones, J. Hazard. Mater. 380 (2019) 120898. https://doi.org/10.1016/j.jhazmat.2019.120898.

[16] J. Xiong, S. Yu, D. Wu, X. Lü, J. Tang, W. Wu, Z. Yao, Pyrolysis treatment of nonmetal fraction of waste printed circuit boards: Focusing on the fate of bromine, Waste Manag. Res. (2020). https://doi.org/10.1177/0734242X19894621.

[17] T.R. Mankhand, K.K. Singh, S.K. Gupta, S. Das, Pyrolysis of Printed Circuit Boards, 1 (2012) 102–107. https://doi.org/10.5923/j.ijmee.20120106.01.

[18] B.B. Uzoejinwa, X. He, S. Wang, A. El-Fatah Abomohra, Y. Hu, Q. Wang, Co-pyrolysis of biomass and waste plastics as a thermochemical conversion technology

for high-grade biofuel production: Recent progress and future directions elsewhere worldwide, Energy Convers. Manag. 163 (2018) 468–492. https://doi.org/10.1016/j.enconman.2018.02.004.

[19] C. Quan, A. Li, N. Gao, Combustion and Pyrolysis of Electronic Waste : Thermogravimetric Analysis and Kinetic Model, Procedia Environ. Sci. 18 (2013) 776–782. https://doi.org/10.1016/j.proenv.2013.04.104.

[20] T. Bridgwater, Challenges and opportunities in fast pyrolysis of biomass: Part I, Johnson Matthey Technol. Rev. 62 (2018) 118–130. https://doi.org/10.1595/205651318X696693.

[21] M.N. Islam, M.H.M. Ali, M. Haziq, Fixed bed pyrolysis of biomass solid waste for bio-oil, AIP Conf. Proc. 1875 (2017). https://doi.org/10.1063/1.4998369.

[22] S.A. El-Sayed, M.E. Mostafa, Pyrolysis characteristics and kinetic parameters determination of biomass fuel powders by differential thermal gravimetric analysis (TGA/DTG), Energy Convers. Manag. 85 (2014) 165–172. https://doi.org/10.1016/j.enconman.2014.05.068.

[23] F.J. Sánchez-Borrego, P. Álvarez-Mateos, J.F. García-Martín, Biodiesel and Other Value-Added Products from Bio-Oil Obtained from Agrifood Waste, Processes. 9 (2021) 797. https://doi.org/10.3390/pr9050797.

[24] P. Hense, K. Reh, M. Franke, J. Aigner, A. Hornung, A. Contin, Pyrolysis of waste electrical and electronic equipment (WEEE) for recovering metals and energy: Previous achievements and current approaches, Environ. Eng. Manag. J. 14 (2015) 1637–1647. https://doi.org/10.30638/eemj.2015.175.

[25] W.J. Liu, K. Tian, H. Jiang, X.S. Zhang, G.X. Yang, Preparation of liquid chemical feedstocks by co-pyrolysis of electronic waste and biomass without formation of polybrominated dibenzo-p-dioxins, Bioresour. Technol. 128 (2013) 1–7. https://doi.org/10.1016/j.biortech.2012.10.160.

[26] F. Abnisa, W.M.A. Wan Daud, A review on co-pyrolysis of biomass: An optional technique to obtain a high-grade pyrolysis oil, Energy Convers. Manag. 87 (2014) 71–85. https://doi.org/10.1016/j.enconman.2014.07.007.

[27] Y. Shen, R. Yuan, X. Chen, X. Ge, M. Chen, Co-pyrolysis of E-waste Non-metallic

Residues with Bio-wastes Co-pyrolysis of E-waste Non-metallic Residues with Bio-wastes, ACS Sustain. Chem. Eng. 6 (2018) 9086–9093. https://doi.org/10.1021/acssuschemeng.8b01439.

[28] P. Madhu, H. Kanagasabapathy, I.N. Manickam, Conversion of cotton residues to bio-oil and chemicals through flash pyrolysis in a fluidised bed reactor, Int. J. Energy Technol. Policy. 14 (2018) 20–33. https://doi.org/10.1504/IJETP.2018.088275.

[29] N. Ali, M. Saleem, K. Shahzad, A. Chughtai, Bio-Oil Production from Fast Pyrolysis of Cotton Stalk in Fluidized Bed Reactor, Arab. J. Sci. Eng. 40 (2015) 3019–3027. https://doi.org/10.1007/s13369-015-1801-z.

[30] V. Pandere, A. Gautam, S. Gautam, Catalytic pyrolysis of metal free ZSM-5 PCB Ca(OH)2, 43 (2022) 1–12. https://doi.org/10.24425/cpe.2022.140820.

[31] L. Rocchetti, A. Amato, F. Beolchini, Printed circuit board recycling: A patent review, Elsevier Ltd, 2018. https://doi.org/10.1016/j.jclepro.2018.01.076.

[32] P.T. Williams, Valorization of printed circuit boards from waste electrical and electronic equipment by pyrolysis, Waste and Biomass Valorization. 1 (2010) 107–120. https://doi.org/10.1007/s12649-009-9003-0.

[33] S.Y. Li, S.Y. Sun, J.Y. Liu, J.Q. Wu, J.J. Zeng, Thermal debromination of waste printed circuit boards by iron-based catalyst, Adv. Mater. Res. 881–883 (2014) 589–593. https://doi.org/10.4028/www.scientific.net/AMR.881-883.589.

[34] Y.F. Huang, S.L. Lo, Energy recovery from waste printed circuit boards using microwave pyrolysis: product characteristics, reaction kinetics, and benefits, Environ. Sci. Pollut. Res. 27 (2020) 43274–43282. https://doi.org/10.1007/s11356-020-10304-2.

[35] Z. Zhang, X. Zhao, E. Kwon, M.J. Calstaldi, Experimental research on microwave induced thermal decomposition of printed circuit board wastes, 18th Annu. North Am. Waste-to-Energy Conf. NAWTEC18. 7 (2010) 15–21. https://doi.org/10.1115/nawtec18-3536.

[36] P. Hense, K. Reh, M. Franke, J. Aigner, A. Hornung, A. Contin, PYROLYSIS OF WASTE ELECTRICAL AND ELECTRONIC EQUIPMENT (WEEE) FOR RECOVERING METALS AND ENERGY : PREVIOUS ACHIEVEMENTS AND

CURRENT APPROACHES, 14 (2015) 1637–1647.

[37] W.J. Hall, P.T. Williams, Removal of organobromine compounds from the pyrolysis oils of flame retarded plastics using zeolite catalysts, J. Anal. Appl. Pyrolysis. 81 (2008) 139–147. https://doi.org/10.1016/j.jaap.2007.09.008.

[38] K. Shiltagh, Novel Concept To Treat Weee for Energy and Metals Recycle Basing on Pyrolysis Process, (2016).

[39] H. Fromme, B. Hilger, E. Kopp, M. Miserok, W. Völkel, Polybrominated diphenyl ethers (PBDEs), hexabromocyclododecane (HBCD) and "novel" brominated flame retardants in house dust in Germany, Environ. Int. 64 (2014) 61–68. https://doi.org/10.1016/j.envint.2013.11.017.

[40] M. Manikkampatti Palanisamy, V.R. Myneni, B. Gudeta, S. Komarabathina, Toxic Metal Recovery from Waste Printed Circuit Boards: A Review of Advanced Approaches for Sustainable Treatment Methodology, Adv. Mater. Sci. Eng. 2022 (2022). https://doi.org/10.1155/2022/6550089.

[41] I. Birloaga, F. Vegliò, Hydrometallurgical processing of waste printed circuit boards, Waste Electr. Electron. Equip. Recycl. Aqueous Recover. Methods. (2018) 95–113. https://doi.org/10.1016/B978-0-08-102057-9.00004-4.

[42] O. Tsydenova, M. Bengtsson, Chemical hazards associated with treatment of waste electrical and electronic equipment, Waste Manag. 31 (2011) 45–58. https://doi.org/10.1016/j.wasman.2010.08.014.

[43] S. Rafique, S.S. Gillani, R. Nazir, Lead and Cadmium Toxic Effects on Human Health : A Review, 11 (2021) 1–6.

[44] U.T. Q. Sohaib, N. Soomro, M. Habib, A. R. Memon, Comparative Analysis of Recycled PVC composites reinforced with nonmetals of printed Circuit Boards Q., 47 (2015) 431–436.

[45] A.C. Marques, J.C. Marrero, C.D.F. Malfatti, A review of the recycling of non-metallic fractions of printed circuit boards, (2013) 1–11.

[46] D. Hu, Z. Jia, J. Li, B. Zhong, W. Fu, Y. Luo, D. Jia, Characterization of Waste Printed Circuit Boards Nonmetals and its Reutilization as Reinforcing Filler in Unsaturated Polyester Resin, J. Polym. Environ. 26 (2018) 1311–1319.

https://doi.org/10.1007/s10924-017-1031-4.

[47] J. Sohaili, S.K. Muniyandi, S.S. Mohamad, A Review on Printed Circuit Boards Waste Recycling Technologies and Reuse of Recovered Nonmetallic Materials, Int. J. Sci. Eng. Res. 3 (2012) 1–7.

[48] Y. Zheng, Z. Shen, C. Cai, S. Ma, Y. Xing, The reuse of nonmetals recycled from waste printed circuit boards as reinforcing fillers in the polypropylene composites, J. Hazard. Mater. 163 (2009) 600–606. https://doi.org/10.1016/j.jhazmat.2008.07.008.

[49] Y. Zheng, Z. Shen, S. Ma, C. Cai, X. Zhao, Y. Xing, A novel approach to recycling of glass fibers from nonmetal materials of waste printed circuit boards, J. Hazard. Mater. 170 (2009) 978–982. https://doi.org/10.1016/j.jhazmat.2009.05.065.

[50] A.M. Cunliffe, P.T. Williams, Characterisation of products from the recycling of glass fibre reinforced polyester waste by pyrolysis, Fuel. 82 (2003) 2223–2230. https://doi.org/10.1016/S0016-2361(03)00129-7.

[51] A.M. Cunliffe, N. Jones, P.T. Williams, Recycling of fibre-reinforced polymeric waste by pyrolysis: Thermo-gravimetric and bench-scale investigations, J. Anal. Appl. Pyrolysis. 70 (2003) 315–338. https://doi.org/10.1016/S0165-2370(02)00161-4.

[52] M. Hu, J. Wang, Z. Xu, Pyrolysis-Based Technology for Recovering Copper from Transistors on Waste Printed Circuit Boards, ACS Sustain. Chem. Eng. 5 (2017) 11354–11361. https://doi.org/10.1021/acssuschemeng.7b02375.

[53] M.I. Jahirul, M.G. Rasul, A.A. Chowdhury, N. Ashwath, Biofuels production through biomass pyrolysis- A technological review, Energies. 5 (2012) 4952–5001. https://doi.org/10.3390/en5124952.

[54] C.Z. Zaman, K. Pal, W.A. Yehye, S. Sagadevan, S.T. Shah, G.A. Adebisi, E. Marliana, R.F. Rafique, R. Bin Johan, Pyrolysis: A Sustainable Way to Generate Energy from Waste, Pyrolysis. (2017) 3–36. https://doi.org/10.5772/intechopen.69036.

[55] E. Stauffer, R. Newman, D. Analysis, Pyrolysis Chemistry and Physics of Fire and Liq- uid Fuels Theory of Extraction Techniques PAINTS | Organic Solvent-Based, (2013).

[56] H. Rate, Principles of Pyrolysis, TNAU Agritech Portal. 1 (2015) 1–8. http://agridr.in/tnauEAgri/eagri50/AENG352/lec10.pdf.

[57] D. Mohan, C.U. Pittman, P.H. Steele, Pyrolysis of Wood / Biomass for Bio-oil : A Critical Review, Energy & Fuels. 20 (2006) 848–889. https://doi.org/https://doi.org/10.1021/ef0502397.

[58] K.M. Qureshi, A.N. Kay Lup, S. Khan, F. Abnisa, W.M.A. Wan Daud, A technical review on semi-continuous and continuous pyrolysis process of biomass to bio-oil, J. Anal. Appl. Pyrolysis. 131 (2018) 52–75. https://doi.org/10.1016/j.jaap.2018.02.010.

[59] I.D. Manariotis, K.N. Fotopoulou, H.K. Karapanagioti, Preparation and Characterization of Biochar Sorbents Produced from Malt Spent Rootlets, Ind. Eng. Chem. Res. 54 (2015) 9577–9584. https://doi.org/10.1021/acs.iecr.5b02698.

[60] T.M. Huggins, A. Haeger, J.C. Biffinger, Z.J. Ren, Granular biochar compared with activated carbon for wastewater treatment and resource recovery, Water Res. 94 (2016) 225–232. https://doi.org/10.1016/j.watres.2016.02.059.

[61] A. V. Bridgwater, D. Meier, D. Radlein, An Overview of Fast Pyrolysis of Biomass, Prog. Thermochem. Biomass Convers. (2008) 977–997. https://doi.org/10.1002/9780470694954.ch80.

[62] A.H. Demirbaş, Yields and heating values of liquids and chars from spruce trunkbark pyrolysis, Energy Sources. 27 (2005) 1367–1373. https://doi.org/10.1080/009083190523208.

[63] A. V. Bridgwater, Principles and practice of biomass fast pyrolysis processes for liquids, J. Anal. Appl. Pyrolysis. 51 (1999) 3–22. https://doi.org/10.1016/S0165-2370(99)00005-4.

[64] T. Cornelissen, J. Yperman, G. Reggers, S. Schreurs, R. Carleer, Flash co-pyrolysis of biomass with polylactic acid. Part 1: Influence on bio-oil yield and heating value, Fuel. 87 (2008) 1031–1041. https://doi.org/10.1016/j.fuel.2007.07.019.

[65] J. Akhtar, N. Saidina Amin, A review on operating parameters for optimum liquid oil yield in biomass pyrolysis, Renew. Sustain. Energy Rev. 16 (2012) 5101–5109. https://doi.org/10.1016/j.rser.2012.05.033.

[66] L. Thesis, Thermochemical Treatment of Electric and Electronic Waste for Energy

Recovery Efthymios Kantarelis, 2009.

[67] F. Diaz, B. Flerus, S. Nagraj, K. Bokelmann, R. Stauber, B. Friedrich, Comparative Analysis About Degradation Mechanisms of Printed Circuit Boards (PCBs) in Slow and Fast Pyrolysis: The Influence of Heating Speed, J. Sustain. Metall. 4 (2018) 205–221. https://doi.org/10.1007/s40831-018-0163-7.

[68] I. Velghe, R. Carleer, J. Yperman, S. Schreurs, Study of the pyrolysis of municipal solid waste for the production of valuable products, J. Anal. Appl. Pyrolysis. 92 (2011) 366–375. https://doi.org/10.1016/j.jaap.2011.07.011.

[69] I. De Marco, B.M. Caballero, M.J. Chomôn, M.F. Laresgoiti, A. Torres, G. Fernández, S. Arnaiz, Pyrolysis of electrical and electronic wastes, J. Anal. Appl. Pyrolysis. 82 (2008) 179–183. https://doi.org/10.1016/j.jaap.2008.03.011.

[70] H.L. Chiang, K.H. Lin, M.H. Lai, T.C. Chen, S.Y. Ma, Pyrolysis characteristics of integrated circuit boards at various particle sizes and temperatures, J. Hazard. Mater. 149 (2007) 151–159. https://doi.org/10.1016/j.jhazmat.2007.03.064.

[71] F. Barontini, V. Cozzani, Formation of hydrogen bromide and organobrominated compounds in the thermal degradation of electronic boards, J. Anal. Appl. Pyrolysis. 77 (2006) 41–55. https://doi.org/10.1016/j.jaap.2006.01.003.

[72] I. Demiral, S. Şensöz, Fixed-bed pyrolysis of hazelnut (Corylus Avellana L.) bagasse: Influence of pyrolysis parameters on product yields, Energy Sources, Part A Recover. Util. Environ. Eff. 28 (2006) 1149–1158. https://doi.org/10.1080/009083190966126.

[73] D. Vamvuka, Bio-oil, solid and gaseous biofuels from biomass pyrolysis processes—An overview, Int. J. ENERGY Res. 35 (2011) 385–862. https://doi.org/10.1002/er.1804.

[74] A. V. Bridgwater, G.V.C. Peacocke, Fast pyrolysis processes for biomass, Renew. Sustain. Energy Rev. 4 (2000) 1–73. https://doi.org/10.1016/S1364-0321(99)00007-6.

[75] W.J. Hall, P.T. Williams, Processing waste printed circuit boards for material recovery, 4 (2007) 43–50. https://doi.org/10.1108/03056120710836936.

[76] W. Scharnhorst, C. Ludwig, J. Wochele, O. Jolliet, Heavy metal partitioning from electronic scrap during thermal End-of-Life treatment, Sci. Total Environ. 373 (2007)

576–584. https://doi.org/10.1016/j.scitotenv.2006.11.023.

[77] J. Sun, W. Wang, Z. Liu, C. Ma, Recycling of waste printed circuit boards by microwave-induced pyrolysis and featured mechanical processing, Ind. Eng. Chem. Res. 50 (2011) 11763–11769. https://doi.org/10.1021/ie2013407.

[78] Y.F. Huang, M.W. Pan, S.L. Lo, Hydrometallurgical metal recovery from waste printed circuit boards pretreated by microwave pyrolysis, Resour. Conserv. Recycl. 163 (2020) 105090. https://doi.org/10.1016/j.resconrec.2020.105090.

[79] Y.F. Huang, P. Te Chiueh, S.L. Lo, A review on microwave pyrolysis of lignocellulosic biomass, Sustain. Environ. Res. 26 (2016) 103–109. https://doi.org/10.1016/j.serj.2016.04.012.

[80] T.R. Abdou, A.B. Botelho Junior, D.C.R. Espinosa, J.A.S. Tenório, Recycling of polymeric composites from industrial waste by pyrolysis: Deep evaluation for carbon fibers reuse, Waste Manag. 120 (2021) 1–9. https://doi.org/10.1016/j.wasman.2020.11.010.

[81] C. Quan, A. Li, N. Gao, Synthesis of carbon nanotubes and porous carbons from printed circuit board waste pyrolysis oil, J. Hazard. Mater. 179 (2010) 911–917. https://doi.org/10.1016/j.jhazmat.2010.03.092.

[82] W.J. Hall, P.T. Williams, Separation and recovery of materials from scrap printed circuit boards, Resour. Conserv. Recycl. 51 (2007) 691–709. https://doi.org/10.1016/j.resconrec.2006.11.010.

[83] W.J. Hall, P.T. Williams, Processing waste printed circuit boards for material recovery, Circuit World. 33 (2007) 43–50. https://doi.org/10.1108/03056120710836936.

[84] Y. Zhou, W. Wu, K. Qiu, Recovery of materials from waste printed circuit boards by vacuum pyrolysis and vacuum centrifugal separation, Waste Manag. 30 (2010) 2299–2304. https://doi.org/10.1016/j.wasman.2010.06.012.

[85] G. Jie, L. Ying-Shun, L. Mai-Xi, Product characterization of waste printed circuit board by pyrolysis, J. Anal. Appl. Pyrolysis. 83 (2008) 185–189. https://doi.org/10.1016/j.jaap.2008.08.007.

[86] H.L. Chiang, C.C. Lo, S.Y. Ma, Characteristics of exhaust gas, liquid products, and

residues of printed circuit boards using the pyrolysis process, Environ. Sci. Pollut. Res. 17 (2010) 624–633. https://doi.org/10.1007/s11356-009-0245-y.

[87] Y.C. Chien, H. Paul Wang, K.S. Lin, Y.J. Huang, Y.W. Yang, Fate of bromine in pyrolysis of printed circuit board wastes, Chemosphere. 40 (2000) 383–387. https://doi.org/10.1016/S0045-6535(99)00251-9.

[88] P. Evangelopoulos, E. Kantarelis, W. Yang, Experimental investigation of pyrolysis of printed circuit boards for energy and materials recovery under nitrogen and steam atmosphere, Energy Procedia. 105 (2017) 986–991. https://doi.org/10.1016/j.egypro.2017.03.435.

[89] M. Heydari, M. Rahman, R. Gupta, Kinetic study and thermal decomposition behavior of lignite coal, Int. J. Chem. Eng. 2015 (2015). https://doi.org/10.1155/2015/481739.

[90] H.M. Ng, N.M. Saidi, F.S. Omar, K. Ramesh, S. Ramesh, S. Bashir, Thermogravimetric Analysis of Polymers, Encycl. Polym. Sci. Technol. (2018) 1–29. https://doi.org/10.1002/0471440264.pst667.

[91] G. Grause, M. Furusawa, A. Okuwaki, T. Yoshioka, Pyrolysis of tetrabromobisphenol-A containing paper laminated printed circuit boards, Chemosphere. 71 (2008) 872–878. https://doi.org/10.1016/j.chemosphere.2007.11.033.

[92] F. Barontini, K. Marsanich, L. Petarca, V. Cozzani, Thermal degradation and decomposition products of electronic boards containing BFRs, Ind. Eng. Chem. Res. 44 (2005) 4186–4199. https://doi.org/10.1021/ie048766l.

[93] Y.M. Kim, T.U. Han, C. Watanabe, N. Teramae, Y.K. Park, S. Kim, B. Hwang, Analytical pyrolysis of waste paper laminated phenolic-printed circuit board (PLP-PCB), J. Anal. Appl. Pyrolysis. 115 (2015) 87–95. https://doi.org/10.1016/j.jaap.2015.06.013.

[94] A.I. Balabanovich, A. Hornung, D. Merz, H. Seifert, The effect of a curing agent on the thermal degradation of fire retardant brominated epoxy resins, Polym. Degrad. Stab. 85 (2004) 713–723. https://doi.org/10.1016/j.polymdegradstab.2004.02.012.

[95] A.I. Balabanovich, M.P. Luda, L. Operti, GC/MS identification of pyrolysis products

from fire-retardant brominated epoxy resin, J. Fire Sci. 23 (2005) 227–245. https://doi.org/10.1177/0734904105047006.

[96] M.P. Luda, A.I. Balabanovich, M. Zanetti, D. Guaratto, Thermal decomposition of fire retardant brominated epoxy resins cured with different nitrogen containing hardeners, Polym. Degrad. Stab. 92 (2007) 1088–1100. https://doi.org/10.1016/j.polymdegradstab.2007.02.004.

[97] M.B. Smith, J. March, March's Advanced Organic Chemistry, 2006. https://doi.org/10.1002/0470084960.

[98] M.N. Siddiqui, H.H. Redhwi, E. V Antonakou, D.S. Achilias, Pyrolysis mechanism and thermal degradation kinetics of poly(bisphenol A carbonate)-based polymers originating in waste electric and electronic equipment, J. Anal. Appl. Pyrolysis. (2018). https://doi.org/10.1016/j.jaap.2018.03.008.

[99] A. Marongiu, G. Bozzano, M. Dente, E. Ranzi, T. Faravelli, Detailed kinetic modeling of pyrolysis of tetrabromobisphenol A, J. Anal. Appl. Pyrolysis. 80 (2007) 325–345. https://doi.org/10.1016/j.jaap.2007.04.003.

[100] P. Bradna, J. Zima, The use of pyrolysis-gas chromatography / mass spectroscopy in the analysis of cured polyfunctional epoxy resins, J. Anal. Appl. Pyrolysis. 21 (1991) 207–220. https://doi.org/10.1016/0165-2370(91)80026-5.

[101] R. Font, A. Ga, J.A. Conesa, J. Molto, Pyrolysis and combustion of electronic wastes, J. Anal. Appl. Pyrolysis. 84 (2009) 68–78. https://doi.org/10.1016/j.jaap.2008.10.023.

[102] M. Blazso, Z. Cze, Pyrolysis and debromination of flame retarded polymers of electronic scrap studied by analytical pyrolysis, J. Anal. Appl. Pyrolysis. 64 (2002) 249–261. https://doi.org/doi.org/10.1016/S0165-2370(02)00035-9.

[103] K.H. Lin, H.L. Chiang, Liquid oil and residual characteristics of printed circuit board recycle by pyrolysis, J. Hazard. Mater. 271 (2014) 258–265. https://doi.org/10.1016/j.jhazmat.2014.02.031.

[104] W.W. Kaeding, R.O. Lindblom, R.G. Temple, H.I. Mahon, Oxidation of toluene and other alkylated aromatic hydrocarbons to benzoic acids and phenols, Ind. Eng. Chem. Process Des. Dev. 4 (1965) 97–101. https://doi.org/10.1021/i260013a022.

[105] M. Riess, T. Ernst, R. Popp, B. Müller, H. Thoma, O. Vierle, M. Wolf, R. Van Eldik,

Analysis of flame retarded polymers and recycling materials, Chemosphere. 40 (2000) 937–941. https://doi.org/10.1016/S0045-6535(99)00336-7.

[106] J. Ebert, M. Bahadir, Formation of PBDD/F from flame-retarded plastic materials under thermal stress, Environ. Int. 29 (2003) 711–716. https://doi.org/10.1016/S0160-4120(03)00117-X.

[107] W.J. Hall, P.T. Williams, Analysis of products from the pyrolysis of plastics recovered from the commercial scale recycling of waste electrical and electronic equipment, J. Anal. Appl. Pyrolysis. 79 (2007) 375–386. https://doi.org/10.1016/j.jaap.2006.10.006.

[108] C. Shimasaki, Y. Muto, N. Takashima, E. Tsukurimichi, T. Yoshimura, K. Hasegawa, Pyrolysis of tetraphenyl imidodiphosphate, J. Anal. Appl. Pyrolysis. 23 (1992) 217–227. https://doi.org/10.1016/0165-2370(92)80018-H.

[109] M.P. k, M. Somasundaram, Co-pyrolysis of Juliflora biomass with low-density polyethylene for bio-oil synthesis, Energy Sources, Part A Recover. Util. Environ. Eff. 43 (2021) 1134–1149. https://doi.org/10.1080/15567036.2019.1635232.

[110] E. Kowalska, J. Radomska, P. Konarski, R. Diduszko, J. Oszczudłowski, T. Opalińska, M. Więch, Z. Duszyc, Thermogravimetric investigation of wastes from electrical and electronic equipment (WEEE), J. Therm. Anal. Calorim. 86 (2006) 137–140. https://doi.org/10.1007/s10973-006-7589-z.

[111] J. Hagberg, Analysis of brominated dioxins and furans by high resolution gas chromatography/high resolution mass spectrometry, J. Chromatogr. A. 1216 (2009) 376–384. https://doi.org/10.1016/j.chroma.2008.10.022.

[112] L. Yang, G. Liu, J. Shen, M. Wang, Q. Yang, M. Zheng, Environmental characteristics and formations of polybrominated dibenzo-p-dioxins and dibenzofurans, Environ. Int. 152 (2021) 106450. https://doi.org/10.1016/j.envint.2021.106450.

[113] H. Bockhorn, A. Hornung, U. Hornung, P. Jakobströer, M. Kraus, Dehydrochlorination of plastic mixtures, J. Anal. Appl. Pyrolysis. 49 (1999) 97–106. https://doi.org/10.1016/S0165-2370(98)00124-7.

[114] S.H. Jung, S.J. Kim, J.S. Kim, Thermal degradation of acrylonitrile-butadiene-styrene

(ABS) containing flame retardants using a fluidized bed reactor: The effects of Ca-based additives on halogen removal, Fuel Process. Technol. 96 (2012) 265–270. https://doi.org/10.1016/j.fuproc.2011.12.039.

[115] C. Vasile, M.A. Brebu, M. Totolin, J. Yanik, T. Karayildirim, H. Darie, Feedstock recycling from the printed circuit boards of used computers, Energy and Fuels. 22 (2008) 1658–1665. https://doi.org/10.1021/ef700659t.

[116] M. Blazsó, Z. Czégény, Catalytic destruction of brominated aromatic compounds studied in a catalyst microbed coupled to gas chromatography/mass spectrometry, J. Chromatogr. A. 1130 (2006) 91–96. https://doi.org/10.1016/j.chroma.2006.05.009.

[117] C.H. Ng, A. Salmiaton, H. Hizam, Catalytic pyrolysis and a pyrolysis kinetic study of shredded printed circuit board for fuel recovery, Bull. Chem. React. Eng. &Amp; Catal. 9 (2014) 224–240. https://doi.org/10.9767/bcrec.9.3.7148.224-240.

[118] Y. Wang, S. Sun, F. Yang, S. Li, J. Wu, J. Liu, S. Zhong, J. Zeng, The effects of activated Al2O3 on the recycling of light oil from the catalytic pyrolysis of waste printed circuit boards, Process Saf. Environ. Prot. 98 (2015) 276–284. https://doi.org/10.1016/j.psep.2015.07.007.

[119] Y. Park, T. Uk, J. Jeong, Y. Kim, Debrominated high quality oil production by the two-step catalytic pyrolysis of phenolic printed circuit boards (PPCB) using natural clays and HY, J. Hazard. Mater. 367 (2019) 50–58. https://doi.org/10.1016/j.jhazmat.2018.12.040.

[120] M.P. Luda, N. Euringer, U. Moratti, M. Zanetti, WEEE recycling: Pyrolysis of fire retardant model polymers, Waste Manag. 25 (2005) 203–208. https://doi.org/10.1016/j.wasman.2004.12.010.

[121] Y. Shen, Effect of chemical pretreatment on pyrolysis of non-metallic fraction recycled from waste printed circuit boards, Waste Manag. (2018). https://doi.org/10.1016/j.wasman.2018.02.036.

[122] O. Terakado, R. Ohhashi, M. Hirasawa, Thermal degradation study of tetrabromobisphenol A under the presence metal oxide: Comparison of bromine fixation ability, J. Anal. Appl. Pyrolysis. 91 (2011) 303–309. https://doi.org/10.1016/j.jaap.2011.03.006.

[123] O. Terakado, R. Ohhashi, M. Hirasawa, Bromine fixation by metal oxide in pyrolysis of printed circuit board containing brominated flame retardant, J. Anal. Appl. Pyrolysis. 103 (2013) 216–221. https://doi.org/10.1016/j.jaap.2012.10.022.

[124] F.R. Xiu, Y. Li, Y. Qi, X. Yu, J. He, Y. Lu, X. Gao, Y. Deng, Z. Song, A novel treatment of waste printed circuit boards by low-temperature near-critical aqueous ammonia: Debromination and preparation of nitrogen-containing fine chemicals, Waste Manag. 84 (2019) 355–363. https://doi.org/10.1016/j.wasman.2018.12.010.

[125] C. Ma, J. Yu, B. Wang, Z. Song, J. Xiang, S. Hu, S. Su, L. Sun, Catalytic pyrolysis of flame retarded high impact polystyrene over various solid acid catalysts, Fuel Process. Technol. 155 (2017) 32–41. https://doi.org/10.1016/j.fuproc.2016.01.018.

[126] D.P. Serrano, J. Aguado, J.M. Escola, Developing advanced catalysts for the conversion of polyolefinic waste plastics into fuels and chemicals, ACS Catal. 2 (2012) 1924–1941. https://doi.org/10.1021/cs3003403.

[127] C. Ma, T. Kamo, Two-stage catalytic pyrolysis and debromination of printed circuit boards: Effect of zero-valent Fe and Ni metals, J. Anal. Appl. Pyrolysis. 134 (2018) 614–620. https://doi.org/10.1016/j.jaap.2018.08.012.

[128] Md. Emdadul Hoque and Fazlur Rashid, Co-Pyrolysis of Biomass Solid Waste and Aquatic Plants, Intech. i (2016) 13. https://doi.org/DOI: 10.5772/intechopen.96228.

[129] X. Yuan, X. Zhang, H. Lv, Y. Xu, T. Bai, Co-Pyrolysis of Cotton Stalks and Low-Density Polyethylene to Synthesize Biochar and Its Application in Pb(II) Removal, Molecules. 27 (2022). https://doi.org/10.3390/molecules27154868.

[130] F. Abnisa, W.M.A. Wan Daud, S. Ramalingam, M.N.B.M. Azemi, J.N. Sahu, Co-pyrolysis of palm shell and polystyrene waste mixtures to synthesis liquid fuel, Fuel. 108 (2013) 311–318. https://doi.org/10.1016/j.fuel.2013.02.013.

[131] P. Ghorbannezhad, S. Park, J.A. Onwudili, Co-pyrolysis of biomass and plastic waste over zeolite- and sodium-based catalysts for enhanced yields of hydrocarbon products, Waste Manag. 102 (2020) 909–918. https://doi.org/10.1016/j.wasman.2019.12.006.

[132] S.A. Babajo, J.S. Enaburekhan, I.A. Rufai, Review on production of liquid fuel from co-pyrolysis of biomass with scrap/waste tire, J. Appl. Sci. Environ. Manag. 23 (2019)

1475. https://doi.org/10.4314/jasem.v23i8.10.

[133] R.M. Soncini, N.C. Means, N.T. Weiland, Co-pyrolysis of low rank coals and biomass: Product distributions, Fuel. 112 (2013) 74–82. https://doi.org/10.1016/j.fuel.2013.04.073.

[134] A. Aboyade, A. Osibote, A. Rabiu, M. Carrier, J. Görgens, Co-pyrolysis of coal and agricultural waste., Int. Proc. Chem. Biol. Environ. Eng. 38 (2012) 88–92. http://search.ebscohost.com/login.aspx?direct=true&db=lah&AN=20133091019&site=ehost-live%5Cnhttp://www.ipcbee.com/vol38/018-ICCCE2012-A036.pdf%5Cnemail: wale.aboyade@gmail.com.

[135] J. Hao, Q. Wang, Co-Pyrolysis Characteristics of Biomass and Coal under Different Mixing Modes, Int. J. Hybrid Inf. Technol. 9 (2016) 433–442. https://doi.org/10.14257/ijhit.2016.9.6.38.

[136] Q. Cao, L. Jin, W. Bao, Y. Lv, Investigations into the characteristics of oils produced from co-pyrolysis of biomass and tire, Fuel Process. Technol. 90 (2009) 337–342. https://doi.org/10.1016/j.fuproc.2008.10.005.

[137] E. Önal, B.B. Uzun, A.E. Pütün, An experimental study on bio-oil production from co-pyrolysis with potato skin and high-density polyethylene (HDPE), Fuel Process. Technol. 104 (2012) 365–370. https://doi.org/10.1016/j.fuproc.2012.06.010.

[138] M.J. Jeon, S.J. Choi, K.S. Yoo, C. Ryu, S.H. Park, J.M. Lee, J.K. Jeon, Y.K. Park, S. Kim, Copyrolysis of block polypropylene with waste wood chip, Korean J. Chem. Eng. 28 (2011) 497–501. https://doi.org/10.1007/s11814-010-0497-8.

[139] J.D. Martínez, A. Veses, A.M. Mastral, R. Murillo, M. V. Navarro, N. Puy, A. Artigues, J. Bartrolí, T. García, Co-pyrolysis of biomass with waste tyres: Upgrading of liquid bio-fuel, Fuel Process. Technol. 119 (2014) 263–271. https://doi.org/10.1016/j.fuproc.2013.11.015.

[140] C. Ma, S. Kumagai, Y. Saito, T. Kameda, T. Yoshioka, Enhanced production of phenol and debromination by co-pyrolysis of the non-metallic fraction of printed circuit boards and waste tires, Green Chem. 23 (2021) 6392–6404. https://doi.org/10.1039/d1gc01176f.

[141] C. Ma, S. Kumagai, Y. Saito, T. Kameda, T. Yoshioka, An integrated utilization

strategy of printed circuit boards and waste tire by fast co-pyrolysis: Value-added products recovery and heteroatoms transformation, J. Hazard. Mater. 430 (2022) 128420. https://doi.org/10.1016/j.jhazmat.2022.128420.

[142] W. Chen, Y. Shu, Y. Li, Y. Chen, J. Wei, Co-pyrolysis of waste printed circuit boards with iron compounds for Br-fixing and material recovery, Environ. Sci. Pollut. Res. 28 (2021) 64642–64651. https://doi.org/10.1007/s11356-021-15506-w.

[143] A. Hornung, S. Donner, A. Balabanovich, H. Seifert, Polypropylene as a reductive agent for dehalogenation of brominated organic compounds, J. Clean. Prod. 13 (2005) 525–530. https://doi.org/10.1016/j.jclepro.2003.09.001.

[144] Y.M. Kim, T.U. Han, S. Kim, J. Jae, J.K. Jeon, S.C. Jung, Y.K. Park, Catalytic co-pyrolysis of epoxy-printed circuit board and plastics over HZSM-5 and HY, J. Clean. Prod. 168 (2017) 366–374. https://doi.org/10.1016/j.jclepro.2017.08.224.

[145] J. Guan, J. Wang, X. Min, W. Wu, The Products Characteristics of Calcium-basic Compounds Pyrolysis with Waste Printed Circuit Boards (PCB), Procedia Environ. Sci. 16 (2012) 461–468. https://doi.org/10.1016/j.proenv.2012.10.063.

[146] Z. Ye, F. Yang, W. Lin, S. Li, S. Sun, Improvement of pyrolysis oil obtained from co-pyrolysis of WPCBs and compound additive during two stage pyrolysis, J. Anal. Appl. Pyrolysis. 135 (2018) 415–421. https://doi.org/10.1016/j.jaap.2018.06.011.

[147] A. Demirbas, Biofuels securing the planet's future energy needs, Energy Convers. Manag. 50 (2009) 2239–2249. https://doi.org/10.1016/j.enconman.2009.05.010.

[148] S. Vitolo, M. Seggiani, P. Frediani, G. Ambrosini, L. Politi, Catalytic upgrading of pyrolytic oils to fuel over different zeolites, Fuel. 78 (1999) 1147–1159. https://doi.org/10.1016/S0016-2361(99)00045-9.

[149] X. Guo, S. Li, Y. Zheng, B. Ci, Preparation and characterization of bio-oil by microwave pyrolysis of biomass, Energy Sources, Part A Recover. Util. Environ. Eff. 38 (2016) 133–139. https://doi.org/10.1080/15567036.2011.649340.

[150] W. Wu, K. Qiu, Vacuum co-pyrolysis of Chinese fir sawdust and waste printed circuit boards. Part I: Influence of mass ratio of reactants, J. Anal. Appl. Pyrolysis. 105 (2014) 252–261. https://doi.org/10.1016/j.jaap.2013.11.011.

[151] N. Joshi, A. Lawal, Hydrodeoxygenation of pyrolysis oil in a microreactor, Chem.

Eng. Sci. 74 (2012) 1–8. https://doi.org/10.1016/j.ces.2012.01.052.

[152] M. Toba, Y. Abe, H. Kuramochi, M. Osako, T. Mochizuki, Y. Yoshimura, Hydrodeoxygenation of waste vegetable oil over sulfide catalysts, Catal. Today. 164 (2011) 533–537. https://doi.org/10.1016/j.cattod.2010.11.049.

[153] A. Veses, M. Aznar, I. Martínez, J.D. Martínez, J.M. López, M. V. Navarro, M.S. Callén, R. Murillo, T. García, Catalytic pyrolysis of wood biomass in an auger reactor using calcium-based catalysts, Bioresour. Technol. 162 (2014) 250–258. https://doi.org/10.1016/j.biortech.2014.03.146.

[154] F.H. Isikgor, C.R. Becer, Lignocellulosic biomass: a sustainable platform for the production of bio-based chemicals and polymers, Polym. Chem. 6 (2015) 4497–4559. https://doi.org/10.1039/c5py00263j.

[155] X. Zhang, H. Lei, S. Chen, J. Wu, Catalytic co-pyrolysis of lignocellulosic biomass with polymers: A critical review, Green Chem. 18 (2016) 4145–4169. https://doi.org/10.1039/c6gc00911e.

[156] E.S. Biris-Dorhoi, D. Michiu, C.R. Pop, A.M. Rotar, M. Tofana, O.L. Pop, S.A. Socaci, A.C. Farcas, Macroalgae—A sustainable source of chemical compounds with biological activities, Nutrients. 12 (2020) 1–23. https://doi.org/10.3390/nu12103085.

[157] T. Mutanda, D. Naidoo, J.K. Bwapwa, A. Anandraj, Biotechnological Applications of Microalgal Oleaginous Compounds: Current Trends on Microalgal Bioprocessing of Products, Front. Energy Res. 8 (2020) 1–21. https://doi.org/10.3389/fenrg.2020.598803.

[158] J. Geng, L.F. Li, W.L. Wang, J.M. Chang, C.L. Xia, L.P. Cai, S.Q. Shi, Fabrication of activated carbon using two-step co-pyrolysis of used rubber and larch sawdust, BioResources. 12 (2017) 8641–8652. https://doi.org/10.15376/biores.12.4.8641-8652.

[159] C. Quan, N. Gao, Copyrolysis of Biomass and Coal: A Review of Effects of Copyrolysis Parameters, Product Properties, and Synergistic Mechanisms, Biomed Res. Int. 2016 (2016). https://doi.org/10.1155/2016/6197867.

[160] D.Y. Hopa, O. Alagöz, N. Yılmaz, M. Dilek, G. Arabacı, T. Mutlu, Biomass co-pyrolysis: Effects of blending three different biomasses on oil yield and quality, Waste

Manag. Res. 37 (2019) 925–933. https://doi.org/10.1177/0734242X19860895.

[161] S. Chakraborthy, Co-pyrolysis of Microalgae, sludge and Lignocellulosic Biomass For aromatic hydrocarbon production, Thesis. (2015).

[162] Sunarno, E. Saputra, M.I. Fermi, P.S. Utama, Non-catalytic co-pyrolysis of empty fruit bunch of palm and solid tire waste into upgrade bio-oil, Int. J. Renew. Energy Res. 10 (2020) 687–692. https://doi.org/10.20508/ijrer.v10i2.10690.g7940.

[163] M.S. Hossain, M.R. Islam, M.S. Rahman, M.A. Kader, H. Haniu, Biofuel from Co-pyrolysis of Solid Tire Waste and Rice Husk, Energy Procedia. 110 (2017) 453–458. https://doi.org/10.1016/j.egypro.2017.03.168.

[164] M. Siva, S. Onenc, S. Uçar, J. Yanik, Influence of oily wastes on the pyrolysis of scrap tire, Energy Convers. Manag. 75 (2013) 474–481. https://doi.org/10.1016/j.enconman.2013.06.055.

[165] M.S.S.A.S. A, B. H, Sultan M. Al-Salem, Animesh Dutta, A review on co-pyrolysis of biomass with plastics and tires: recent progress, catalyst development, and scaling up potential, (n.d.). https://doi.org/https://doi.org/10.1007/s13399-021-01818-x.

[166] Z. Wang, S. An, J. Zhao, P. Sun, H. Lyu, W. Kong, B. Shen, Plastic regulates its co-pyrolysis process with biomass: Influencing factors, model calculations, and mechanisms, Front. Ecol. Evol. 10 (2022) 1–17. https://doi.org/10.3389/fevo.2022.964936.

[167] B. Bernard, X. He, S. Wang, A.E. Abomohra, Y. Hu, Q. Wang, Co-pyrolysis of biomass and waste plastics as a thermochemical conversion technology for high-grade biofuel production : Recent progress and future directions elsewhere worldwide, Energy Convers. Manag. 163 (2018) 468–492. https://doi.org/10.1016/j.enconman.2018.02.004.

[168] H.W. Ryu, D.H. Kim, J. Jae, S.S. Lam, E.D. Park, Y.K. Park, Recent advances in catalytic co-pyrolysis of biomass and plastic waste for the production of petroleum-like hydrocarbons, Bioresour. Technol. 310 (2020) 123473. https://doi.org/10.1016/j.biortech.2020.123473.

[169] V.I. Sharypov, N. Marin, N.G. Beregovtsova, S. V. Baryshnikov, B.N. Kuznetsov, V.L. Cebolla, J. V. Weber, Co-pyrolysis of wood biomass and synthetic polymer

mixtures. Part I: Influence of experimental conditions on the evolution of solids, liquids and gases, J. Anal. Appl. Pyrolysis. 64 (2002) 15–28. https://doi.org/10.1016/S0165-2370(01)00167-X.

[170] Y. Zhao, Y. Wang, D. Duan, R. Ruan, L. Fan, Y. Zhou, L. Dai, J. Lv, Y. Liu, Fast microwave-assisted ex-catalytic co-pyrolysis of bamboo and polypropylene for bio-oil production, Bioresour. Technol. 249 (2018) 69–75. https://doi.org/10.1016/j.biortech.2017.09.184.

[171] K. Ding, A. He, D. Zhong, L. Fan, S. Liu, Y. Wang, Y. Liu, P. Chen, H. Lei, R. Ruan, Improving hydrocarbon yield via catalytic fast co-pyrolysis of biomass and plastic over ceria and HZSM-5: An analytical pyrolyzer analysis, Bioresour. Technol. 268 (2018) 1–8. https://doi.org/10.1016/j.biortech.2018.07.108.

[172] K. Praveen Kumar, S. Srinivas, Catalytic Co-pyrolysis of Biomass and Plastics (Polypropylene and Polystyrene) Using Spent FCC Catalyst, Energy and Fuels. 34 (2020) 460–473. https://doi.org/10.1021/acs.energyfuels.9b03135.

[173] J. Wang, J. Jiang, Z. Zhong, K. Wang, X. Wang, B. Zhang, R. Ruan, M. Li, A.J. Ragauskas, Catalytic fast co-pyrolysis of bamboo sawdust and waste plastics for enhanced aromatic hydrocarbons production using synthesized CeO2/Γ-Al2O3 and HZSM-5, Energy Convers. Manag. 196 (2019) 759–767. https://doi.org/10.1016/j.enconman.2019.06.009.

[174] M.S. Hossain, J. Ferdous, M.S. Islam, M.R. Islam, N.N. Mustafi, H. Haniu, Production of liquid fuel from co-pyrolysis of polythene waste and rice straw, Energy Procedia. 160 (2019) 116–122. https://doi.org/10.1016/j.egypro.2019.02.126.

[175] R. Kumar Mishra, K. Mohanty, Co-pyrolysis of waste biomass and waste plastics (polystyrene and waste nitrile gloves) into renewable fuel and value-added chemicals, Carbon Resour. Convers. 3 (2020) 145–155. https://doi.org/10.1016/j.crcon.2020.11.001.

[176] H. Hassan, B.H. Hameed, J.K. Lim, Co-pyrolysis of sugarcane bagasse and waste high-density polyethylene: Synergistic effect and product distributions, Energy. 191 (2020) 116545. https://doi.org/10.1016/j.energy.2019.116545.

[177] W. Wu, K. Qiu, Vacuum co-pyrolysis of Chinese fir sawdust and waste printed circuit boards. Part II: Influence of heating conditions, J. Anal. Appl. Pyrolysis. 111 (2015)

216–223. https://doi.org/10.1016/j.jaap.2014.11.006.

[178] A. Pratap, S. Chouhan, A Slow Pyrolysis of Cotton Stalk (Gossypium arboretum) Waste for Bio-Oil Production, J. Pharm. Chem. Biol. Sci. 3 (2015) 143–149. http://www.jpcbs.info.

[179] G. Mailto, R.B. Mahar, I.N. Unar, K.M. Brohi, Kinetic Study of Cotton Stalk and Rice Husk Samples under an Inert and Oxy Combustion Atmospheres, Mehran Univ. Res. J. Eng. Technol. 37 (2018) 327–336. https://doi.org/10.22581/muet1982.1802.09.

[180] D. Chen, E. Shuang, L. Liu, Analysis of pyrolysis characteristics and kinetics of sweet sorghum bagasse and cotton stalk, J. Therm. Anal. Calorim. 131 (2018) 1899–1909. https://doi.org/10.1007/s10973-017-6585-9.

[181] S.A.Y. Shah, M. Zeeshan, M.Z. Farooq, N. Ahmed, N. Iqbal, Co-pyrolysis of cotton stalk and waste tire with a focus on liquid yield quantity and quality, Renew. Energy. 130 (2019) 238–244. https://doi.org/10.1016/j.renene.2018.06.045.

[182] Z. Wang, J. Wang, L. Xie, H. Zhu, X. Shu, Influence of the Addition of Cotton Stalk during Co-pyrolysis with Sewage Sludge on the Properties, Surface Characteristics, and Ecological Risks of Biochars, J. Therm. Sci. 28 (2019) 755–762. https://doi.org/10.1007/s11630-019-1100-1.

[183] T. Miranda, I. Montero, F.J. Sepúlveda, J.I. Arranz, C.V. Rojas, S. Nogales, A review of pellets from different sources, Materials (Basel). 8 (2015) 1413–1427. https://doi.org/10.3390/ma8041413.

[184] C. Henkel, P.D. Muley, K.K. Abdollahi, C. Marculescu, D. Boldor, Pyrolysis of energy cane bagasse and invasive Chinese tallow tree (Triadica sebifera L.) biomass in an inductively heated reactor, Energy Convers. Manag. 109 (2016) 175–183. https://doi.org/10.1016/j.enconman.2015.12.013.

[185] W.A. Bizzo, R.A. Figueiredo, V.F. De Andrade, Characterization of printed circuit boards for metal and energy recovery after milling and mechanical separation, Materials (Basel). 7 (2014) 4555–4566. https://doi.org/10.3390/ma7064555.

[186] P.P.M. Ribeiro, I.D. Dos Santos, A.J.B. Dutra, Copper and metals concentration from printed circuit boards using a zig-zag classifier, J. Mater. Res. Technol. 8 (2019) 513–

520. https://doi.org/10.1016/j.jmrt.2018.05.003.

[187] G.N. Lewis, Autocatalytic Decomposition of Silver Oxide, Proc. Am. Acad. Arts Sci. 40 (1905) 719. https://doi.org/10.2307/20022019.

[188] P. Holba, Temperature dependence of activation energy of endothermic processes and related imperfections of non-isothermal kinetic evaluations, J. Therm. Anal. Calorim. 129 (2017) 609–614. https://doi.org/10.1007/s10973-017-6088-8.

[189] J.M. Criado, L.A. Pérez-Maqueda, P.E. Sánchez-Jiménez, Dependence of the preexponential factor on temperature: Errors in the activation energies calculated by assuming that A is constant, J. Therm. Anal. Calorim. 82 (2005) 671–675. https://doi.org/10.1007/s10973-005-0948-3.

[190] S. Vyazovkin, Kinetic concepts of thermally stimulated reactions in solids: A view from a historical perspective, Int. Rev. Phys. Chem. 19 (2000) 45–60. https://doi.org/10.1080/014423500229855.

[191] P. Šimon, Isoconversional methods: Fundamentals, meaning and application, J. Therm. Anal. Calorim. 76 (2004) 123–132. https://doi.org/10.1023/B:JTAN.0000027811.80036.6c.

[192] S. Vyazovkin, Model-free kinetics: Staying free of multiplying entities without necessity, J. Therm. Anal. Calorim. 83 (2006) 45–51. https://doi.org/10.1007/s10973-005-7044-6.

[193] Z. Yao, S. Yu, W. Su, W. Wu, J. Tang, W. Qi, Kinetic studies on the pyrolysis of plastic waste using a combination of model-fitting and model-free methods, Waste Manag. Res. 38 (2020) 77–85. https://doi.org/10.1177/0734242X19897814.

[194] Zhitong Yao, Thermal behavior and kinetic study on the co-pyrolysis of biomass with polymer waste, Biomass Convers. Biorefinery. (2022). https://doi.org/https://doi.org/10.1007/s13399-022-02480-7.

[195] A. Dhaundiyal, S.B. Singh, M.M. Hanon, R. Rawat, Determination of Kinetic Parameters for the Thermal Decomposition of Parthenium hysterophorus, Environ. Clim. Technol. 22 (2018) 5–21. https://doi.org/10.1515/rtuect-2018-0001.

[196] H. Mahmood, A. Shakeel, A. Abdullah, M.I. Khan, M. Moniruzzaman, A comparative study on suitability of model-free and model-fitting kinetic methods to

non-isothermal degradation of lignocellulosic materials, Polymers (Basel). 13 (2021). https://doi.org/10.3390/polym13152504.

[197] M.Y. Guida, A. Hannioui, Evaluation of Reliability of Coats-Redfern and Criado Methods for Kinetics Analysis of Olive Mill Solid Waste and Olive Mill Wastewater, Int. J. Sci. Eng. Res. 7 (2016) 193–203.

[198] M. Venkatesh, P. Ravi, S.P. Tewari, Isoconversional kinetic analysis of decomposition of nitroimidazoles: Friedman method vs Flynn-Wall-Ozawa method, J. Phys. Chem. A. 117 (2013) 10162–10169. https://doi.org/10.1021/jp407526r.

[199] X. Yongjiang, X. Huaqing, W. Hongyan, L. Zhiping, F. Chaohe, Kinetics of isothermal and non-isothermal pyrolysis of oil shale, Oil Shale. 28 (2011) 415–424. https://doi.org/10.3176/oil.2011.3.05.

[200] Y. Hu, Z. Wang, X. Cheng, C. Ma, Non-isothermal TGA study on the combustion reaction kinetics and mechanism of low-rank coal char, RSC Adv. 8 (2018) 22909–22916. https://doi.org/10.1039/C8RA02618A.

[201] A. Caballero, J.A. Conesa, Mathematical considerations for nonisothermal kinetics in thermal decomposition, 73 (2005) 85–100. https://doi.org/10.1016/j.jaap.2004.12.003.

[202] E. Kantarelis, W. Yang, W. Blasiak, C. Forsgren, A. Zabaniotou, Thermochemical treatment of E-waste from small household appliances using highly pre-heated nitrogen-thermogravimetric investigation and pyrolysis kinetics, Appl. Energy. 88 (2011) 922–929. https://doi.org/10.1016/j.apenergy.2010.08.022.

[203] S.A. El-Sayed, M.E. Mostafa, Thermal pyrolysis and kinetic parameter determination of mango leaves using common and new proposed parallel kinetic models, RSC Adv. 10 (2020) 18160–18179. https://doi.org/10.1039/d0ra00493f.

[204] M.J. Starink, The determination of activation energy from linear heating rate experiments : a comparison of the accuracy of isoconversion methods, 404 (2003) 163–176. https://doi.org/10.1016/S0040-6031(03)00144-8.

[205] S. Vyazovkin, A time to search: Finding the meaning of variable activation energy, Phys. Chem. Chem. Phys. 18 (2016) 18643–18656. https://doi.org/10.1039/c6cp02491b.

[206] P.L. Vol, D. Method, F.O.R. The, D. Of, A. Energy, T.D. The, A quick, direct method for the determination of activation energy, 4 (1966) 323–328.

[207] M. Sakakibara, F. Okada, M. Horiuchi, K. Suzuki, Kinetic Analysis of Thermogravimetric Data, Nippon Kagaku Kaishi. 1989 (1989) 1729–1732. https://doi.org/10.1246/nikkashi.1989.1729.

[208] N. Koga, Ozawa's kinetic method for analyzing thermoanalytical curves: History and theoretical fundamentals, J. Therm. Anal. Calorim. 113 (2013) 1527–1541. https://doi.org/10.1007/s10973-012-2882-5.

[209] C. Păcurariu, R.I. Lazău, I. Lazău, D. Tiţa, Kinetics of non-isothermal crystallization of some glass-ceramics based on basalt, J. Therm. Anal. Calorim. 88 (2007) 647–652. https://doi.org/10.1007/s10973-006-8024-1.

[210] A. Aboulkas, K. El Harfi, Study of the kinetics and mechanisms of thermal decomposition of Moroccan Tarfaya oil shale and its kerogen, Oil Shale. 25 (2008) 426–443. https://doi.org/10.3176/oil.2008.4.04.

[211] H.E. Kissinger, Reaction Kinetics in Differential Thermal Analysis, Anal. Chem. 303 (1957) 1702–1706. https://doi.org/10.1021/ac60131a045.

[212] G. MY, B. H, E.M. L, M. A, A. A, E. harfi K, H. A, Utilization of Starink Approach and Avrami Theory to Evaluate the Kinetic Parameters of the Pyrolysis of Olive Mill Solid Waste and Olive Mill Wastewater, J. Adv. Chem. Eng. 07 (2017) 1–8. https://doi.org/10.4172/2090-4568.1000155.

[213] J.M. Criado, J. Málek, A. Ortega, Applicability of the master plots in kinetic analysis of non-isothermal data, Thermochim. Acta. 147 (1989) 377–385. https://doi.org/10.1016/0040-6031(89)85192-5.

[214] J.M. Criado, F.J. Gotor, J. Málek, A UNIFIED THEORY FOR THE KINETIC ANALYSIS OF SOLID STATE REACTIONS UNDER ANY THERMAL PATHWAY, 72 (2003) 901–906.

[215] J. Málek, The kinetic analysis of non-isothermal data, Thermochim. Acta. 200 (1992) 257–269. https://doi.org/10.1016/0040-6031(92)85118-F.

[216] V. Pistor, F.G. Ornaghi, H.L. Ornaghi, A.J. Zattera, Degradation kinetic of epoxy nanocomposites containing different percentage of epoxycyclohexyl-POSS, Polym.

Compos. 33 (2012) 1224–1232. https://doi.org/10.1002/pc.22181.

[217] J. Costa, J. Martins, T. Arantes, M. Gonçalves, L. Durão, F.P. Brito, Experimental assessment of the performance and emissions of a spark-ignition engine using waste-derived biofuels as additives, Energies. 14 (2021). https://doi.org/10.3390/en14165209.

[218] C. Quan, A. Li, N. Gao, Thermogravimetric analysis and kinetic study on large particles of printed circuit board wastes, Waste Manag. 29 (2009) 2353–2360. https://doi.org/10.1016/j.wasman.2009.03.020.

[219] A. Anca-Couce, Reaction mechanisms and multi-scale modelling of lignocellulosic biomass pyrolysis, Prog. Energy Combust. Sci. 53 (2016) 41–79. https://doi.org/10.1016/j.pecs.2015.10.002.

[220] V. Georgieva, L. Vlaev, K. Gyurova, Non-isothermal degradation kinetics of CaCO3 from different origin, J. Chem. 2013 (2013). https://doi.org/10.1155/2013/872981.

[221] M. Van de Velden, J. Baeyens, A. Brems, B. Janssens, R. Dewil, Fundamentals, kinetics and endothermicity of the biomass pyrolysis reaction, Renew. Energy. 35 (2010) 232–242. https://doi.org/10.1016/j.renene.2009.04.019.

[222] S. Munir, S.S. Daood, W. Nimmo, A.M. Cunliffe, B.M. Gibbs, Thermal analysis and devolatilization kinetics of cotton stalk, sugar cane bagasse and shea meal under nitrogen and air atmospheres, Bioresour. Technol. 100 (2009) 1413–1418. https://doi.org/10.1016/j.biortech.2008.07.065.

[223] D. V. Suriapparao, S.P. Batchu, S. Jayasurya, R. Vinu, Selective production of phenolics from waste printed circuit boards via microwave assisted pyrolysis, Elsevier Ltd, 2018. https://doi.org/10.1016/j.jclepro.2018.06.203.

[224] N. Sbirrazzuoli, Advanced isoconversional kinetic analysis for the elucidation of complex reaction mechanisms: A new method for the identification of rate-limiting steps, Molecules. 24 (2019). https://doi.org/10.3390/molecules24091683.

[225] A.S. Patnaik, J.L. Goldfarb, Continuous activation energy representation of the Arrhenius equation for the pyrolysis of cellulosic materials: Feed corn stover and cocoa shell biomass, Cellul. Chem. Technol. 50 (2016) 311–320.

[226] G.D. Mumbach, J.L.F. Alves, J.C.G. da Silva, M. Di Domenico, R.F. de Sena, C.

Marangoni, R.A.F. Machado, A. Bolzan, Pyrolysis of cocoa shell and its bioenergy potential: evaluating the kinetic triplet, thermodynamic parameters, and evolved gas analysis using TGA-FTIR, Biomass Convers. Biorefinery. 12 (2022) 723–739. https://doi.org/10.1007/s13399-020-01058-5.

[227] C. Zheng, D. Li, M. Ek, Mechanism and kinetics of thermal degradation of insulating materials developed from cellulose fiber and fire retardants, J. Therm. Anal. Calorim. 135 (2019) 3015–3027. https://doi.org/10.1007/s10973-018-7564-5.

[228] Y. Chen, J. Yang, Y. Zhang, K. Liu, S. Liang, X. Xu, J. Hu, H. Yao, B. Xiao, Kinetic simulation and prediction of pyrolysis process for non-metallic fraction of waste printed circuit boards by discrete distributed activation energy model compared with isoconversional method, Environ. Sci. Pollut. Res. 25 (2018) 3636–3646. https://doi.org/10.1007/s11356-017-0763-y.

[229] M. Carrier, L. Auret, A. Bridgwater, J.H. Knoetze, Using Apparent Activation Energy as a Reactivity Criterion for Biomass Pyrolysis, Energy and Fuels. 30 (2016) 7834–7841. https://doi.org/10.1021/acs.energyfuels.6b00794.

[230] A. Mianowski, T. Radko, T. Siudyga, Kinetic compensation effect of isoconversional methods, React. Kinet. Mech. Catal. 132 (2021) 37–58. https://doi.org/10.1007/s11144-020-01898-2.

[231] N.U. Hasan, M.M. Rahman, R.I. Rahat, Characteristics comparison of pyrolysed oils obtained from waste of plastic, tyres and biomass solid, 4th Int. Conf. Adv. Electr. Eng. ICAEE 2017. 2018-Janua (2017) 450–454. https://doi.org/10.1109/ICAEE.2017.8255398.

[232] S. Adhikari, H. Nam, J.P. Chakraborty, Conversion of solid wastes to fuels and chemicals through pyrolysis, Elsevier B.V., 2018. https://doi.org/10.1016/B978-0-444-63992-9.00008-2.

[233] J. lu Zheng, W. ming Yi, N. na Wang, Bio-oil production from cotton stalk, Energy Convers. Manag. 49 (2008) 1724–1730. https://doi.org/10.1016/j.enconman.2007.11.005.

[234] Q. Lu, W.Z. Li, X.F. Zhu, Overview of fuel properties of biomass fast pyrolysis oils, Energy Convers. Manag. 50 (2009) 1376–1383. https://doi.org/10.1016/j.enconman.2009.01.001.

[235] A. Oasmaa, C. Peacocke, S. Gust, D. Meier, R. McLellan, Norms and standards for pyrolysis liquids. End-user requirements and specifications, Energy and Fuels. 19 (2005) 2155–2163. https://doi.org/10.1021/ef040094o.

[236] A. Oasmaa, S. Czernik, Fuel oil quality of biomass pyrolysis oils - state of the art for the end users, Energy and Fuels. 13 (1999) 914–921. https://doi.org/10.1021/ef980272b.

[237] S. Şensöz, D. Angin, Pyrolysis of safflower (Charthamus tinctorius L.) seed press cake: Part 1. The effects of pyrolysis parameters on the product yields, Bioresour. Technol. 99 (2008) 5492–5497. https://doi.org/10.1016/j.biortech.2007.10.046.

[238] Q. Zhang, J. Chang, T. Wang, Y. Xu, Review of biomass pyrolysis oil properties and upgrading research, Energy Convers. Manag. 48 (2007) 87–92. https://doi.org/10.1016/j.enconman.2006.05.010.

[239] A.E. Pütün, N. Özbay, E.P. Önal, E. Pütün, Fixed-bed pyrolysis of cotton stalk for liquid and solid products, Fuel Process. Technol. 86 (2005) 1207–1219. https://doi.org/10.1016/j.fuproc.2004.12.006.

[240] Q.J. Yu, Experimental Study on Pyrolysis of Non-Metallic Materials Separated from Printed Circuit Board Waste via TGA and Analytical Vacuum Fast Pyrolysis of Non-Metallic Fraction of Printed Circuit Board Waste after Copper Separation, Glob. Environ. Eng. 6 (2019) 1–15. https://doi.org/10.15377/2410-3624.2019.06.1.

[241] Y. Shen, X. Chen, X. Ge, M. Chen, Thermochemical treatment of non-metallic residues from waste printed circuit board: Pyrolysis vs. combustion, J. Clean. Prod. 176 (2018) 1045–1053. https://doi.org/10.1016/j.jclepro.2017.11.232.

[242] M. Gu, Z. Shen, L. Yang, W. Dong, L. Kong, W. Zhang, B.Y. Peng, Y. Zhang, Reaction Route Selection for Cellulose Hydrogenolysis into C2/C3 Glycols by ZnO-Modified Ni-W/β-zeolite Catalysts, Sci. Rep. 9 (2019) 1–10. https://doi.org/10.1038/s41598-019-48103-6.

[243] Z. Fang, R.L. Smith, L. Xu, Production of Biofuels and Chemicals with Pyrolysis, 2015. http://link.springer.com/10.1007/978-94-017-9612-5.

[244] P.R. Patwardhan, R.C. Brown, B.H. Shanks, Product distribution from the fast pyrolysis of hemicellulose, ChemSusChem. 4 (2011) 636–643.

https://doi.org/10.1002/cssc.201000425.

[245] J. Li, C. Wang, Z. Yang, Production and separation of phenols from biomass-derived bio-petroleum, J. Anal. Appl. Pyrolysis. 89 (2010) 218–224. https://doi.org/10.1016/j.jaap.2010.08.004.

[246] J. Yan, Q. Meng, X. Shen, B. Chen, Y. Sun, J. Xiang, H. Liu, B. Han, Selective valorization of lignin to phenol by direct transformation of Csp2-Csp3 and C-O bonds, Sci. Adv. 6 (2020) 1–11. https://doi.org/10.1126/SCIADV.ABD1951.

[247] X. Huang, J.M. Ludenhoff, M. Dirks, X. Ouyang, M.D. Boot, E.J.M. Hensen, Selective Production of Biobased Phenol from Lignocellulose-Derived Alkylmethoxyphenols, ACS Catal. 8 (2018) 11184–11190. https://doi.org/10.1021/acscatal.8b03430.

[248] X. Ouyang, X. Huang, M.D. Boot, E.J.M. Hensen, Efficient Conversion of Pine Wood Lignin to Phenol, ChemSusChem. 13 (2020) 1705–1709. https://doi.org/10.1002/cssc.202000485.

[249] J.G. Kim, Chemical recycling of poly(bisphenol A carbonate), Polym. Chem. 11 (2020) 4830–4849. https://doi.org/10.1039/c9py01927h.

[250] D. Kim, B.K. Kim, Y. Cho, M. Han, B.S. Kim, Kinetics of polycarbonate glycolysis in ethylene glycol, Ind. Eng. Chem. Res. 48 (2009) 685–691. https://doi.org/10.1021/ie8010947.

[251] C. Ma, T. Kamo, Effect of steam-iron reaction on product characteristics and debromination during pyrolysis of epoxy-printed circuit boards, J. Hazard. Mater. 379 (2019) 120803. https://doi.org/10.1016/j.jhazmat.2019.120803.

[252] M. Xing, F.S. Zhang, Degradation of brominated epoxy resin and metal recovery from waste printed circuit boards through batch sub/supercritical water treatments, Chem. Eng. J. 219 (2013) 131–136. https://doi.org/10.1016/j.cej.2012.12.066.

[253] H.Y. Zhao, K. Peng, M. Li, S.Q. Li, Q. Song, Q. Yao, Distribution of Bromine in the Pyrolysis of Printed Circuit Board Wastes, 8thAsia-Pacific Int. Symp. Combust. Energy Util. (2006). http://apisceu.narod.ru/PDF/ec-104.pdf.

[254] V. Sahajwalla, R. Cayumil, R. Khanna, M. Ikram-Ul-Haq, R. Rajarao, P.S. Mukherjee, A. Hill, Recycling Polymer-Rich Waste Printed Circuit Boards at High

Temperatures: Recovery of Value-Added Carbon Resources, J. Sustain. Metall. 1 (2015) 75–84. https://doi.org/10.1007/s40831-014-0002-4.

[255] M. Bardalai, D.K. Mahanta, A review of physical properties of biomass pyrolysis oil, Int. J. Renew. Energy Res. 5 (2015) 277–286. https://doi.org/10.20508/ijrer.12755.

[256] H. Panchasara, N. Ashwath, Effects of Pyrolysis Bio-Oils on Fuel Atomisation—A Review, Energies. 14 (2021) 794. https://doi.org/10.3390/en14040794.

[257] W.J. Hall, N. Miskolczi, J. Onwudili, P.T. Williams, Thermal processing of toxic flame-retarded polymers using a waste fluidized catalytic cracker (FCC) catalyst, Energy and Fuels. 22 (2008) 1691–1697. https://doi.org/10.1021/ef800043g.

[258] T. Rieger, J.C. Oey, V. Palchyk, A. Hofmann, M. Franke, A. Hornung, Chemical recycling of WEEE plastics—production of high purity monocyclic aromatic chemicals, Processes. 9 (2021) 1–16. https://doi.org/10.3390/pr9030530.

[259] S. Zhang, Y. Yan, T. Li, Z. Ren, Upgrading of liquid fuel from the pyrolysis of biomass, Bioresour. Technol. 96 (2005) 545–550. https://doi.org/10.1016/j.biortech.2004.06.015.

[260] Y. Xu, X. Hu, W. Li, Y. Shi, Preparation and Characterization of Bio-oil from Biomass, Prog. Biomass Bioenergy Prod. (2011). https://doi.org/10.5772/16466.

[261] Y.Y. Chong, S. Thangalazhy-Gopakumar, H.K. Ng, P.B. Ganesan, S. Gan, L.Y. Lee, V.S.A.R. Manickavel, C.M. Ong, H.S.R. Al Hinai, Emulsification of bio-oil and diesel, Chem. Eng. Trans. 56 (2017) 1801–1806. https://doi.org/10.3303/CET1756301.

[262] M. Theses, S.J. Eaton, Accelerated Poisoning of Diesel Oxidation Catalysts by Zinc Dialkyldithiophosphate-Derived Phosphorus, TRACE Tennessee Res. Creat. Exch. Masters. (2006). https://trace.tennessee.edu/utk_gradthes/1544.

[263] L. Negahdar, A. Gonzalez-Quiroga, D. Otyuskaya, H.E. Toraman, L. Liu, J.T.B.H. Jastrzebski, K.M. Van Geem, G.B. Marin, J.W. Thybaut, B.M. Weckhuysen, Characterization and Comparison of Fast Pyrolysis Bio-oils from Pinewood, Rapeseed Cake, and Wheat Straw Using 13C NMR and Comprehensive GC × GC, ACS Sustain. Chem. Eng. 4 (2016) 4974–4985. https://doi.org/10.1021/acssuschemeng.6b01329.

[264] C. Guizani, K. Haddad, L. Limousy, M. Jeguirim, New insights on the structural evolution of biomass char upon pyrolysis as revealed by the Raman spectroscopy and elemental analysis, Carbon N. Y. 119 (2017) 519–521. https://doi.org/10.1016/j.carbon.2017.04.078.

[265] R. Al Afif, S.S. Anayah, C. Pfeifer, Batch pyrolysis of cotton stalks for evaluation of biochar energy potential, Renew. Energy. 147 (2020) 2250–2258. https://doi.org/10.1016/j.renene.2019.09.146.

[266] C. Guizani, M. Jeguirim, S. Valin, L. Limousy, S. Salvador, Biomass chars: The effects of pyrolysis conditions on their morphology, structure, chemical properties and reactivity, Energies. 10 (2017) 1–18. https://doi.org/10.3390/en10060796.

[267] O.D. Nartey, B. Zhao, Biochar preparation, characterization, and adsorptive capacity and Its effect on Bioavailability of contaminants: An overview, Adv. Mater. Sci. Eng. 2014 (2014). https://doi.org/https://doi.org/10.1155/2014/715398.

[268] Y. Deng, T. Zhang, Q. Wang, Biochar Adsorption Treatment for Typical Pollutants Removal in Livestock Wastewater: A Review, Eng. Appl. Biochar. (2017). https://doi.org/10.5772/intechopen.68253.

[269] B. Chen, Z. Chen, S. Lv, A novel magnetic biochar efficiently sorbs organic pollutants and phosphate, Bioresour. Technol. 102 (2011) 716–723. https://doi.org/10.1016/j.biortech.2010.08.067.

[270] C. Fang, T. Zhang, P. Li, R.F. Jiang, Y.C. Wang, Application of magnesium modified corn biochar for phosphorus removal and recovery from swine wastewater, Int. J. Environ. Res. Public Health. 11 (2014) 9217–9237. https://doi.org/10.3390/ijerph110909217.

[271] Y. Yao, B. Gao, M. Inyang, A.R. Zimmerman, X. Cao, P. Pullammanappallil, L. Yang, Removal of phosphate from aqueous solution by biochar derived from anaerobically digested sugar beet tailings, J. Hazard. Mater. 190 (2011) 501–507. https://doi.org/10.1016/j.jhazmat.2011.03.083.

[272] L. Suárez-Hernández, A.N. Ardila-A., R. Barrera-Zapata, Morphological and physicochemical characterization of biochar produced by gasification of selected forestry species, Rev. Fac. Ing. 26 (2017) 123–130. https://doi.org/10.19053/01211129.v26.n46.2017.7324.

[273] M. Waqas, A.S. Aburiazaiza, R. Miandad, M. Rehan, M.A. Barakat, A.S. Nizami, Development of biochar as fuel and catalyst in energy recovery technologies, J. Clean. Prod. 188 (2018) 477–488. https://doi.org/10.1016/j.jclepro.2018.04.017.

[274] A. Shaaban, S.M. Se, M.F. Dimin, J.M. Juoi, M.H. Mohd Husin, N.M.M. Mitan, Influence of heating temperature and holding time on biochars derived from rubber wood sawdust via slow pyrolysis, J. Anal. Appl. Pyrolysis. 107 (2014) 31–39. https://doi.org/10.1016/j.jaap.2014.01.021.

[275] K.S.W. Sing, Reporting physisorption data for gas / solid systems with Special Reference to the Determination of S, Pure Appl. Chem. 54 (1982) 2201–2218.

[276] H. Abdullah, H. Wu, Biochar as a fuel: 1. Properties and grindability of biochars produced from the pyrolysis of mallee wood under slow-heating conditions, Energy and Fuels. 23 (2009) 4174–4181. https://doi.org/10.1021/ef900494t.

[277] J.C. Groen, L.A.A. Peffer, J. Pérez-Ramírez, Pore size determination in modified micro- and mesoporous materials. Pitfalls and limitations in gas adsorption data analysis, Microporous Mesoporous Mater. 60 (2003) 1–17. https://doi.org/10.1016/S1387-1811(03)00339-1.

[278] O. Kadlec, M.M. Dubinin, Comments on the limits of applicability of the mechanism of capillary condensation, J. Colloid Interface Sci. 31 (1969) 479–489. https://doi.org/10.1016/0021-9797(69)90049-6.

[279] S. Storck, H. Bretinger, W.F. Maier, Characterization of micro- and mesoporous solids by physisorption methods and pore-size analysis, Appl. Catal. A Gen. 174 (1998) 137–146. https://doi.org/10.1016/S0926-860X(98)00164-1.

[280] R.K. Sharma, J.B. Wooten, V.L. Baliga, P.A. Martoglio-Smith, M.R. Hajaligol, Characterization of char from the pyrolysis of tobacco, J. Agric. Food Chem. 50 (2002) 771–783. https://doi.org/10.1021/jf0107398.

[281] S.P. Sohi, E. Krull, E. Lopez-Capel, R. Bol, A review of biochar and its use and function in soil, Adv. Agron. 105 (2010) 47–82. https://doi.org/10.1016/S0065-2113(10)05002-9.

[282] T. Liu, Z. Li, W. Li, C. Shi, Y. Wang, Preparation and characterization of biomass carbon-based solid acid catalyst for the esterification of oleic acid with methanol,

Bioresour. Technol. 133 (2013) 618–621. https://doi.org/10.1016/j.biortech.2013.01.163.

[283] M. Li, Y. Zheng, Y. Chen, X. Zhu, Biodiesel production from waste cooking oil using a heterogeneous catalyst from pyrolyzed rice husk, Bioresour. Technol. 154 (2014) 345–348. https://doi.org/10.1016/j.biortech.2013.12.070.

[284] R.S. Varma, Biomass-Derived Renewable Carbonaceous Materials for Sustainable Chemical and Environmental Applications, ACS Sustain. Chem. Eng. 7 (2019) 6458–6470. https://doi.org/10.1021/acssuschemeng.8b06550.

[285] A.B. Syuhada, J. Shamshuddin, C.I. Fauziah, A.B. Rosenani, A. Arifin, Biochar as soil amendment: Impact on chemical properties and corn nutrient uptake in a Podzol, Can. J. Soil Sci. 96 (2016) 400–412. https://doi.org/10.1139/cjss-2015-0044.

[286] X. xia Guo, H. tao Liu, J. Zhang, The role of biochar in organic waste composting and soil improvement: A review, Waste Manag. 102 (2020) 884–899. https://doi.org/10.1016/j.wasman.2019.12.003.

APPENDIX A

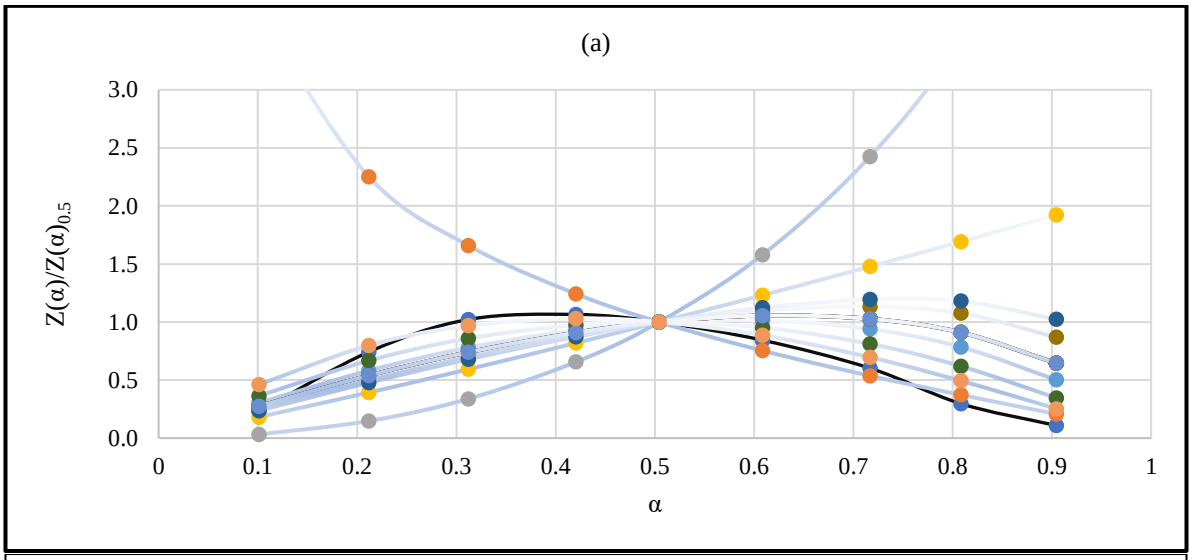
(a)
3.0
2.5
2.0
1.5
1.0
0.5
0.0
Z(α)/Z(α)0.5
0
0.1
0.2
0.3
0.4
0.5
0.6
0.7
0.8
0.9
1
α

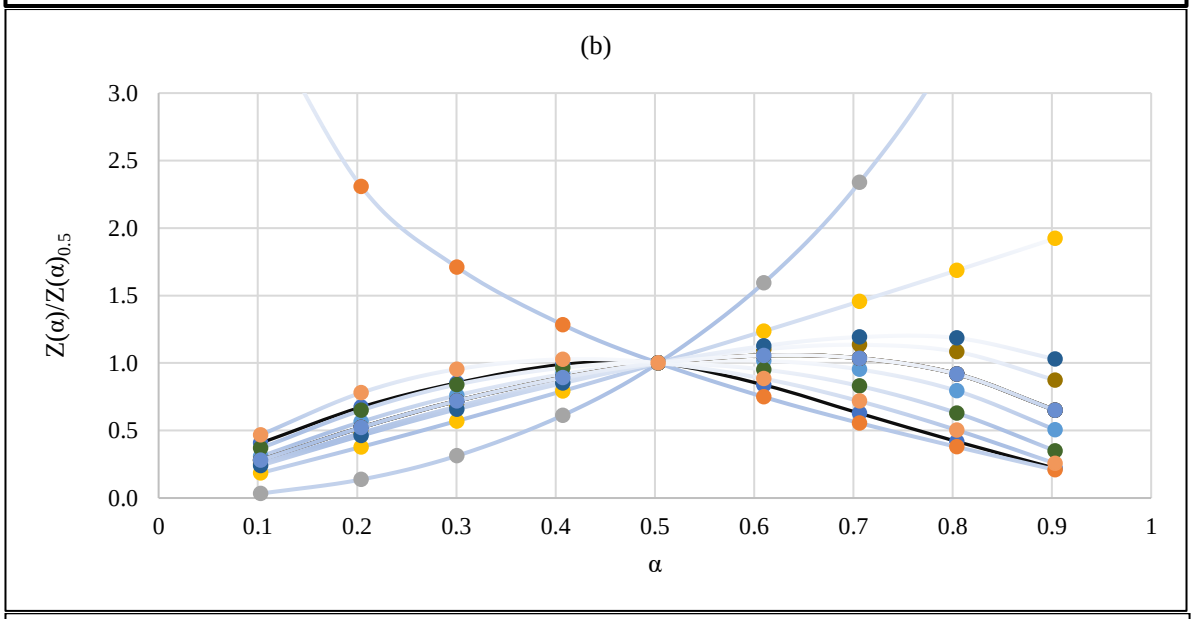
(b)
3.0
2.5
2.0
1.5
1.0
0.5
0.0
Z(α)/Z(α)0.5
0
0.1
0.2
0.3
0.4
0.5
0.6
0.7
0.8
0.9
1
α

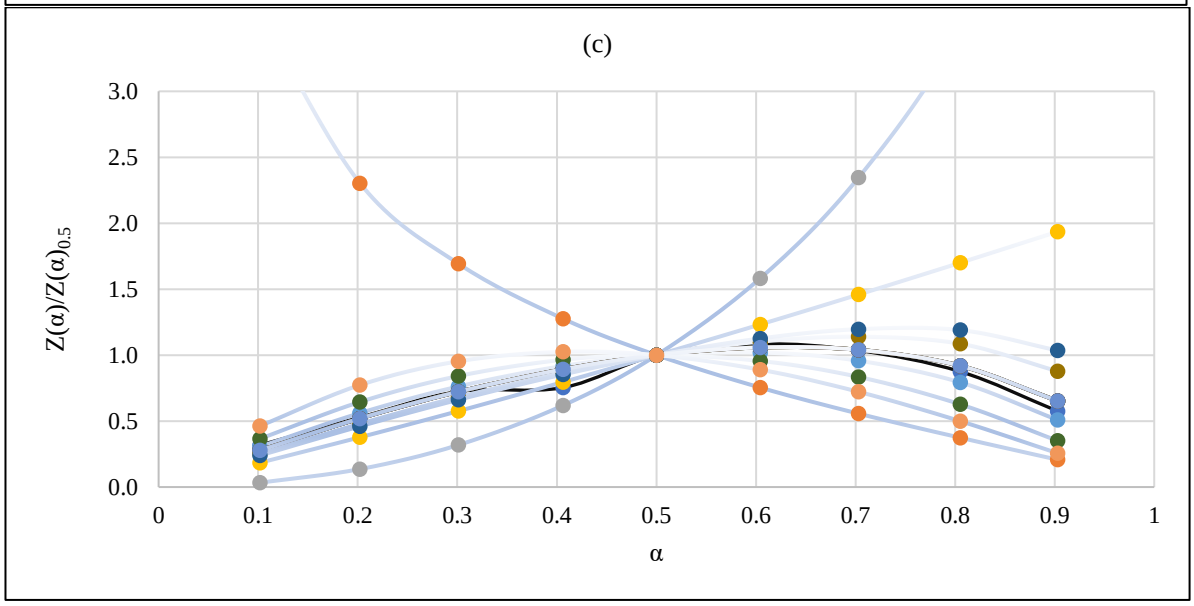
(c)
3.0
2.5
2.0
1.5
1.0
0.5
0.0
Z(α)/Z(α)0.5
0
0.1
0.2
0.3
0.4
0.5
0.6
0.7
0.8
0.9
1
α

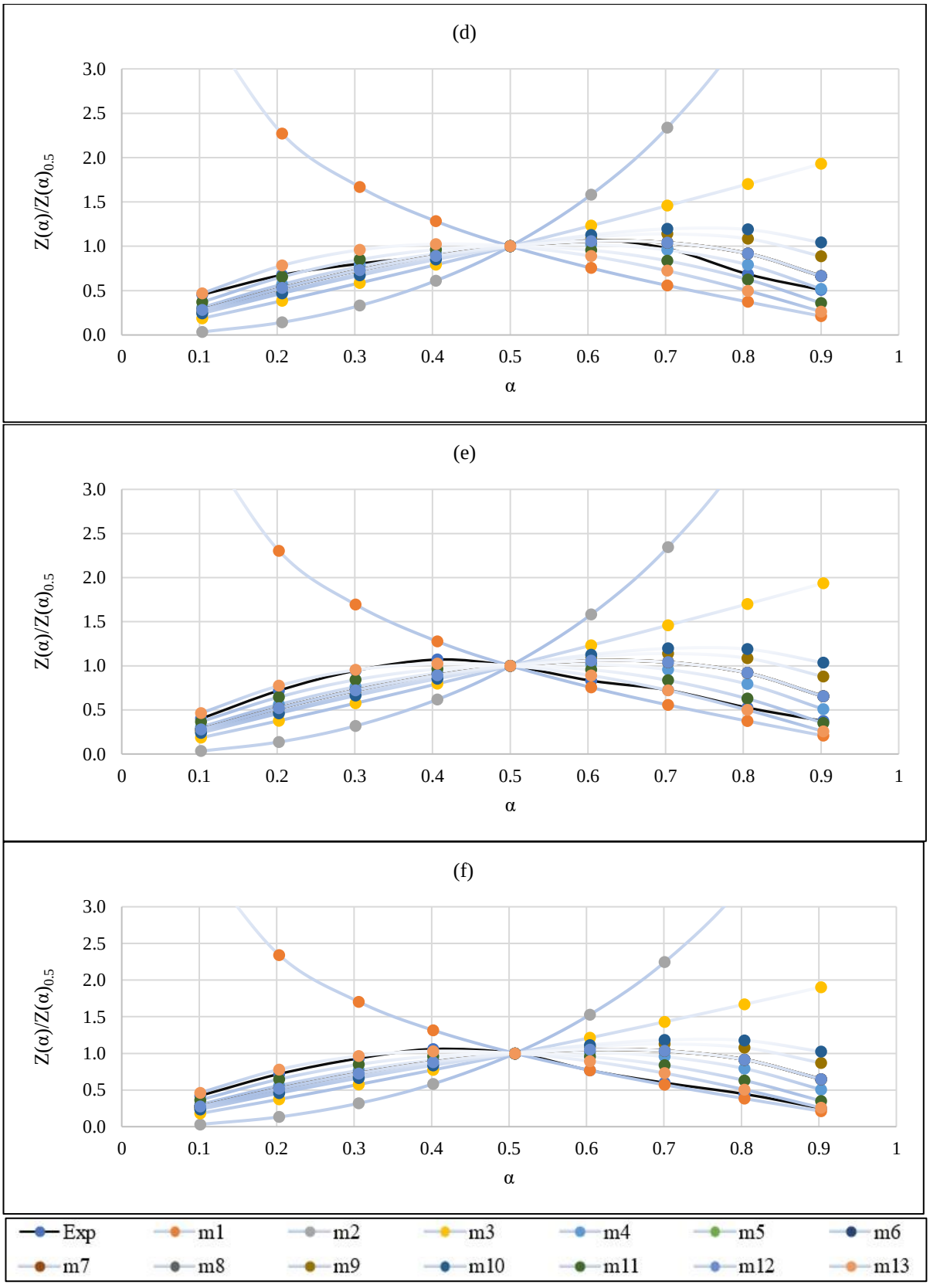

FIGURE 1: Criado plots of PCB (a), CS(b), CS30(c), CS40(d), CS50(e) and CS60(f) for First zone.

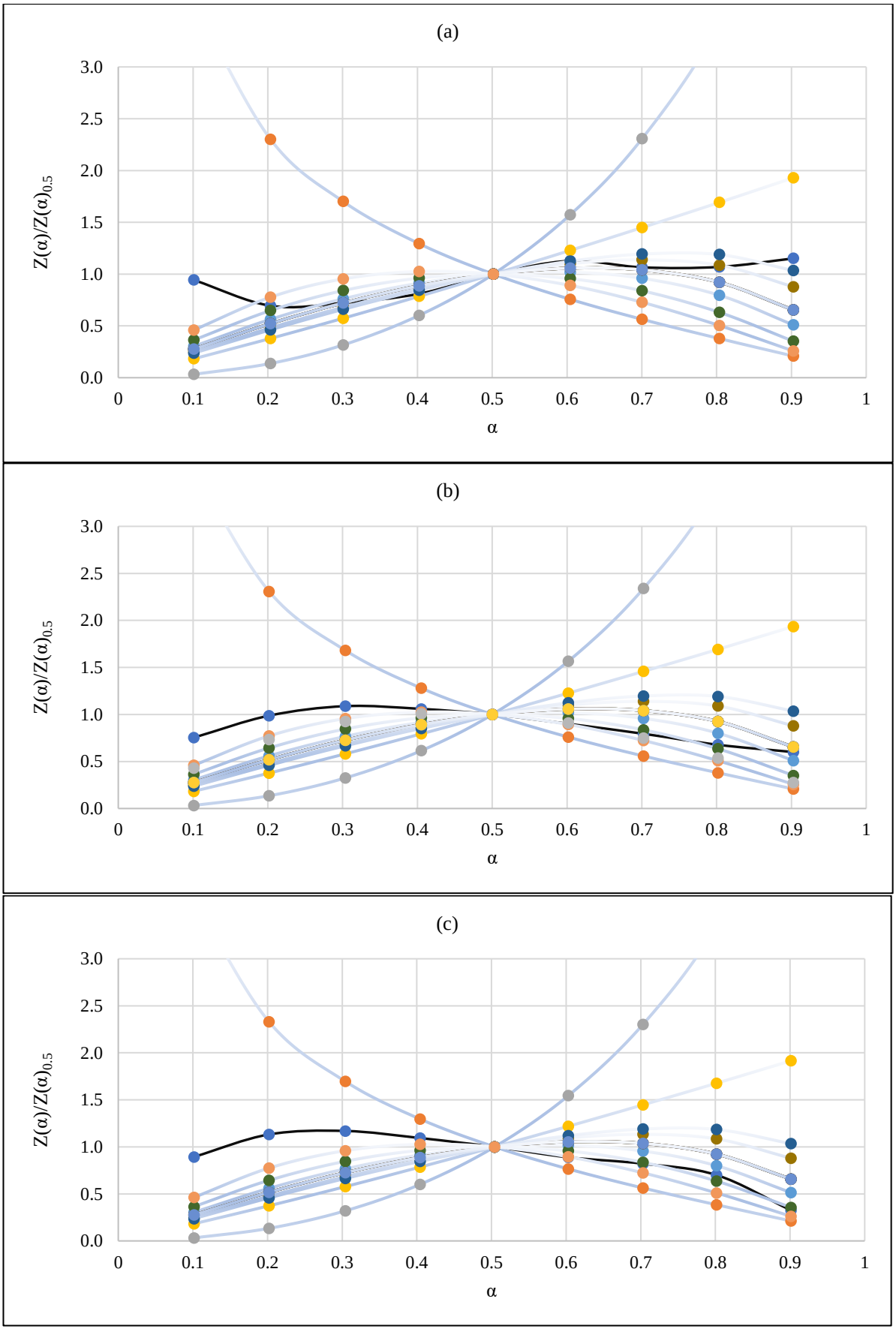
(a)
3.0
2.5
2.0
1.5
1.0
0.5
0.0
Z(α)/Z(α)0.5
0
0.1
0.2
0.3
0.4
0.5
0.6
0.7
0.8
0.9
1
α
(b)
3.0
2.5
2.0
1.5
1.0
0.5
0.0
Z(α)/Z(α)0.5
0
0.1
0.2
0.3
0.4
0.5
0.6
0.7
0.8
0.9
1
α
(c)
3.0
2.5
2.0
1.5
1.0
0.5
0.0
Z(α)/Z(α)0.5
0
0.1
0.2
0.3
0.4
0.5
0.6
0.7
0.8
0.9
1
α

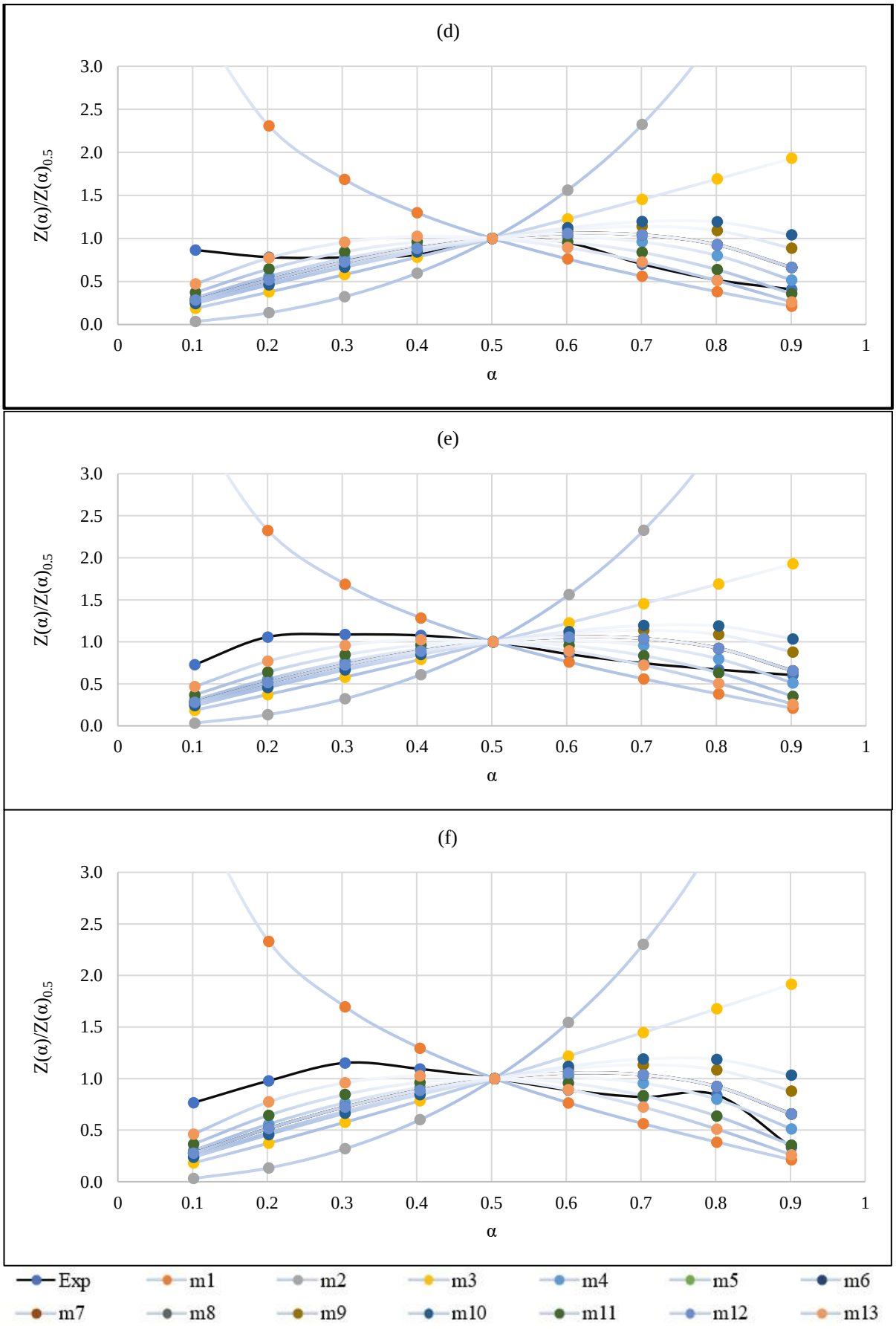

FIGURE 2: Criado plots of PCB (a), CS(b), CS30(c), CS40(d), CS50(e) and CS60(f) for Second zone.

APPENDIX B

List of Publication:

Journal:

1. S.B. Prajapati, A. Gautam, S. Gautam, Biomass and Bioenergy **Non-isothermal kinetic study by TGA analysis of printed circuit boards and cotton stalk**, Biomass and Bioenergy. 172 (2023) 106746. https://doi.org/10.1016/j.biombioe.2023.106746. (Impact Factor: 5.774) (SCIE & SCOPUS)

2. S.B. Prajapati, A. Gautam, S. Gautam, **Debromination and improved phenol content in fuel oil generated from co - pyrolysis of non - metallic PCB and biomass,** Biomass Convers. Biorefinery (2022). https://doi.org/10.1007/s13399-022-03139-z (Impact Factor: 4.050) (SCIE & SCOPUS)

3. S.B. Prajapati, A. Gautam, S. Gautam, **The Effect of Cotton Stalk Concentration on Morphology and Fixing Bromine Content in Char while Co-Pyrolysis with Non-Metal Fractions of PCB,** Biomass Convers. Biorefinery (2022) https://doi.org/10.1007/s13399-022-03515-9 (Impact Factor: 4.050) (SCIE & SCOPUS)

4. S. B. Prajapati, A. Gautam, S. Gautam, Z. Yao , F. Tesfaye, X. Lü, **Co-pyrolysis behaviour, kinetic and mechanism of waste printed circuit board with Biomass,** Processes, (2023) 1–21. https://doi.org/10.3390/pr11010229. (Impact Factor: 3.352) (SCIE & SCOPUS)

5. S.B. Prajapati, A. Gautam, S. Gautam, **Co-pyrolysis of PCB and cotton stalk: Towards enhanced phenol production and debromination of pyrolysis oil**, Chemical and Process Engineering 2022, 43 (2), 1–14. DOI: 10.24425/cpe.2022.140823. (Impact Factor: 0.679) (SCOPUS)

6. S. B. Prajapati, A. Gautam, S. Gautam, **Co-pyrolysis of PCB: Towards enhanced phenol production and debromination - Review,** Biomass and Bioenergy - Under Review

Conference Proceedings:

1. Sonal Prajapati, S. Gautam, **Co-pyrolysis of PCB with Cotton stalk: Product Characterization**, International Chemical Engineering Conference 2021, Organised by Department of Chemical Engineering Dr. B.R. Ambedkar National Institute of Technology, Jalandhar.

2. Sonal Prajapati, S. Gautam, **Pyrolysis of E-waste for Fuel oil Generation: A Review,** Schemcon (2019), 15^{th} annual session of student's chemical engineering congress, Shroff S. R. Rotary Institute of Chemical technology, Ankleshwar.